Supplementary Information for

Scalable and selective deuteration of *N*-heteroarenes via single-atom photocatalysis

Jie Xu[1,2], Rui Cao[1,2], Shao-Zhen Yang[1,2], Yi-Ming Guo[1], Tong Xia[1,2], Da Zhao[3], Ting-Rui Pan[2], K.M. Liew[4], Flemming Besenbacher[5], Yi-Tao Dai[1,2]*

[1]Key Laboratory of Precision and Intelligent Chemistry, School of Nano Science and Technology, School of Chemistry and Materials Science, University of Science and Technology of China; Hefei, Anhui 230026, China

[2]Sustainable Energy and Environmental Materials Innovation Center, Center for Intelligent Medical Equipment and Devices, Suzhou Institute for Advanced Research, University of Science and Technology of China; Suzhou, Jiangsu 215123, China

[3]School of Chemical Sciences, University of Chinese Academy of Sciences; Beijing 101408, China

[4]Department of Architecture and Civil Engineering, Centre for Nature-Inspired Engineering, City University of Hong Kong, Kowloon, Hong Kong, China

[5]Interdisciplinary Nanoscience Center (iNANO), Aarhus University; DK-8000 Aarhus C, Denmark

*Corresponding author. Email: yitaodai@ustc.edu.cn

Table of Contents

1. General information

Unless otherwise noted, all reagents, substrates and solvents were obtained from commercial suppliers (including Bidepharm: https://www.bidepharm.com/; Aladdin: https://www.aladdin-e.com/; Macklin: https://www.macklin.cn/; Leyan: https://www.leyan.com/; Energy: https://www.energy-chemical.com/; Topbatt: http://www.topbatt.net/; Rhawn: https://www.rhawn.cn/; Sinopharm: https://www.sinoreagent.com/) and used without further purification. NMR spectra were recorded on a Bruker spectrometer at 400 MHz (^{1}H NMR), 101 MHz (^{13}C NMR), 376 MHz (^{19}F NMR). Chemical shifts were reported relative to tetramethylsilane, D_2O (4.79 ppm for ^{1}H), $CDCl_3$ (2.50 ppm for ^{1}H, 77.0 ppm for ^{13}C), DMSO-d_6 (2.50 ppm for ^{1}H, 39.6 ppm for ^{13}C). The following abbreviations (or combinations thereof) were used to explain multiplicities: s = singlet, d = doublet, t = triplet, q = quartet, m = multiplet, br = broad. Coupling constants, *J*, were reported in the Hertz unit (Hz). All measurements were carried out at room temperature unless otherwise stated. The ^{1}H NMR of the substrates was measured directly without further purification. The degree of deuterium incorporation was determined by the decrease of ^{1}H NMR signal intensities in comparison with the unlabelled one. To get a precise integration by quantitative NMRs, we did as follows: (1) checking for a proper phase correction. (2) making appropriate baseline correction (baseline must be flat and, most importantly, situated at zero value of the vertical (y) axis). (3) using always the same integration region, the width of which is defined by a constant multiple of the signal half-width. d) using the signals of the undeuterated C−H positions as internal references, which have equal intensities in contrast to reactants. In cases where deuterium exchange happened at all the C(sp^2)−H positions without the unlabelled parts as internal references, *e.g.* **14b**, **17b**, **25b**, and **33b-36b**, we introduced an internal standard 1,4-dioxane to identify the deuterium content of products.

2. Procedure for the preparation of photocatalysts

Raw Materials: the following noble-metals, semiconductors and solvents were obtained from commercial suppliers: K_2PdCl_4 (Aladdin, ⩾99.95% metals basis), K_2PtCl_4 (Aladdin, ⩾99.9% metals basis), $RuCl_3·3H_2O$ (Macklin, 98%), $RhCl_3·3H_2O$ (Macklin, 99.95% metals basis), $IrCl_3·3H_2O$ (Energy, 98%), $AuCl_3$ (Aladdin, ⩾99.9% metals basis), Pd/C (Macklin, 10% Pd), TiO_2-R (Aladdin, rutile, 99.8% metals basis), Nb_2O_5 (Macklin, 99.99% metals basis), $SrTiO_3$ (Macklin, 99.5% metals basis), SiC (Bidepharm, 99%), BiOCl (Aladdin, ⩾99%), $BiVO_4$ (Energy, 99.9% metals basis), Bi_2WO_6 (Rhawn, 99.9% metals basis), $Ti(OBu)_4$ (Aladdin, ⩾99%), EtOH (Sinopharm, Ar, ⩾99.7%), $NH_3·H_2O$ (Sinopharm, Ar), *i*-PrOH (Macklin, HPLC⩾99.9%).

2.1 Preparation of TiO_2-h

30 mL $Ti(OBu)_4$ was added to 100 mL absolute ethanol, which was stirred on a thermostatic stirrer for 10 min to form a uniform light yellow color solution **A**. Then, 10 mL deionized water was added to solution **A** dropwise slowly. The mixture was stirred for 1 h and filtrated through a funnel. The obtained solid was washed with deionized water 3 times, and then dried at 70 °C for 12 h. The sample was transferred to a ceramic crucible and placed in a muffle furnace, which was heated at 500 °C for 2 h (at a heating rate of 10 °C/min). After cooling down, TiO_2-h as a white powder was obtained.

2.2 Preparation of Pd_1/TiO_2-h

As-prepared 500 mg TiO_2-h and 7.67 mg K_2PdCl_4 were added to a 20 mL water-isopropanol solution (volume ratio of deionized water : *i*-PrOH was 5 : 1), which were stirred on a thermostatic stirrer for 10 min. Then the mixture was irradiated with 410 nm LED under Ar atmosphere at room temperature. After 5 h irradiation, the light grey solids were collected via centrifugation and further washed with water. After drying in a vacuum oven, the sample **Pd_1/TiO_2-h** was obtained, which was directly used for characterizations and photocatalytic tests. The loading amount of Pd was easily tuned by introducing different amounts of K_2PdCl_4.

2.3 Preparation of Pd_n/TiO_2-h

According to the literature[1], 300 mg TiO_2-h was dispersed in 50 mL deionized water with a certain amount of H_2PdCl_4 and was stirred at room temperature. Then, H_2 was introduced to the

suspension. H_2PdCl_4 was rapidly reduced into small Pd^0 nanoparticles. The light grey solids were collected via centrifugation and further washed with water. After drying, the sample **Pd_n/TiO_2-h** was obtained.

2.4 Preparation of other photocatalysts (Metal/Semiconductor)

In_2O_3: it was prepared according to the literature[2], 7 mmol $In(NO_3)_3 \cdot 6H_2O$ were dissolved in 50 mL of deionized water under magnetic stirring. Then, $NH_3 \cdot H_2O$ was added dropwise until no further precipitation occurred. The resulting white slurry was then placed in a thermostatic water bath and aged at 80 °C for 1 h. Later, the product was separated by centrifugation. The sediment was washed twice with deionized water and then twice with ethanol before drying for 5 hours at 60 °C. Finally, the dried sediment was transferred to a crucible, heated at 350 °C for 3 h in a muffle furnace at a heating rate of 5 °C/min.

According to the synthesis method of Pd_1/TiO_2-h, 500 mg semiconductors and required amounts of noble-metals salt were dissolved in a 20 mL water-isopropanol solution (volume ratio of deionized water : *i*-PrOH = 5 : 1) under stirring. Then the mixture was irradiated with 410 nm LED under Ar atmosphere at room temperature. After 5 h irradiation, the photocatalyst was collected via centrifugation and further washed with water. After drying in a vacuum oven, photocatalysts of **M/TiO_2-h** or **Pd/Semiconductors** were obtained. The metal loading was easily tuned by introducing different amounts of noble metals. Specificially, Pt/TiO_2-h, Ru/TiO_2-h, Rh/TiO_2-h, Ir/TiO_2-h, Au/TiO_2-h, Pd/TiO_2-R, Pd/In_2O_3, Pd/Nb_2O_5, $Pd/SrTiO_3$, Pd/SiC, Pd/In_2O_3, Pd/BiClO, $Pd/BiVO_4$, and Pd/Bi_2WO_6 were prepared accordingly.

3. Characterizations of photocatalysts

3.1 X-ray Diffraction (XRD)

To investigate the crystal structures of samples, XRD data were collected on all samples using a Rigaku smartlab X-ray diffractometer equipped with a Cu Kα source (40 kV, 200 mA; λ=1.54178 Å). The XRD patterns were recorded using the conventional θ-2θ geometry (Bragg-Brentano) and a scan range from 20 to 80 ° with a step size of 0.02 ° and a scan rate of 20 °/min.

3.2 Electron Microscopy

Scanning electron microscope (SEM) images were collected on GeminiSEM 500. Transmission electron microscopy (TEM) images were collected on JEM-2100 Plus. High-resolution TEM (HRTEM) images and energy-dispersive X-ray spectroscopy (EDS) elemental mapping were obtained on Talos F200S and Talos F200X. Aberration-corrected high-angle annular dark-field scanning transmission electron microscopy (AC HAADF-STEM) analysis was performed on ThemisZ transmission electron microscope (accelerating voltage of 300 kV).

3.3 Inductively Coupled Plasma-mass Spectrometry (ICP-MS)

The metal loadings of photocatalysts were precisely analyzed by inductively coupled plasma mass spectrometer (ICP and Agilent 720ES). For each measurement, a 100 mg sample was dissolved in the mixture of aqua regia and HF for analysis.

3.4 UV-Vis Diffuse Reflectance Spectroscopy (UV-Vis DRS) and Photoluminescence (PL)

The UV-Vis DRS profiles were recorded at room temperature (r.t.) covering 300-800 nm via a PerkinElmer Lambda 365 UV-vis spectrophotometer with $BaSO_4$ (spectroscopy grade) as reference. For each measurement, a 100 mg sample was loaded for analysis. According to the Kubelka-Munk theory[3], Tauc plots of a direct semiconductor can be drawn by plotting $[F(R)\cdot h\nu]^2$ versus $h\nu$ (incident photon energy)[4], where $F(R) = (1-R)^2/(2R)$ and R is the measured reflectance. To investigate the possible interaction between *N*-heteroarenes and photocatalyst samples, 0.15 mL 2-aminopyrimidine solution was directly mixed with dry sample powders to get a wet sample adsorbed with *N*-heteroarenes, which was subsequently analyzed by spectrophotometer to obtain the UV-Vis DRS data.

Photoluminescence (PL) spectra were recorded on a Cary Eclipse fluorescence spectrophotometer using the excitation wavelength of 300 nm.

3.5 X-ray Photoelectron Spectroscopy (XPS)

XPS measurements were performed with a spectrometer from Escalab 250Xi. The monochromatized Al Kα X-ray source (E=1486.6 eV) was operated at 15 kV and 200W. For the narrow scans, 20 eV pass energy was applied. The medium area mode was used as lens mode. The base pressure during the experiment in the analysis chamber was $5x10^{-10}$ mbar. Considering charging effects, all spectra have been referred to C 1s at 284.8 eV.

3.6 *In-situ* Mass Spectrometry

To identify the gas composition during photocatalytic hydrogen isotope exchange (HIE) of 2-aminopyrimidine in D_2O, the gas phase was analyzed qualitatively and quantitatively using an *in-situ* mass spectrometer (MS, HPR-20, Hiden) in SynCat@Beijing, Synfuels China Technology Co. Ltd. Since the system had a well-defined volume and was leak tight, the quantity of evolved gases can be calculated based on their partial pressure by applying the ideal gas law calibrated with the MS sensitivity factor. The *in-situ* MS system can be employed to monitor the evolution of several gases (e.g., H_2, HD, D_2) all at once.

3.7 Fourier Transform Infrared Spectroscopy (FT-IR)

3.7.1. Diffuse Reflectance Infrared Fourier Transform Spectroscopy (DRIFTs) analysis

DRIFTs experiments were conducted using the Praying Mantis accessory (Harrick) in a Nicolet iS20 spectrometer equipped with an MCT detector. The fresh powder sample (e.g., TiO_2-h, Pd/TiO_2-h, and organic substrates mixed with KBr) was placed in the catalytic reaction chamber equipped with two ZnSe windows and one SiO_2 window dome and coupled with a temperature controller for heating. Firstly, the sample was heated from R.T. to 120 °C for 30 min under Ar flow (20 mL/min) to remove the adsorbed water molecules. After the sample was cooled down to r.t. under Ar flow, IR spectra were recorded.

3.7.2. In-situ Diffuse Reflectance Infrared Fourier Transform Spectroscopy (DRIFTs) analysis

As shown in Supplementary Fig. 31, an *in-situ* DRIFT setup was home-built to investigate the HIE process at the surface of the photocatalyst. The setup consisted of the following parts: (1) a Nicolet iS20 spectrometer equipped with an MCT detector and a Praying Mantis^{TM} HVC accessory enclosed with a three-window dome (Harrick Scientific Products, Inc.); (2) an ATC temperature controller with a cooling water circulating system; (3) 410 nm LED lamp for light irradiation; (4) Ar as carrier gas introduced by a mass flow controller (MFC).

To study the possible reaction pathway during the HIE of *N*-heteroarenes, *in-situ* DRIFTs experiments were conducted. Initially, the fresh powder sample (e.g., Pd_1/TiO_2-h) was loaded in the reaction chamber equipped with two ZnSe windows and one quartz window. Then, the sample was heated at 120 °C for 30 min under Ar flow (20 mL/min) to remove the adsorbed water. After cooling down to r.t., NMP (*N*-methyl pyrrole) vapor (15 mL) was introduced into the chamber via a syringe. Later, the sample was flushed with Ar flow (20 mL/min) for 1 h to remove physically adsorbed NMP, IR spectra were recorded in dark and light irradiation, respectively. To investigate the dynamic changes under light irradiation in the presence of D_2O, sufficient vapor of D_2O (50 mL) was introduced into the chamber via a syringe. Subsequently, photocatalysts covered with NMP and D_2O molecules in the closed chamber were irradiated by a 410 nm LED lamp. Simultaneously, IR spectra were recorded repeatedly with a certain time interval.

3.8 X-ray Absorption Spectroscopy (XAS)

3.8.1 XAS measurements and data processing

The X-ray absorption spectra at the Pd K-edge were recorded at the XAS station (BL14W1) of the Shanghai Synchrotron Radiation Facility (SSRF). The electron storage ring was operated at 3.5 GeV. Using Si (311) double-crystal monochromator, the data collection was carried out in transmission mode for Pd K-edge XAFS. All spectra were collected in ambient conditions. By using the third ionization chamber, standard samples including Pd foil and PdO were measured simultaneously for energy calibrations. The beam size was limited by the horizontal and vertical slits with an area of 1×4 mm^2 during XAFS measurements. The as-obtained, raw XAFS data were processed using WinXAS version 3.1.

3.8.2 XAS data analysis

The EXAFS data were processed according to the standard procedures using the Athena and Artemis implemented in the IFEFFIT software packages. The EXAFS spectra were obtained by subtracting the post-edge background from the overall absorption and then normalizing with respect to the edge-jump step. Subsequently, the $\chi(k)$ data of Fourier were transformed to real (R) space using a hanning windows (dk=1.0 $Å^{-1}$) to separate the EXAFS contributions from different coordination shells. To obtain the quantitative structural parameters around central atoms, least-squares curve parameter fitting was performed using the ARTEMIS module of IFEFFIT software packages.

The following EXAFS equation was employed:

$$\chi(k) = \sum_j \frac{N_j S_o^2 F_j(k)}{k R_j^2} \exp[-2k^2\sigma_j^2] \exp[\frac{-2R_j}{\lambda(k)}] \sin[2kR_j + \phi_j(k)]$$

S_0^2 is the amplitude reduction factor, $F_j(k)$ is the effective curved-wave backscattering amplitude, N_j is the number of neighbors in the j^{th} atomic shell, R_j is the distance between the X-ray absorbing central atom and the atoms in the j^{th} atomic shell (backscatterer), λ is the mean free path in Å, $\phi_j(k)$ is the phase shift (including the phase shift for each shell and the total central atom phase shift), σ_j is the Debye-Waller parameter of the j^{th} atomic shell (variation of distances around the average R_j). The functions $F_j(k)$, λ, and $\phi_j(k)$ were calculated with the ab initio code FEFF8.2. The coordination numbers of model samples were fixed as the nominal values. The obtained S_0^2 was fixed in the subsequent fitting. While the internal atomic distances R, Debye-Waller factor δ^2, and the edge-energy shift ΔE_0 were allowed to run freely.

3.9 High-resolution Mass Spectrometry (HR-MS)

High-resolution Mass Spectra (HR-MS) were measured with a Waters Xevo G2-XS QTof spectrometer. Accurate masses were reported for the molecular ion + hydrogen ($[M+H^+]$), the molecular ion + sodium ($[M+Na^+]$) and the molecular ion + potassium ($[M+K^+]$). For each measurement, 90% methanol (including 0.1% formic acid) was used as the mobile phase.

3.10 Electron Paramagnetic Resonance (EPR)

Electron paramagnetic resonance (EPR) measurements were performed at an EMXplus electron paramagnetic resonance spectrometer to investigate possible radicals with 5,5′-dimethyl-

1-pyrroline-N-oxide (DMPO) as the radical scavenger. First, in the glove box, a suspension with 25 mg photocatalysts and 0.1 mmol DMPO in 1 mL D_2O was prepared. Then, a certain amount of the suspension was sucked into a capillary (inner diameter of 0.9 mm). After sealing one end of the capillary, it was transferred to an EPR quartz tube (inner diameter of 4 mm) with a leak-tight cap. Later, the EPR tests were performed with the suspension in the quartz tube irradiated by 410 nm LED. In addition, the suspension without light irradiation was tested with EPR as well for comparison.

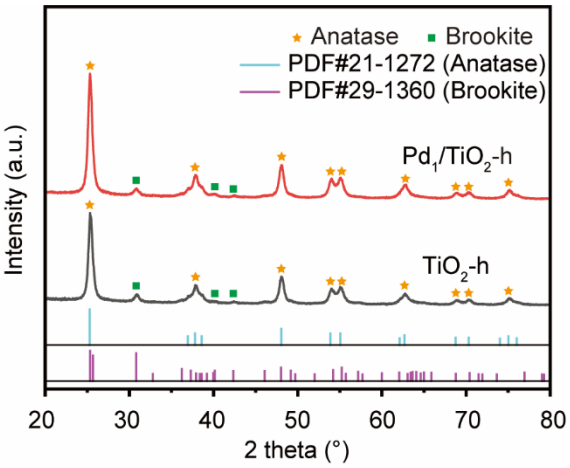

Supplementary Figure 1. XRD patterns of TiO_2-h and Pd_1/TiO_2-h. The standard JCPDS cards of anatase (PDF#21-1272) and brookite (PDF#29-1360) TiO_2 were incorporated for comparison.

In comparison with the pristine homemade TiO_2 (TiO_2-h), the XRD pattern of the sample loaded with Pd (Pd_1/TiO_2-h) showed that there was no significant change in crystal phases without the observation of diffraction peaks attributed to Pd nanoparticles.

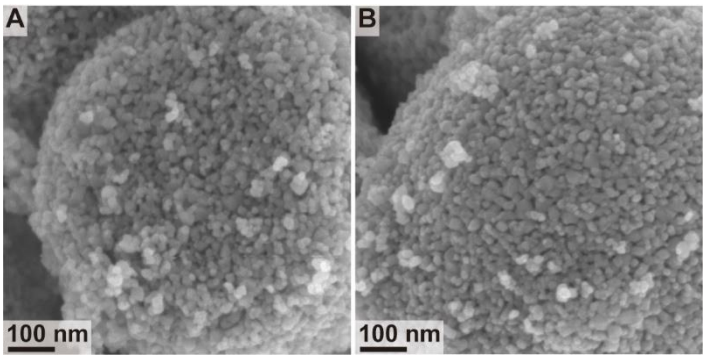

Supplementary Figure 2. SEM images of (A) TiO_2-h and (B) Pd_1/TiO_2-h.

The SEM data of TiO_2-h showed the aggregation of spherical particles, with the particle size ranging between 15-25 nm. Moreover, there is no significant change in morphology for the sample loaded with Pd (Pd_1/TiO_2-h) in comparison with pristine TiO_2-h.

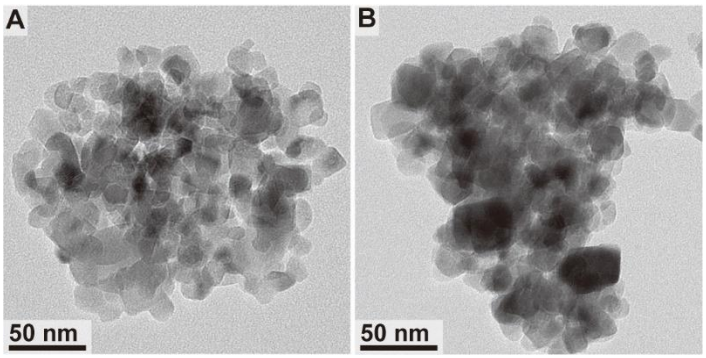

Supplementary Figure 3. TEM images of (A) TiO_2-h and (B) Pd_1/TiO_2-h.

To further clarify the microstructures of the photocatalysts, we conducted TEM characterizations. TEM images revealed that TiO_2-h has a well-defined nanoparticle structure and no significant change in morphology appeared after loading Pd via the photo-deposition method. Moreover, we did not observe any Pd nanoparticles.

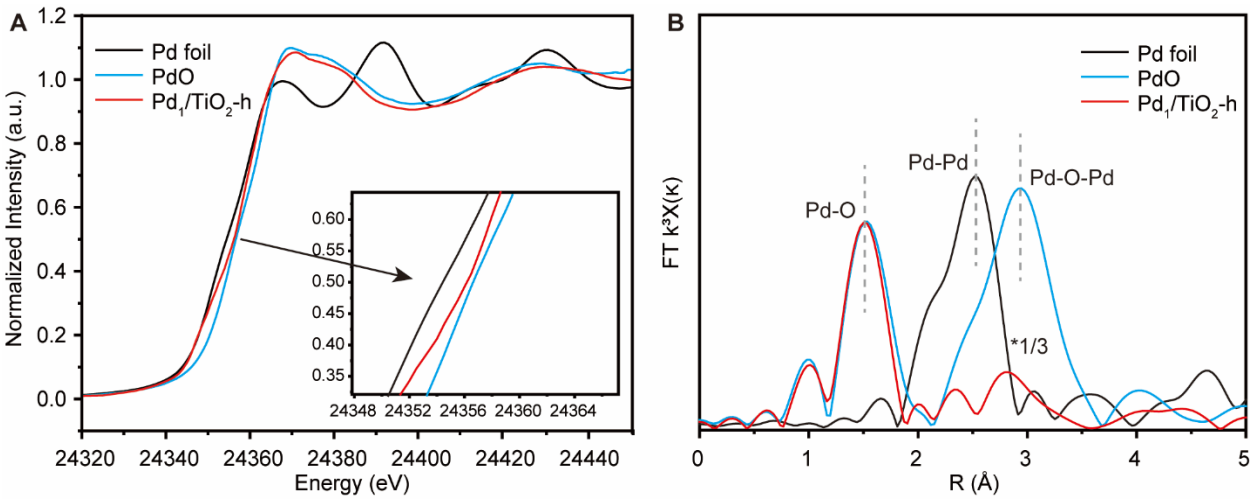

Supplementary Figure 4. (A) X-ray absorption near-edge structure (XANES) of Pd K-edge for Pd_1/TiO_2-h catalyst with reference materials Pd foil and PdO. (B) Fourier transforms of k^3-weighted Pd K-edge EXAFS experimental data for Pd foil, PdO, and Pd_1/TiO_2-h.

The electronic properties of Pd species in Pd_1/TiO_2-h were studied by XANES spectroscopy with Pd foil and PdO as reference samples. As shown in Supplementary Fig. 4A, XANES spectra displayed that the Pd K-edge absorption edge for Pd_1/TiO_2-h was located between that of Pd foil and PdO, indicating the existence of $Pd^{\delta+}$ rather than Pd^0 ($0<\delta<2$). Besides, the near-edge structure of Pd_1/TiO_2-h was similar to that of PdO reference. The low-intensity oscillations directly following the near-edge region indicated the short-range and low-coordinate environment of Pd on TiO_2-h.

For Pd_1/TiO_2-h there was only one notable peak at 1.51 Å from the Pd-O contribution without the appearance of a signal at 2.55 Å from the Pd-Pd contribution (Supplementary Fig. 4B), confirming the dominant presence of atomically dispersed Pd atoms in Pd_1/TiO_2-h.

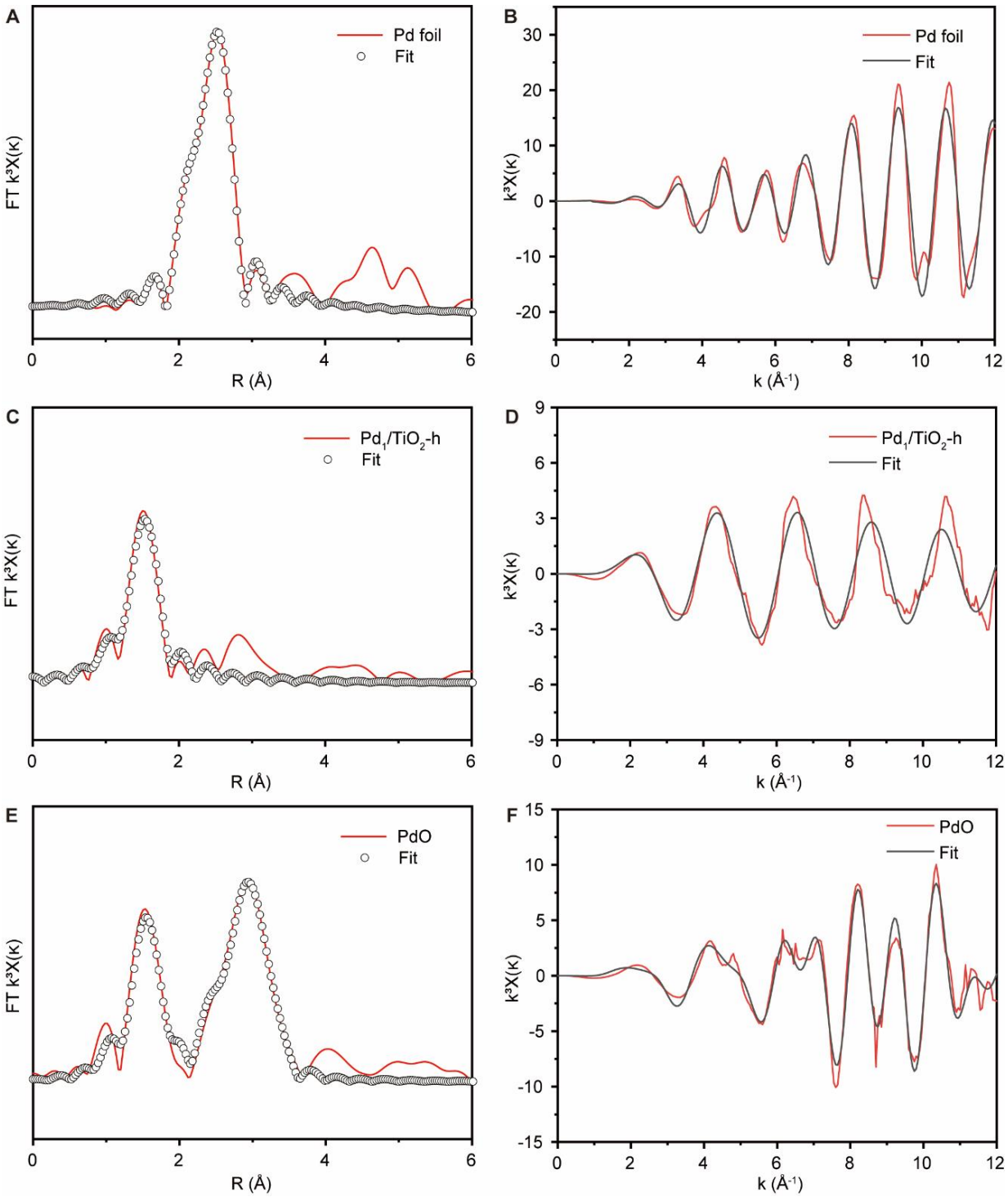

Supplementary Figure 5. EXAFS R space fitting curves (circle) and the experimental ones (red line), k space fitting curves (red line) and the experimental ones (black line) of (A, B) Pd foil, (C, D) Pd_1/TiO_2-h and (E, F) PdO, respectively.

Supplementary Table S1. Fitting parameters extracted from the Pd K-edge EXAFS fitting. (S_0^2=0.86 from Pd foil)

Sample	Scattering path	CN	R (Å)	δ^2(Å^2)	ΔE_0 (eV)	R factor
Pd foil	Pd-Pd	12	2.73 ± 0.01	0.0053	3.8 ± 0.1	0.0016
PdO	Pd-O	4	2.01 ± 0.01	0.0011	1.7 ± 0.1	0.039
Pd_1/TiO_2-h	Pd-O	4.2 ± 0.1	2.01 ± 0.01	0.0029	0.7 ± 1.0	0.0023

S_0^2 is the amplitude reduction factor; CN is the coordination number; R is interatomic distance (the bond length between central atoms and surrounding coordination atoms); δ^2 is Debye-Waller factor (a measure of thermal and static disorder in absorber-scatterer distances); ΔE_0 is edge-energy shift (the difference between the zero kinetic energy value of the sample and that of the theoretical model). R factor is used to value the goodness of the fitting. Error bounds that characterize the structural parameters obtained by EXAFS spectroscopy were estimated as N ± 20%; R ± 1%; δ^2 ± 20%.

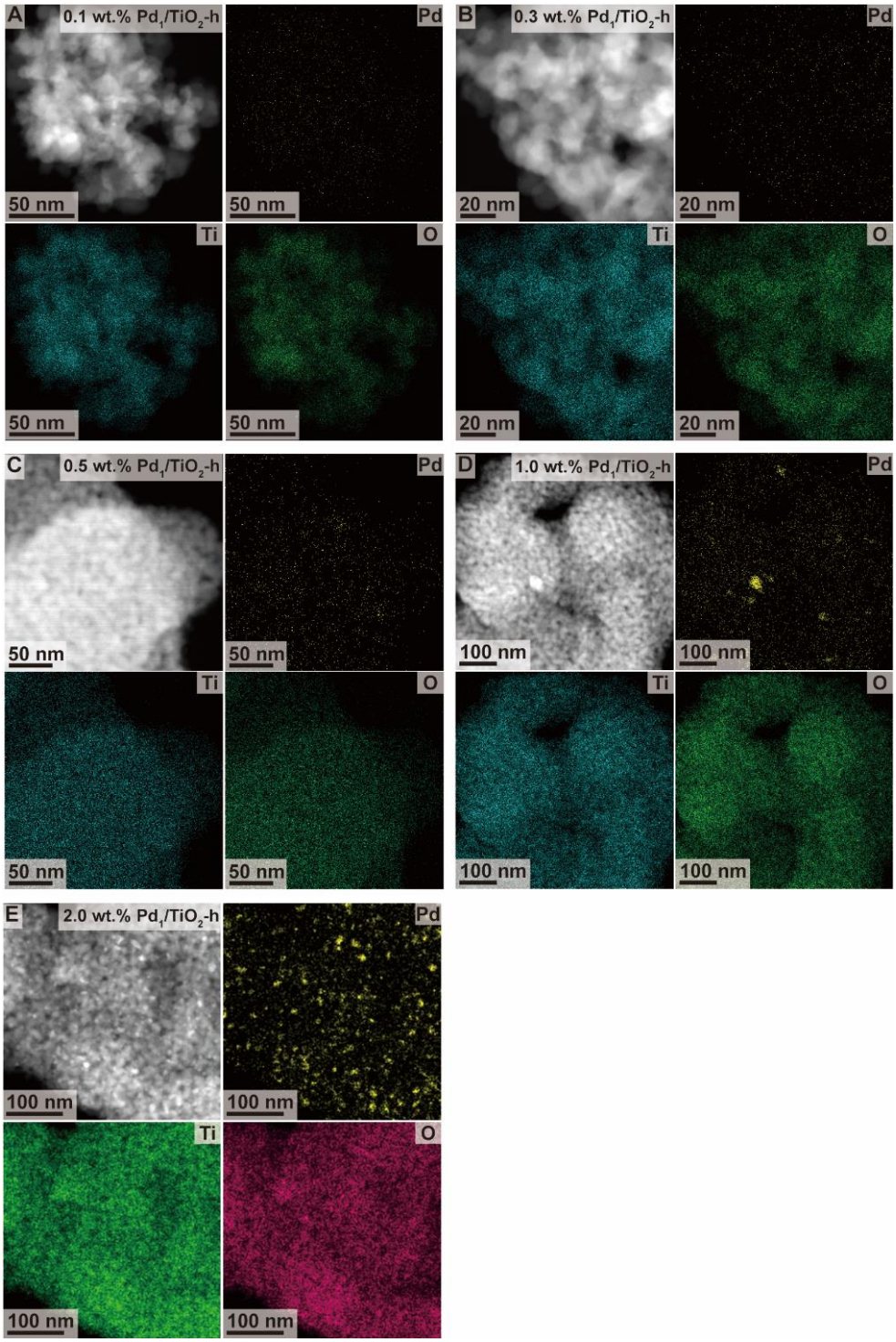

Supplementary Figure 6. STEM-EDS elemental mapping of Pd_1/TiO_2-h with different Pd loading amounts. (A) 0.1 wt.% Pd_1/TiO_2-h; (B) 0.3 wt.% Pd_1/TiO_2-h; (C) 0.5 wt.% Pd_1/TiO_2-h; (D) 1.0 wt.% Pd_1/TiO_2-h; (E) 2.0 wt.% Pd_1/TiO_2-h.

With the increase of Pd loading, coverage of Pd species atomically dispersed on TiO_2-h became higher. In addition, for the samples with 1.0 wt.% and 2.0 wt.% loadings, the dominant Pd species still existed as SA sites, even though we observed the appearance of some Pd clusters or nanoparticles (Supplementary Figs. 6D and 6E).

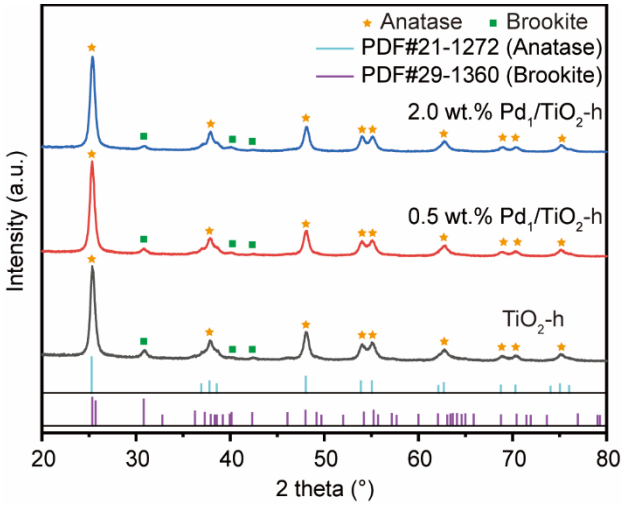

Supplementary Figure 7. XRD patterns of Pd_1/TiO_2-h samples with different Pd loadings. The standard JCPDS cards of anatase (PDF#21-1272) and brookite (PDF#29-1360) TiO_2 were incorporated for comparison.

These two Pd_1/TiO_2-h samples with different Pd loading (0.5 and 2.0 wt.%) presented the same XRD patterns with pristine TiO_2-h. This also implied that the SA Pd sites dominated in 2.0 wt.% Pd_1/TiO_2-h. Otherwise, the diffraction peaks assigned to Pd nanoparticles could be observed like the case 2.0 wt.% Pd/TiO_2-R (Supplementary Fig. 14).

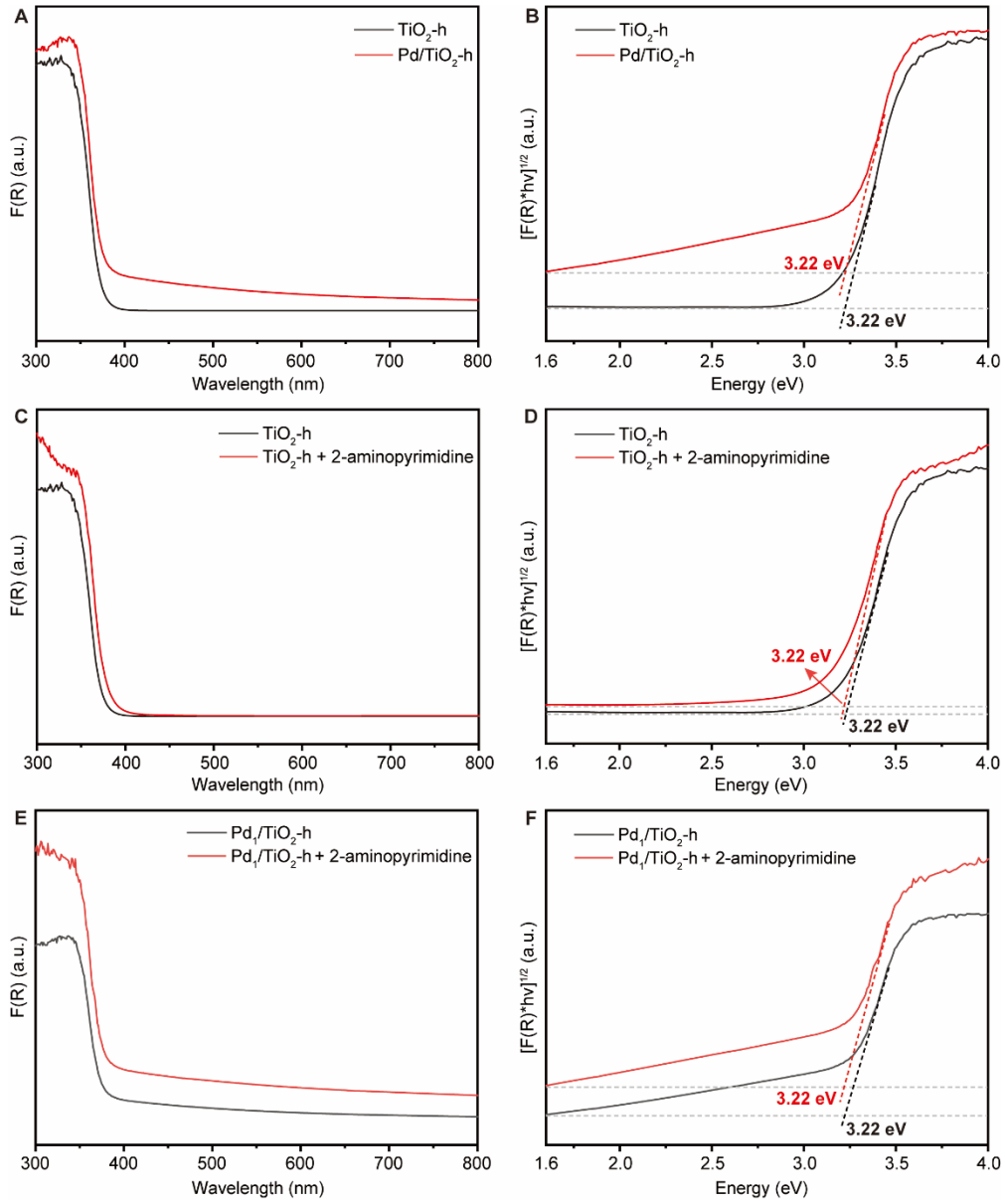

Supplementary Figure 8. (A) UV-Vis DRS and (B) Tauc plots of TiO_2-h and Pd_1/TiO_2-h. (C) UV-Vis DRS and (D) Tauc plots of TiO_2-h with the adsorption of 2-aminopyrimidine. (E) UV-Vis DRS and (F) Tauc plots of Pd_1/TiO_2-h with the adsorption of 2-aminopyrimidine.

Supplementary Fig. 8A shows that TiO_2-h exhibited good light absorption in the ultraviolet region (<400 nm) and limited light absorption in the visible region (>400 nm). After Pd loadings, the absorption edge of the sample Pd_1/TiO_2-h presented an absorption tail till ~600 nm. Based on UV-Vis DRS and Tauc plots, the main bandgap of Pd_1/TiO_2-h was the same as that of TiO_2-h (3.22 eV). Furthermore, the adsorption of 2-aminopyrimidine onto the surface of TiO_2-h extended the

absorption spectrum of TiO_2-h to the visible-light region (~420 nm, Supplementary Fig. 8D). It originated from the surface complexation between heteroatom-containing substrates (e.g., O, N, or S) and TiO_2[5]. Specifically, the surface complex via weak coordination could create new electron donor levels above the valence band of TiO_2 from the 2p orbital of N, resulting in weak visible light absorbance. A similar phenomenon was observed as well in Pd_1/TiO_2-h (Supplementary Fig. 8E).

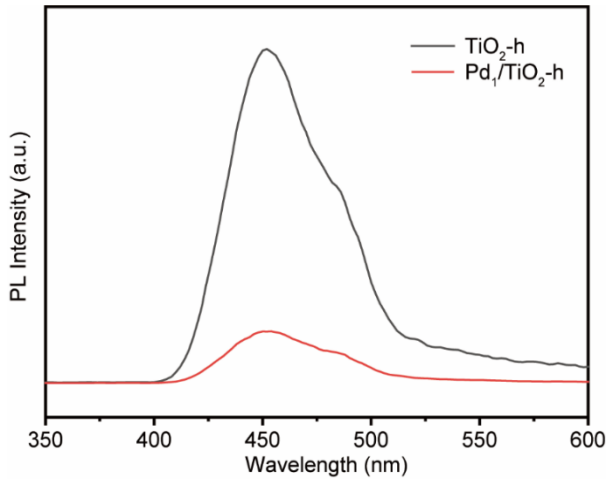

Supplementary Figure 9. PL spectra of TiO_2-h and Pd_1/TiO_2-h.

As shown in Supplementary Fig. 9, TiO_2-h and Pd_1/TiO_2-h samples exhibited a broad peak at 450 nm in PL spectra, which can be attributed to the irradiative recombination of electrons and holes from the conduction band (CB) and valence band (VB), respectively. The Pd_1/TiO_2-h sample showed a lower peak intensity than pristine TiO_2-h, indicating the suppressed charge recombination because of the electron reservoir ability from loaded Pd species. Thus, more photogenerated charges could be available on the surface of the Pd_1/TiO_2-h photocatalyst.

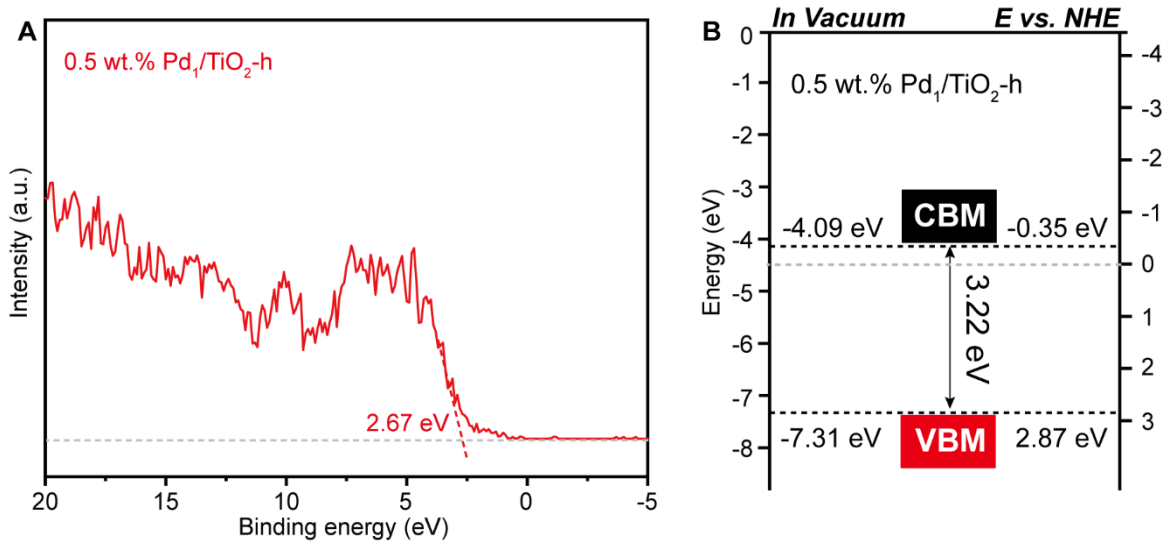

Supplementary Figure 10. (A) Valence band spectrum from XPS of 0.5 wt.% Pd_1/TiO_2-h. (B) Estimated conduction band minimum (CBM) and valance band maximum (VBM) of 0.5 wt.% Pd_1/TiO_2-h.

Considering UV-Vis DRS and Tauc plots in Supplementary Fig. 8, the bandgap of Pd_1/TiO_2-h was 3.22 eV. According to the valence band spectrum from XPS, the E_{VBM} value of Pd_1/TiO_2-h was 2.67 eV. Based on calculation equation (1), the E_{VBM} and E_{CBM} (*vs.* NHE, pH = 7) of Pd_1/TiO_2-h was calculated to be 2.87 V and -0.35 eV, respectively.

Specifically, the valance band maximum (VBM) position was calculated as follows:

E_{VB} (NHE)= E_{VBM} + Work function (Φ) - 4.44 equation (1)

E_{VB}: Valence band position

E_{VBM}: Valence band maximum (From XPS)

Φ: Work function of the sample (4.64 eV for anatase TiO_2[6])

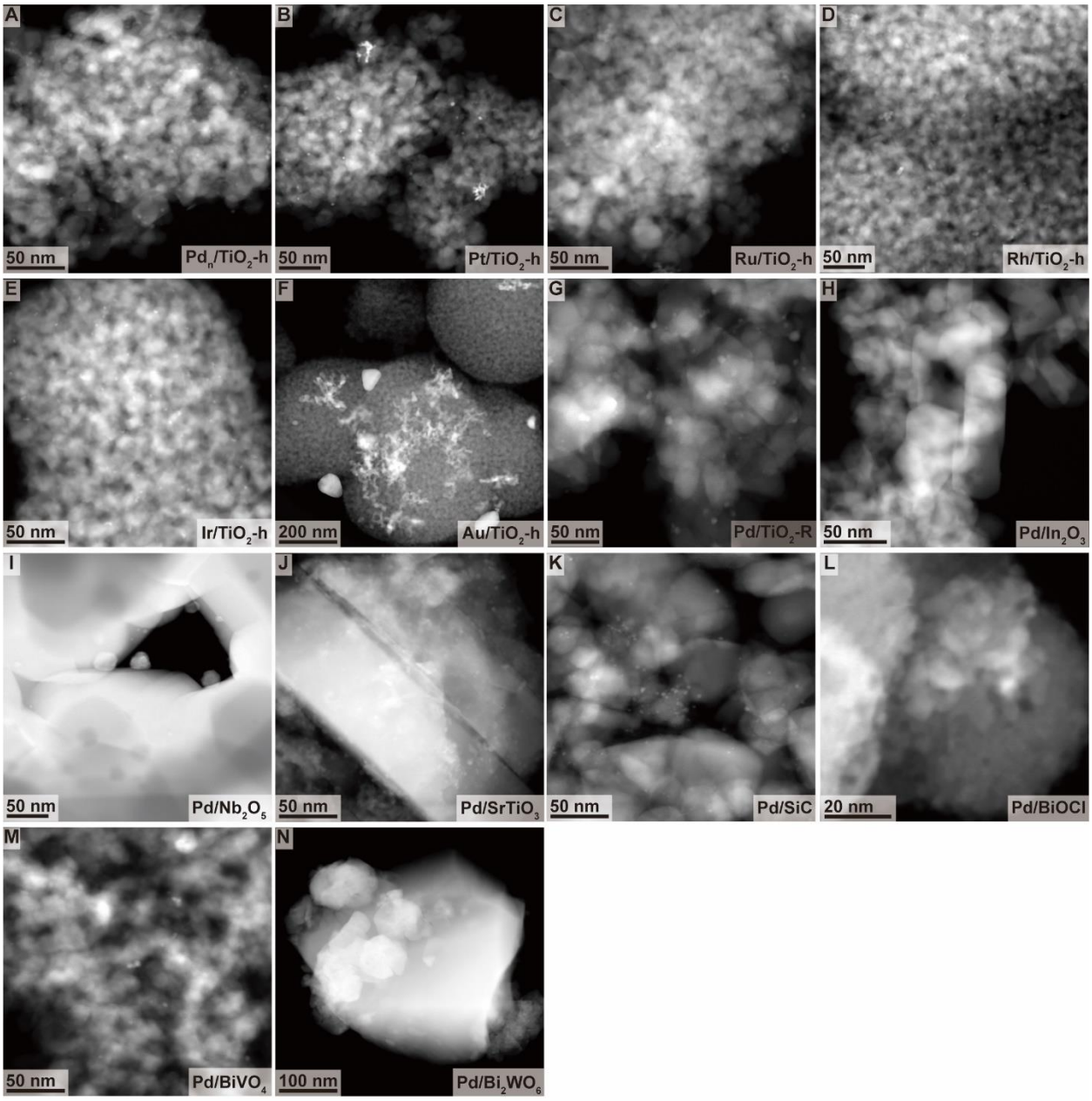

Supplementary Figure 11. TEM dark-field images of different photocatalysts. (A) Pd_n/TiO_2-h; (B) Pt/TiO_2-h; (C) Ru/TiO_2-h; (D) Rh/TiO_2-h; (E) Ir/TiO_2-h; (F) Au/TiO_2-h; (G) Pd/TiO_2-R; (H) Pd/In_2O_3; (I) Pd/Nb_2O_5; (J) $Pd/SrTiO_3$; (K) Pd/SiC; (L) Pd/BiOCl; (M) $Pd/BiVO_4$; (N) Pd/Bi_2WO_6.

Based on the above TEM analysis in Supplementary Fig. 11, all noble metals were deposited on supports in the form of nanoparticles. Specifically, the particles size of Pd in Pd_n/TiO_2-h was about 1-5 nm; the particles size of Pt in Pt/TiO_2-h was about 5-10 nm; the particles size of Ru in Ru/TiO_2-h was about 1-5 nm; the particles size of Rh in Rh/TiO_2-h was about 5-10 nm; the

particles size of Ir in Ir/TiO_2-h was about 1-5 nm; the particles size of Au in Au/TiO_2-h was about 20-100 nm; the particles size of Pd in Pd/TiO_2-R was about 2-10 nm; the particles size of Pd in Pd/In_2O_3 was about 10-40 nm; the particles size of Pd in Pd/Nb_2O_5 was about 10-25 nm; the particles size of Pd in Pd/$SrTiO_3$ was about 1-5 nm; the particles size of Pd in Pd/SiC was about 1-5 nm; the particles size of Pd in Pd/BiOCl was about 5-10 nm; the particles size of Pd in Pd/$BiVO_4$ was about 5-20 nm; the particles size of Pd in Pd/Bi_2WO_6 was about 100-200 nm. For the samples in which the Pd species could not be clearly observed, the characterizations of STEM-EDS elemental mapping were conducted to identify the loading state of Pd species (as shown in Supplementary Fig. 12).

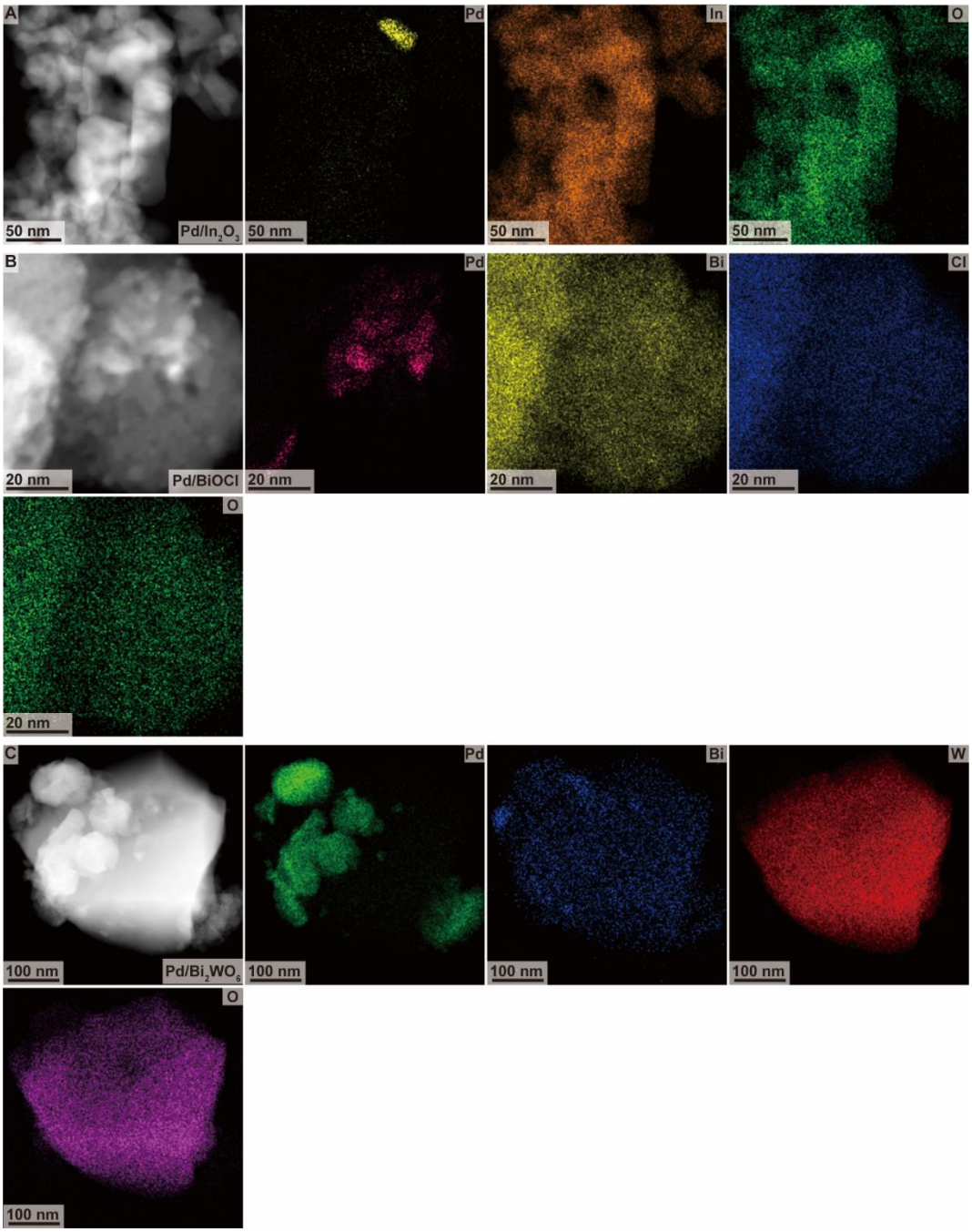

Supplementary Figure 12. STEM-EDS elemental mapping of unclear samples. (A) Pd/In_2O_3; (B) Pd/BiOCl; (C) Pd/Bi_2WO_6.

Based on STEM-EDS analysis in Supplementary Fig. 12, the size of the Pd particles in Pd/In_2O_3 was about 10-40 nm. The size of the Pd particles in Pd/BiOCl was about 5-10 nm. The size of the Pd particles in Pd/Bi_2WO_6 was about 100-200 nm.

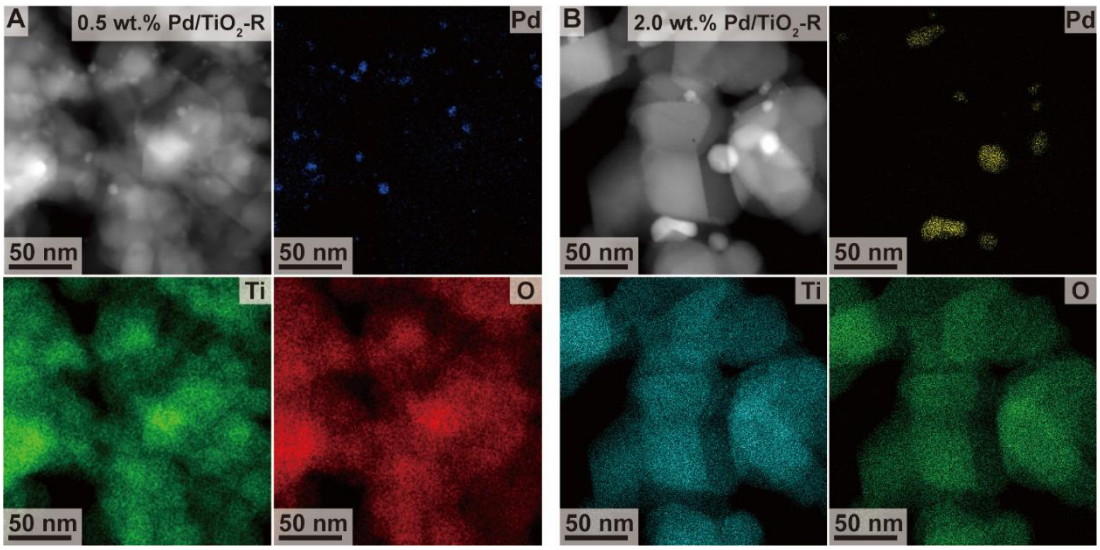

Supplementary Figure 13. STEM-EDS elemental mapping of Pd/TiO_2-R with different Pd loading amounts. (A) 0.5 wt.% Pd/TiO_2-R; (B) 2.0 wt.% Pd/TiO_2-R.

Based on STEM-EDS analysis, Pd species were attached to TiO_2-R in the form of nanoparticles, even for the low Pd loading of 0.5 wt.%. The size of Pd particles in 0.5 wt.% Pd/TiO_2-R was about 1-10 nm, while this particle size was increased to 10-50 nm when loading reached 2.0 wt.%. Notably, Pd nanoparticles dominated on rutile crystals, while Pd ions prevailed on our TiO_2-h with anatase as the main crystal phase.

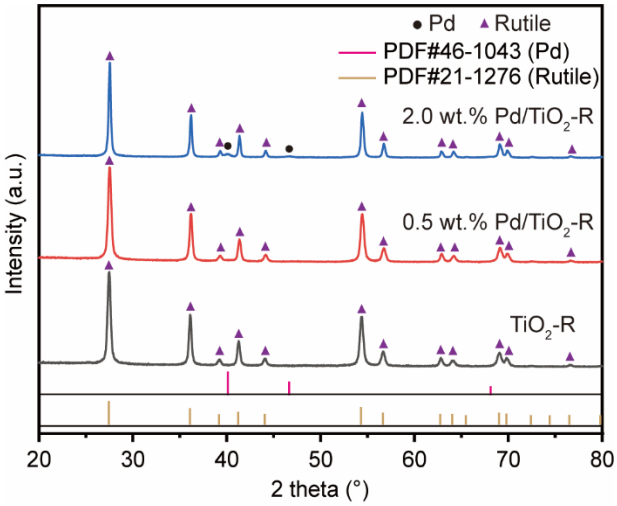

Supplementary Figure 14. XRD patterns of Pd_1/TiO_2-R samples with different Pd loadings. The standard JCPDS cards of rutile (PDF#21-1276) TiO_2 and Pd (PDF#46-1043) were incorporated for comparison.

The rutile-based sample 2.0 wt.% Pd/TiO_2-R showed the diffraction peaks of Pd metal. This also well agreed with the appearance of Pd nanoparticles in 2.0 wt.% Pd/TiO_2-R sample (Supplementary Fig. 13B).

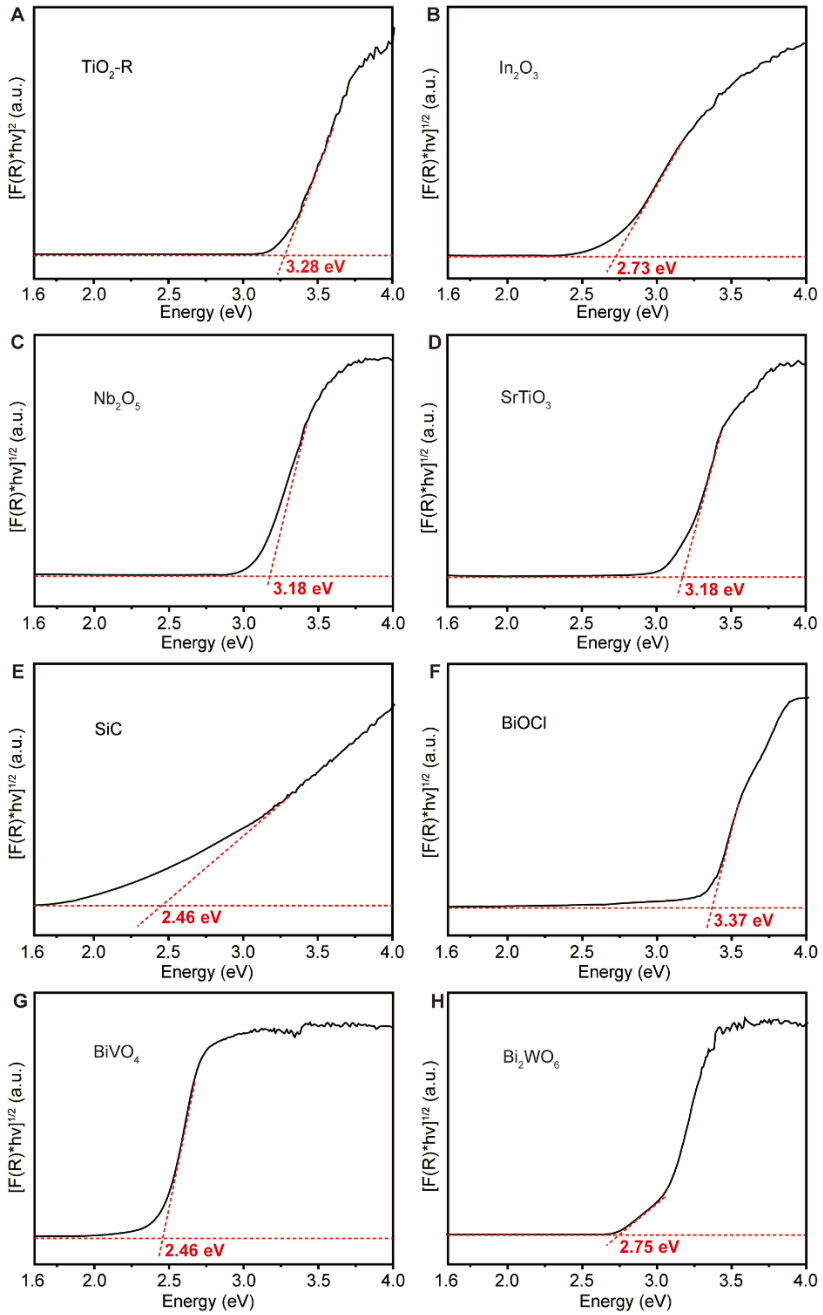

Supplementary Figure 15. The optical absorption analysis of various semiconductors. (A) TiO_2-R. (B) In_2O_3. (C) Nb_2O_5. (D) $SrTiO_3$. (E) SiC. (F) BiOCl. (G) $BiVO_4$. (H) Bi_2WO_6.

Based on Tauc plots (Supplementary Fig. 15), the bandgaps of TiO_2-R, In_2O_3, Nb_2O_5, $SrTiO_3$, SiC, BiOCl, $BiVO_4$, and Bi_2WO_6 were estimated to be 3.28, 2.73, 3.18, 3.18, 2.46, 3.37, 2.46, and 2.75 eV, respectively.

4. General procedure for the photocatalytic HIE reactions

In a 7 mL glass vial fitted with a magnetic stirring bar, Pd_1/TiO_2-h (50 mg) and substrate (0.1 mmol) were added. After adding the solvent D_2O (2.0 mL), the vial was placed into a 20 mL stainless-steel autoclave with a quartz window. The autoclave was purged with Ar at 10 bar and then degassed to the ambient pressure (1 bar). It was repeated for 6 times to remove O_2 maximally. Next, it was seated into an aluminum cooling jacket with water circulating from the chiller to keep the room temperature (25 ^{o}C). Later, the monochromatic LED lamp (light wavelength of 365 nm, 410 nm, 450 nm, 500 nm, 530 nm, or 600 nm) was placed on top of the autoclave and irradiated the suspension through the quartz window for 24 h. After the photocatalytic HIE reaction, the suspension was transferred from the autoclave to a centrifuge tube, and then centrifuged to obtain the supernatant. The deuterium incorporation (D incorporation) and selectivity of products can be obtained by ^{1}H NMR analysis of the supernatant (see below for calculation equations). For the product isolation, after the removal of all D_2O in vacuo, the desired products were obtained.

$$\text{D incorporation (\%)} = \left(1 - \frac{\text{Residual integral}}{\text{Integral of unlabeled C-H site}}\right) * 100\%$$

$$\text{Selectivity (\%)} = \left(\frac{\text{The molar number of substrates participating in the deuteration reaction}}{\text{The molar number of reacted substrates}}\right) * 100\%$$

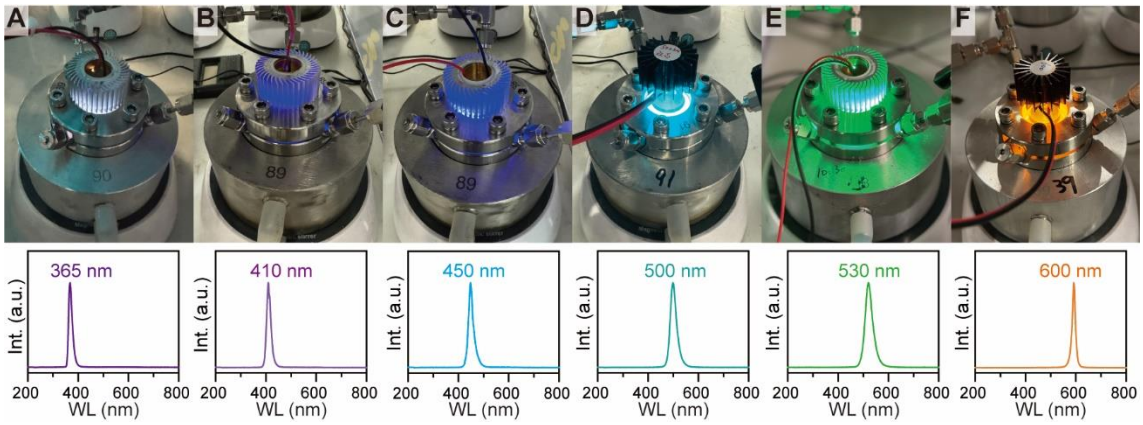

Supplementary Figure 16. Images of the homemade batch-mode photocatalytic reactors under LED light irradiation with different wavelengths. (A) 365 nm; (B) 410 nm; (C) 450 nm; (D) 500 nm; (E) 530 nm; (F) 600 nm.

5. Photocatalytic properties of Pd_1/TiO_2-h in HIE

Initially, we employed 2-aminopyrimidine as a model substrate to investigate photocatalytic HIE over Pd_1/TiO_2-h. After a series of optimization experiments, the deuterated product was obtained in high D incorporation (99%) by using 0.5 wt.% Pd_1/TiO_2-h as the photocatalyst, D_2O as the solvent, irradiated with 410 nm LED under Ar atmosphere at room temperature for 24 h. The control tests (no photocatalyst, no light, no Pd deposition, in air, or heating in dark) showed the HIE of *N*-heteroarenes could not occur in the absence of light and SA photocatalysts. Even external heating (120 °C) failed to realize HIE reactions without light irradiation.

Supplementary Table S2. The photocatalytic performance of Pd_1/TiO_2-h for the H/D exchange reaction of 2-aminopyrimidine in D_2O.

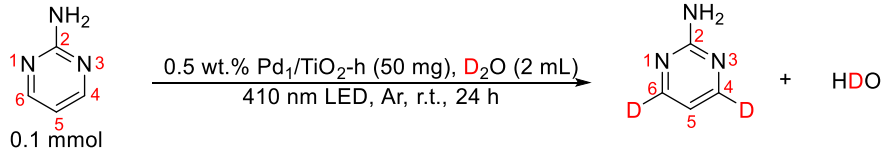

Entry	Variation from the standard conditions[a]	D incorporation (%)[b]
1	None (standard condition)	**99**
2	No photocatalyst	0
3	No light	0
4	No palladium co-catalyst	0
5	Air	0
6	In dark, 120 °C instead of r.t.	0

[a]Standard conditions: 2-aminopyrimidine (0.1 mmol), 0.5 wt.% Pd_1/TiO_2-h (50 mg), D_2O (2.0 mL), 410 nm LED (95 mW/cm^2), Ar (1 bar), r.t., 24 h; [b]D incorporation determined by quantitative ^{1}H NMR: decrease of the signal corresponding to the aromatic protons, using the pyrimidine 5-site proton signals as internal calibration.

The concentration of HDO after reactions was determined by quantitative ^{1}H NMR. Firstly, we performed the ^{1}H NMR analysis of D_2O without 2-aminopyrimidine after 24 h light irradiation as the blank test, using 1,4-dioxane as internal calibration. Then, we obtained the ^{1}H NMR spectra of the reaction solution after HIE under standard conditions with 1,4-dioxane for internal calibration. In principle, when 0.1 mmol of 2-aminopyrimidine was deuterated with the D incorporation of 99%, 0.4 mmol HDO would be generated. From the NMR results, we calculated the actual molar number of increased HDO to be 0.34 mmol, which was a little lower than the theoretical value. This may be due to HDO partially adsorbed by the photocatalyst during HIE reactions and characterization errors of ^{1}H NMR.

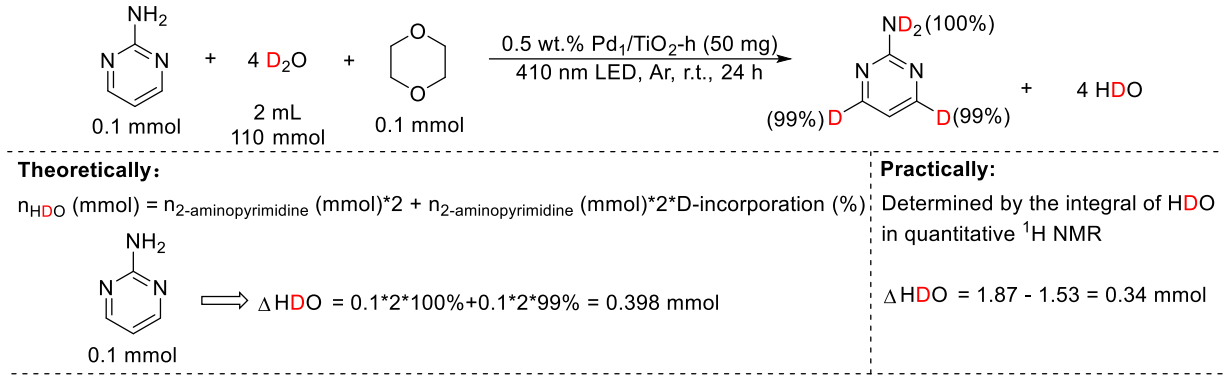

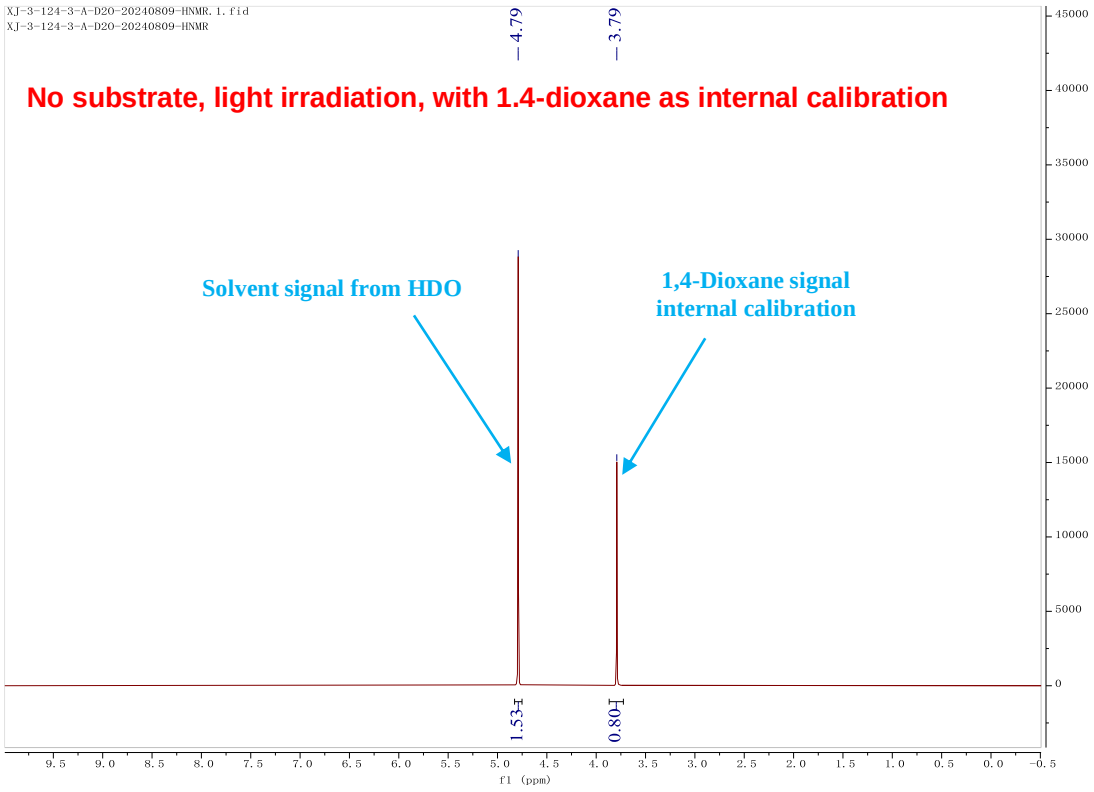

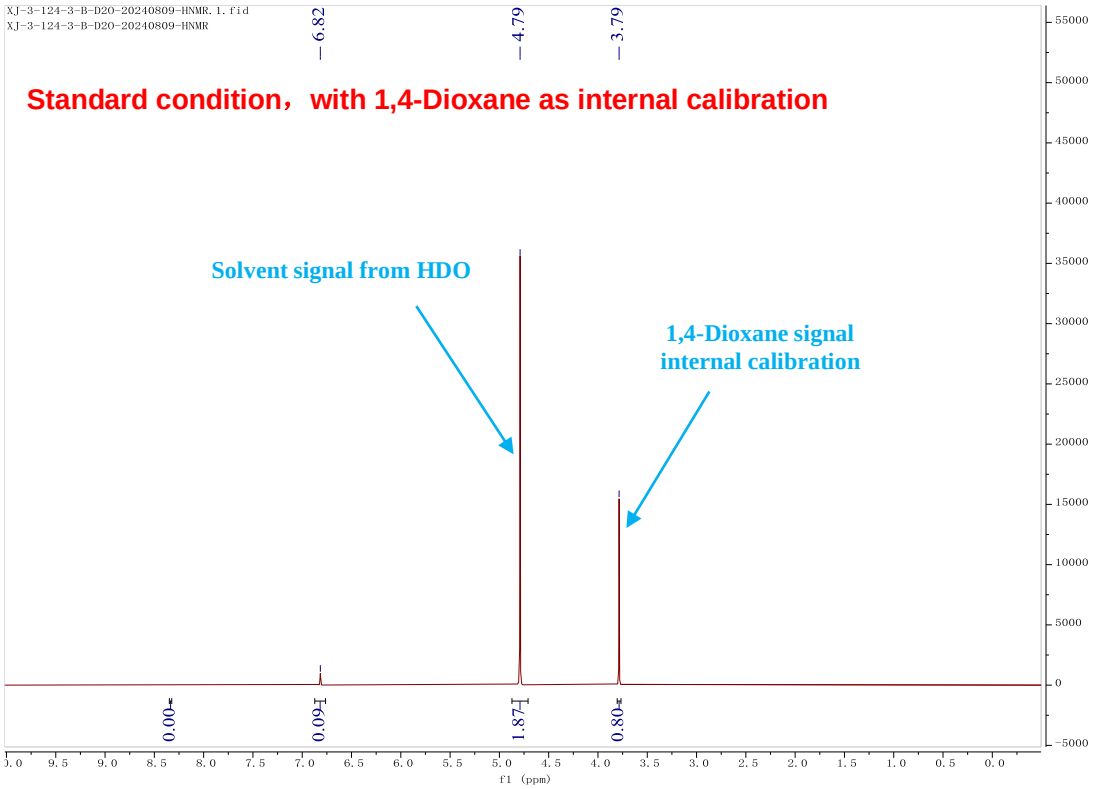

^{2}H NMR (600 MHz, $CDCl_3$) of the product:

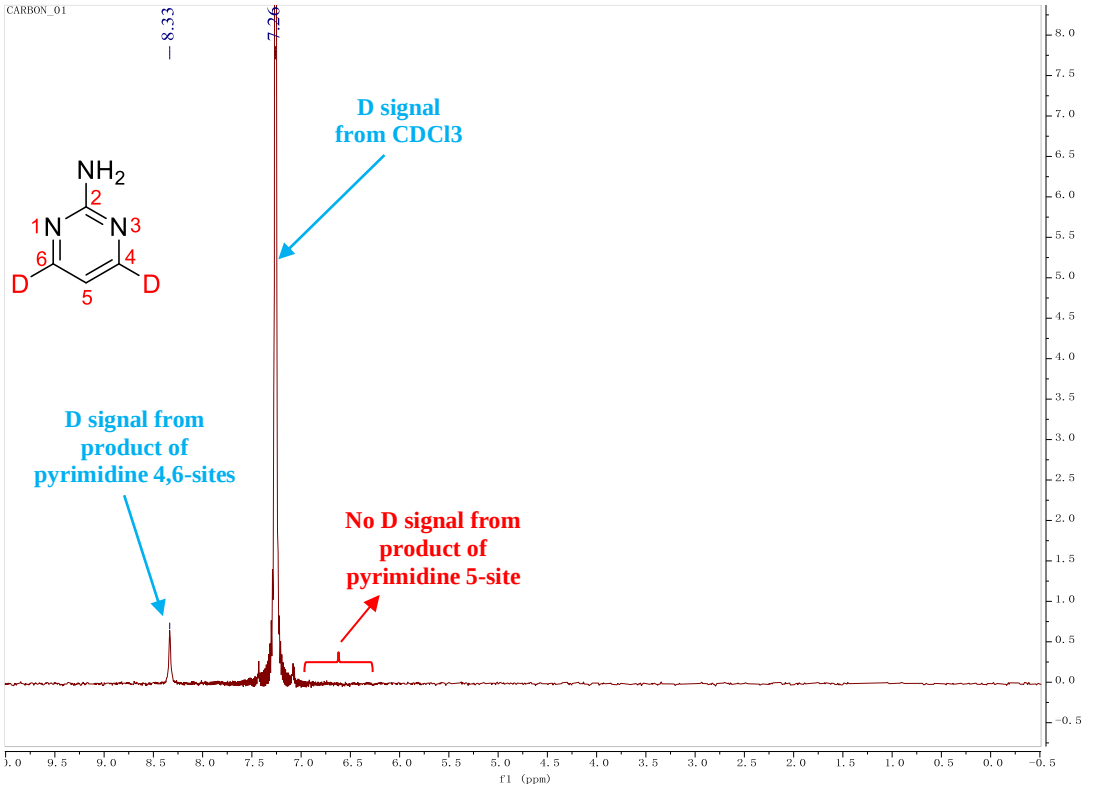

^{2}H NMR spectra of the product indicated only C−H bonds at pyrimidine 4,6-sites were deuterated.

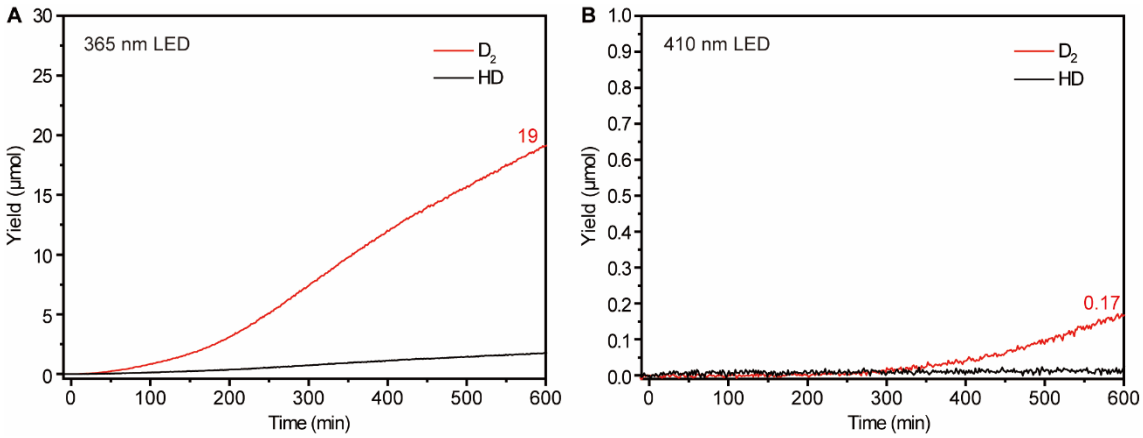

Supplementary Figure 17. Yield of D_2 and HD under LED light irradiation with different wavelengths. (A) 365 nm LED; (B) 410 nm LED.

In-situ MS showed 19 μmol D_2 was evolved in the photoreactor under 365 nm LED irradiation for 10 h. This D_2 amount is 112 times higher than the case under 410 nm LED irradiation, in which 0.17 μmol D_2 was produced. Therefore, we reasoned that D_2 may poison the SA photocatalyst by occupying active sites.

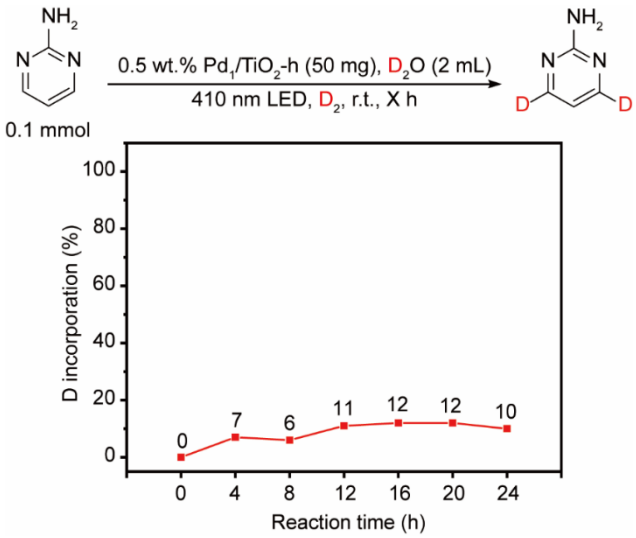

Supplementary Figure 18. Time-dependent photocatalytic HIE of 2-aminopyrimidine in the presence of D_2 over 0.5 wt.% Pd_1/TiO_2-h under 410 nm irradiation. Reaction conditions: 2-aminopyrimidine (0.1 mmol), photocatalyst (50 mg), D_2O (2.0 mL), 410 nm LED (95 mW/cm^2), D_2 (1 bar), r.t., 0-24 h.

After changing the inert reaction atmosphere (Ar) to D_2 gas, poor photocatalytic deuteration (around 10% D incorporation) was observed after 24 h irradiation, indicating that D_2 had a pronounced negative effect on the reaction. It could be the reason that D_2 poisoned the photocatalyst Pd_1/TiO_2-h by occupying its active sites of SA Pd species.

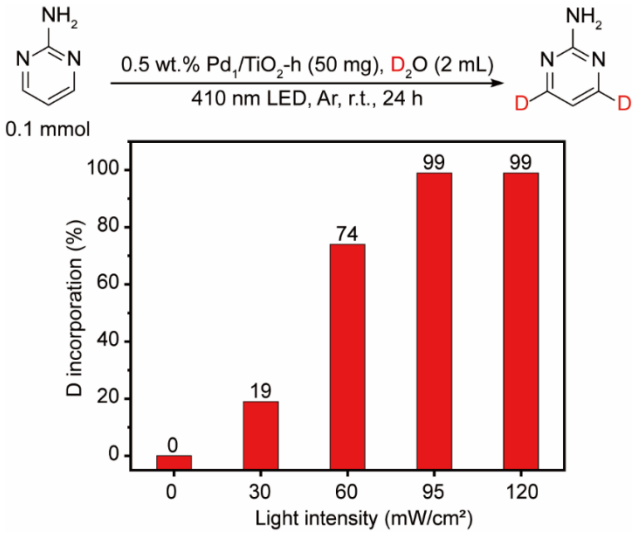

Supplementary Figure 19. Photocatalytic deuterium incorporation of 2-aminopyrimidine in D_2O over 0.5 wt.% Pd_1/TiO_2-h under 410 nm irradiation with different light intensity. Reaction conditions: 2-aminopyrimidine (0.1 mmol), photocatalyst (50 mg), D_2O (2.0 mL), 410 nm LED (0-120 mW/cm^2), Ar (1 bar), r.t., 24 h.

Under the light irradiation from 410 nm LED, the D incorporation gradually increased (from 0 to 99%) with the light intensity from 0 to 95 mW/cm^2. Higher light intensity of 120 mW/cm2 resulted in 99% D incorporation as well, which indicated the light saturation under this circumstance. Thus, we chose 95 mW/cm^2 as the optimal light intensity.

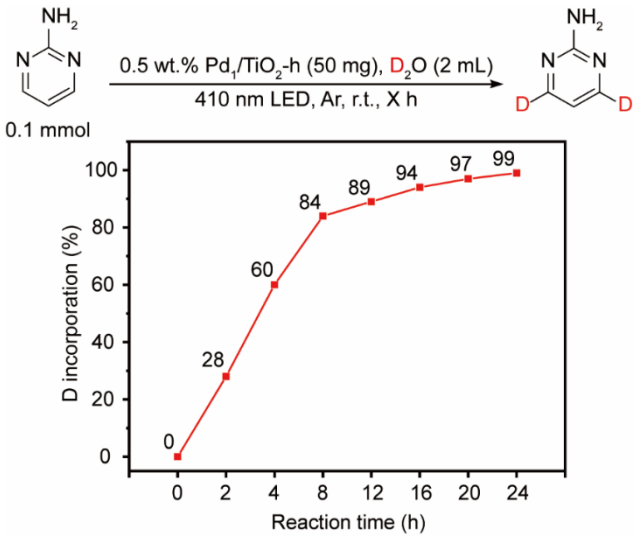

Supplementary Figure 20. Photocatalytic deuterium incorporation of 2-aminopyrimidine in D_2O over 0.5 wt.% Pd_1/TiO_2-h under 410 nm irradiation with different reaction time. Reaction conditions: 2-aminopyrimidine (0.1 mmol), photocatalyst (50 mg), D_2O (2.0 mL), 410 nm LED (95 mW/cm^2), Ar (1 bar), r.t., 0-24 h.

The deuterium incorporation showed a growth trend with the reaction time. Within 0-8 hours, the deuterium incorporation increased rapidly, reaching 84%. Then, the deuteration rate slowed down from 8-24 h, because the collision chance between active sites of photocatalysts and unreacted molecules dramatically decreased when most reactants were deuterated. The satisfactory deuteration (99% D incorporation) was realized after 24 h irradiation. Thus, we chose 24 h as the optimal reaction time.

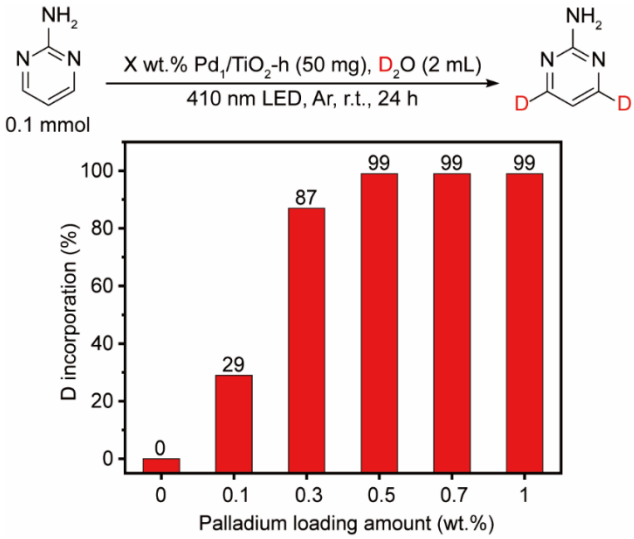

Supplementary Figure 21. Photocatalytic deuterium incorporation of 2-aminopyrimidine in D_2O under 410 nm irradiation over photocatalyst Pd_1/TiO_2-h with different Pd loading amounts. Reaction conditions: 2-aminopyrimidine (0.1 mmol), photocatalyst (50 mg), D_2O (2.0 mL), 410 nm LED (95 mW/cm^2), Ar (1 bar), r.t., 24 h.

With the increase of Pd loadings from 0 to 0.5 wt.%, the D incorporation showed a growth trend, reaching 99% for 0.5 wt.% Pd_1/TiO_2-h. The further increase of Pd loading (0.7 and 1 wt.%) presented 99% D incorporation as well. It implied that the active sites of Pd_1/TiO_2-h with Pd loading ranging from 0.5 to 1 wt.% were saturated for HIE reactions in this circumstance. Considering the cost of Pd metal, we chose the Pd loading amount of 0.5 wt.% for the following studies.

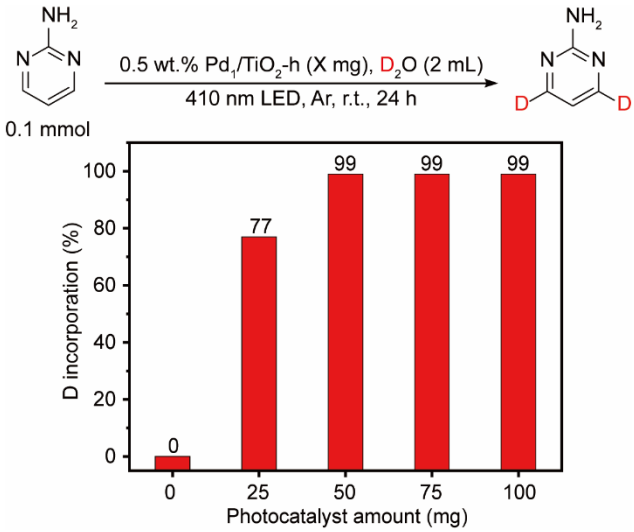

Supplementary Figure 22. Optimization of photocatalyst amount. Reaction conditions: 2-aminopyrimidine (0.1 mmol), 0.5 wt.% Pd_1/TiO_2-h (0-100 mg), D_2O (2.0 mL), 410 nm LED (95 mW/cm^2), Ar (1 bar), r.t., 24 h.

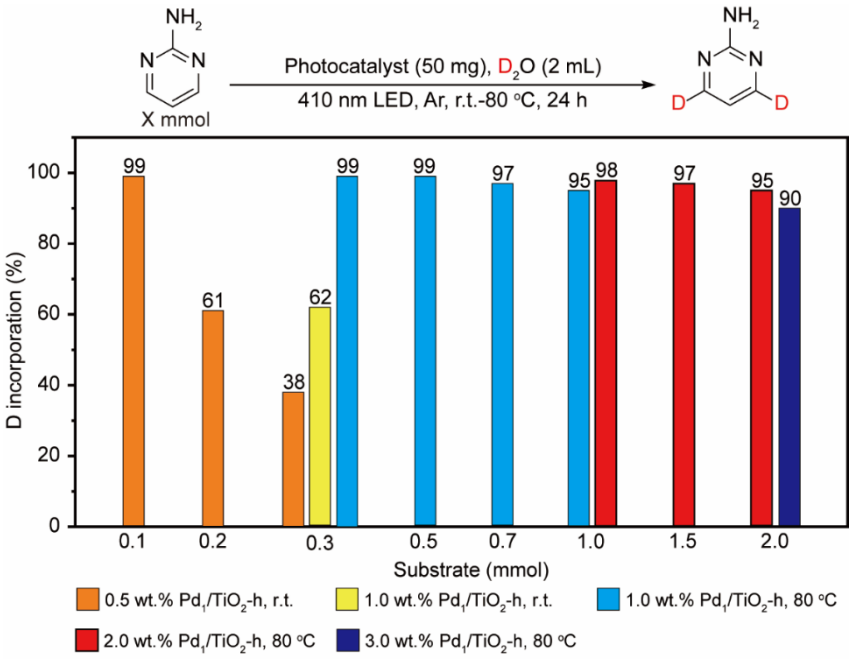

Supplementary Figure 23. Photocatalytic deuterium incorporation of 2-aminopyrimidine in D_2O over different substrate concentrations. Reaction conditions: 2-aminopyrimidine (0.1-2.0 mmol), photocatalyst (50 mg), D_2O (2.0 mL), 410 nm LED (95 mW/cm^2), Ar (1 bar), r.t.-80 °C, 24 h.

When the substrate amount was increased from 0.1 to 0.3 mmol, the deuteration performance became poor with D incorporation decreased from 99% to 38%. When conditions were strengthened, a higher temperature of 80 °C and Pd_1/TiO_2-h with a Pd loading of 1.0 wt.% could realize decent D incorporation (95%-99%) for the cases of 0.3-1.0 mmol substrates. When the substrate amount was increased to 2.0 mmol, excellent deuteration (95% D incorporation) could be achieved by use of 2.0 wt.% Pd_1/TiO_2-h. Besides, when the Pd loading rose to 3.0 wt.%, the D incorporation decreased to 90% instead. It may be ascribed to the phenomenon that photocatalyst Pd_1/TiO_2-h with high Pd loadings presented more Pd clusters or nanoparticles, which were inactive for photocatalytic HIE of *N*-heteroarenes.

Supplementary Table S3. Pd loading amounts of photocatalysts based on ICP-mass analysis.

Photocatalyst	Pd loading amount （wt.%）
0.5 wt.% Pd_1/TiO_2-h (Fresh)	0.49
0.5 wt.% Pd_1/TiO_2-h (5^{th} used)	0.45

After the photocatalyst was reused for five cycles, the amount of Pd loading presented a slight drop from 0.49 to 0.45 wt.%. It may come from the long-time stirring of the photocatalyst in D_2O (around 120 h).

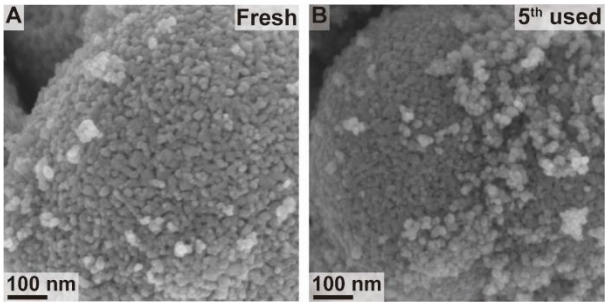

Supplementary Figure 24. SEM images of (A) fresh 0.5 wt.% Pd_1/TiO_2-h and (B) the used photocatalyst after 5 rounds of recycling tests.

The SEM images showed that the particle size and morphology of the photocatalyst Pd_1/TiO_2-h had no significant change after 5 rounds of recycling tests.

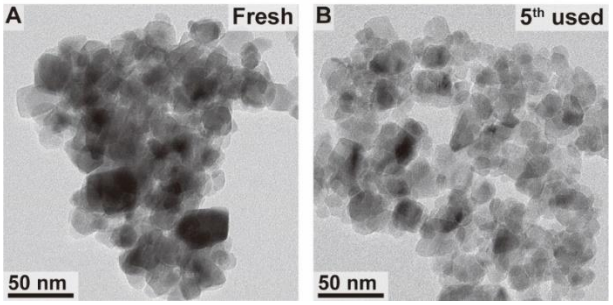

Supplementary Figure 25. TEM images of (A) fresh 0.5 wt.% Pd_1/TiO_2-h and (B) the used photocatalyst after 5 rounds of recycling tests.

The TEM images showed that the particle size and morphology of the photocatalyst Pd_1/TiO_2-h had no significant change after 5 rounds of recycling tests as well. Additionally, we did not observe any Pd nanoparticles.

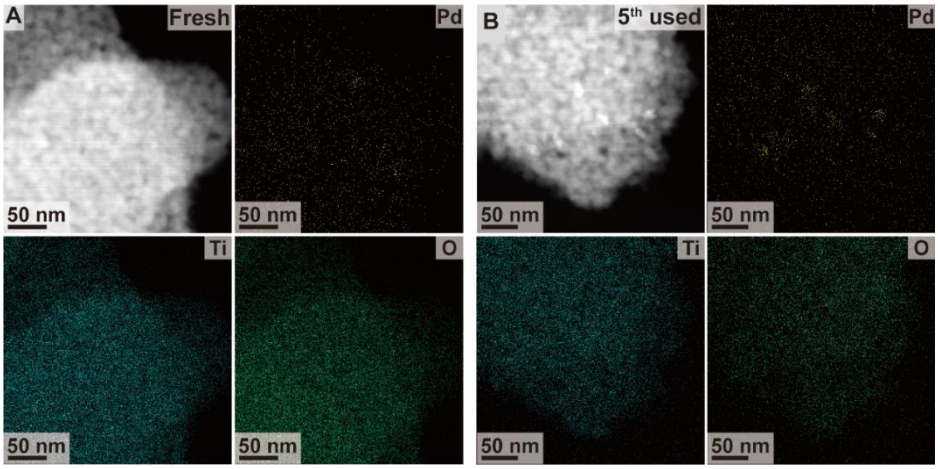

Supplementary Figure 26. STEM-EDS elemental mapping of (A) fresh 0.5 wt.% Pd_1/TiO_2-h and (B) the used photocatalyst after 5 rounds of recycling tests.

The STEM-EDS elemental mapping showed that the distribution of elements Pd, Ti, and O in the photocatalyst Pd_1/TiO_2-h was similar to that of the fresh sample. The main Pd species in the 5^{th} used photocatalyst still presented as SA sites, even though a tiny amount of aggregated Pd clusters or nanoparticles appeared. It makes sense that minor SA Pd sites were mobile and aggregated to form clusters or nanoparticles after 5-round recycling tests.

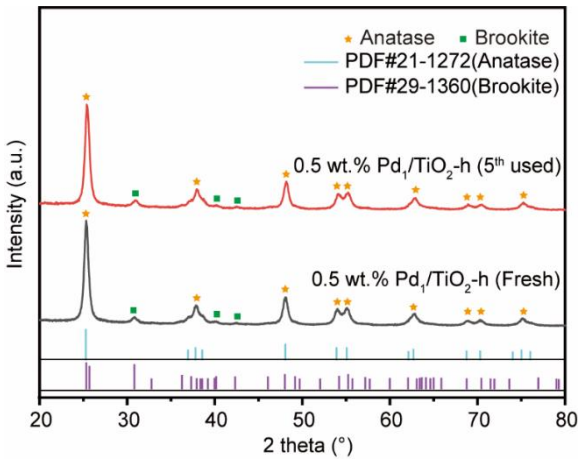

Supplementary Figure 27. XRD patterns of fresh 0.5 wt.% Pd_1/TiO_2-h and the used photocatalyst after 5 rounds of recycling tests. The standard JCPDS cards of anatase (PDF#21-1272) and brookite (PDF#29-1360) TiO_2 were incorporated for comparison.

The XRD pattern of the 5th used photocatalyst was the same as that of the fresh sample. Moreover, no peaks attributed to Pd nanoparticles were detected.

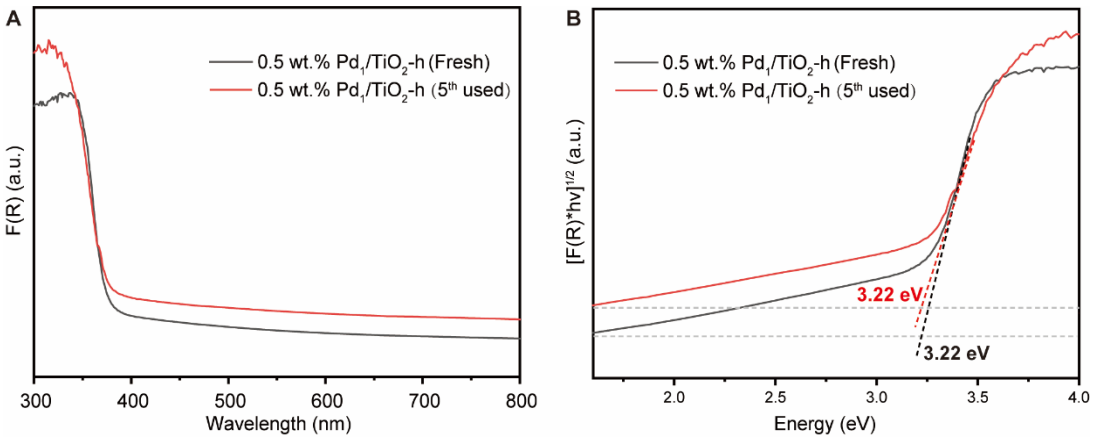

Supplementary Figure 28. (A) UV-Vis DRS and (B) Tauc plots of fresh 0.5 wt.% Pd_1/TiO_2-h and the used photocatalyst after 5 rounds of recycling tests.

The optical absorption capability of the 5th used photocatalyst was similar to that of the fresh sample with the bandgap unchanged at 3.22 eV.

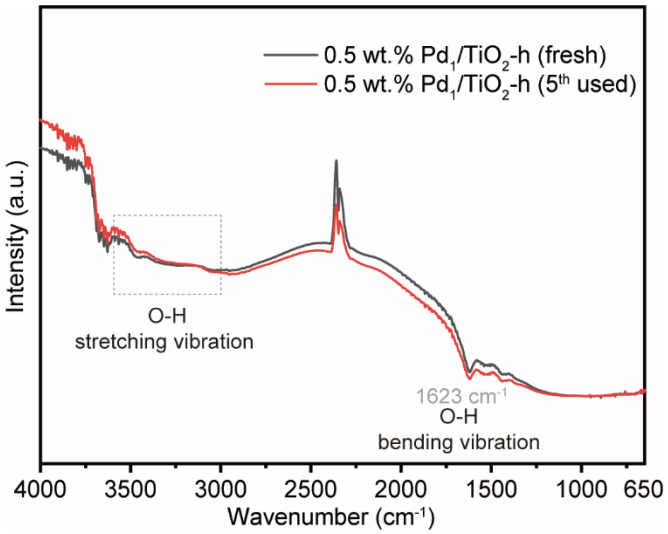

Supplementary Figure 29. DRIFT spectra of fresh 0.5 wt.% Pd_1/TiO_2-h and the used photocatalyst after 5 rounds of recycling tests.

The DRIFT spectrum of the 5th used photocatalyst was the same as that of the fresh sample. No IR absorption signals belonging to organic reactants/products were observed on the photocatalyst, indicating the clean surface after the HIE reaction.

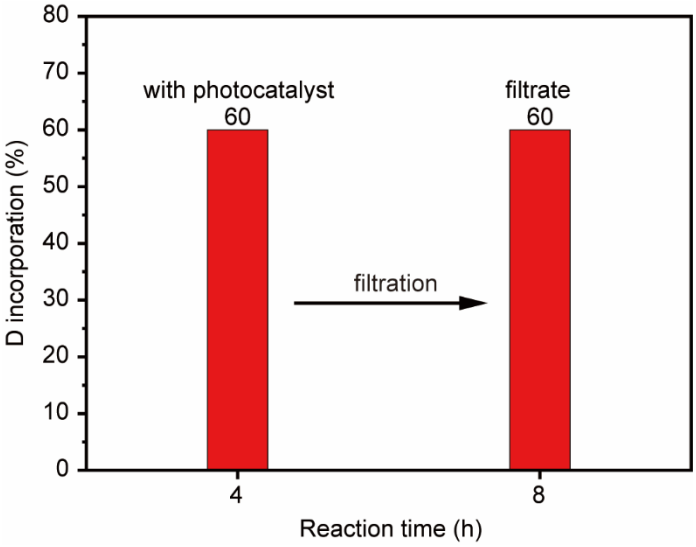

Supplementary Figure 30 The reaction results of the hot filtration test.

After 4 h light irradiation under standard reaction conditions, the SA photocatalyst was removed by filtration. The filtrate was irradiated for another 4 h. Since no increase in D-incorporation was observed, the soluble active species could be ruled out. It confirmed that the heterogenous SA photocatalyst drove the HIE of *N*-heteroarenes in D_2O.

6. Mechanistic studies

6.1. Kinetic isotope effect study

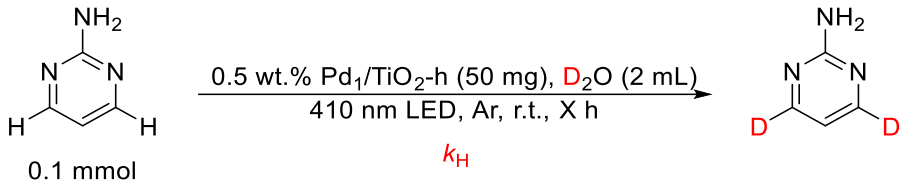

The reaction conditions involved 0.5 wt.% Pd_1/TiO_2-h (50 mg), 2-aminopyrimidine (9.5 mg, 0.1 mmol), D_2O (2 mL), 410 nm LED (95 mW/cm^2), Ar (1 bar), r.t., and 0-5 h irradiation. The time-dependent reaction performance was obtained by analyzing the solution after 0-5 h irradiation with ^{1}H NMR.

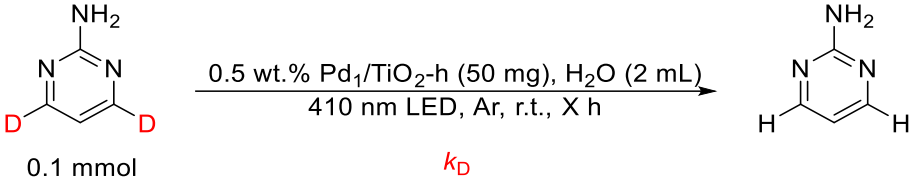

The reaction conditions involved 0.5 wt.% Pd_1/TiO_2-h (50 mg), 2-aminopyrimidine-4,6-d_2 (9.7 mg, 0.1 mmol), H_2O (2 mL), 410 nm LED (95 mW/cm^2), Ar (1 bar), r.t., and 0-5 h irradiation. The time-dependent reaction performance was obtained by analyzing the solution after 0-5 h irradiation with ^{1}H NMR. To eliminate the influence of H_2O in ^{1}H NMR tests, the solvent of H_2O was removed in vacuo for each sample, which was then measured in $CDCl_3$.

6.2. In-situ DRIFT

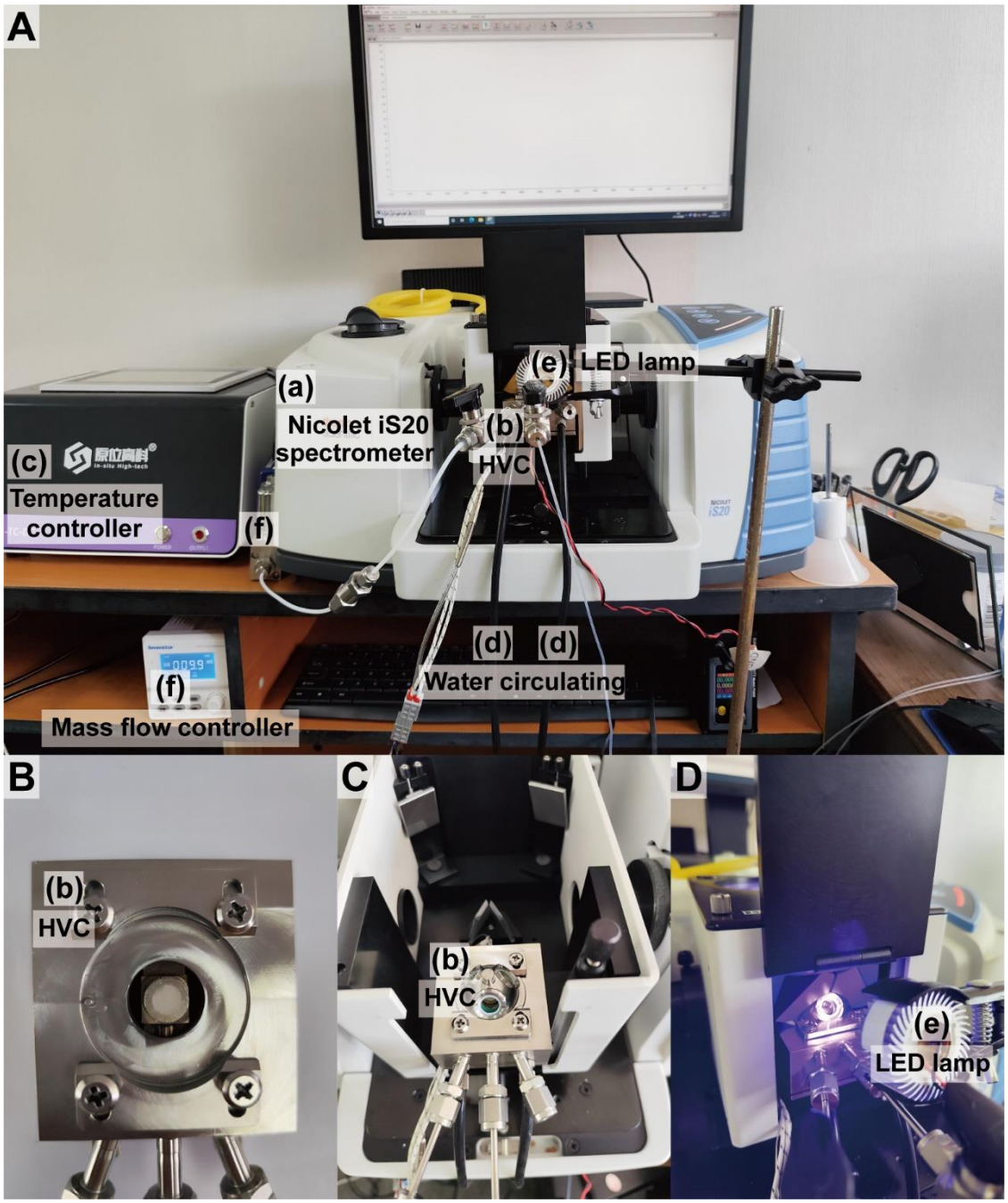

Supplementary Figure 31. Photographs of (A) *in-situ* DRIFT setup; (B) HVC loaded with fresh Pd_1/TiO_2-h powder sample; (C) Praying Mantis^{TM} HVC accessory enclosed with a three-window dome; (D) HVC with light irradiation from 410 nm LED.

6.3 CO adsorption

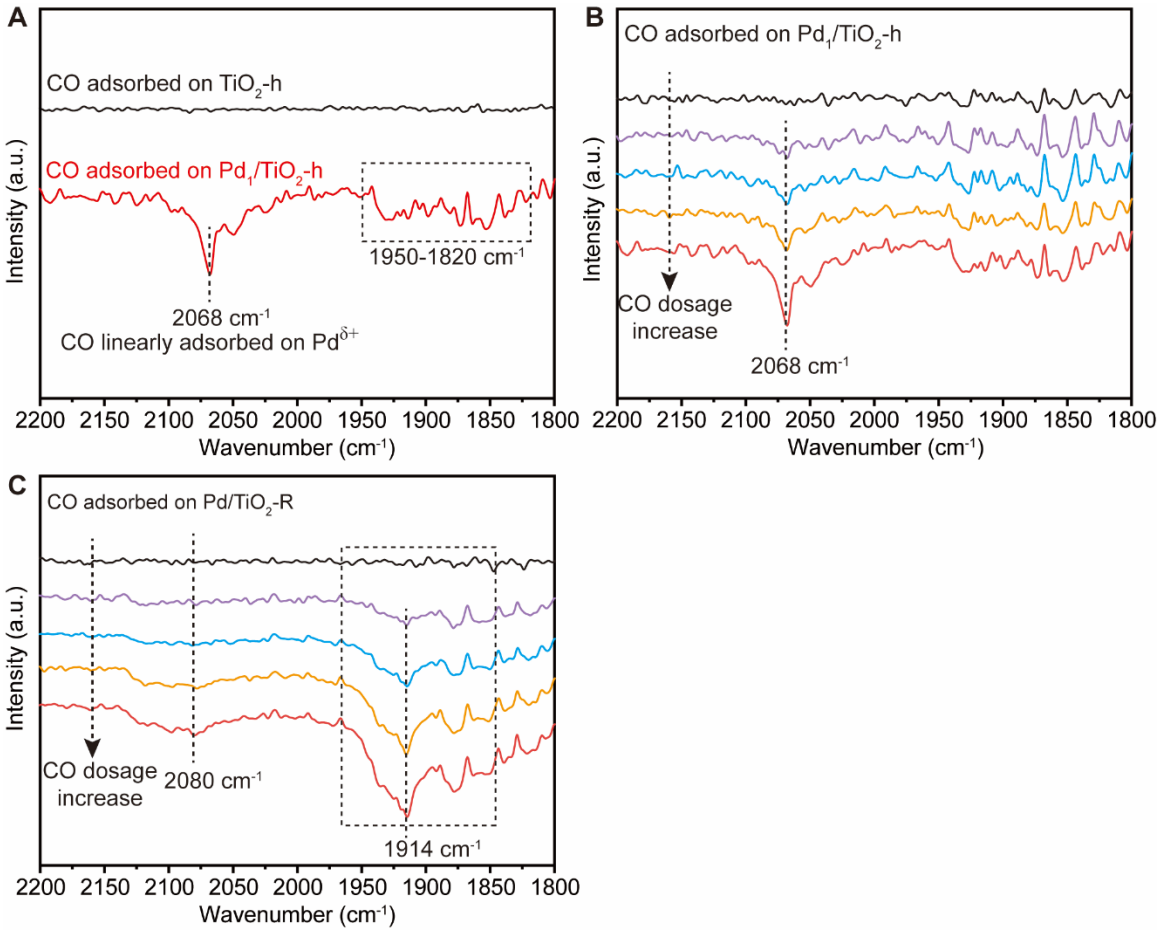

Supplementary Figure 32. (A) DRIFT spectra of CO adsorbed on TiO_2-h and 0.5 wt.% Pd_1/TiO_2-h. (B) DRIFT spectra of CO adsorbed on 0.5 wt.% Pd_1/TiO_2-h with CO dosage increase. (C) DRIFT spectra of CO adsorbed on 0.5 wt.% Pd/TiO_2-R with CO dosage increase.

The strong and main IR band at 2068 cm^{-1} was ascribed to CO linearly adsorbed on SA $Pd^{\delta+}$ sites in the case of Pd_1/TiO_2-h (Supplementary Figs. 32A and 32B). Besides, a weak and broad absorption band (from 1950-1820 cm^{-1}) could be observed as well, which was mainly ascribed to the bridged or multi-bonded CO on Pd^0 sites[7-9]. These spectra indicated that the majority of Pd species in the sample of Pd_1/TiO_2-h were the SA Pd sites with the co-existence of tiny Pd clusters or nanoparticles. In contrast, the IR band appearing around 1914 cm^{-1} dominated for the Pd/TiO_2-R sample, while the IR signal related to linear CO adsorption (~2080 cm^{-1}) was very weak (Supplementary Fig. 32C). Thus, the main Pd species in Pd/TiO_2-R could be Pd^0 clusters or nanoparticles, which agreed well with the TEM data in Supplementary Figs. 11 and 13.

6.4 *N*-methyl pyrrole (NMP) adsorption

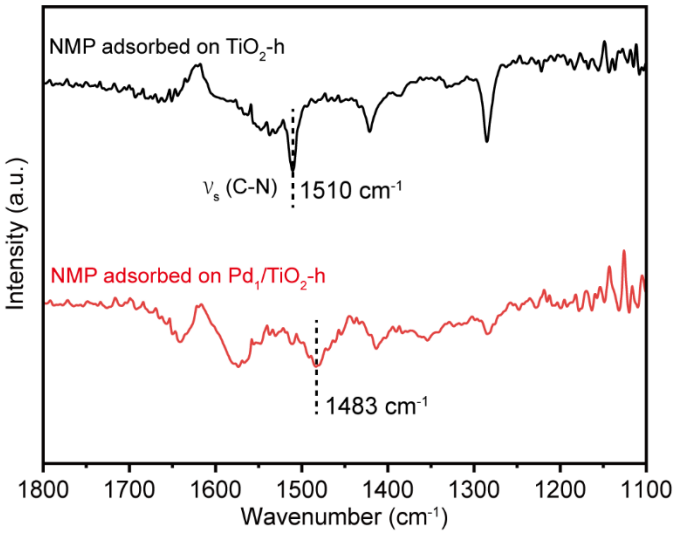

Supplementary Figure 33. DRIFT spectra of NMP adsorbed on TiO_2-h, Pd_1/TiO_2-h and Pd_n/TiO_2-h.

As shown in Supplementary Fig. 33, after loading with Pd, the SA $Pd^{\delta+}$ sites captured the reactant molecules (NMP) via the coordination between Pd and N atoms, which was evidenced by the red-shifted absorption band of C−N vibration in reactants (from 1510 to 1483 cm^{-1})[10].

6.5 *In-situ* DRIFTs analysis of photocatalysts for HIE reactions

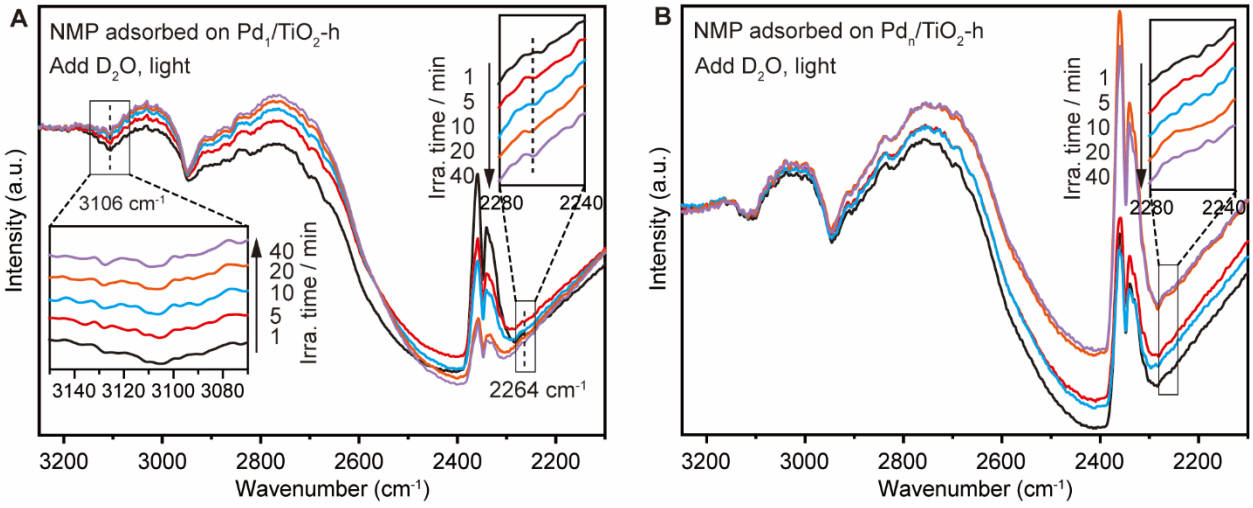

Supplementary Figure 34. (A) DRIFT spectra of *in-situ* photocatalytic H/D exchange reaction over Pd_1/TiO_2-h. (B) DRIFT spectra of in-situ photocatalytic H/D exchange reaction over Pd_n/TiO_2-h.

After D_2O was introduced to the cell of DRIFTs, the absorption band belonging to $C(sp^2)-H$ (at 3106 cm^{-1})[10] gradually weakened with irradiation time using Pd_1/TiO_2-h (Supplementary Fig. 34A). It could be ascribed to the H/D exchange step with D_2O, accompanied by the appearance of a new absorption peak at 2264 cm^{-1} assigned to C−D bonds from deuterated NMP. In contrast, the absorption band at 3106 cm^{-1} did not change with irradiation time in the case of Pd_n/TiO_2-h sample (Supplementary Fig. 34B), where no new peaks around 2264 cm^{-1} were observed as well.

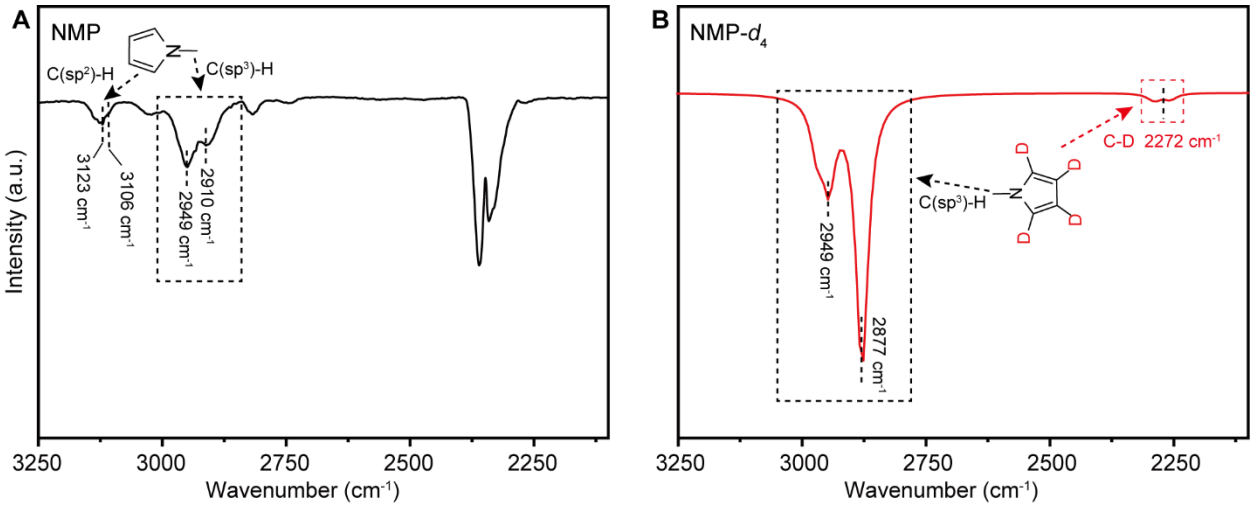

Supplementary Figure 35. (A) DRIFT spectra of NMP adsorbed on KBr. (B) Calculated IR spectra of NMP-d_4.

Supplementary Fig. 35A showed the IR spectrum of NMP on KBr, where absorption peaks at 3123 cm^{-1} and 3106 cm^{-1} were attributed to the symmetric stretching vibration of aromatic C(sp^2)−H bonds in NMP[10]. In addition, the absorption peaks at 2949 cm^{-1} and 2910 cm^{-1} were ascribed to the asymmetric stretching vibration of C(sp^3)−H bonds from the methyl group of NMP. To further determine the position of the C−D bond in IR, we carried out the infrared theoretical calculation of the product NMP-d_4. The calculation results in Supplementary Fig. 35B showed that the absorption position of the C−D bond was located at 2272 cm^{-1}. Accordingly, the absorption band at 2264 cm^{-1} from our *in-situ* DRFITs experiments could be assigned to the C−D bond.

Calculation Methods

All calculations were performed with Gaussian 16, Rev. C01[11]. Unless specified otherwise, geometry optimizations were computed with default convergence thresholds and without symmetry constraints using the M06-2X[12,13] density functional at 298 K. The 6-31+G(d)[14] basis set was employed on all atoms. Frequency analysis was performed at the same level of theory with the geometry optimization to confirm that the optimized structures are local minima, and to gain the molecular vibrational frequency. The correction factor used to obtain the exact fundamental frequency was set to 0.9400[15].

Coordinates

NMP

C	-0.17222300	-1.11578700	-0.01350400
C	-1.48870500	-0.71096700	0.01482900
C	-1.48879000	0.71086800	0.01463500
C	-0.17234100	1.11580400	-0.01337400
N	0.62217600	0.00004900	-0.03707400
H	0.26835900	-2.10324100	-0.02321000
H	-2.35138600	-1.36235000	0.02213100
H	-2.35153600	1.36216200	0.02177700
H	0.26815200	2.10329400	-0.02298400
C	2.06910400	-0.00001200	0.02528600
H	2.45310100	0.88938700	-0.47884300
H	2.42198300	-0.00522100	1.06154000
H	2.45382800	-0.88380600	-0.48812900

NMP-d_4

C	-0.17222300	-1.11578700	-0.01350400
C	-1.48870500	-0.71096700	0.01482900
C	-1.48879000	0.71086800	0.01463500
C	-0.17234100	1.11580400	-0.01337400
N	0.62217600	0.00004900	-0.03707400
H(Iso=2)	0.26835900	-2.10324100	-0.02321000
H(Iso=2)	-2.35138600	-1.36235000	0.02213100
H(Iso=2)	-2.35153600	1.36216200	0.02177700
H(Iso=2)	0.26815200	2.10329400	-0.02298400
C	2.06910400	-0.00001200	0.02528600
H	2.45310100	0.88938700	-0.47884300
H	2.42198300	-0.00522100	1.06154000
H	2.45382800	-0.88380600	-0.48812900

6.6 EPR spectra

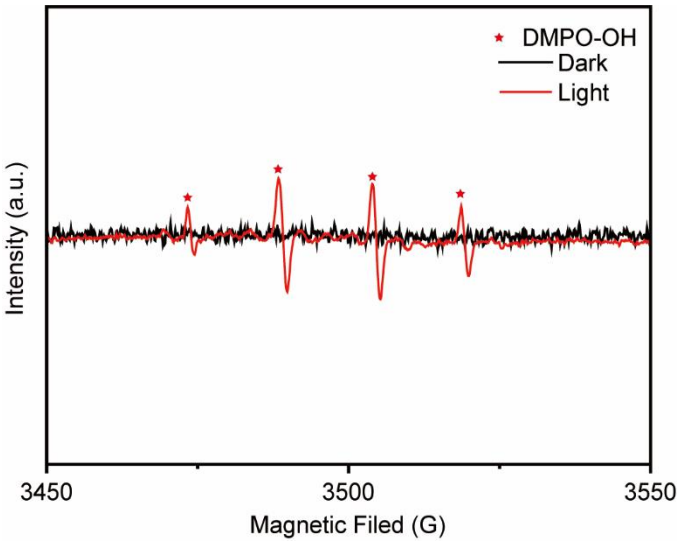

Supplementary Figure 36. EPR spectra of the suspension samples in D_2O with or without light irradiation.

Characteristic signals from hydroxyl radicals were clearly observed in the EPR spectra of the suspension in D_2O under light irradiation[16], which were absent in the case without illumination. Thus, hydroxyl radicals would be produced in the reaction system during photocatalytic HIE. Additionally, the fluctuation of the baseline appeared probably due to the presence of solid photocatalysts in the solution during EPR tests. The hydroxyl radicals could originate from the oxidation of D_2O or surface hydroxyl groups on TiO_2-h by photo-generated holes. Besides, the hydroxyl radicals may play the role of oxidizing the partially reduced sites of $Pd^{\delta*}$ back to $Pd^{\delta+}$ in the photocatalytic cycle.

7. Scale-up synthesis of deuterated *N*-heteroarenes via SA photocatalysis

7.1 Photocatalytic HIE using one homemade batch-mode photoreactor

In comparison with the reaction scale in a 20 mL stainless-steel autoclave (0.1 mmol reactant, 50 mg photocatalyst, 2 mL D_2O), the reactant amount can be scaled up to **1580 times** (158 mmol) by use of a homemade glass photoreactor (250 mL, as shown in Supplementary Fig. 37C and 37H).

1st round:

In a 250 mL Schlenk bottle fitted with a magnetic stirrer, 2.0 wt.% Pd_1/TiO_2-h (3.75 g) and 2-aminopyrimidine (15 g, 158 mmol) were added. Then, the bottle was flushed with the Schlenk Line in Ar atmosphere for 3 times. Subsequently, **fresh D_2O** (150 mL, 8276 mmol) was introduced. Later, it was placed into a homemade light box (equipped with 410 nm LED strips) and irradiated for 48 h. Additionally, the temperature of the reaction after 48 h irradiation was detected to be around 60-70 ^oC, which came from the absorption of photon energy and the heat released from LED strips when working. At the end of the reaction, the suspension was centrifuged to obtain the used photocatalyst and supernatant, which was analyzed by ^1H NMR directly. After the removal of D_2O in vacuo, the desired products were obtained. The used photocatalyst and D_2O were employed in the 2nd round HIE reaction (see below).

2nd round:

Used 2.0 wt.% Pd_1/TiO_2-h (3.75 g, **recycled from the 1st round**) and fresh 2-aminopyrimidine (15 g, 158 mmol) were added into a 250 mL Schlenk bottle fitted with a magnetic stirrer. After purging the bottle with Ar, the **used D_2O** (150 mL, 8276 mmol, **recycled from the 1st round**) was introduced. Same with the 1st round synthesis, the suspension was irradiated for 48 h. At the end of the reaction, the suspension was centrifuged to obtain the used photocatalyst and supernatant, which was analyzed by ^1H NMR directly. After the removal of D_2O in vacuo, the desired products were obtained. The used photocatalyst and D_2O were employed again in the 3rd round HIE reaction (see below).

3rd round:

Used 2.0 wt.% Pd_1/TiO_2-h (3.75 g, **recycled from the 2nd round**) and fresh 2-aminopyrimidine (10 g, 105 mmol) were added into a 250 mL Schlenk bottle fitted with a magnetic

stirrer. After purging the bottle with Ar, the **used D_2O** (150 mL, 8276 mmol, **recycled from the 2nd round**) was introduced. Same with the 2nd round synthesis, the suspension was irradiated for 48 h. At the end of the reaction, the suspension was centrifuged to obtain the used photocatalyst and supernatant, which was analyzed by ^1H NMR directly. After the removal of D_2O in vacuo, the desired products were obtained. The photocatalyst was reused for the synthesis of products with excellent deuterium incorporation (see below).

Further synthesis of products with excellent deuterium incorporation:

Used 2.0 wt.% Pd_1/TiO_2-h (3.75 g, **recycled from the 3rd round**) and deuterated 2-aminopyrimidine (50 g, 515 mmol, from products in the 3rd round) were added into a 250 mL Schlenk bottle fitted with a magnetic stirrer. After purging the bottle with Ar, **fresh D_2O** (150 mL, 8276 mmol) was introduced. Then, the suspension was irradiated for 48 h in the homemade light box with 410 nm LED strips. At the end of the reaction, the suspension was centrifuged to obtain the used photocatalyst and supernatant, which was analyzed by ^1H NMR directly. After the removal of D_2O in vacuo, the desired products were obtained.

7.2 Photocatalytic HIE using a photocatalytic bed equipped with 30 homemade photoreactors

Usually, this facile duplication is quite challenging since most catalytic systems require harsh and hazardous reaction conditions (e.g., ≥ 120 °C or 20 bar H_2/D_2) or complicated catalyst preparation (e.g., metal complexes). In contrast, we successfully duplicated the scale-up synthesis with 30 photoreactors in a compact bed (80 cm × 60 cm × 190 cm, as shown in Supplementary Fig. 37J) due to facile assembly of photoreactors, scaled preparation of photocatalysts, mild reaction conditions, and small usage of D_2O.

We obtained **1.157 kg deuterated product 18b** with high deuterium content (**92%** on average at 4,6 C-H sites) by reusing the photocatalyst and D_2O for three times, which demonstrates the practicality of this photocatalytic synthesis protocol.

1st round: 433 g (isolated yield: 94.3%), 4.46 mol, 95% D incorporation (Fresh D_2O and photocatalyst).

2nd round: 434 g (isolated yield: 94.6%), 4.47 mol, 91% D incorporation (Reused D_2O and photocatalyst from 1st round).

3rd round: 290 g (isolated yield: 94.8%), 2.99 mol, 90% D incorporation (Reused D_2O and photocatalyst from 2nd round).

Overall, by use of 4.5 L D_2O (249 mol), 1.157 kg 2-aminopyrimidine-4,6-d_2 (11.93 mol) was obtained. The molar ratio of D_2O/reactant was dramatically reduced to 19.7.

Supplementary Figure 37. The operation process of scale-up photocatalytic HIE reactions. (A) Substrate of 2-aminopyrimidine. (B) 120 g photocatalysts (2.0 wt.% Pd_1/TiO_2-h). (C) 250 mL Schlenk bottle. (D) 30 Schlenk bottles (250 mL for each bottle) filled with substrates and photocatalysts. (E) Purging with the Schlenk Line in Ar atmosphere for 3 times. (F) 4.5 L D_2O. (G) Adding D_2O. (H) 250 mL batch-mode photoreactor equipped with 410 nm LED strips covered by Al foils. (I) Loading photoreactors. (J) Photoreactor bed equipped with 30 photoreactors in operation.

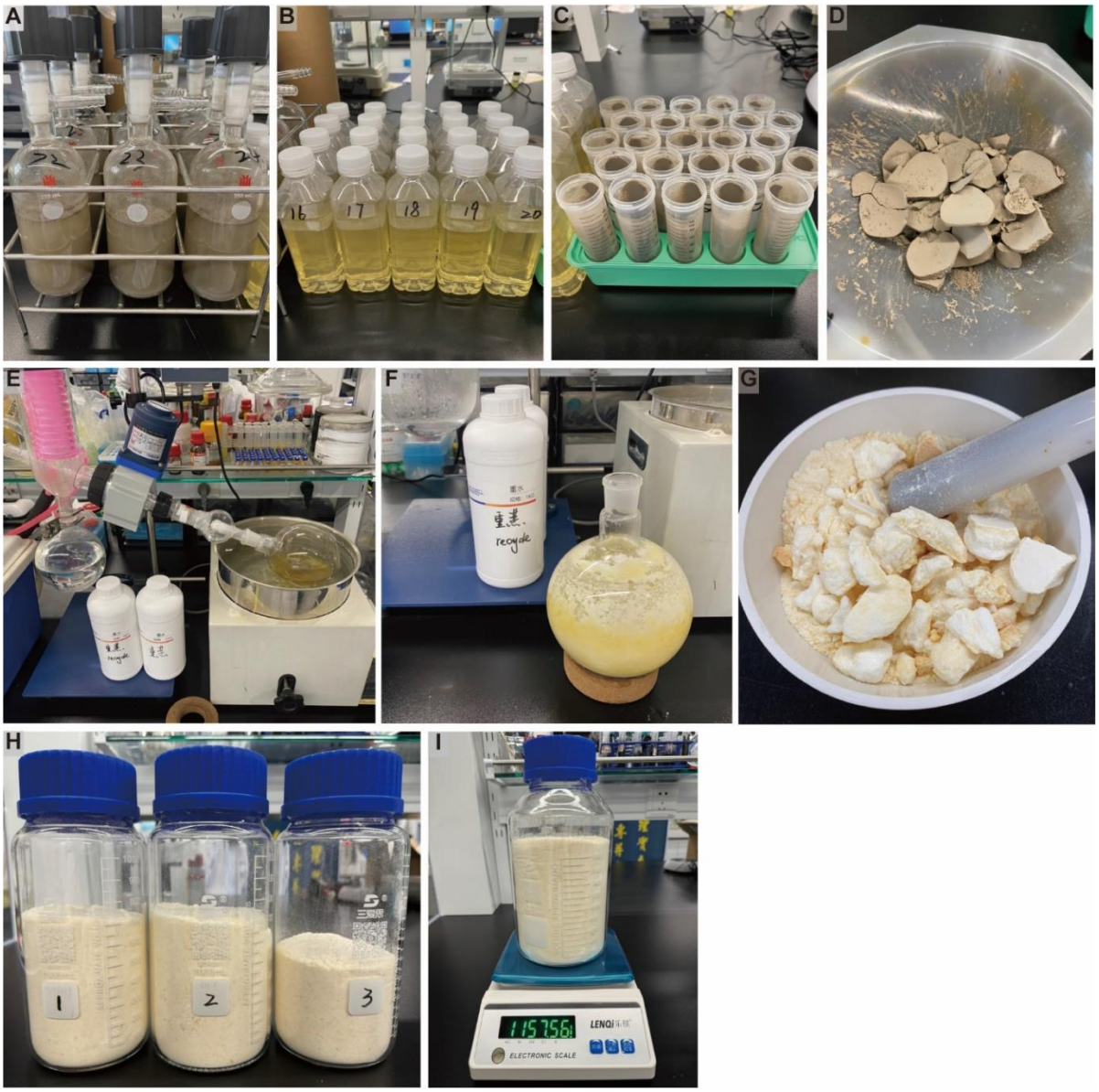

Supplementary Figure 38. Isolation processes of used D_2O, photocatalysts, and deuterated products. (A) 30 bottles of reaction suspensions after photocatalytic HIE. (B-C) Supernatants and used photocatalysts separated by centrifuging. (D) The powders of used photocatalysts after drying in air at 100 ^oC for 12 h (they can be employed in the next round of photocatalytic HIE reactions). (E) The rotary evaporation of supernatants in vacuum (the used D_2O could be obtained). (F) The deuterated products and used D_2O separated from evaporation. (G) The powders of deuterated products after drying in air at 60 ^oC for 12 h. (H) The isolated deuterated products from the 1st, 2nd and 3rd round of photocatalytic HIE reactions. (I) The deuterated products in total collected from three rounds of photocatalytic HIE reactions.

Supplementary Table S4. Pd loading amounts of photocatalysts based on ICP-mass analysis.

Photocatalyst	Pd loading amount （wt.%）
2.0 wt.% Pd_1/TiO_2-h (Fresh)	1.90
2.0 wt.% Pd_1/TiO_2-h (3^{rd} used)	1.89

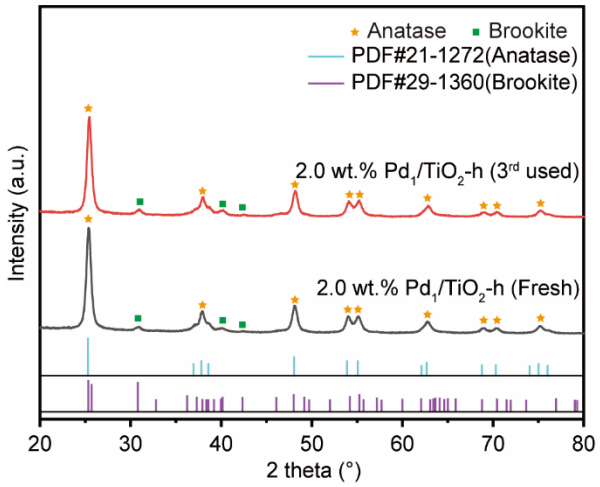

Supplementary Figure 39. XRD patterns of fresh 2.0 wt.% Pd_1/TiO_2-h and the used photocatalyst after 3 rounds of recycling tests. The standard JCPDS cards of anatase (PDF#21-1272) and brookite (PDF#29-1360) TiO_2 were incorporated for comparison.

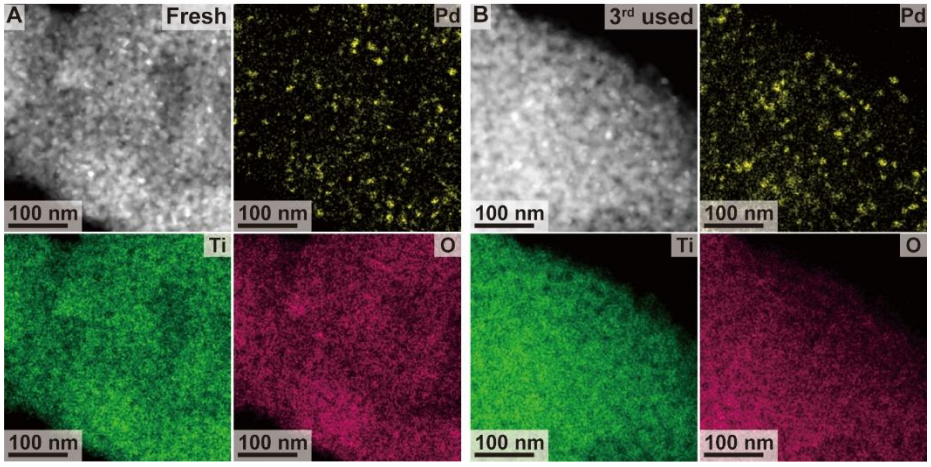

Supplementary Figure 40. STEM-EDS elemental mapping of (A) fresh 2.0 wt.% Pd_1/TiO_2-h and (B) the used photocatalyst after 3 rounds of recycling tests.

The concentrations of HDO after each round of HIE reactions were determined by quantitative ^{1}H NMR. Firstly, we tested the ^{1}H NMR spectra of the fresh D_2O using 1,4-dioxane for internal calibration. Then, we tested the ^{1}H NMR spectra of the used D_2O after reactions with 1,4-dioxane for internal calibration. In principle, when 158 mmol of 2-aminopyrimidine was deuterated with D incorporation of 95% in the 1st round of HIE reactions, 616 mmol HDO would be generated. In the 2nd round, when 158 mmol of 2-aminopyrimidine was deuterated with D incorporation of 92%, 607 mmol HDO would be generated. In the case of 3rd round, when 105 mmol of 2-aminopyrimidine was deuterated with D incorporation of 90%, accordingly 399 mmol HDO would be generated.

Based on the NMR results, the molar amounts of HDO in D_2O after each round of HIE reactions were 9-16% higher than the theoretical values. This difference may be due to a few reasons: (1) some H_2O was introduced during the process of recycling D_2O by rotary evaporation; (2) H_2O adsorbed on the surface of photocatalysts could be introduced into the reaction solution; (3) characterization errors of ^{1}H NMR.

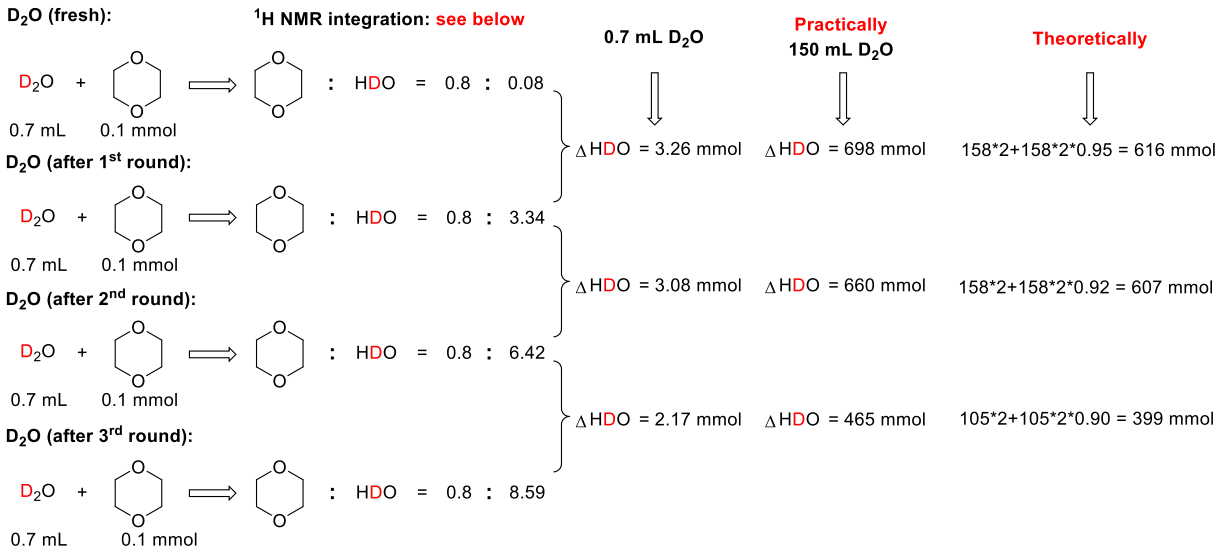

The calculation of HDO amount in D_2O after HIE reactions:

1st round:

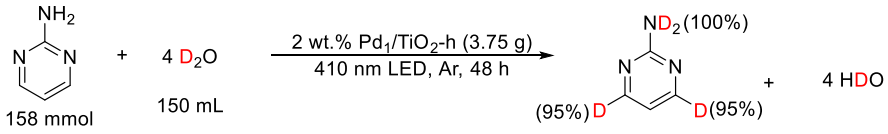

Theoretically:

n_{HDO} (mmol) = $n_{2\text{-aminopyrimidine}}$ (mmol)*2 + $n_{2\text{-aminopyrimidine}}$ (mmol)*2*D-incorporation (%)

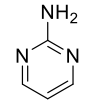

$\Longrightarrow$ △HDO = 158*2*100%+158*2*95% = 616 mmol

Practically:

Determined by the integral of HDO in quantitative ^{1}H NMR

$$\triangle HDO = \frac{3.34 - 0.08}{0.7} * 150 = 698 \text{ mmol}$$

2nd round:

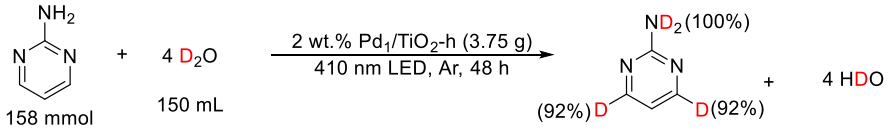

Theoretically:

n_{HDO} (mmol) = $n_{2\text{-aminopyrimidine}}$ (mmol)*2 + $n_{2\text{-aminopyrimidine}}$ (mmol)*2*D-incorporation (%)

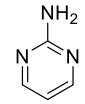

$\Longrightarrow$ △HDO = 158*2*100%+158*2*92% = 607 mmol

Practically:

Determined by the integral of HDO in quantitative ^{1}H NMR

$$\triangle HDO = \frac{6.42 - 3.34}{0.7} * 150 = 660 \text{ mmol}$$

3rd round:

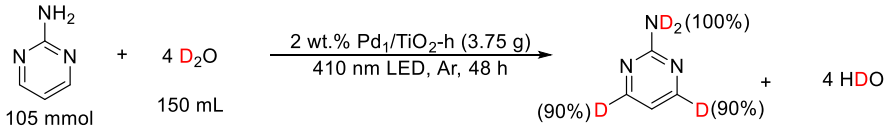

Theoretically:

n_{HDO} (mmol) = $n_{2\text{-aminopyrimidine}}$ (mmol)*2 + $n_{2\text{-aminopyrimidine}}$ (mmol)*2*D-incorporation (%)

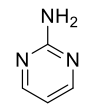

$\Longrightarrow$ △HDO = 105*2*100%+105*2*90% = 399 mmol

Practically:

Determined by the integral of HDO in quantitative ^{1}H NMR

$$\triangle HDO = \frac{8.59 - 6.42}{0.7} * 150 = 465 \text{ mmol}$$

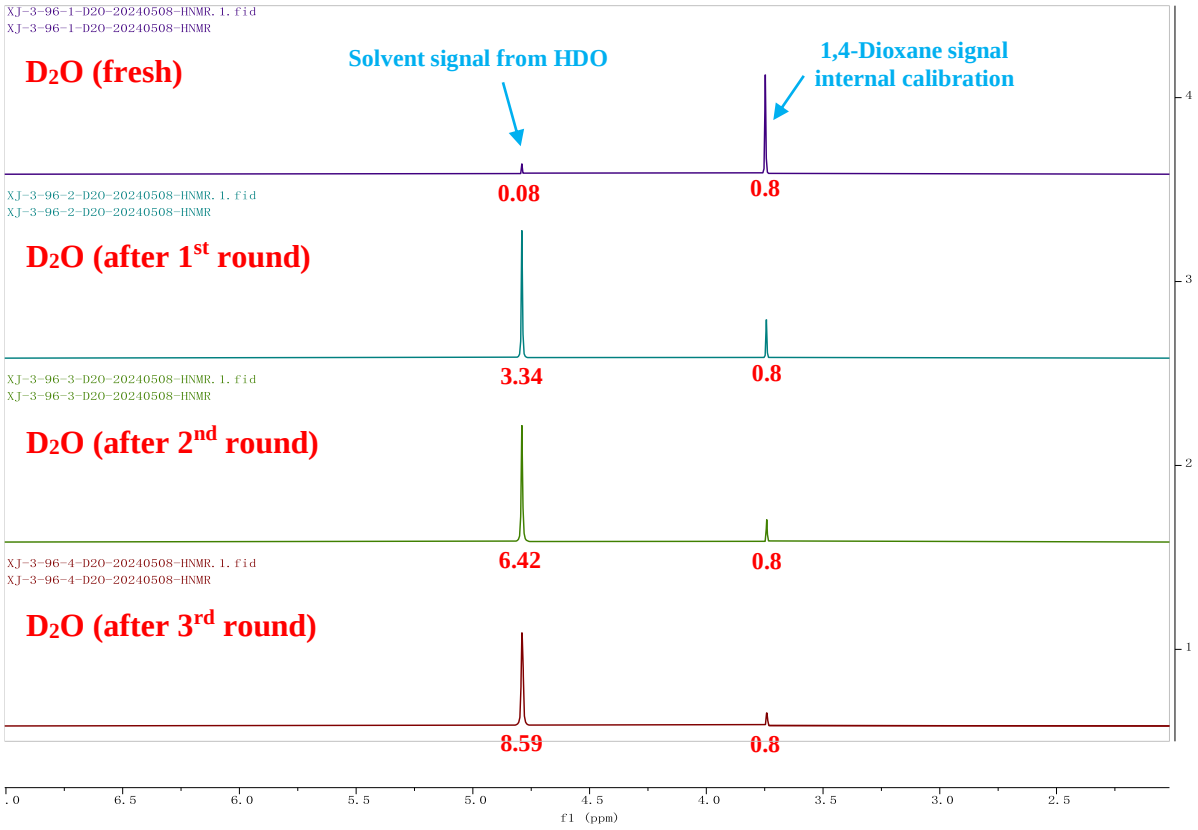

Supplementary Figure 41. ^{1}H NMR of fresh D_2O and reused D_2O, using the signals from 1,4-Dioxane as internal calibration.

NMR and HR-MS analysis of feed material.

^{1}H NMR (400 MHz, D_2O) of feed material **18a**:

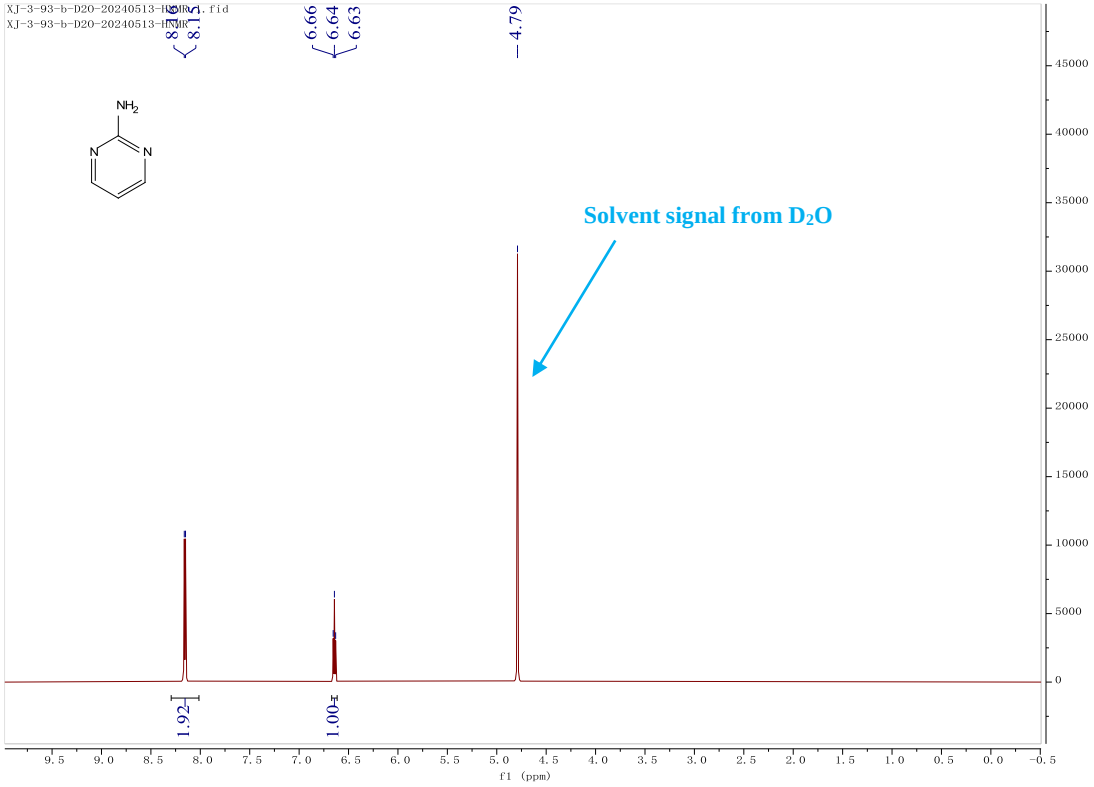

^{13}C NMR (101 MHz, D_2O) of feed material **18a**:

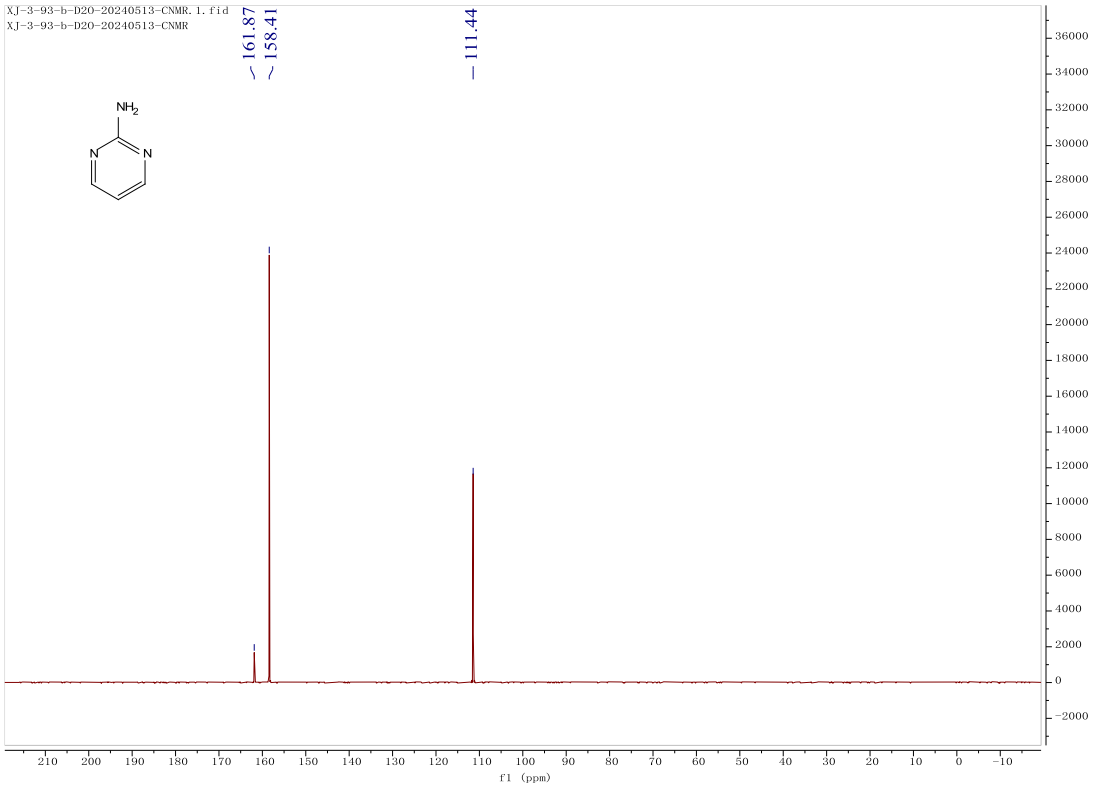

HR-MS of feed material **18a**:

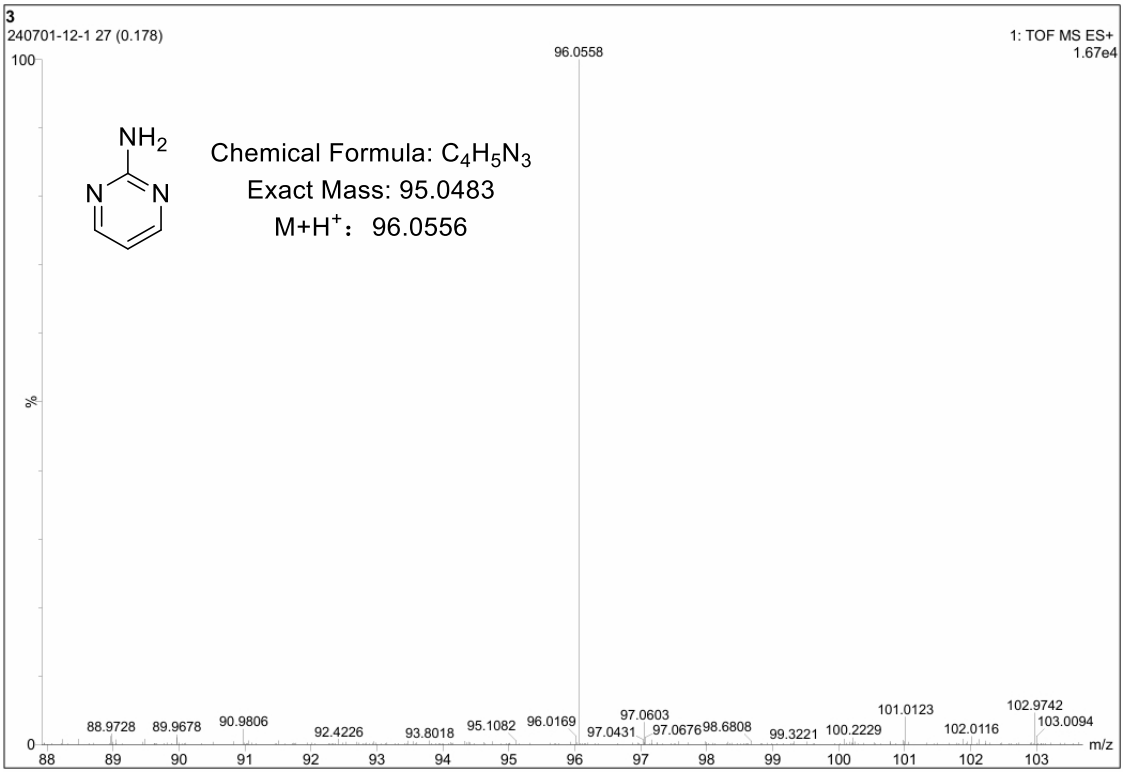

NMR and HR-MS analysis of collected products from the 1st round HIE reaction using 30 homemade photoreactors.

^{1}H NMR (400 MHz, D_2O) of product **18b:**

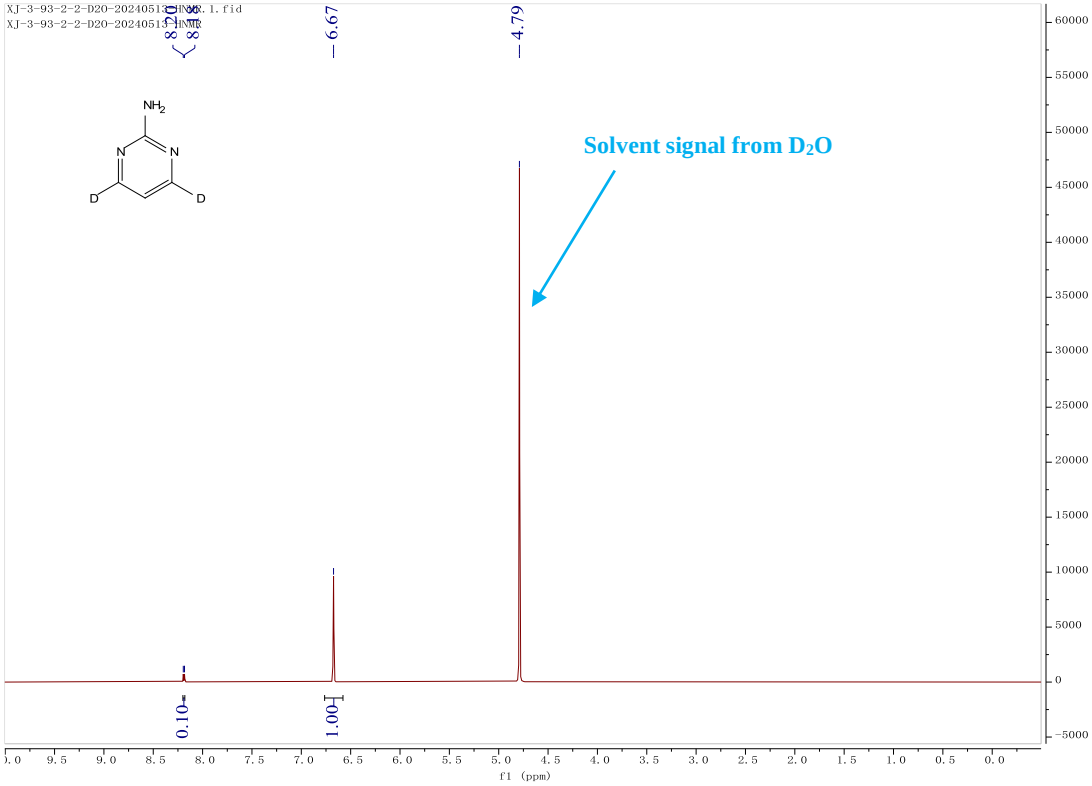

^{13}C NMR (101 MHz, D_2O) of product **18b:**

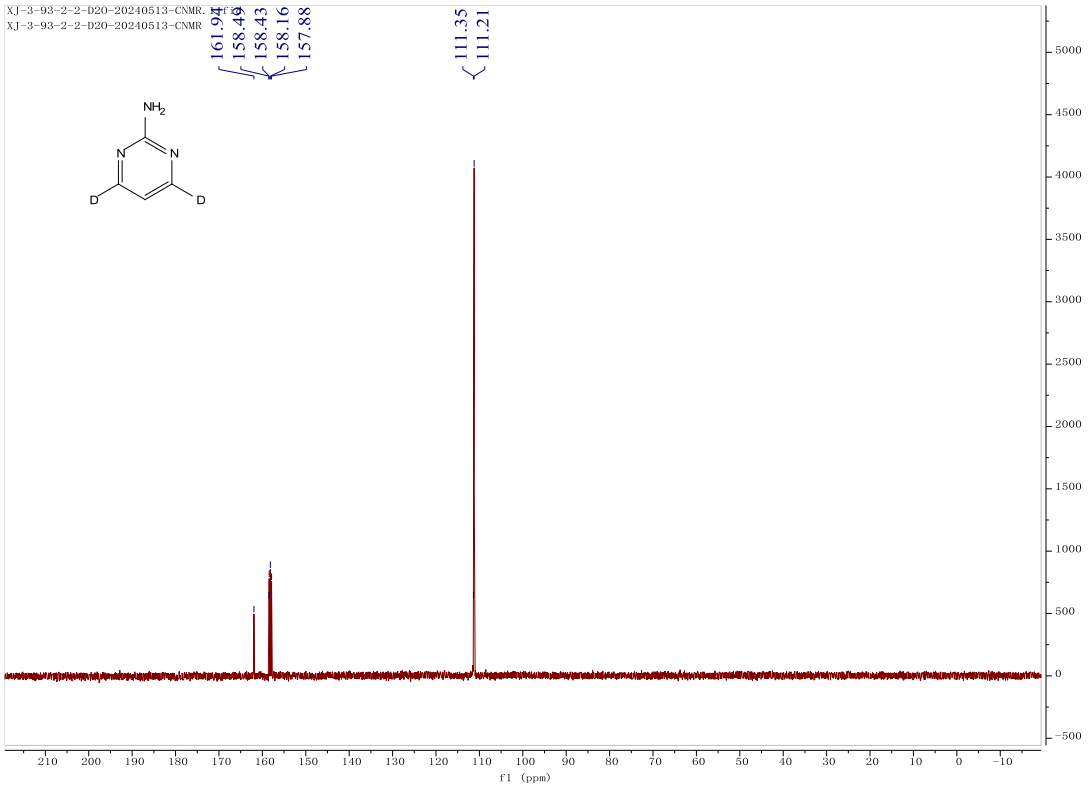

HR-MS of product **18b**:

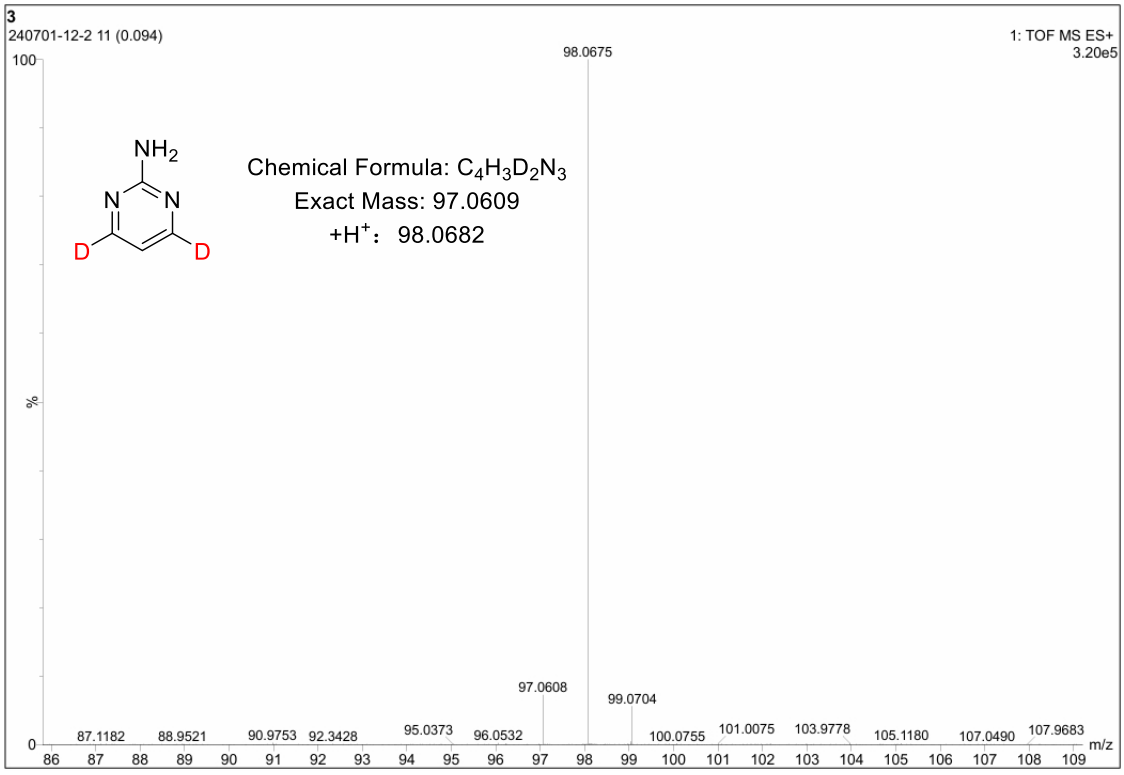

NMR and HR-MS analysis of collected products from the 2nd round HIE reaction using 30 homemade photoreactors.

^{1}H NMR (400 MHz, D_2O) of product **18b:**

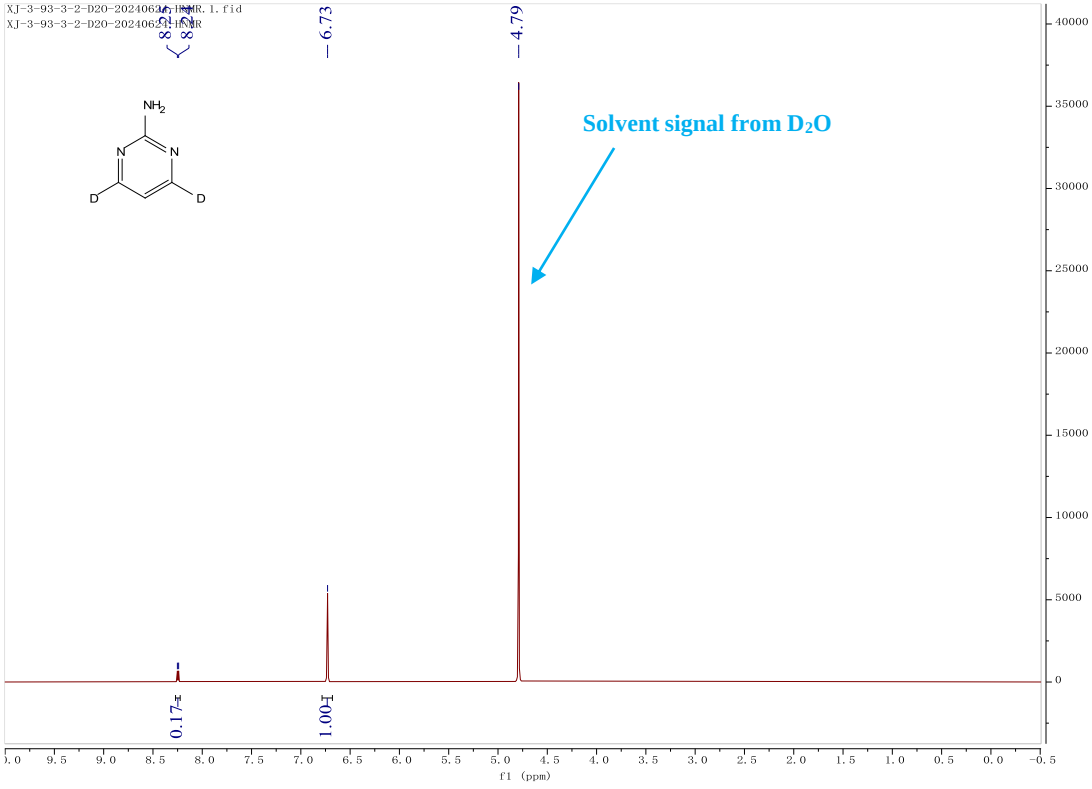

^{13}C NMR (101 MHz, D_2O) of product **18b:**

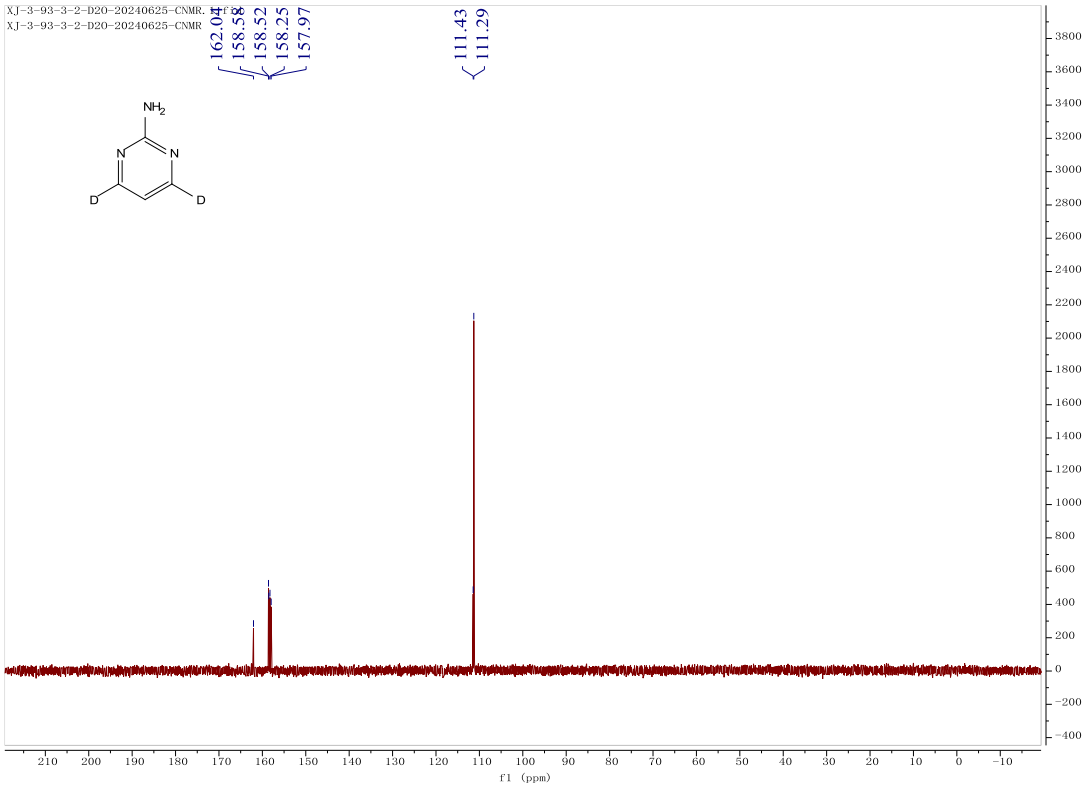

HR-MS of product **18b:**

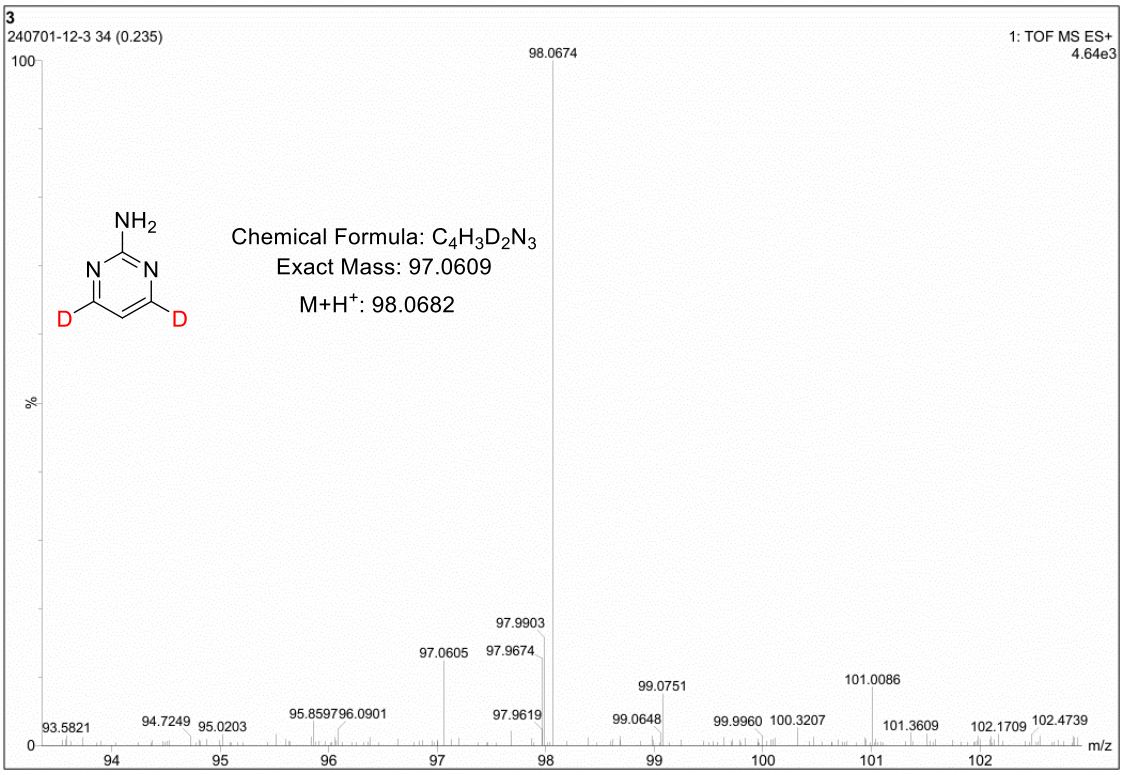

NMR and HR-MS analysis of collected products from the 3rd round HIE reaction using 30 homemade photoreactors.

^{1}H NMR (400 MHz, D_2O) of product **18b:**

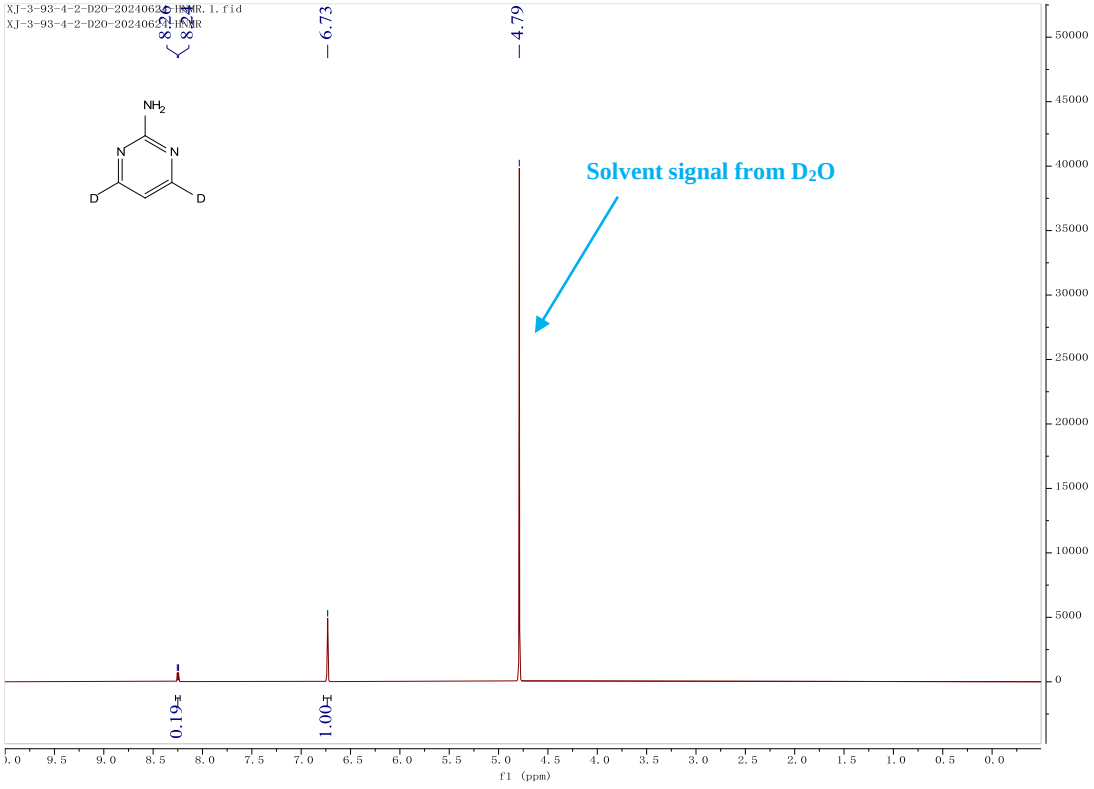

^{13}C NMR (101 MHz, D_2O) of product **18b:**

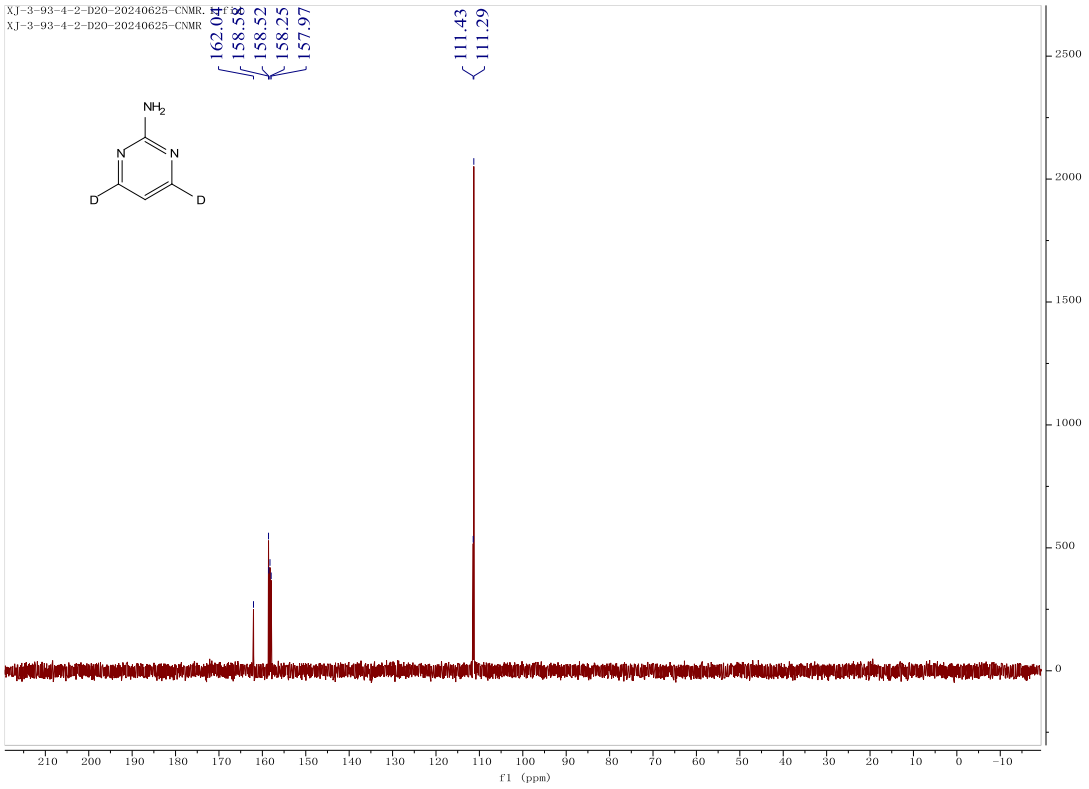

HR-MS of product **18b**:

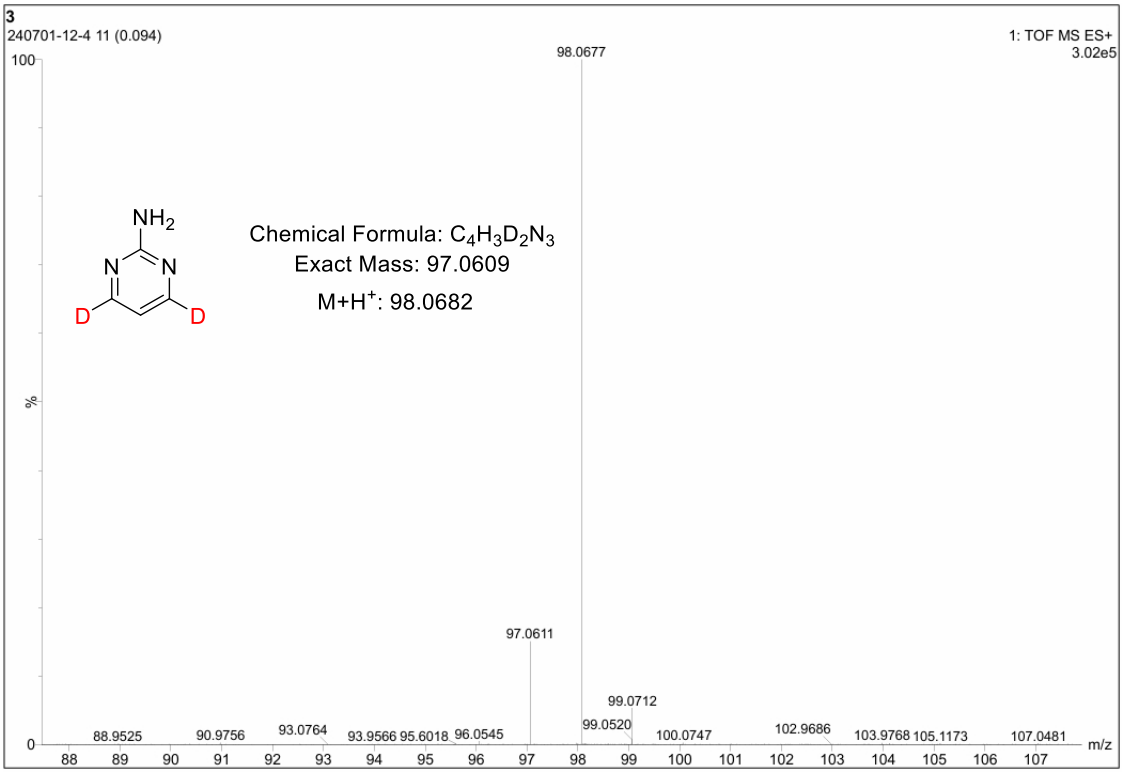

NMR and HR-MS analysis of the collected products with excellent D incorporation.

^{1}H NMR (400 MHz, D_2O) of product **18b:**

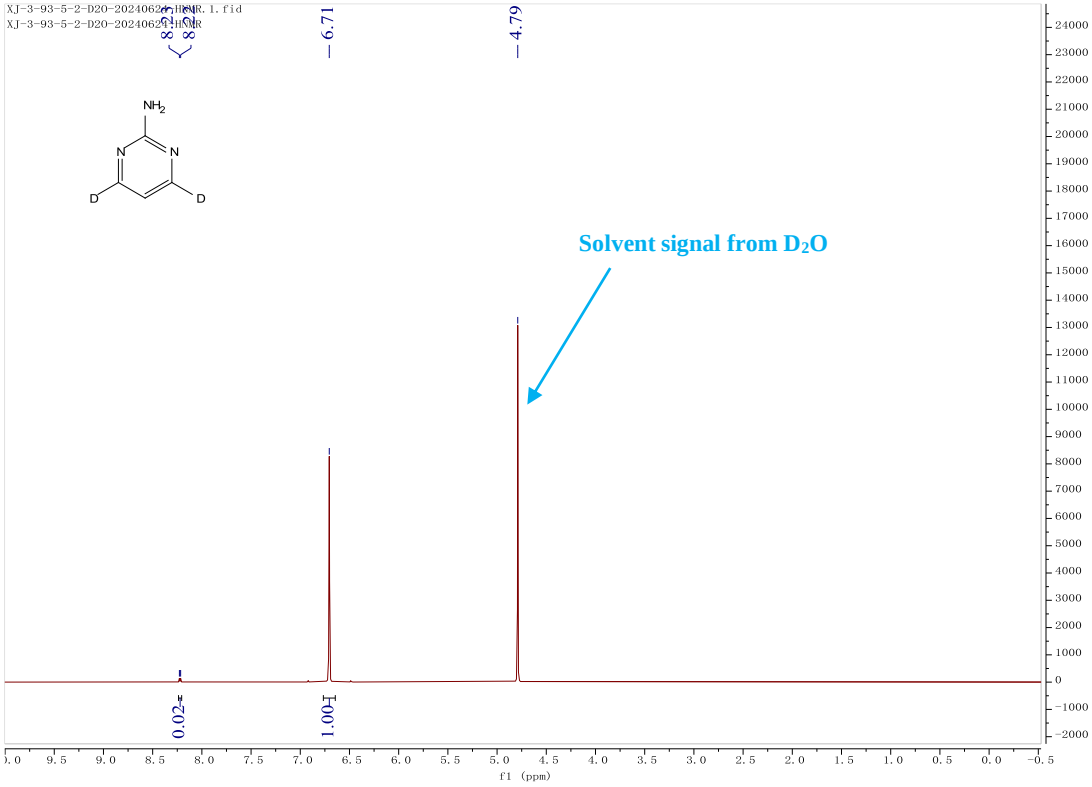

^{13}C NMR (101 MHz, D_2O) of product **18b:**

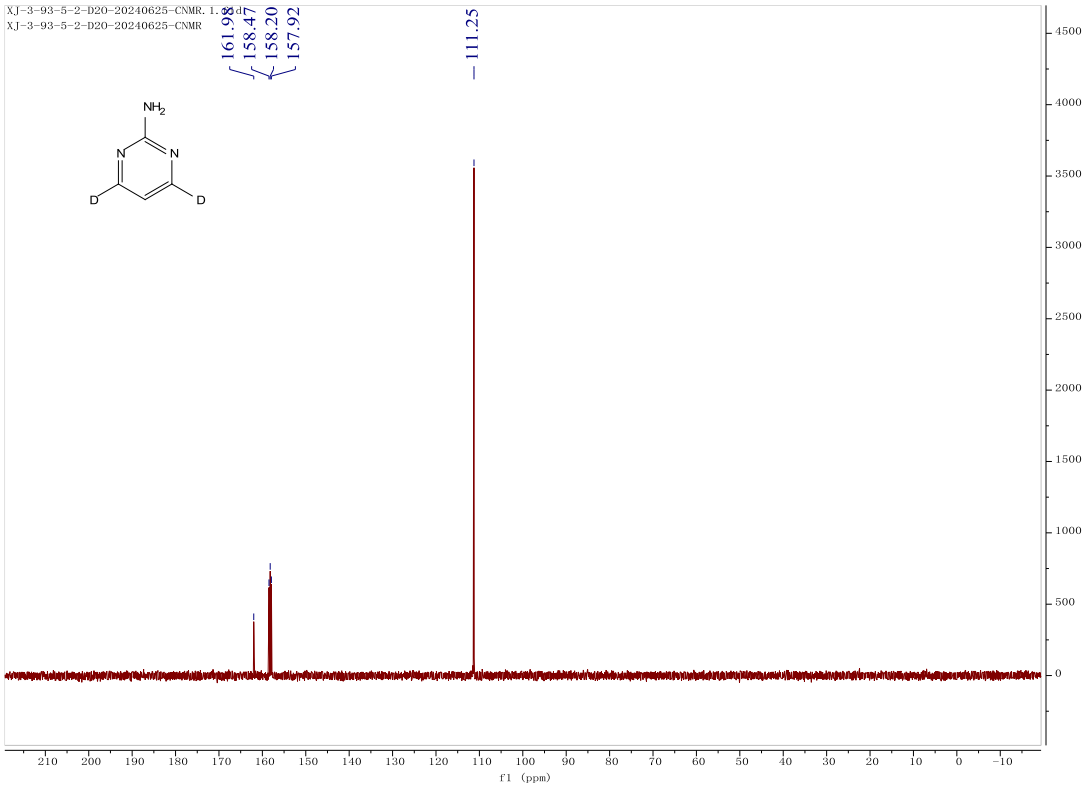

^{2}H NMR (400 MHz, $CDCl_3$) of product **18b:**

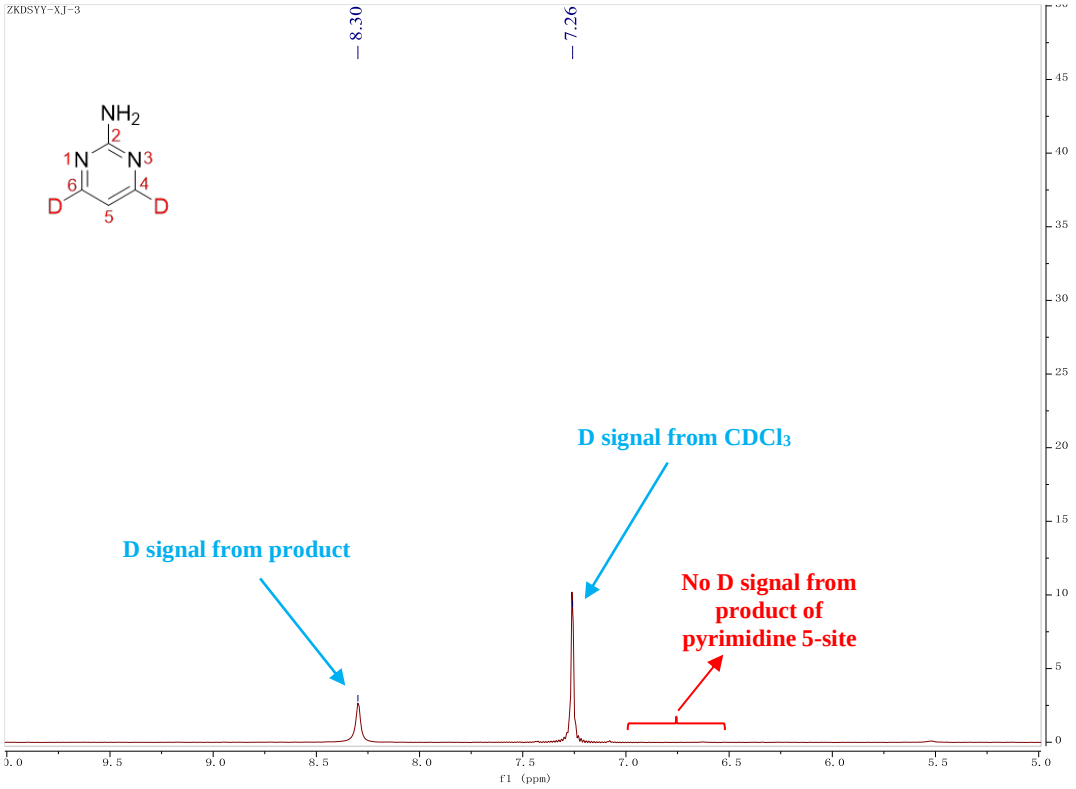

HR-MS of product **18b**:

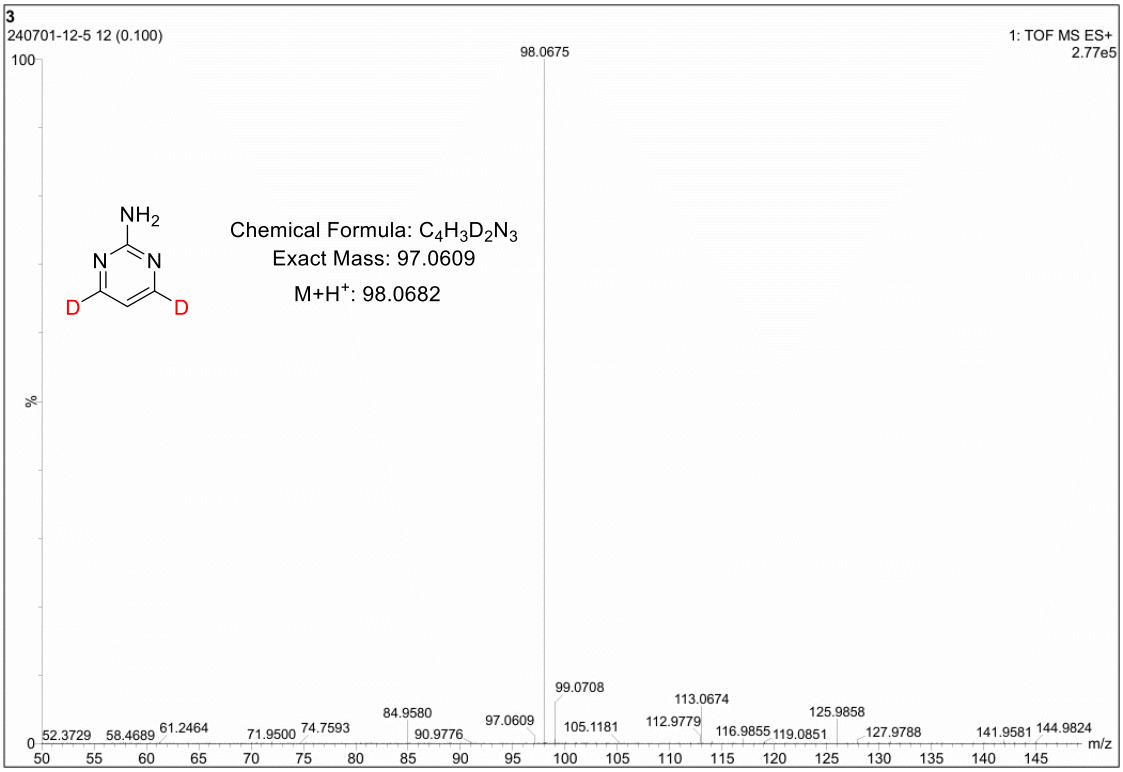

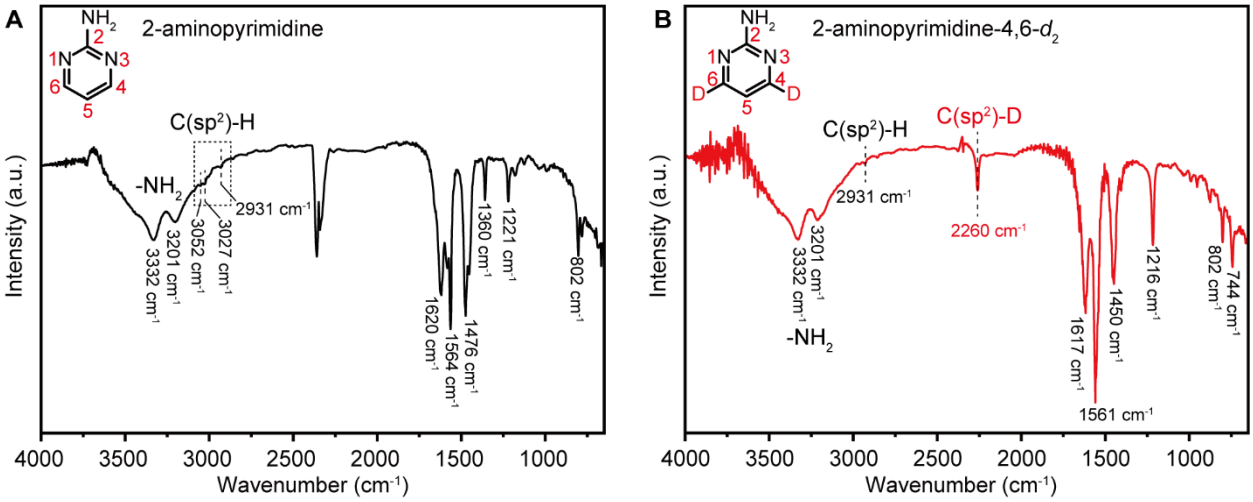

Supplementary Figure 42. DRIFT spectra of (A) 2-aminopyrimidine and (B) 2-aminopyrimidine-4,6-d_2.

By comparing the IR spectra of the feed material (2-aminopyrimidine) and the deuterated product (2-aminopyrimidine-4,6-d_2), a new absorption peak was observed at 2260 cm^{-1}, which was attributed to the formation of the C(sp^2)−D bond. Moreover, the weak absorption bands at 3052 and 3027 cm^{-1}, corresponding to the symmetric stretching vibrations of C(sp^2)−H bonds at pyrimidine 4,6-sites[17], disappeared in the IR spectrum of the deuterated products. Instead, the absorption band assigned to the C(sp^2)−H bond at pyrimidine 5-site (at 2931 cm^{-1})[17] remained in deuterated products. Thus, it indicated the selective and efficient HIE at pyrimidine 4,6-sites via SA photocatalysis, well complying with the data from ^{2}H NMR.

8. NMR analysis of substrates and products

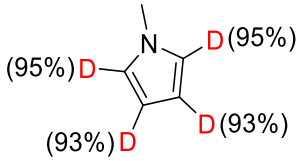

1b

According to GP, 0.5 wt.% Pd_1/TiO_2-h (50 mg), substrate (8.1 mg, 0.1 mmol), D_2O (2 mL), 410 nm LED (95 mW/cm^2), Ar (1 bar), r.t., 24 h. The product **1b** was obtained (Selectivity > 99%, detected by ^{1}H NMR).

Feed material 1a: ^{1}H NMR (400 MHz, D_2O) δ 6.76 (t, *J* = 4 Hz, 2H), 6.17 (t, *J* = 4 Hz, 2H), 3.66 (s, 3H).

Product 1b: ^{1}H NMR (400 MHz, D_2O) δ 6.76 (s, 0.10H), 6.16 (s, 0.12H), 3.66 (s, 3H).

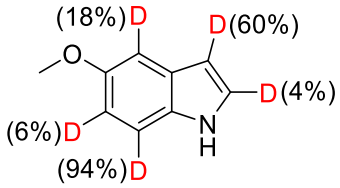

2b

According to GP, 0.5 wt.% Pd_1/TiO_2-h (50 mg), substrate (14.7 mg, 0.1 mmol), D_2O (1.6 mL), acetone (0.4 mL), 410 nm LED (95 mW/cm^2), Ar (1 bar), r.t., 24 h. The product **2b** was obtained (Selectivity > 99%, detected by ^{1}H NMR).

Feed material 2a: ^{1}H NMR (400 MHz, $CDCl_3$) δ 8.06 (s, 1H), 7.28 (d, *J* = 8 Hz, 1H), 7.18 (t, *J* = 4 Hz, 1H), 7.13 (d, *J* = 4 Hz, 1H), 6.88 (dd, *J* = 12, 4 Hz, 1H), 6.51 – 6.49 (m, 1H), 3.87 (s, 3H).

Product 2b: ^{1}H NMR (400 MHz, $CDCl_3$) δ 8.05 (s, 1H), 7.28 (d, *J* = 8 Hz, 0.77H), 7.18 (s, 0.06H), 7.13 (d, *J* = 4 Hz, 0.90H), 6.88 (dd, *J* = 8, 4 Hz, 0.92H), 6.49 (s, 0.38H), 3.86 (s, 3H).

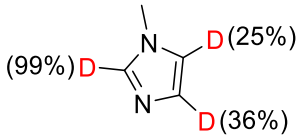

3b

According to GP, 0.5 wt.% Pd_1/TiO_2-h (50 mg), substrate (8.2 mg, 0.1 mmol), D_2O (2 mL), 410 nm LED (95 mW/cm^2), Ar (1 bar), r.t., 24 h. The product **3b** was obtained (Selectivity > 99%, detected by ^{1}H NMR).

Feed material 3a: ^{1}H NMR (400 MHz, D_2O) δ 7.58 (s, 1H), 7.08 (s, 1H), 6.98(s, 1H), 3.68 (s, 3H).

Product 3b: ^{1}H NMR (400 MHz, D_2O) δ 7.70 (s, 0.01H), 7.15 (s, 0.54H), 7.05 (s, 0.65H), 3.76 (s, 3H).

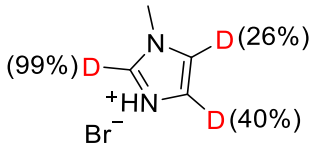

4b

According to GP, 0.5 wt.% Pd_1/TiO_2-h (50 mg), substrate (16.3 mg, 0.1 mmol), D_2O (2 mL), 410 nm LED (95 mW/cm^2), Ar (1 bar), r.t., 24 h. The product **4b** was obtained (Selectivity > 99%, detected by ^{1}H NMR).

Feed material 4a: ^{1}H NMR (400 MHz, D_2O) δ 8.26 (s, 1H), 7.33 (s, 1H), 7.28(s, 1H), 3.86 (s, 3H).

Product 4b: ^{1}H NMR (400 MHz, D_2O) δ 8.32 (s, 0.01H), 7.35 (s, 0.52H), 7.31 (s, 0.64H), 3.88 (s, 3H).

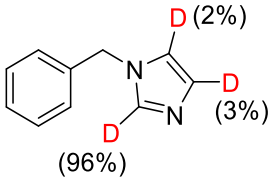

5b

According to GP, 0.5 wt.% Pd_1/TiO_2-h (50 mg), substrate (15.8 mg, 0.1 mmol), D_2O (1.6 mL), acetone (0.4 ml), 410 nm LED (95 mW/cm^2), Ar (1 bar), r.t., 24 h. The product **5b** was obtained (Selectivity > 99%, detected by ^{1}H NMR).

Feed material 5a: ^{1}H NMR (400 MHz, $CDCl_3$) δ 7.53 (s, 1H), 7.37 – 7.28 (m, 3H), 7.15 (dd, *J* = 8, 4 Hz, 2H), 7.08 (s, 1H), 6.89 (s, 1H), 5.10 (s, 2H).

Product 5b: ^{1}H NMR (400 MHz, $CDCl_3$) δ 7.55 (s, 0.03H), 7.37 – 7.30 (m, 3H), 7.16 – 7.12 (m,, 2H), 7.08 (s, 0.95H), 6.90 (s, 0.92H), 5.11 (s, 2H).

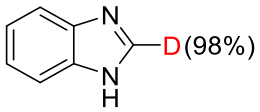

6b

According to GP, 0.5 wt.% Pd_1/TiO_2-h (50 mg), substrate (11.8 mg, 0.1 mmol), D_2O (1.6 mL), acetone (0.4 mL), 410 nm LED (95 mW/cm^2), Ar (1 bar), r.t., 24 h. The product **6b** was obtained (Selectivity > 99%, detected by ^{1}H NMR).

Feed material 6a: ^{1}H NMR (400 MHz, DMSO-d_6) δ 12.47 (s, 1H), 8.22 (s, 1H), 7.59 (t, *J* = 4 Hz, 2H), 7.19 (dd, *J* = 8, 4 Hz, 2H).

Product 6b: ^{1}H NMR (400 MHz, DMSO-d_6) δ 8.23 (s, 0.02H), 7.59 (dd, *J* = 8, 4 Hz, 2H), 7.19 (dd, *J* = 8, 4 Hz, 2H).

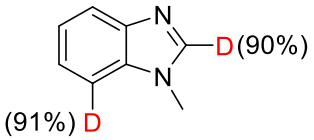

7b

According to GP, 0.5 wt.% Pd_1/TiO_2-h (50 mg), substrate (13.2 mg, 0.1 mmol), D_2O (1.6 mL), acetone (0.4 mL), 410 nm LED (95 mW/cm^2), Ar (1 bar), r.t., 24 h. The product **7b** was obtained (Selectivity > 99%, detected by ^{1}H NMR).

Feed material 7a: ^{1}H NMR (400 MHz, $CDCl_3$) δ 7.87 (s, 1H), 7.82 – 7.79 (m, 1H), 7.39 – 7.37 (m, 1H), 7.34 – 7.27 (m, 2H), 3.82 (s, 3H).

Product 7b: ^{1}H NMR (400 MHz, $CDCl_3$) δ 7.85 (s, 0.09H), 7.74 – 7.72 (m, 0.09H), 7.34 – 7.31 (m, 1H), 7.27 – 7.19 (m, 2H), 3.77 (s, 3H).

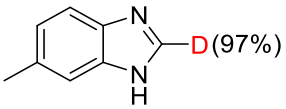

8b

According to GP, 0.5 wt.% Pd_1/TiO_2-h (50 mg), substrate (13.2 mg, 0.1 mmol), D_2O (1.6 mL), acetone (0.4 mL), 410 nm LED (95 mW/cm^2), Ar (1 bar), r.t., 24 h. The product **8b** was obtained (Selectivity > 99%, detected by ^{1}H NMR).

Feed material 8a: ^{1}H NMR (400 MHz, $CDCl_3$) δ 9.17 (s, 1H), 8.09 (s, 1H), 7.58 (d, *J* = 12 Hz, 1H), 7.46 (s, 1H), 7.13 (dd, *J* = 8, 4 Hz, 1H), 2.48 (s, 3H).

Product 8b: ^{1}H NMR (400 MHz, $CDCl_3$) δ 8.88 (s, 1H), 8.08 (s, 0.03H), 7.57 (d, *J* = 8 Hz, 1H), 7.45 (s, 1H), 7.12 (d, *J* = 8 Hz, 1H), 2.48 (s, 3H).

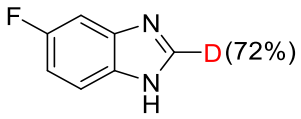

9b

According to GP, 0.5 wt.% Pd_1/TiO_2-h (50 mg), substrate (13.6 mg, 0.1 mmol), D_2O (1.6 mL), acetone (0.4 mL), 410 nm LED (95 mW/cm^2), Ar (1 bar), r.t., 24 h. The product **9b** was obtained (Selectivity > 99%, detected by ^{1}H NMR).

Feed material 9a: ^{1}H NMR (400 MHz, DMSO-d_6) δ 12.55 (s, 1H), 8.25 (s, 1H), 7.58 (dd, *J* = 8, 4 Hz, 1H), 7.39 (dd, *J* = 8, 4 Hz, 1H), 7.05 (td, *J* = 8, 4 Hz, 1H); ^{19}F NMR(376 MHz, DMSO-d_6) δ -121.34.

Product 9b: ^{1}H NMR (400 MHz, DMSO-d_6) δ 8.27 (s, 0.27H), 7.59 (dd, *J* = 8, 4 Hz, 1H), 7.39 (dd, *J* = 12, 4 Hz, 1H), 7.05 (td, *J* = 12, 4 Hz , 1H); ^{19}F NMR(376 MHz, DMSO-d_6) δ -121.25.

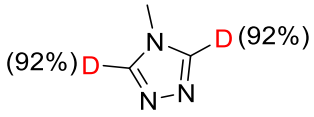

10b

According to GP, 0.5 wt.% Pd_1/TiO_2-h (50 mg), substrate (8.3 mg, 0.1 mmol), D_2O (2 mL), 410 nm LED (95 mW/cm^2), Ar (1 bar), r.t., 24 h. The product **10b** was obtained (Selectivity > 99%, detected by ^{1}H NMR).

Feed material 10a: ^{1}H NMR (400 MHz, D_2O) δ 8.43 (s, 2H), 3.78 (s, 3H).

Product 10b: ^{1}H NMR (400 MHz, D_2O) δ 8.45 (s, 0.11H), 3,79 (s, 3H).

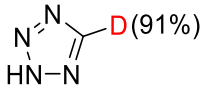

11b

According to GP, 2.0 wt.% Pd_1/TiO_2-h (50 mg), substrate (7.0 mg, 0.1 mmol), D_2O (2 mL), 410 nm LED (95 mW/cm^2), Ar (1 bar), 80 ^{o}C, 24 h. The product **11b** was obtained (Selectivity > 99%, detected by ^{1}H NMR).

Feed material 11a: ^{1}H NMR (400 MHz, D_2O) δ 9.26 (s, 1H).

Product 11b: ^{1}H NMR (400 MHz, D_2O) δ 9.26 (s, 0.07H).

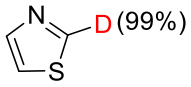

12b

According to GP, 0.5 wt.% Pd_1/TiO_2-h (50 mg), substrate (8.5 mg, 0.1 mmol), D_2O (2 mL), 410 nm LED (95 mW/cm^2), Ar (1 bar), 80 °C, 24 h. The product **12b** was obtained (Selectivity > 99%, detected by ^{1}H NMR).

Feed material 12a: ^{1}H NMR (400 MHz, D_2O) δ 9.01 (d, *J* = 4 Hz, 1H), 7.94 (d, *J* = 4 Hz, 1H), 7.65 – 7.63 (m, 1H).

Product 12b: ^{1}H NMR (400 MHz, D_2O) δ 9.04 (s, 0.01H), 7.97 (d, *J* = 4 Hz, 1H), 7.67 (d, *J* = 4 Hz, 1H).

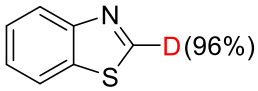

13b

According to GP, 2.0 wt.% Pd_1/TiO_2-h (50 mg), substrate (13.5 mg, 0.1 mmol), D_2O (1.6 mL), acetone (0.4 mL), 410 nm LED (95 mW/cm^2), Ar (1 bar), 80 °C, 24 h. The product **13b** was obtained (Selectivity > 99%, detected by ^{1}H NMR).

Feed material 13a: ^{1}H NMR (400 MHz, D_2O) δ 9.23 (s, 1H), 8.06 (d, *J* = 8 Hz, 2H), 7.58 (t, *J* = 8 Hz, 1H), 7.51 (t, *J* = 8 Hz, 1H).

Product 13b: ^{1}H NMR (400 MHz, D_2O) δ 9.31 (s, 0.03H), 8.15 (t, *J* = 8 Hz, 2H), 7.67 (t, *J* = 8 Hz, 1H), 7.60 (t, *J* = 8 Hz, 1H).

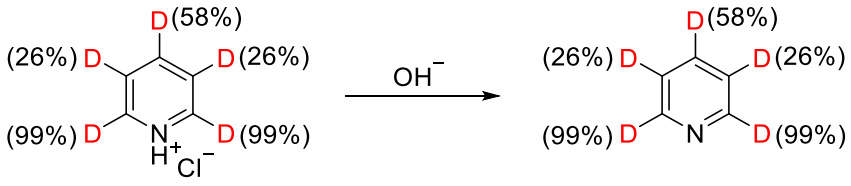

14b **15b**

According to GP, 2.0 wt.% Pd_1/TiO_2-h (50 mg), substrate (11.5 mg, 0.1 mmol), D_2O (2 mL), 410 nm LED (95 mW/cm^2), Ar (1 bar), 80 °C, 24 h. The product **14b** was obtained (Selectivity > 99%, detected by ^{1}H NMR).

Feed material 14a: ^{1}H NMR (400 MHz, D_2O) δ 8.80 (d, *J* = 4 Hz, 2H), 8.64 (t, *J* = 8 Hz, 1H), 8.09 (t, *J* = 8 Hz, 2H).

Product 14b: ^{1}H NMR (400 MHz, D_2O) δ 8.81 (d, *J* = 4 Hz, 0H), 8.66 (t, *J* = 8 Hz, 0.06H), 8.10 (t, *J* = 8 Hz, 0.21H). (0.1426 mmol product and 0.1045 mmol 1,4-dioxane)

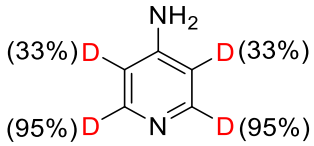

16b

According to GP, 0.5 wt.% Pd_1/TiO_2-h (50 mg), substrate (9.4 mg, 0.1 mmol), D_2O (2 mL), 410 nm LED (95 mW/cm^2), Ar (1 bar), r.t., 24 h. The product **16b** was obtained (Selectivity > 99%, detected by ^{1}H NMR).

Feed material 16a: ^{1}H NMR (400 MHz, $CDCl_3$) δ 8.20 (d, *J* = 4 Hz, 2H), 6.50 (d, *J* = 8 Hz, 2H), 4.21 (s, 2H).

Product 16b: ^{1}H NMR (400 MHz, $CDCl_3$) δ 8.20 (t, *J* = 4 Hz, 0.10H), 1.28 (s, 1.28H), 4.16 (s, 2H).

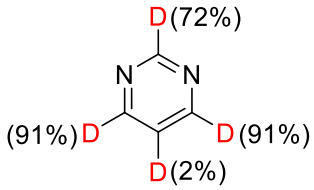

17b

According to GP, 0.5 wt.% Pd_1/TiO_2-h (50 mg), substrate (8.0 mg, 0.1 mmol), D_2O (2 mL), 410 nm LED (95 mW/cm^2), Ar (1 bar), r.t., 48 h. The product **17b** was obtained (Selectivity > 99%, detected by ^{1}H NMR).

Feed material 17a: ^{1}H NMR (400 MHz, D_2O) δ 9.17 (s, 1H), 8.85 (d, *J* = 4 Hz, 2H), 7.63 (td, *J* = 8, 4 Hz, 1H).

Product 17b: ^{1}H NMR (400 MHz, D_2O) δ 9.17 (s, 0.25H), 8.85 (d, *J* = 4 Hz, 0.16H), 7.63 (s, 0.92H).

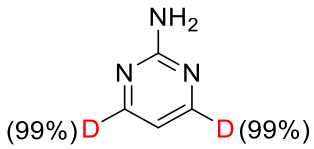

18b

According to GP, 0.5 wt.% Pd_1/TiO_2-h (50 mg), substrate (9.5 mg, 0.1 mmol), D_2O (2 mL), 410 nm LED (95 mW/cm^2), Ar (1 bar), r.t., 24 h. The product **18b** was obtained (Selectivity > 99%, detected by ^{1}H NMR).

Feed material 18a: ^{1}H NMR (400 MHz, D_2O) δ 8.30 (d, *J* = 8 Hz, 2H), 6.50 (t, *J* = 8 Hz, 1H).

Product 18b: ^{1}H NMR (400 MHz, D_2O) δ 8.30 (d, *J* = 4 Hz, 0.02H), 6.78 (s, 1H).

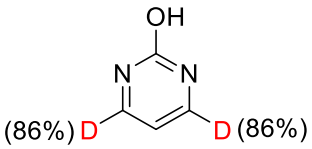

19b

According to GP, 0.5 wt.% Pd_1/TiO_2-h (50 mg), substrate (9.6 mg, 0.1 mmol), D_2O (2 mL), 410 nm LED (95 mW/cm^2), Ar (1 bar), r.t., 36 h. The product **19b** was obtained (Selectivity > 99%, detected by ^{1}H NMR).

Feed material 19a: ^{1}H NMR (400 MHz, D_2O) δ 8.40 (d, *J* = 8 Hz, 2H), 6.73 (t, *J* = 4 Hz, 1H).

Product 19b: ^{1}H NMR (400 MHz, D_2O) δ 8.39 (d, *J* = 4 Hz, 0.27H), 6.72 (s, 1H).

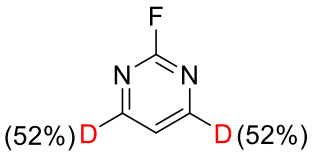

20b

According to GP, 0.5 wt.% Pd_1/TiO_2-h (50 mg), substrate (9.8 mg, 0.1 mmol), D_2O (2 mL), 410 nm LED (95 mW/cm^2), Ar (1 bar), r.t., 24 h. The product **20b** was obtained (Selectivity > 99%, detected by ^{1}H NMR).

Feed material 20a: ^{1}H NMR (400 MHz, D_2O) δ 8.76 (dd, *J* = 8, 4 Hz, 2H), 7.56 – 7.52 (m, 1H); ^{19}F NMR (376 MHz, D_2O) δ -47.27.

Product 20b: ^{1}H NMR (400 MHz, D_2O) δ 8.75 (dd, *J* = 8, 4 Hz, 0.94H), 7.53 (s, 1H); ^{19}F NMR (376 MHz, D_2O) δ -47.27.

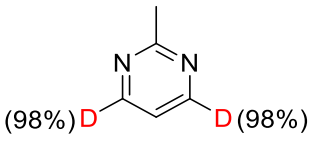

21b

According to GP, 2.0 wt.% Pd_1/TiO_2-h (50 mg), substrate (9.4 mg, 0.1 mmol), D_2O (2 mL), 410 nm LED (95 mW/cm^2), Ar (1 bar), r.t., 24 h. The product **21b** was obtained (Selectivity > 99%, detected by ^{1}H NMR).

Feed material 21a: ^{1}H NMR (400 MHz, D_2O) δ 8.61 (d, *J* = 4 Hz, 2H), 7.33 (t, *J* = 8 Hz, 1H), 2.60 (s, 3H).

Product 21b: ^{1}H NMR (400 MHz, D_2O) δ 8.69 (dd, *J* = 8 Hz, 0.04H), 7.39 (s, 1H), 2.68 (s, 3H).

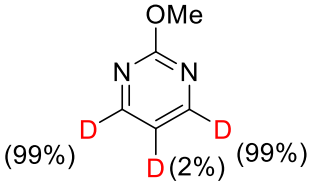

22b

According to GP, 2.0 wt.% Pd_1/TiO_2-h (50 mg), substrate (11.0 mg, 0.1 mmol), D_2O (2 mL), 410 nm LED (95 mW/cm^2), Ar (1 bar), 80 °C, 24 h. The product **22b** was obtained (Selectivity > 99%, detected by ^{1}H NMR).

Feed material 22a: ^{1}H NMR (400 MHz, D_2O) δ 8.54 (d, *J* = 4 Hz, 2H), 7.15 (t, *J* = 8 Hz, 1H), 3.97 (s, 3H).

Product 22b: ^{1}H NMR (400 MHz, D_2O) δ 8.60 (dd, *J* = 8 Hz, 0.01H), 7.20 (s, 0.87H), 4.03 (s, 3H).

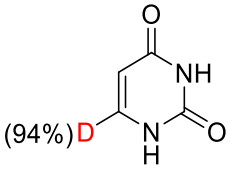

23b

According to GP, 0.5 wt.% Pd_1/TiO_2-h (50 mg), substrate (11.2 mg, 0.1 mmol), D_2O (2 mL), 410 nm LED (95 mW/cm^2), Ar (1 bar), 80 °C, 24 h. The product **23b** was obtained (Selectivity > 99%, detected by ^{1}H NMR).

Feed material 23a: ^{1}H NMR (400 MHz, D_2O) δ 7.53 (d, *J* = 8 Hz, 1H), 5.80 (d, *J* = 8 Hz, 1H).

Product 23b: ^{1}H NMR (400 MHz, D_2O) δ 7.54 (d, *J* = 8 Hz, 0.06H), 5.81 (s, 1H).

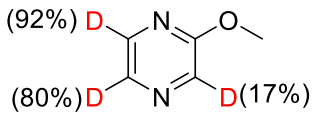

24b

According to GP, 0.5 wt.% Pd_1/TiO_2-h (50 mg), substrate (11.0 mg, 0.1 mmol), D_2O (2 mL), 410 nm LED (95 mW/cm^2), Ar (1 bar), r.t., 24 h. The product **24b** was obtained (Selectivity > 99%, detected by ^{1}H NMR).

Feed material 24a: ^{1}H NMR (400 MHz, D_2O) δ 8.26 (s, 1H), 8.18 - 8.17 (m, 1H), 8.17 (d, *J* = 4 Hz, 1H), 4.00 (s, 3H).

Product 24b: ^{1}H NMR (400 MHz, D_2O) δ 8.23 (s, 0.17H), 8.14 (s, 0.72H), 8.12 (d, *J* = 4 Hz, 0.07H), 3.95 (s, 3H).

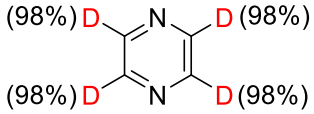

25b

According to GP, 1.0 wt.% Pd_1/TiO_2-h (50 mg), substrate (8.0 mg, 0.1 mmol), D_2O (2 mL), 410 nm LED (95 mW/cm^2), Ar (1 bar), r.t., 48 h. The product **25b** was obtained (Selectivity > 99%, detected by ^{1}H NMR).

Feed material 25a: ^{1}H NMR (400 MHz, D_2O) δ 8.62 (s, 4H).

Product 25b: ^{1}H NMR (400 MHz, D_2O) δ 8.62 (s, 0.09H).

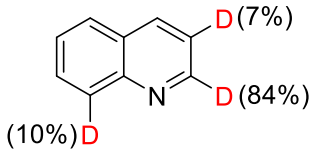

26b

According to GP, 0.5 wt.% Pd_1/TiO_2-h (50 mg), substrate (12.9 mg, 0.1 mmol), D_2O (2.0 mL), 410 nm LED (95 mW/cm^2), Ar (1 bar), r.t., 48 h. The product **26b** was obtained (Selectivity > 99%, detected by ^{1}H NMR).

Feed material 26a: ^{1}H NMR (400 MHz, DMSO-d_6) δ 8.91 (dd, *J* = 8, 4 Hz, 1H), 8.33 (d, *J* = 4 Hz, 1H), 8.04 (d, *J* = 4 Hz, 1H), 7.96 (d, *J* = 4 Hz, 1H), 7.77 – 7.73 (m, 1H), 7.61 – 7.57 (m, 1H), 7.51 (dd, *J* = 8, 4 Hz, 1H).

Product 26b: ^{1}H NMR (400 MHz, D_2O) δ 8.78 (dd, *J* = 8, 4 Hz, 0.15H), 8.33 (d, *J* = 8 Hz, 1H), 7.97 (d, *J* = 8 Hz, 0.87H), 7.92 (d, *J* = 8 Hz , 1H), 7.80 – 7.76 (m, 1H), 7.61 (t, *J* = 8 Hz, 1H), 7.50 (d, *J* = 8 Hz, 0.92H).

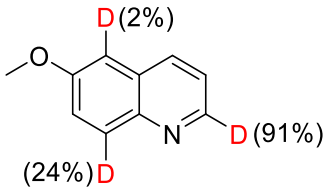

27b

According to GP, 0.5 wt.% Pd_1/TiO_2-h (50 mg), substrate (15.9 mg, 0.1 mmol), D_2O (1.6 mL), acetone (0.4 ml), 410 nm LED (95 mW/cm^2), Ar (1 bar), r.t., 48 h. The product **27b** was obtained (Selectivity > 99%, detected by ^{1}H NMR).

Feed material 27a: ^{1}H NMR (400 MHz, $CDCl_3$) δ 8.76 (dd, *J* = 8, 4 Hz, 1H), 8.03 (d, *J* = 8 Hz, 1H), 7.99 (d, *J* = 8 Hz, 1H), 7.37 – 7.32 (m, 2H), 7.05 (d, *J* = 4 Hz,1H), 3.91 (s, 3H).

Product 27b: ^{1}H NMR (400 MHz, $CDCl_3$) δ 8.78 (s, 0.08H), 8.07 (d, *J* = 8 Hz, 1H), 8.02 (d, *J* = 8 Hz, 0.71H), 7.39 – 7.36 (m, 2H), 7.08 (d, *J* = 4 Hz, 0.94H), 3.93 (s, 3H).

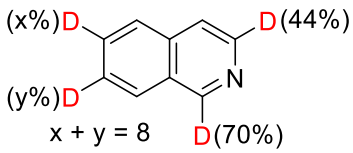

28b

According to GP, 0.5 wt.% Pd_1/TiO_2-h (50 mg), substrate (12.9 mg, 0.1 mmol), D_2O (2 mL), 410 nm LED (95 mW/cm^2), Ar (1 bar), 80 °C, 24 h. The product **28b** was obtained (Selectivity > 99%, detected by ^{1}H NMR).

Feed material 28a: ^{1}H NMR (400 MHz, D_2O) δ 9.11 (s, 1H), 8.33 (d, *J* = 8 Hz, 1H), 8.02 (d, *J* = 8 Hz, 1H), 7.89 (d, *J* = 12 Hz, 1H), 7.79 – 7.75 (m, 2H), 7.67 (t, *J* = 8 Hz, 1H).

Product 28b: ^{1}H NMR (400 MHz, D_2O) δ 9.17 (s, 0.29H), 8.37 (d, *J* = 8 Hz, 0.55H), 8.07 (d, *J* = 8 Hz, 1H), 7.93 (d, *J* = 8 Hz, 1H), 7.82 – 7.79 (m, 1.98H), 7.70 (t, *J* = 8 Hz, 1H).

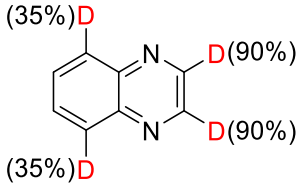

29b

According to GP, 0.5 wt.% Pd_1/TiO_2-h (50 mg), substrate (13.0 mg, 0.1 mmol), D_2O (2 mL), 410 nm LED (95 mW/cm^2), Ar (1 bar), 80 °C, 24 h. The product **29b** was obtained (Selectivity > 99%, detected by ^{1}H NMR).

Feed material 29a: ^{1}H NMR (400 MHz, D_2O) δ 8.35 (s, 2H), 7.46 – 7.37 (m, 4H).

Product 29b: ^{1}H NMR (400 MHz, D_2O) δ 8.73 (s, 0.19H), 7.91 – 7.86 (m, 1.31H), 7.80 – 7.77 (m, 2H).

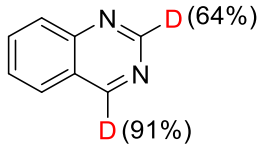

30b

According to GP, 0.5 wt.% Pd_1/TiO_2-h (50 mg), substrate (13.0 mg, 0.1 mmol), D_2O (2.0 mL), 410 nm LED (95 mW/cm^2), Ar (1 bar), r.t., 48 h. The product **30b** was obtained (Selectivity > 99%, detected by ^{1}H NMR).

Feed material 30a: ^{1}H NMR (400 MHz, D_2O) δ 9.24 (s, 1H), 8.95 (s, 1H), 7.94 – 7.88 (m, 2H), 7.76 (d, *J* = 12 Hz, 1H), 7.68 – 7.63 (m, 1H).

Product 30b: ^{1}H NMR (400 MHz, D_2O) δ 9.26 (s, 0.09H), 8.97 (s, 0.32H), 7.95 – 7.91 (m, 2H), 7.78 (d, *J* = 8 Hz, 1H), 7.68 – 7.64 (m, 1H).

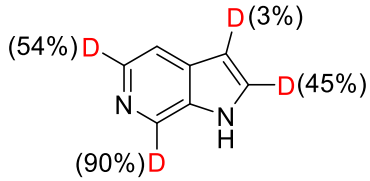

31b

According to GP, 0.5 wt.% Pd_1/TiO_2-h (50 mg), substrate (11.8 mg, 0.1 mmol), D_2O (1.6 mL), acetone (0.4 mL), 410 nm LED (95 mW/cm^2), Ar (1 bar), r.t., 24 h. The product **31b** was obtained (Selectivity > 99%, detected by ^{1}H NMR).

Feed material 31a: ^{1}H NMR (400 MHz, DMSO-d_6) δ 11.59 (s, 1H), 8.76 (s, 1H), 8.08 (d, *J* = 4 Hz, 1H), 7.59 (t, *J* = 4 Hz, 1H), 7.52 (dd, *J* = 8, 4 Hz, 1H), 6.50 (d, *J* = 4 Hz, 1H).

Product 31b: ^{1}H NMR (400 MHz, DMSO-d_6) δ 11.62 (s, 1H), 8.76 (s, 0.10H), 8.08 (d, *J* = 4 Hz, 0.48H), 7.61 (d, *J* = 4 Hz, 0.55H), 7.53 (t, *J* = 4 Hz, 1H), 6.51 (d, *J* = 4 Hz, 0.95H).

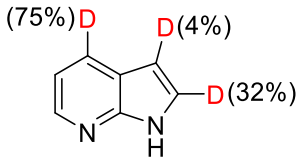

32b

According to GP, 0.5 wt.% Pd_1/TiO_2-h (50 mg), substrate (11.8 mg, 0.1 mmol), D_2O (1.6 mL), acetone (0.4 mL), 410 nm LED (95 mW/cm^2), Ar (1 bar), r.t., 24 h. The product **32b** was obtained (Selectivity > 99%, detected by ^{1}H NMR).

Feed material 32a: ^{1}H NMR (400 MHz, DMSO-d_6) δ 11.60 (s, 1H), 8.20 (dd, *J* = 8, 4 Hz, 1H), 7.94 (dd, *J* = 8, 4 Hz, 1H), 7.46 (d, *J* = 4 Hz, 1H), 7.04 (dd, *J* = 8, 8 Hz, 1H), 6.44 (d, *J* = 4 Hz, 1H).

Product 32b: ^{1}H NMR (400 MHz, DMSO-d_6) δ 11.60 (s, 1H), 8.20 (dd, *J* = 4, 4 Hz, 0.24H), 7.94 (d, *J* = 8 Hz, 1H), 7.46 – 7.44 (m, 0.67H), 7.04 (dt, *J* = 8, 4 Hz, 1H), 6.44 – 6.43 (m, 0.92H).

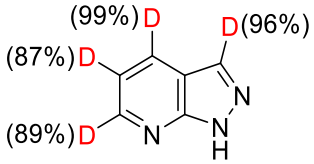

33b

According to GP, 0.5 wt.% Pd_1/TiO_2-h (50 mg), substrate (11.9 mg, 0.1 mmol), D_2O (1.6 mL), acetone (0.4 mL), 410 nm LED (95 mW/cm^2), Ar (1 bar), 80 °C, 24 h. The product **33b** was obtained (Selectivity > 99%, detected by ^{1}H NMR).

Feed material 33a: ^{1}H NMR (400 MHz, $CDCl_3$) δ 8.65 (d, *J* = 4 Hz, 1H), 8.16 (d, *J* = 8 Hz, 1H), 8.13 (s, 1H), 7.20 (dd, *J* = 8, 4 Hz, 1H).

Product 33b: ^{1}H NMR (400 MHz, $CDCl_3$) δ 8.59 (s, 0.01H), 8.13 (d, *J* = 8 Hz, 0.1H), 8.10 (s, 0.03H), 7.17 (d, *J* = 8 Hz, 0.12H). (0.0878 mmol product and 0.10 mmol 1,4-dioxane)

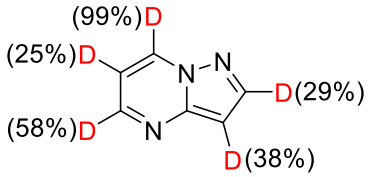

34b

According to GP, 0.5 wt.% Pd_1/TiO_2-h (50 mg), substrate (11.9 mg, 0.1 mmol), D_2O (1.6 mL), acetone (0.4 mL), 410 nm LED (95 mW/cm^2), Ar (1 bar), r.t., 24 h. The product **34b** was obtained (Selectivity > 99%, detected by ^{1}H NMR).

Feed material 34a: ^{1}H NMR (400 MHz, $CDCl_3$) δ 8.69 (d, *J* = 8 Hz, 1H), 8.49 – 8.48 (m, 1H), 8.14 (d, *J* = 4 Hz, 1H), 6.83 – 6.80 (m, 1H), 6.72 (d, *J* = 4 Hz, 1H).

Product 34b: ^{1}H NMR (400 MHz, $CDCl_3$) δ 8.70 (s, 0.01H), 8.49 (d, *J* = 4 Hz, 0.28H), 8.13 (s, 0.48H), 6.81 (s, 0.50H), 6.71 (d, *J* = 4 Hz, 0.40H). (0.0677 mmol product and 0.099 mmol 1,4-dioxane)

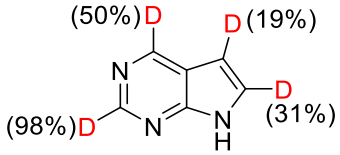

35b

According to GP, 0.5 wt.% Pd_1/TiO_2-h (50 mg), substrate (11.9 mg, 0.1 mmol), D_2O (1.6 mL), acetone (0.4 mL), 410 nm LED (95 mW/cm^2), Ar (1 bar), r.t., 24 h. The product **35b** was obtained (Selectivity > 99%, detected by ^{1}H NMR).

Feed material 35a: ^{1}H NMR (400 MHz, $CDCl_3$) δ 10.52 (s, 1H), 9.05 (s, 1H), 8.93 (s, 1H), 7.39 (t, *J* = 4 Hz, 1H), 6.64 – 6.62 (m, 1H).

Product 35b: ^{1}H NMR (400 MHz, $CDCl_3$) δ 11.20 (s, 0.60H), 9.03 (s, 0.02H), 8.92 (s, 0.41H), 7.40 – 7.39 (m, 0.58H), 6.62 – 6.61 (m, 0.68H). (0.0837 mmol product and 0.098 mmol 1,4-dioxane)

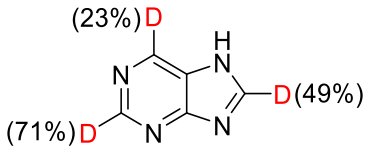

36b

According to GP, 0.5 wt.% Pd_1/TiO_2-h (50 mg), substrate (12.0 mg, 0.1 mmol), D_2O (2.0 mL), 410 nm LED (95 mW/cm^2), Ar (1 bar), r.t., 36 h. The product **36b** was obtained (Selectivity > 99%, detected by ^{1}H NMR).

Feed material 36a: ^{1}H NMR (400 MHz, D_2O) δ 9.10 (s, 1H), 8.93 (s, 1H), 8.58 (s, 1H).

Product 36b: ^{1}H NMR (400 MHz, D_2O) δ 9.11 (s, 0.29H), 8.93 (s, 0.75H), 8.58 (s, 0.49H).

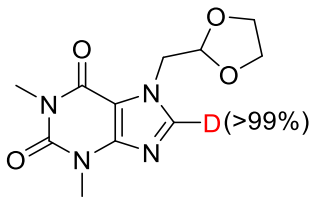

37b

According to GP, 0.5 wt.% Pd_1/TiO_2-h (50 mg), substrate (26.6 mg, 0.1 mmol), D_2O (2.0 mL), 410 nm LED (95 mW/cm^2), Ar (1 bar), r.t., 24 h. The product **37b** was obtained (Selectivity > 99%, detected by ^{1}H NMR).

Feed material 37a: ^{1}H NMR (400 MHz, D_2O) δ 8.00 (s, 1H), 5.34 (t, *J* = 4 Hz,1H), 4.60 (d, *J* = 4 Hz, 2H), 3.92 – 3.89 (m, 2H), 3.78 – 3.74 (m, 2H), 3.53 (s, 3H), 3.34 (s, 3H).

Product 37b: ^{1}H NMR (400 MHz, D_2O) δ 7.98 (s, 0.00H), 5.32 (t, *J* = 4 Hz,1H), 4.58 (d, *J* = 4 Hz, 2H), 3.91 – 3.87 (m, 2H), 3.76 – 3.73 (m, 2H), 3.51 (s, 3H), 3.32 (s, 3H).

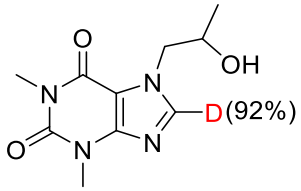

38b

According to GP, 0.5 wt.% Pd_1/TiO_2-h (50 mg), substrate (23.8 mg, 0.1 mmol), D_2O (2.0 mL), 410 nm LED (95 mW/cm^2), Ar (1 bar), r.t., 24 h. The product **38b** was obtained (Selectivity > 99%, detected by ^{1}H NMR).

Feed material 38a: ^{1}H NMR (400 MHz, D_2O) δ 7.93 (s, 1H), 4.37 – 4.31 (m, 1H), 4.17 – 4.07 (m, 2H), 3.45 (s, 3H), 3.26 (s, 3H), 1.21 (d, *J* = 4 Hz, 3H).

Product 38b: ^{1}H NMR (400 MHz, D_2O) δ 7.94 (s, 0.09H), 4.42 – 4.33 (m, 1H), 4.20 – 4.10 (m, 2H), 3.49 (s, 3H), 3.30 (s, 3H), 1.22 (d, *J* = 4 Hz, 3H).

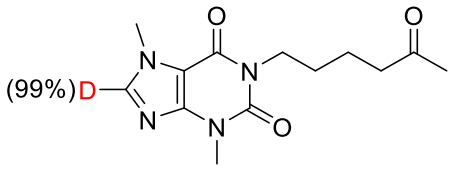

39b

According to GP, 0.5 wt.% Pd_1/TiO_2-h (50 mg), substrate (27.8 mg, 0.1 mmol), D_2O (2.0 mL), 410 nm LED (95 mW/cm^2), Ar (1 bar), r.t., 24 h. The product **39b** was obtained (Selectivity > 99%, detected by ^{1}H NMR).

Feed material 39a: ^{1}H NMR (400 MHz, D_2O) δ 7.88 (s, 1H), 3.92 (s, 3H), 3.89 (t, *J* = 8 Hz, 2H), 3.47 (s, 3H), 2.62 (t, *J* = 8 Hz, 2H), 2.21 (s, 3H), 1.58 – 1.55 (m, 4H).

Product 39b: ^{1}H NMR (400 MHz, D_2O) δ 7.86 (s, 0.01H), 3.89 (s, 3H), 3.86 (t, *J* = 8 Hz, 2H), 3.43 (s, 3H), 2.60 (t, *J* = 8 Hz, 2H), 2.19 (s, 3H), 1.55 – 1.52 (m, 4H).

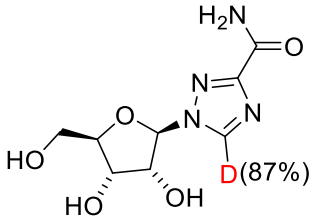

40b

According to GP, 0.5 wt.% Pd_1/TiO_2-h (50 mg), substrate (24.4 mg, 0.1 mmol), D_2O (2.0 mL), 410 nm LED (95 mW/cm^2), Ar (1 bar), r.t., 24 h. The product **40b** was obtained (Selectivity > 99%, detected by ^{1}H NMR).

Feed material 40a: ^{1}H NMR (400 MHz, D_2O) δ 8.76 (s, 1H), 6.08 (d, *J* = 4 Hz, 1H), 4.67 (dd, *J* = 8, 4 Hz, 1H), 4.51 (t, *J* = 4 Hz, 1H), 4.24 (td, *J* = 8, 4 Hz, 1H), 3.89 (dd, *J* = 12, 4 Hz, 1H), 3.78 (dd, *J* = 16, 8 Hz, 1H).

Product 40b: ^{1}H NMR (400 MHz, D_2O) δ 8.78 (s, 0.11H), 6.10 (d, *J* = 4 Hz, 1H), 4.69 (dd, *J* = 8, 4 Hz, 1H), 4.53 (t, *J* = 8 Hz, 1H), 4.26 (td, *J* = 8, 4 Hz, 1H), 3.91 (dd, *J* = 12, 8 Hz, 1H), 3.80 (dd, *J* = 12, 8 Hz, 1H).

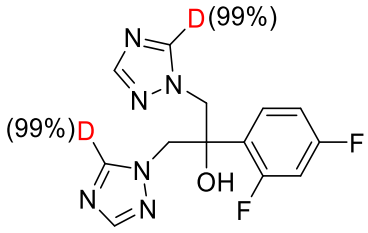

41b

According to GP, 0.5 wt.% Pd_1/TiO_2-h (50 mg), substrate (30.6 mg, 0.1 mmol), D_2O (1.6 mL), MeOH (0.4mL), 410 nm LED (95 mW/cm^2), Ar (1 bar), 80 °C, 48 h. The product **41b** was obtained (Selectivity > 99%, detected by ^{1}H NMR).

Feed material 41a: ^{1}H NMR (400 MHz, DMSO-d_6) δ 8.32 (s, 2H), 7.80 (s, 2H), 7.24 – 7.13 (m, 2H), 6.88 (td, *J* = 12, 4 Hz, 1H), 6.35 (s, 1H), 4.73 (d, *J* = 16 Hz, 2H), 4.56 (d, *J* = 12 Hz, 2H).

Product 41b: ^{1}H NMR (400 MHz, DMSO-d_6) δ 8.32 (s, 0.02H), 7.79 (s, 2H), 7.24 – 7.13 (m, 2H), 6.88 (td, *J* = 8, 4 Hz, 1H), 6.36 (s, 1H), 4.73 (d, *J* = 16 Hz, 2H), 4.56 (d, *J* = 12 Hz, 2H).

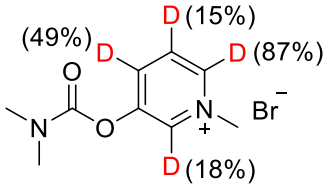

42b

According to GP, 2.0 wt.% Pd_1/TiO_2-h (50 mg), substrate (26.1 mg, 0.1 mmol), D_2O (2.0 mL), 410 nm LED (95 mW/cm^2), Ar (1 bar), 80 ^{o}C, 24 h. The product **42b** was obtained (Selectivity > 99%, detected by ^{1}H NMR).

Feed material 42a: ^{1}H NMR (400 MHz, D_2O) δ 8.89 (s, 1H), 8.75 (d, *J* = 4 Hz, 1H), 8.43 (dd, *J* = 8, 4 Hz, 1H), 8.13 (dd, *J* = 8, 4 Hz, 1H), 4.47 (s, 3H), 3.20 (s, 3H), 3.07 (s, 3H).

Product 42b: ^{1}H NMR (400 MHz, D_2O) δ 8.88 (d, *J* = 4 Hz, 0.80H), 8.75 (s, 0.13H), 8.44 – 8.42 (m, 0.83H), 8.12 (d, *J* = 8 Hz, 0.52H), 4.46 (s, 3H), 3.19 (s, 3H), 3.06 (s, 3H).

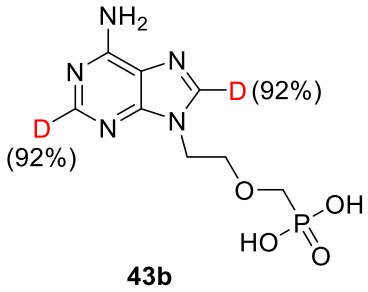

43b

According to GP, 2.0 wt.% Pd_1/TiO_2-h (50 mg), substrate (27.3 mg, 0.1 mmol), D_2O (2.0 mL), 410 nm LED (95 mW/cm^2), Ar (1 bar), 80 ^{o}C, 24 h. The product **43b** was obtained (Selectivity > 99%, detected by ^{1}H NMR).

Feed material 43a: ^{1}H NMR (400 MHz, D_2O) δ 8.46 (d, *J* = 4 Hz, 2H), 4.57 (t, *J* = 4 Hz, 2H), 4.03 (t, *J* = 4 Hz, 2H), 3.68 (d, *J* = 8 Hz, 2H).

Product 43b: ^{1}H NMR (400 MHz, D_2O) δ 8.22 (s, 0.15H), 4.44 (t, *J* = 4 Hz, 2H), 3.97 (t, *J* = 4 Hz, 2H), 3.51 (d, *J* = 8 Hz, 2H).

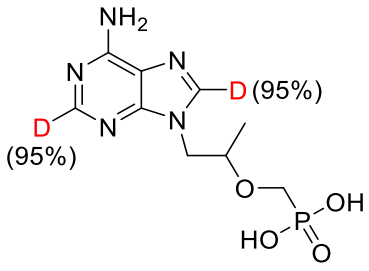

44b

According to GP, 2.0 wt.% Pd_1/TiO_2-h (50 mg), substrate (28.7 mg, 0.1 mmol), D_2O (2.0 mL), 410 nm LED (95 mW/cm^2), Ar (1 bar), 80 °C, 24 h. The product **44b** was obtained (Selectivity > 99%, detected by ^{1}H NMR).

Feed material 44a: ^{1}H NMR (400 MHz, D_2O) δ 8.45 (d, *J* = 4 Hz, 2H), 4.55 – 4.51 (m, 1H), 4.37 – 4.32 (m, 1H), 4.05 – 4.01 (m, 1H), 3.75 – 3.69 (m, 1H), 3.55 – 3.49 (m, 1H), 1.23 (d, *J* = 4 Hz, 3H).

Product 44b: ^{1}H NMR (400 MHz, D_2O) δ 8.43 (d, *J* = 4 Hz, 0.09H), 4.54 – 4.50 (m, 1H), 4.36 – 4.31 (m, 1H), 4.07 – 3.99 (m, 1H), 3.74 – 3.69 (m, 1H), 3.55 – 3.49 (m, 1H), 1.22 (d, *J* = 8 Hz, 3H).

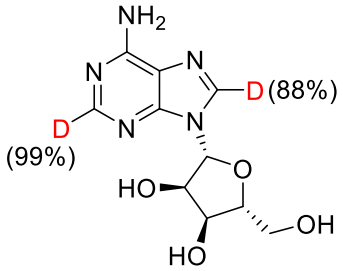

45b

According to GP, 2.0 wt.% Pd_1/TiO_2-h (50 mg), substrate (26.7 mg, 0.1 mmol), D_2O (2.0 mL), 410 nm LED (95 mW/cm^2), Ar (1 bar), 80 °C, 24 h. The product **45b** was obtained (Selectivity > 99%, detected by ^{1}H NMR).

Feed material 45a: ^{1}H NMR (400 MHz, D_2O) δ 8.34 (s, 1H), 8.24 (s, 1H), 6.08 (d, *J* = 8 Hz, 1H), 4.82 (d, *J* = 8 Hz, 1H), 4.46 – 4.44 (m, 1H), 4.32 (q, *J* = 8, 4 Hz, 1H), 3.94 (dd, *J* = 12, 4 Hz, 1H), 3.86 (dd, *J* = 16, 4 Hz, 1H).

Product 45b: ^{1}H NMR (400 MHz, D_2O) δ 8.32 (s, 0.01H), 8.21 (s, 0.10H), 6.06 (d, *J* = 8 Hz, 1H), 4.81 (s, 1H), 4.45 – 4.43 (m, 1H), 4.31 (q, *J* = 8, 4 Hz, 1H), 3.94 (dd, *J* = 12, 4 Hz, 1H), 3.85 (dd, *J* = 12, 4 Hz, 1H).

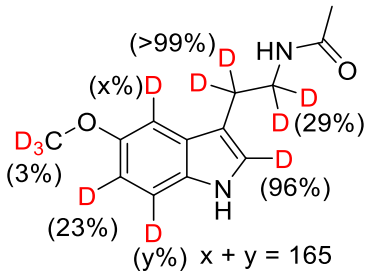

46b

According to GP, 2.0 wt.% Pd_1/TiO_2-h (50 mg), substrate (23.2 mg, 0.1 mmol), D_2O (2.0 mL), 410 nm LED (95 mW/cm^2), Ar (1 bar), 80 ^{o}C, 24 h. The product **46b** was obtained (Selectivity > 99%, detected by ^{1}H NMR).

Feed material 46a: ^{1}H NMR (400 MHz, D_2O) δ 7.45 (d, *J* = 8 Hz, 1H), 7.25 (t, *J* = 4 Hz, 2H), 6.99 (dd, *J* = 8, 4 Hz, 1H), 3.92 (s, 3H), 3.50 (t, *J* = 8 Hz, 2H), 2.97 (t, *J* = 8 Hz, 2H), 1.92 (s, 3H).

Product 46b: ^{1}H NMR (400 MHz, D_2O) δ 7.44 (d, *J* = 8 Hz, 0.04H), 7.23 (d, *J* = 4 Hz, 0.35H), 6.93 (s, 0.79H), 3.91 (s, 3.01H), 3.47 (s, 1.51H), 2.93 (s, 0.01H), 1.92 (s, 3H).

9. ^{1}H NMR, ^{13}C NMR and ^{19}F NMR spectra for substrates and products

^{1}H NMR (400 MHz, D_2O) of feed material **1a**

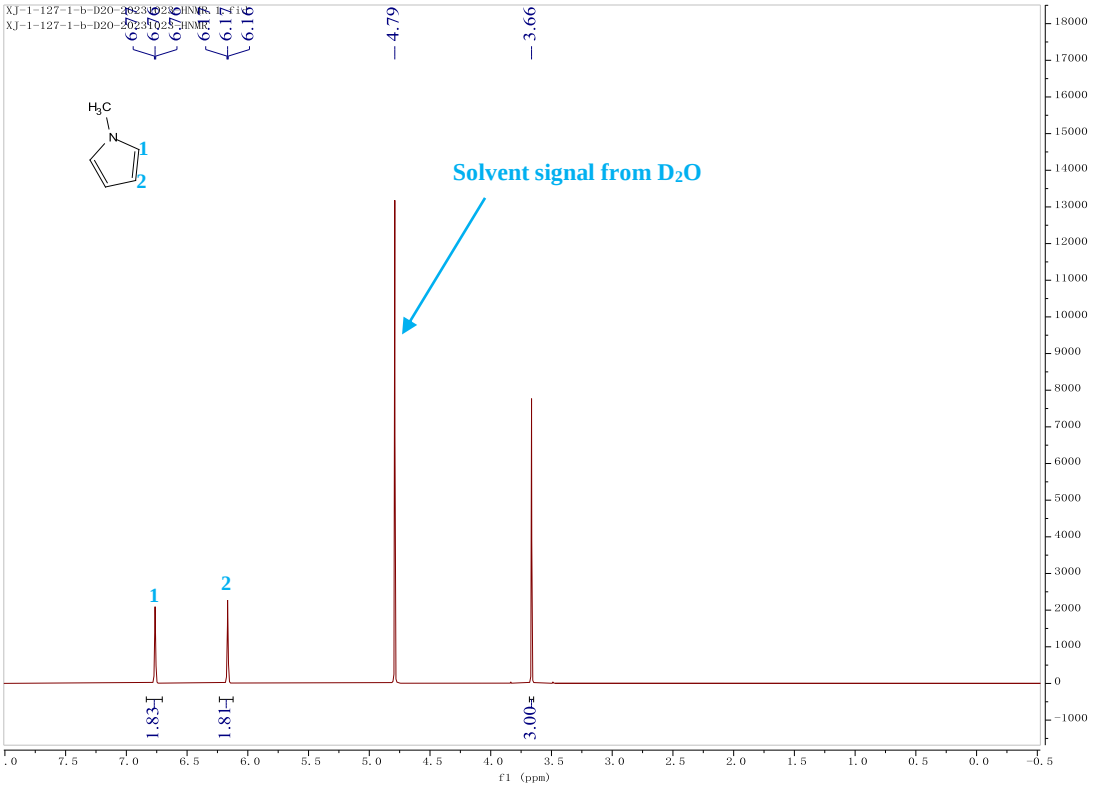

^{1}H NMR (400 MHz, D_2O) of product **1b**

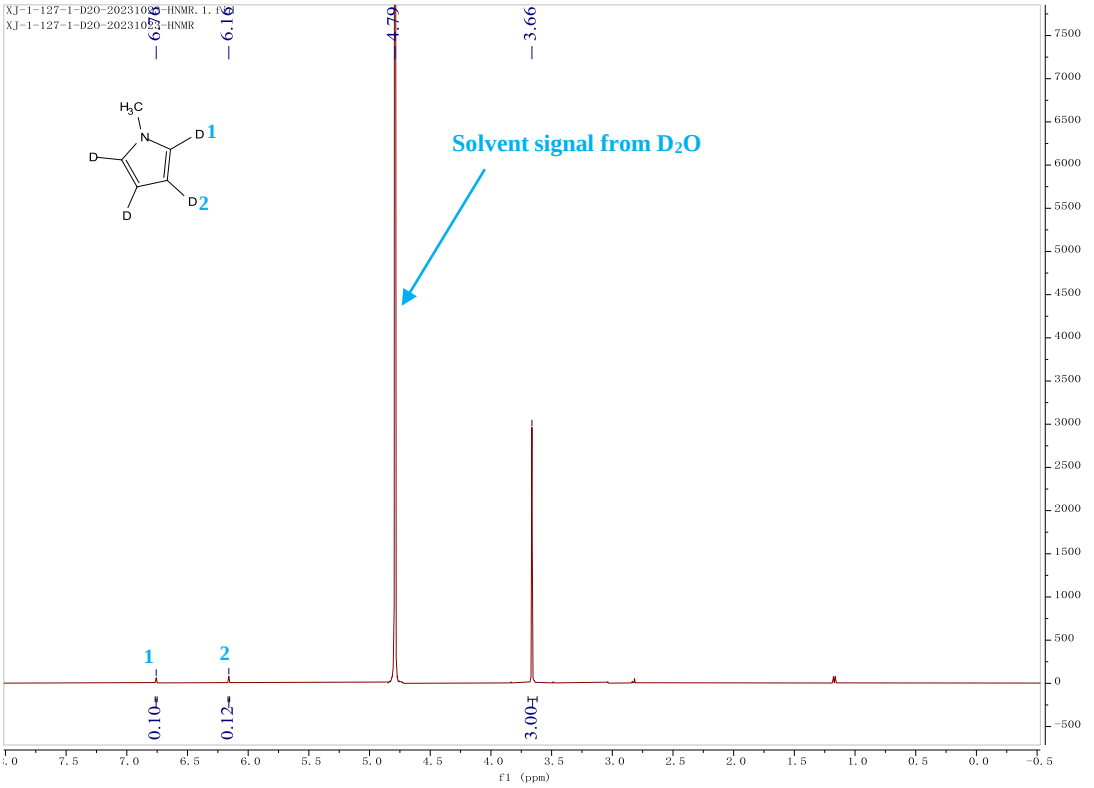

^{1}H NMR (400 MHz, $CDCl_3$) of feed material **2a**

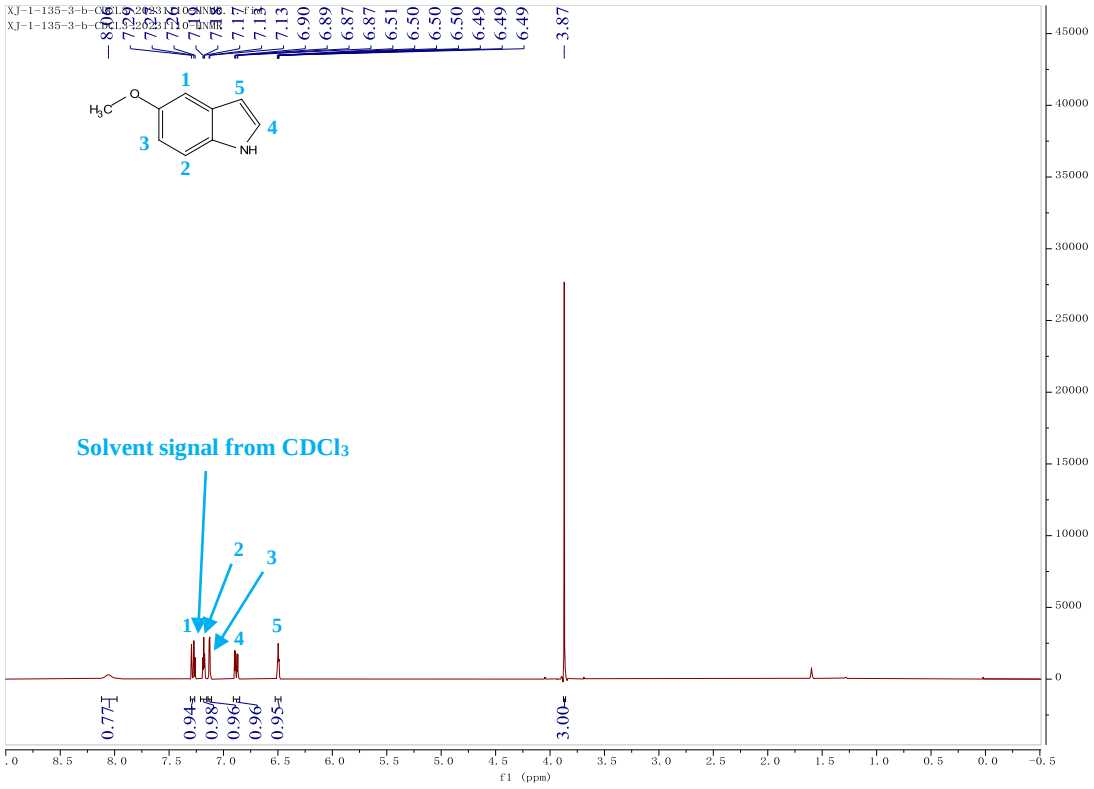

^{1}H NMR (400 MHz, $CDCl_3$) of product **2b**

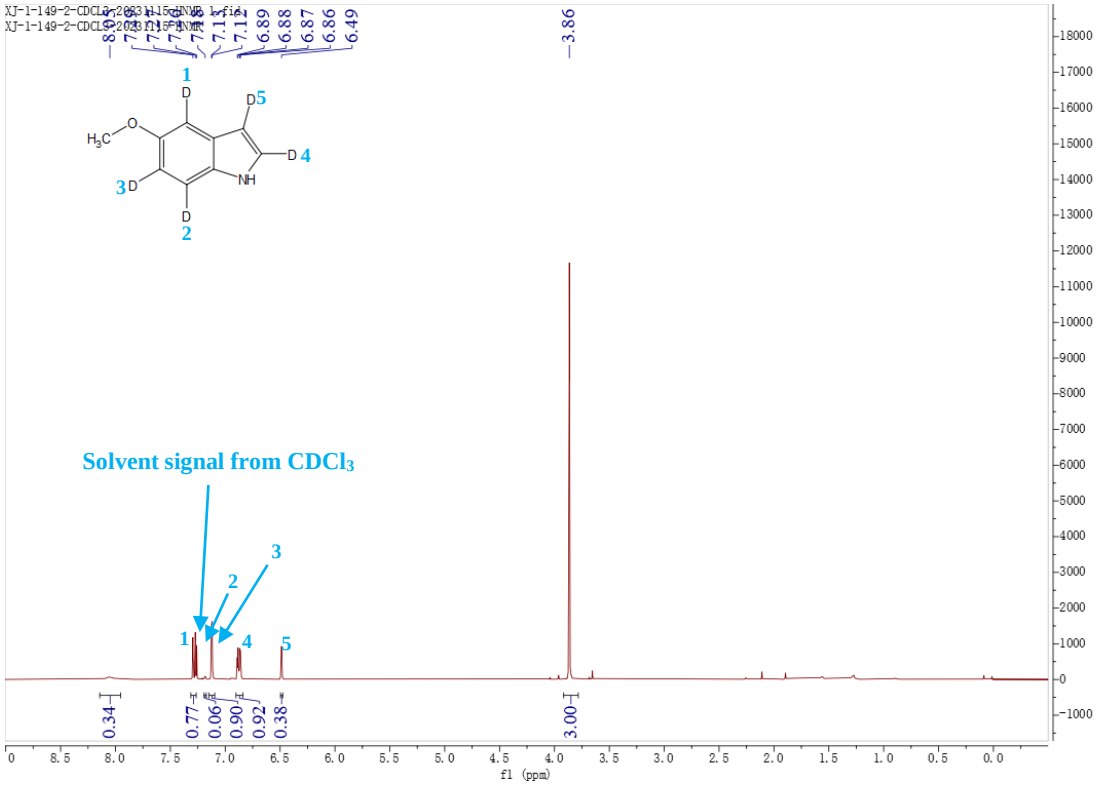

^{1}H NMR (400 MHz, D_2O) of feed material **3a**

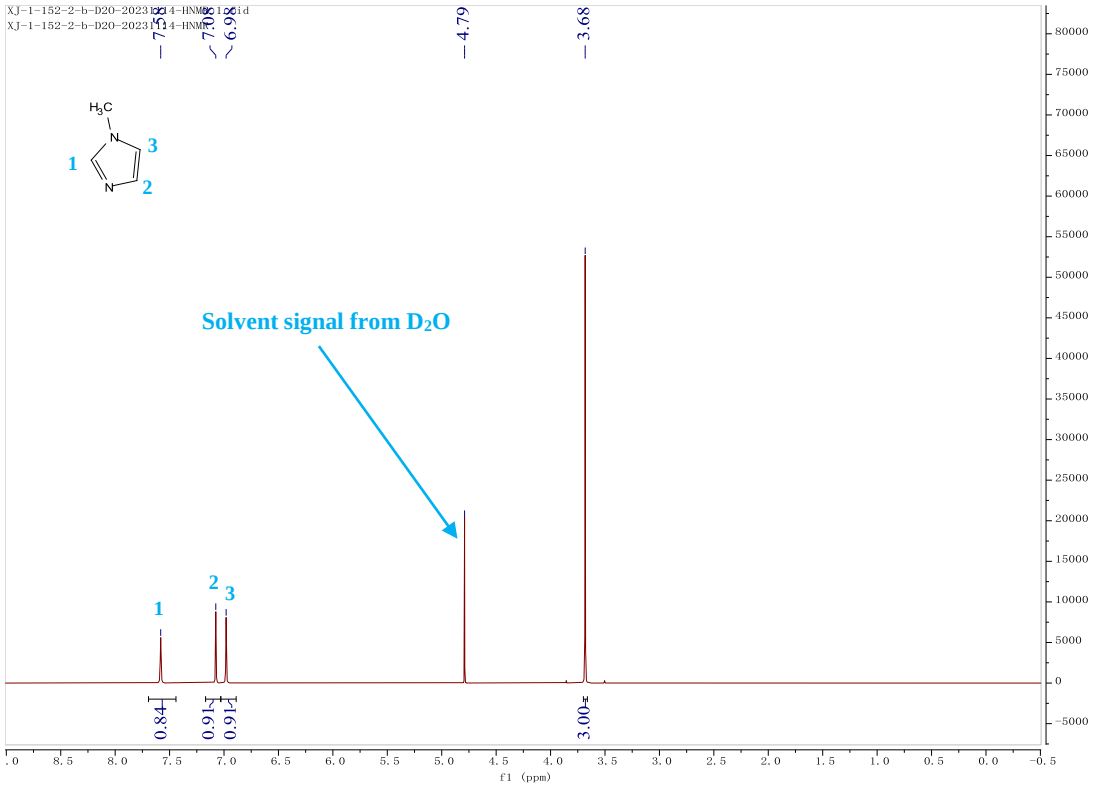

^{1}H NMR (400 MHz, D_2O) of product **3b**

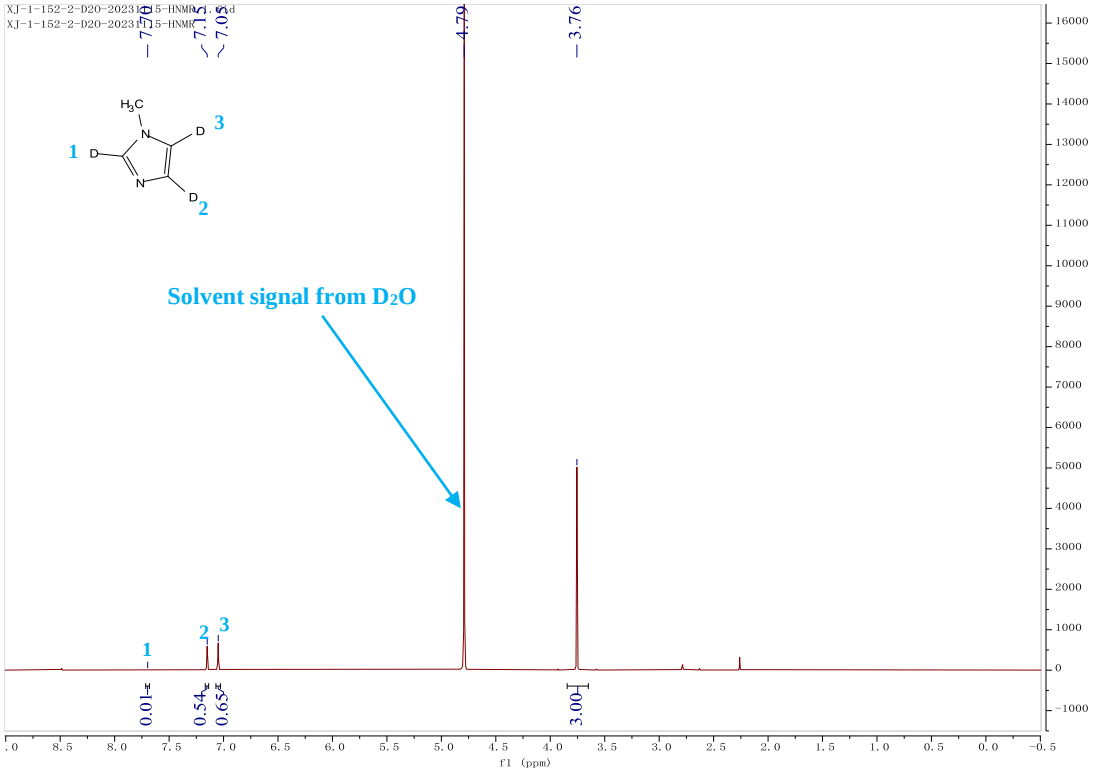

^{1}H NMR (400 MHz, D_2O) of feed material **4a**

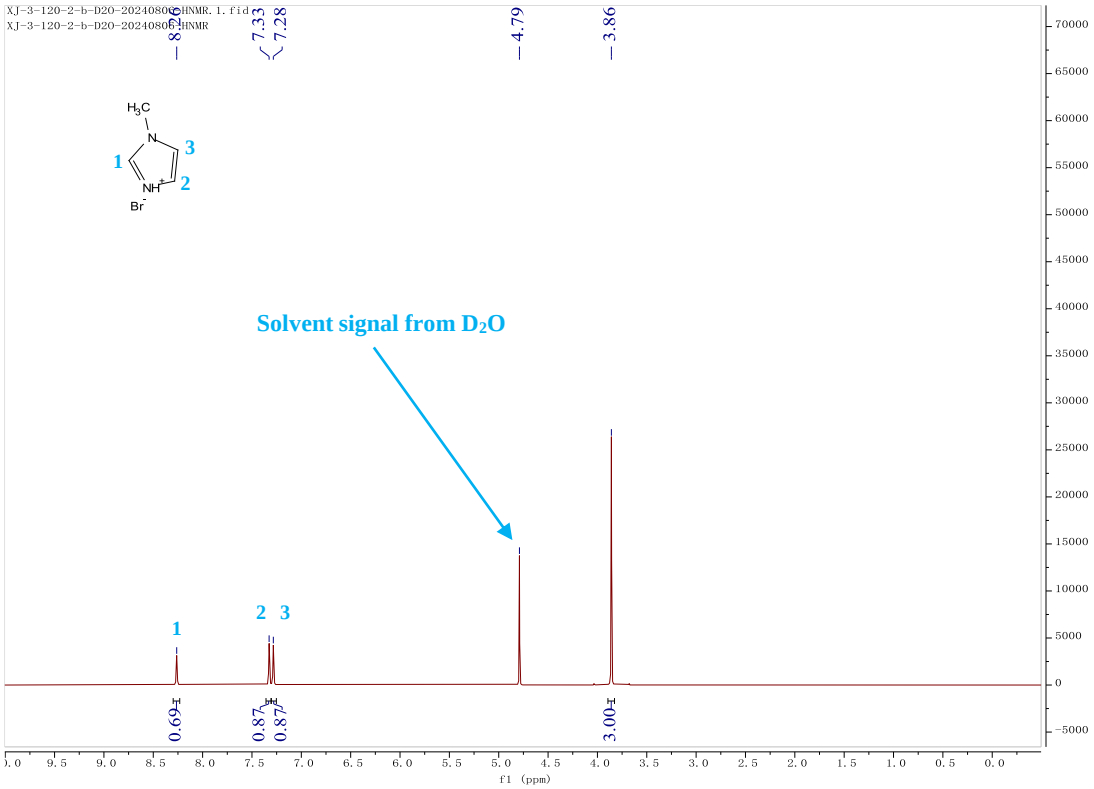

^{1}H NMR (400 MHz, D_2O) of product **4b**

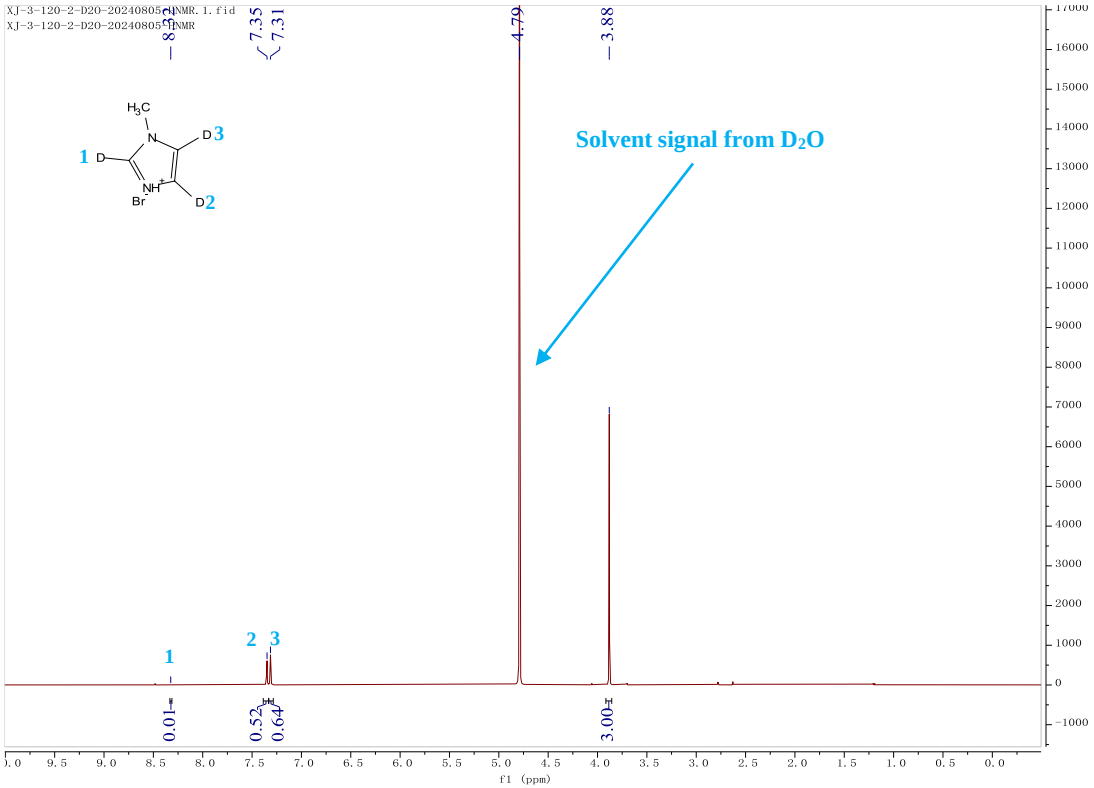

^{1}H NMR (400 MHz, $CDCl_3$) of feed material **5a**

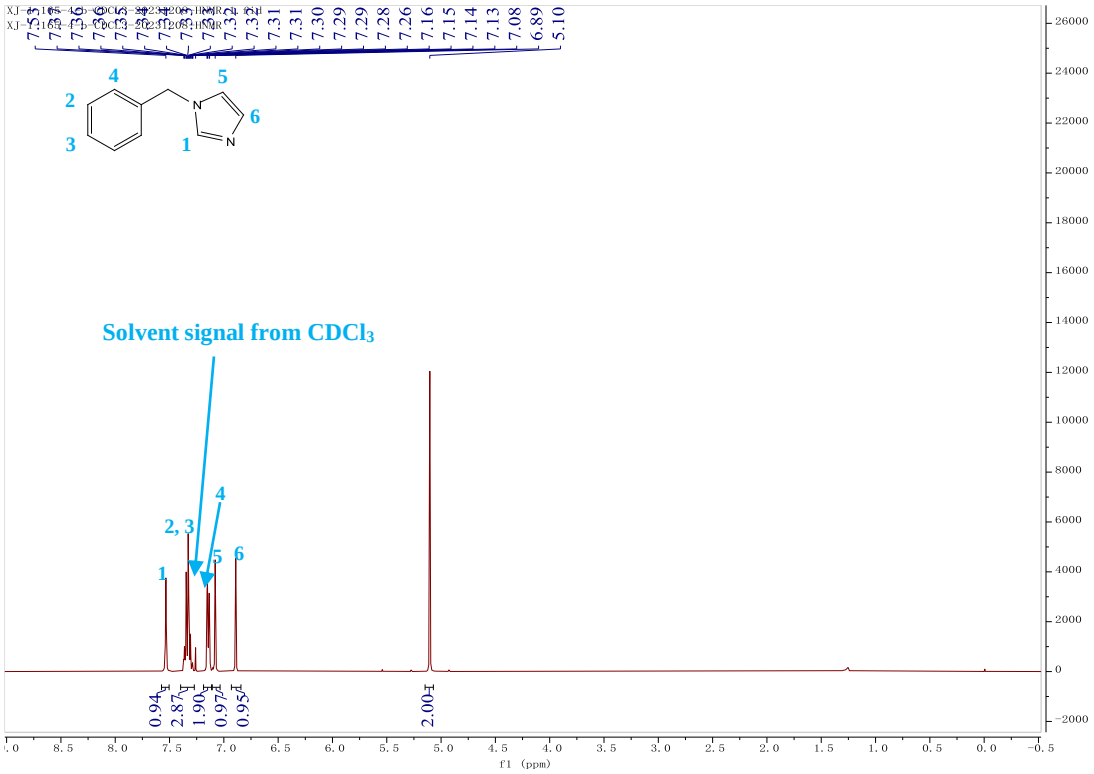

^{1}H NMR (400 MHz, $CDCl_3$) of product **5b**

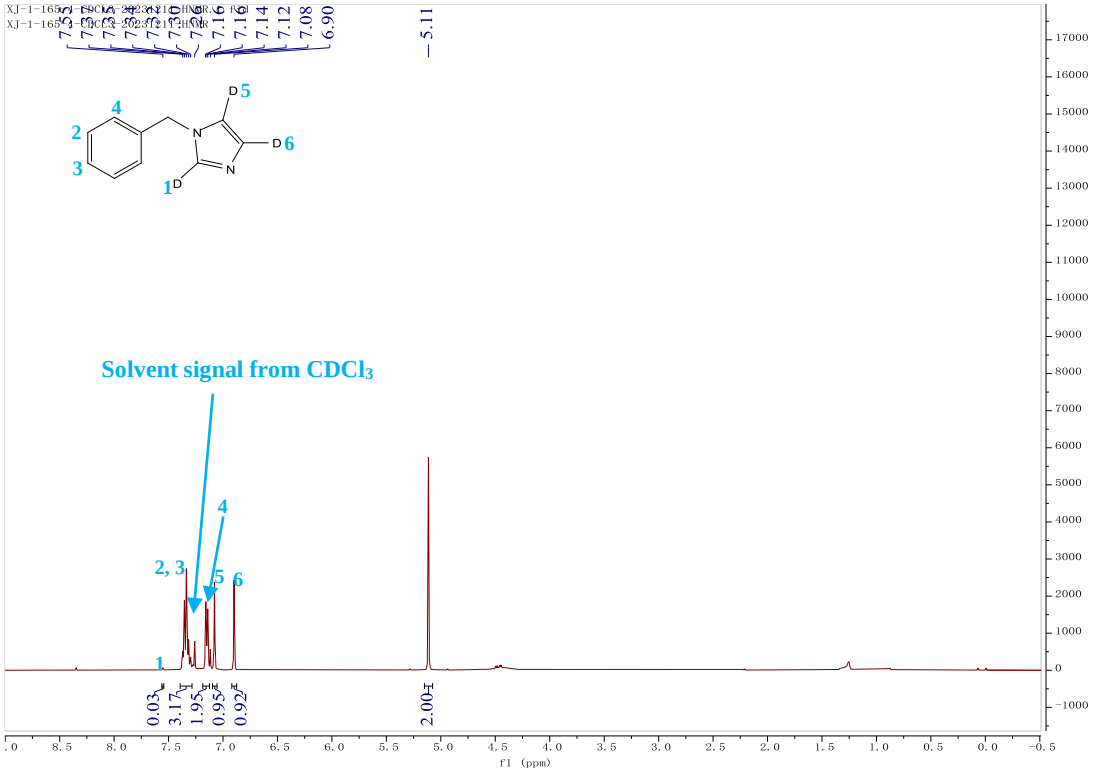

^{1}H NMR (400 MHz, DMSO-d_6) of feed material **6a**

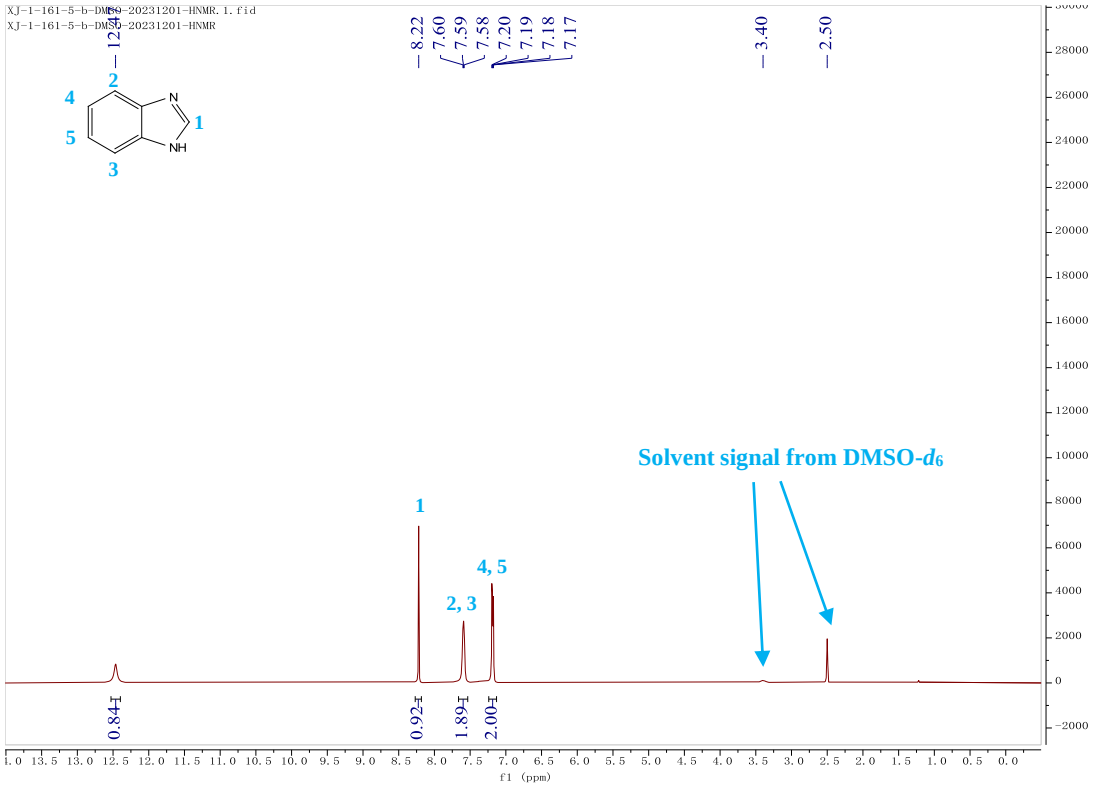

^{1}H NMR (400 MHz, DMSO-d_6) of product **6b**

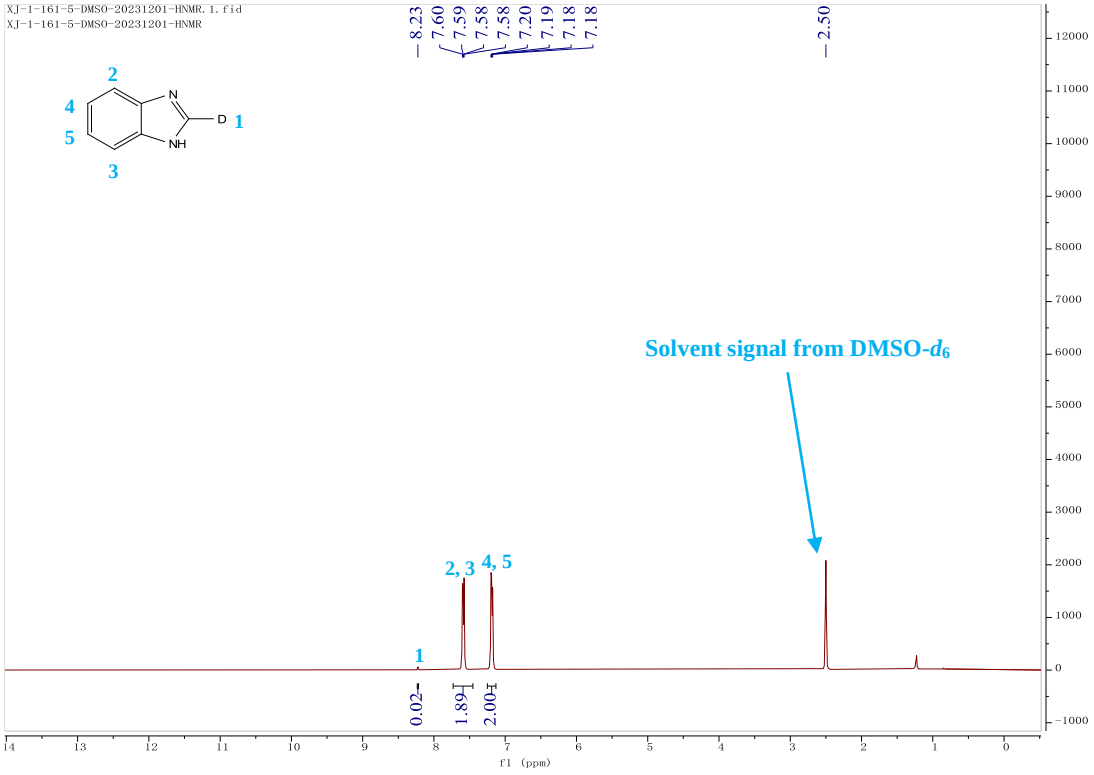

^{1}H NMR (400 MHz, $CDCl_3$) of feed material**7a**

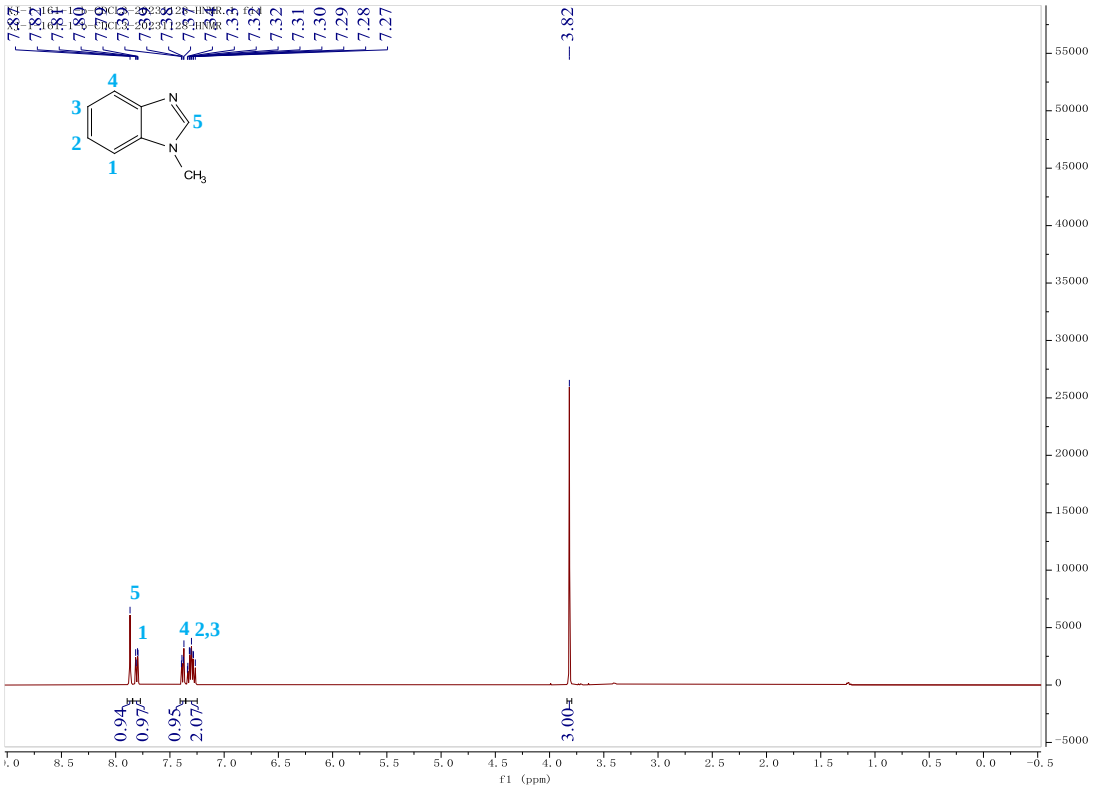

^{1}H NMR (400 MHz, $CDCl_3$) of product **7b**

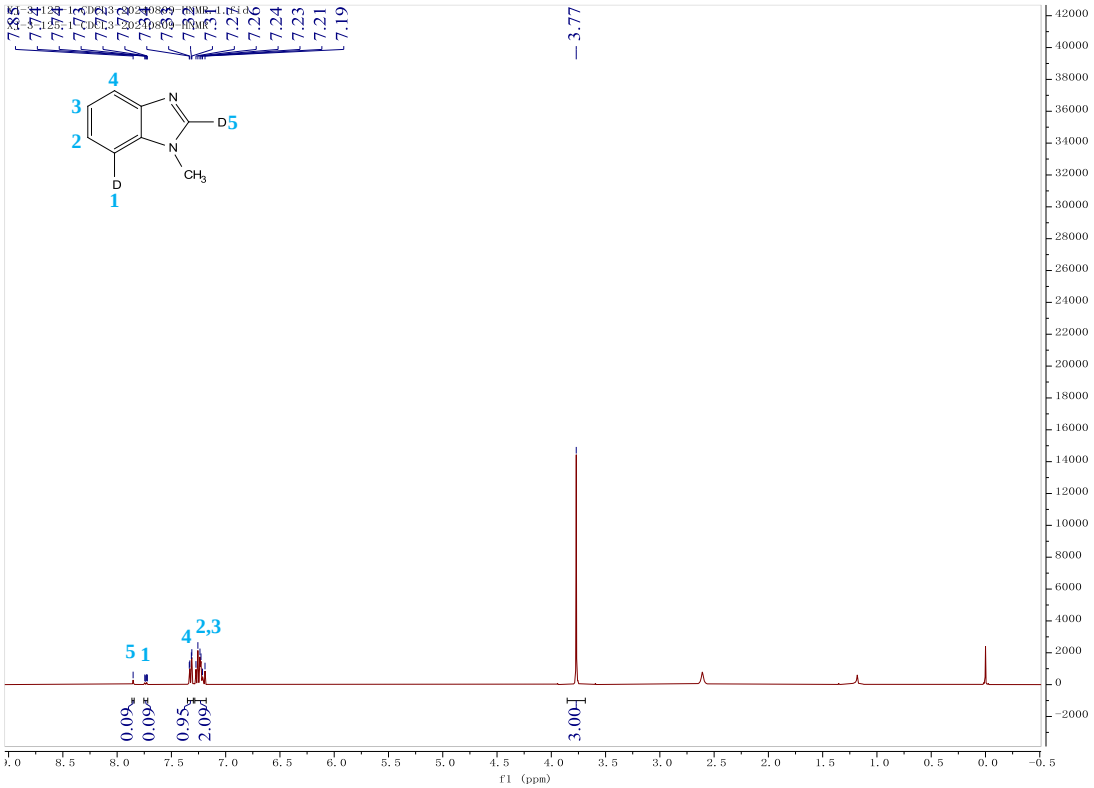

^{1}H NMR (400 MHz, $CDCl_3$) of feed material **8a**

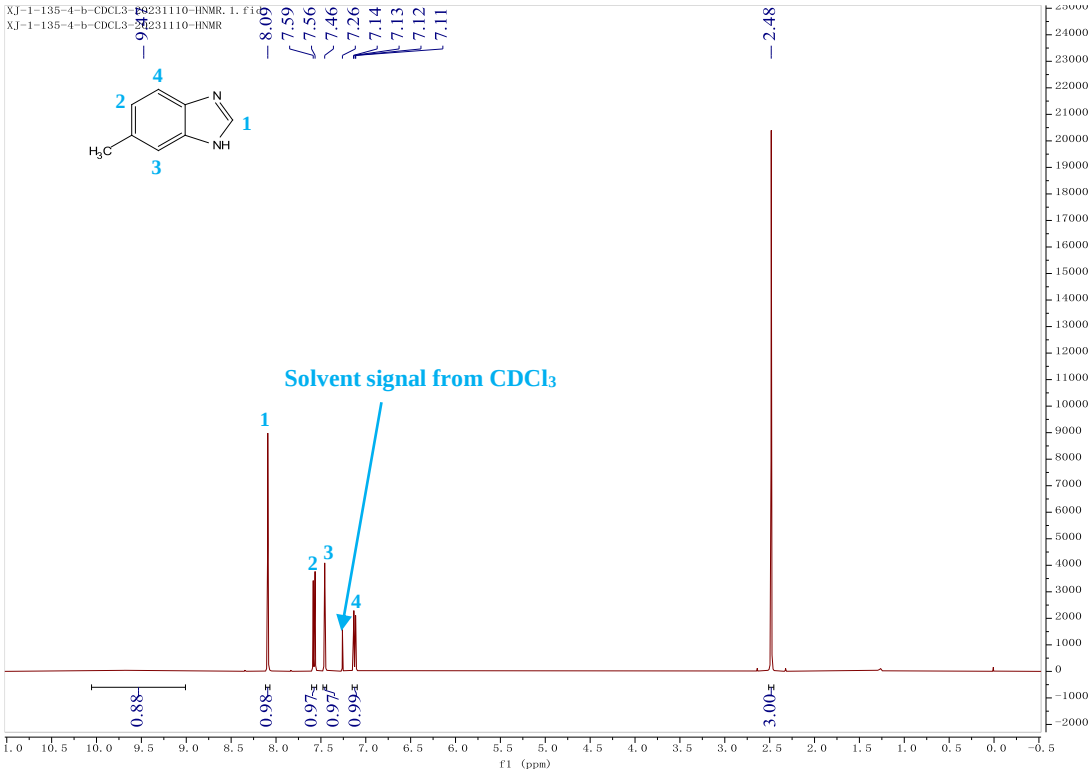

^{1}H NMR (400 MHz, $CDCl_3$) of product **8b**

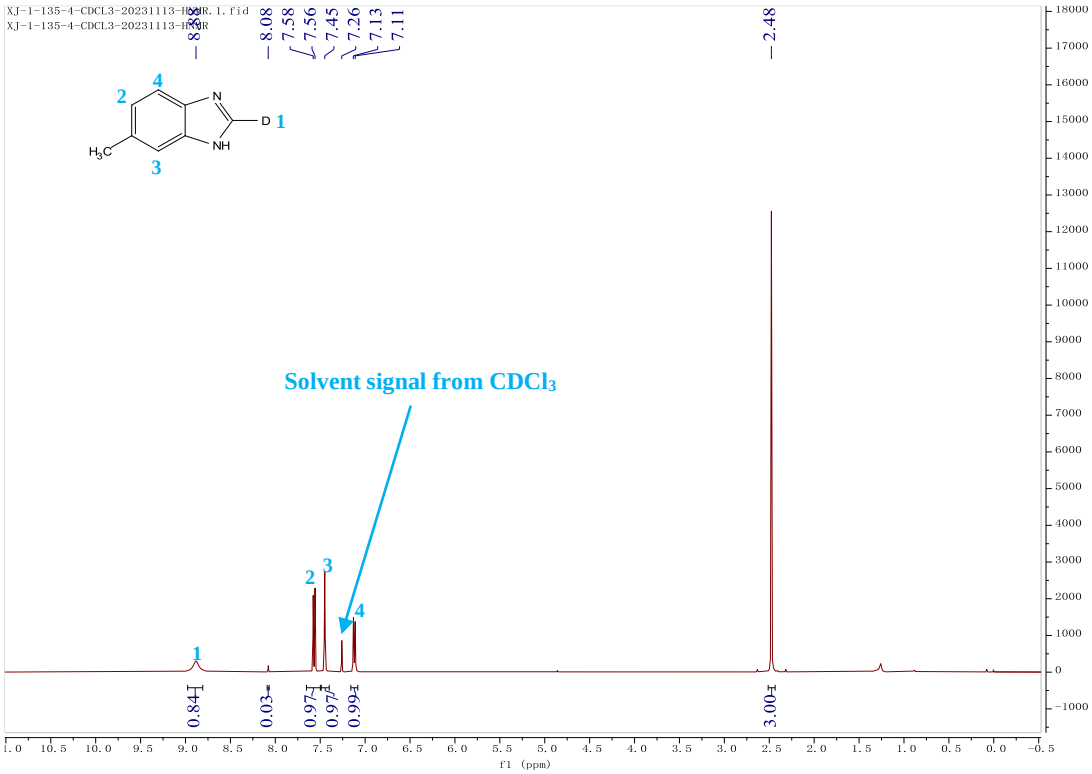

^{1}H NMR (400 MHz, DMSO-d_6) of feed material **9a**

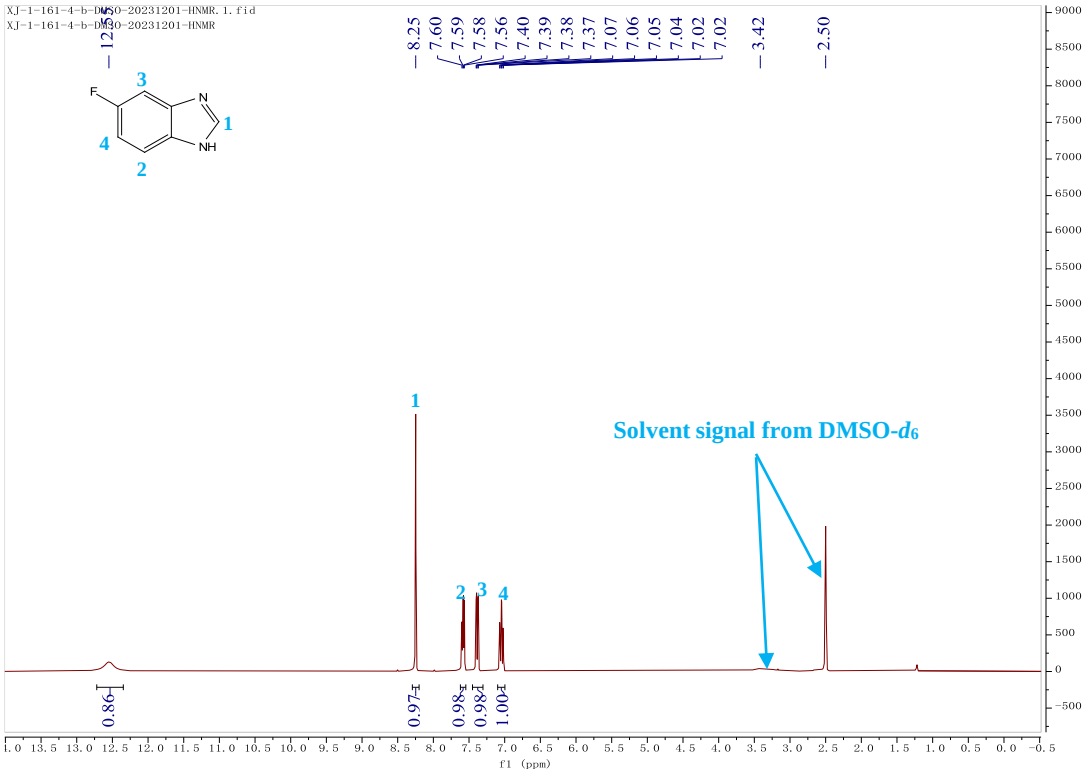

^{19}F NMR (376 MHz, DMSO-d_6) of feed material **9a**

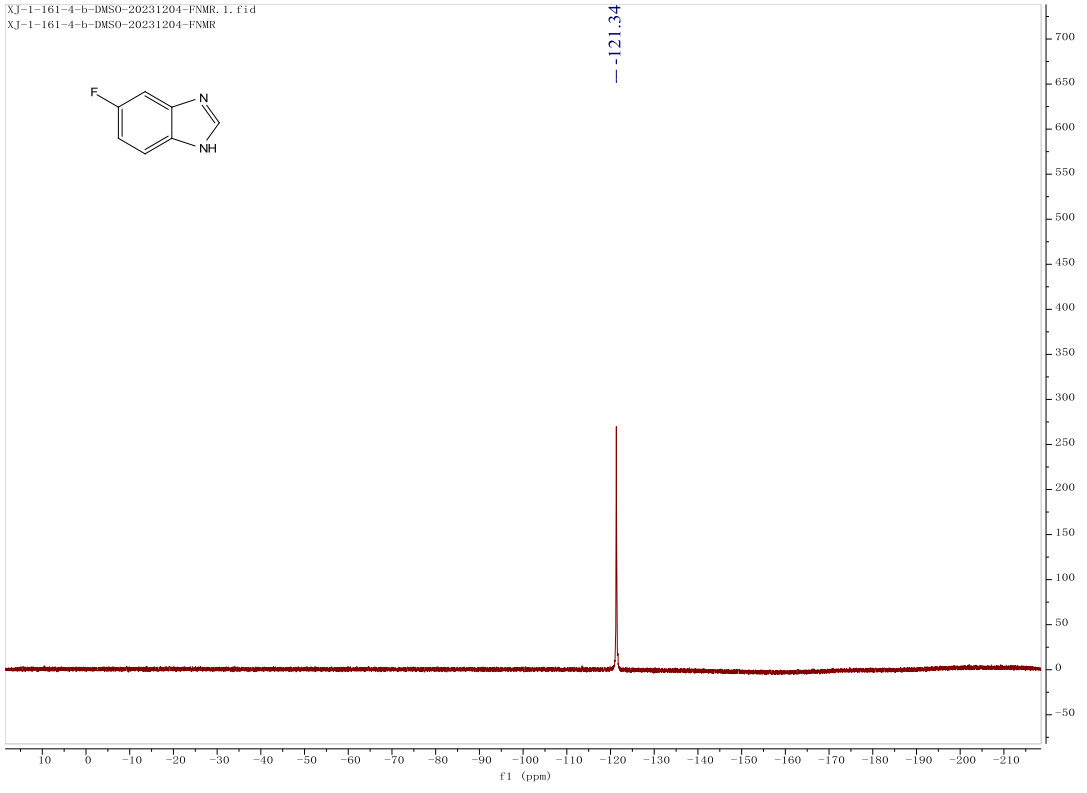

^{1}H NMR (400 MHz, DMSO-d_6) of product **9b**

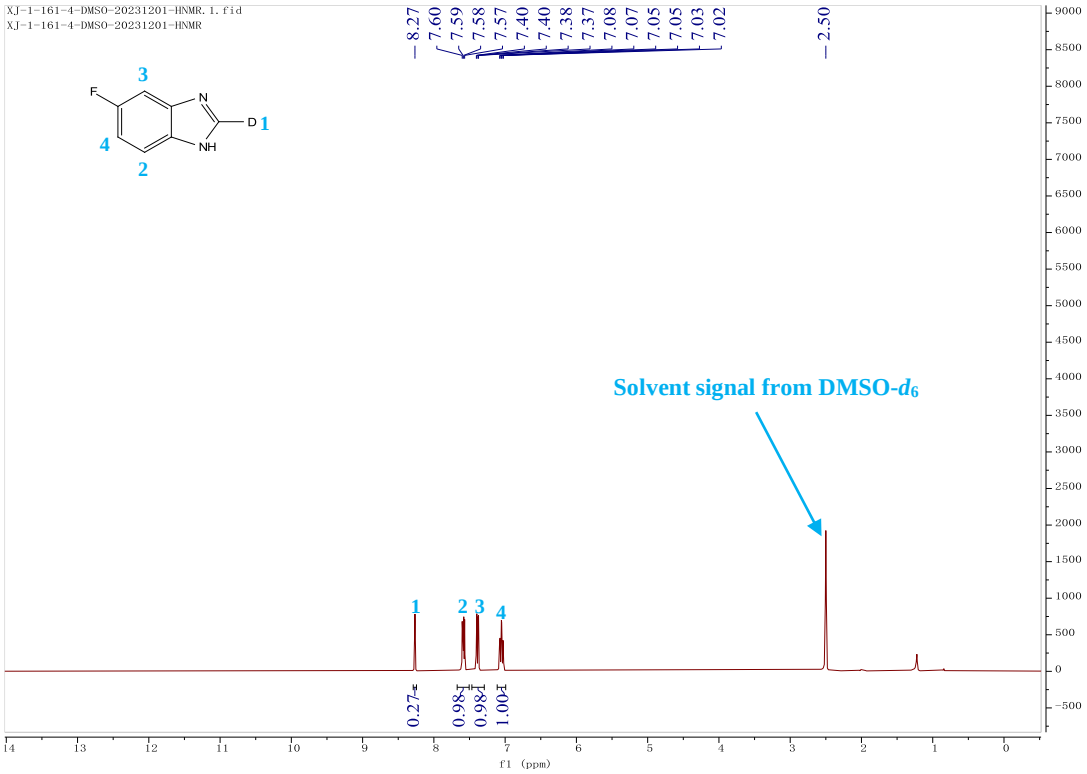

^{19}F NMR (376 MHz, DMSO-d_6) of product **9b**

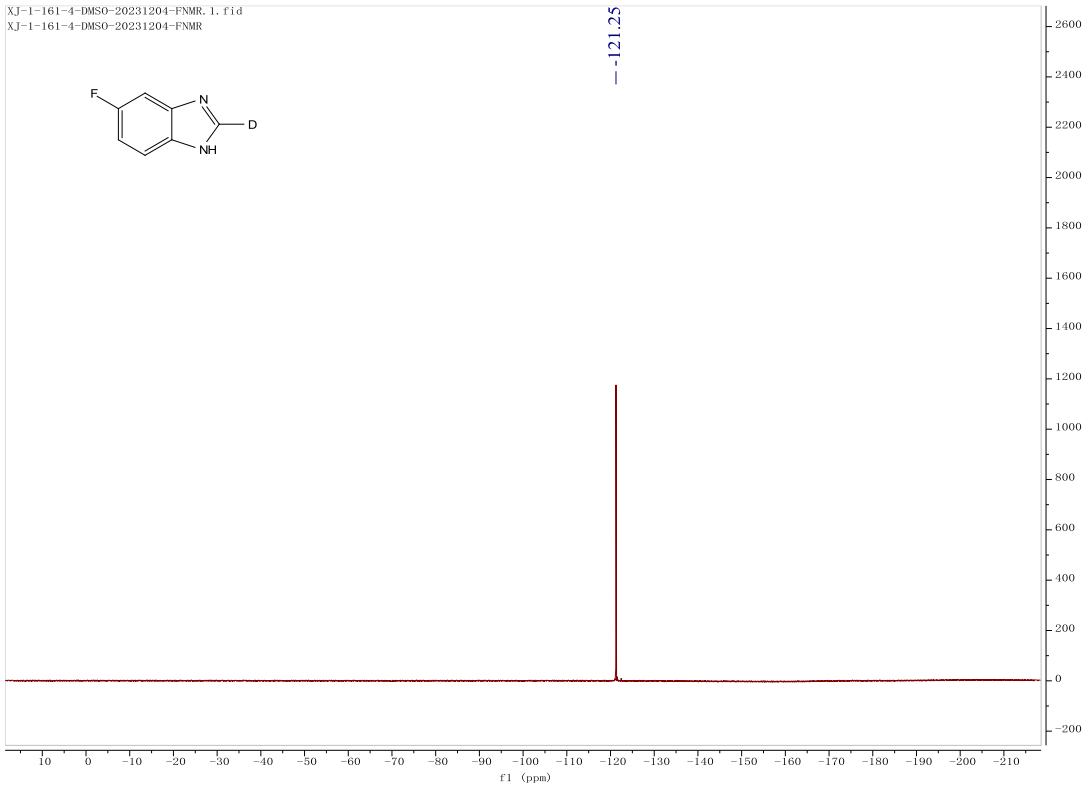

^{1}H NMR (400 MHz, D_2O) of feed material **10a**

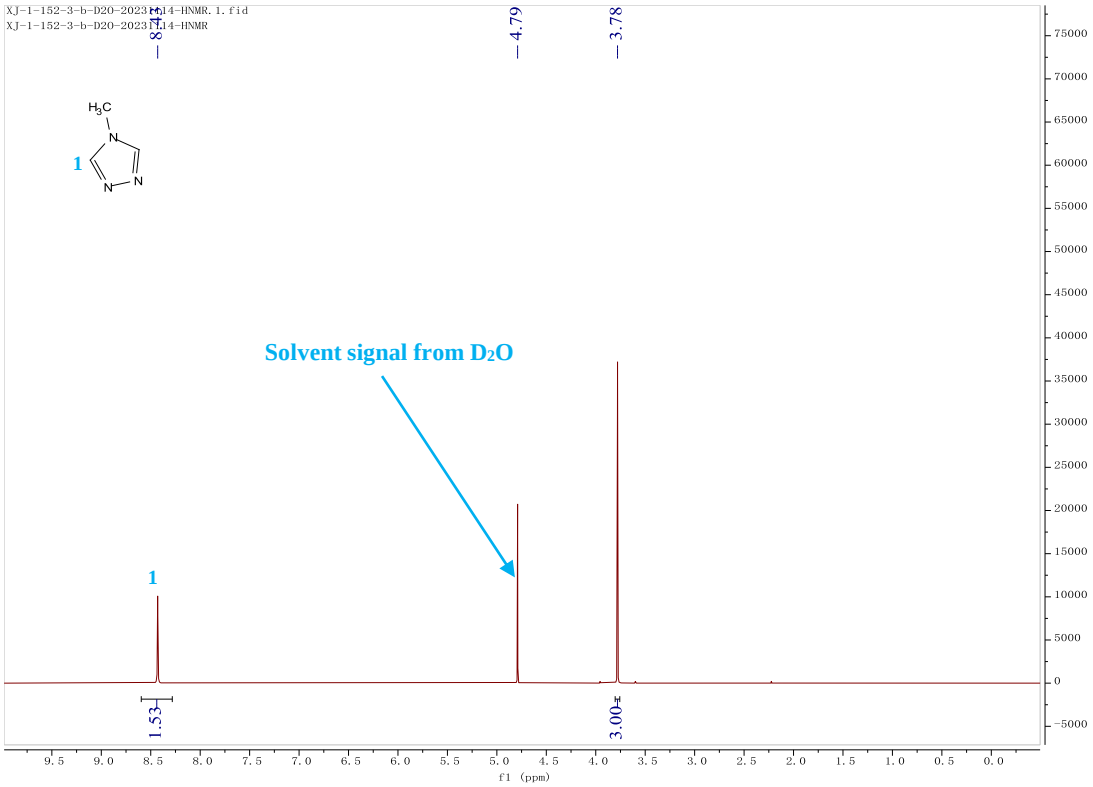

^{1}H NMR (400 MHz, D_2O) of product **10b**

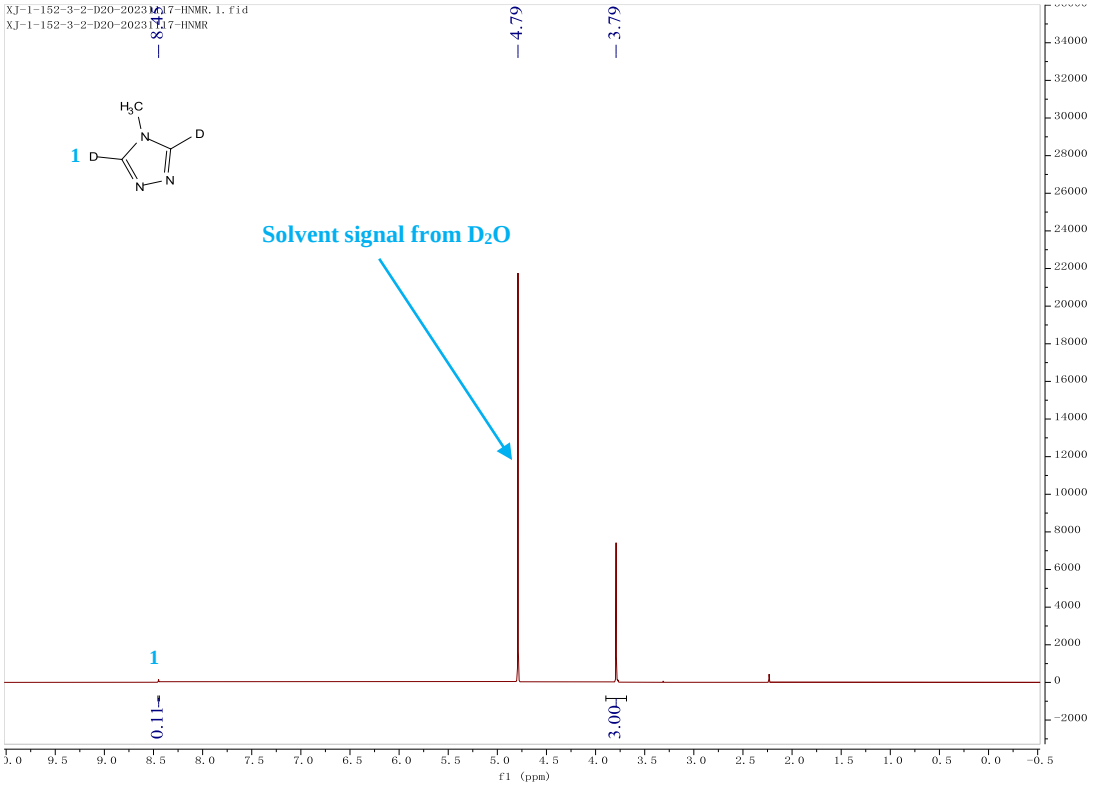

^{1}H NMR (400 MHz, D_2O) of feed material **11a**

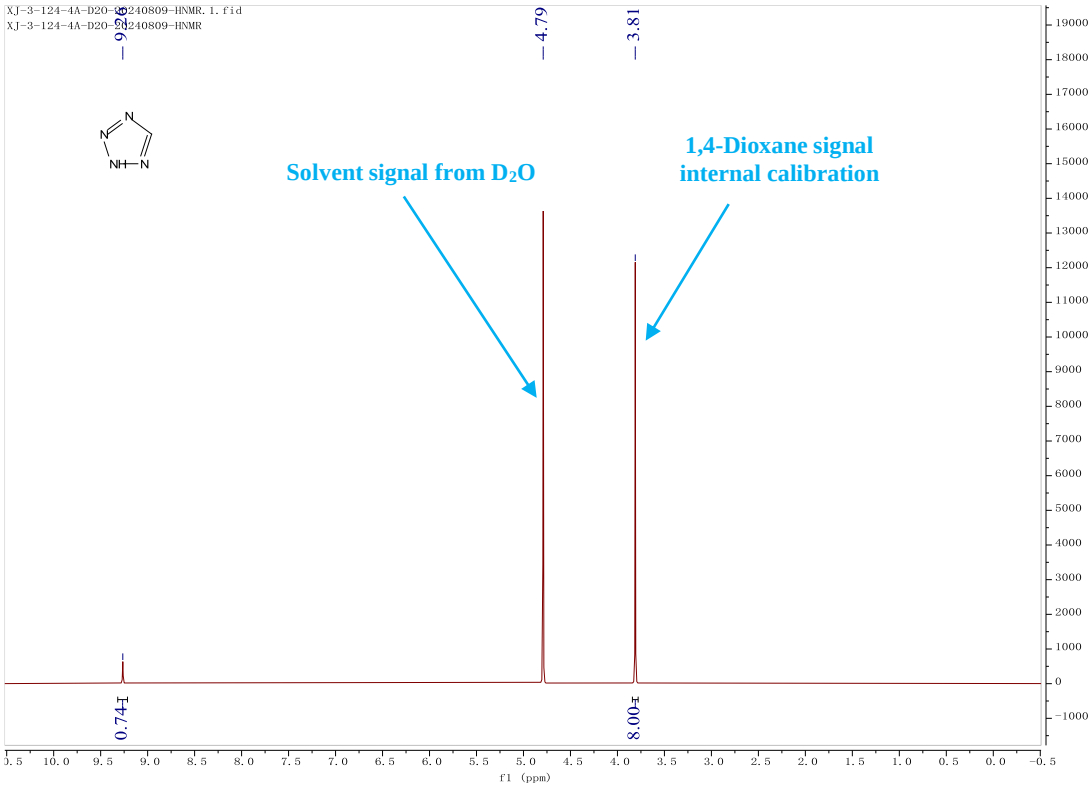

^{1}H NMR (400 MHz, D_2O) of product **11b**

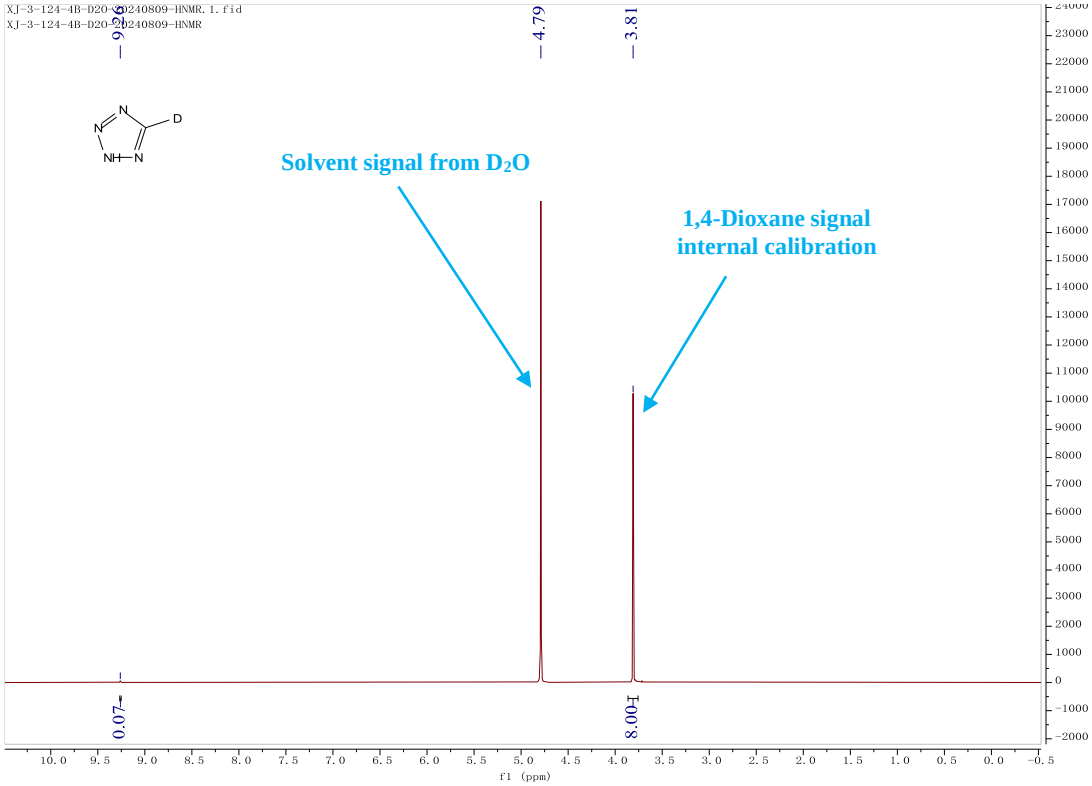

^{1}H NMR (400 MHz, D_2O) of feed material **12a**

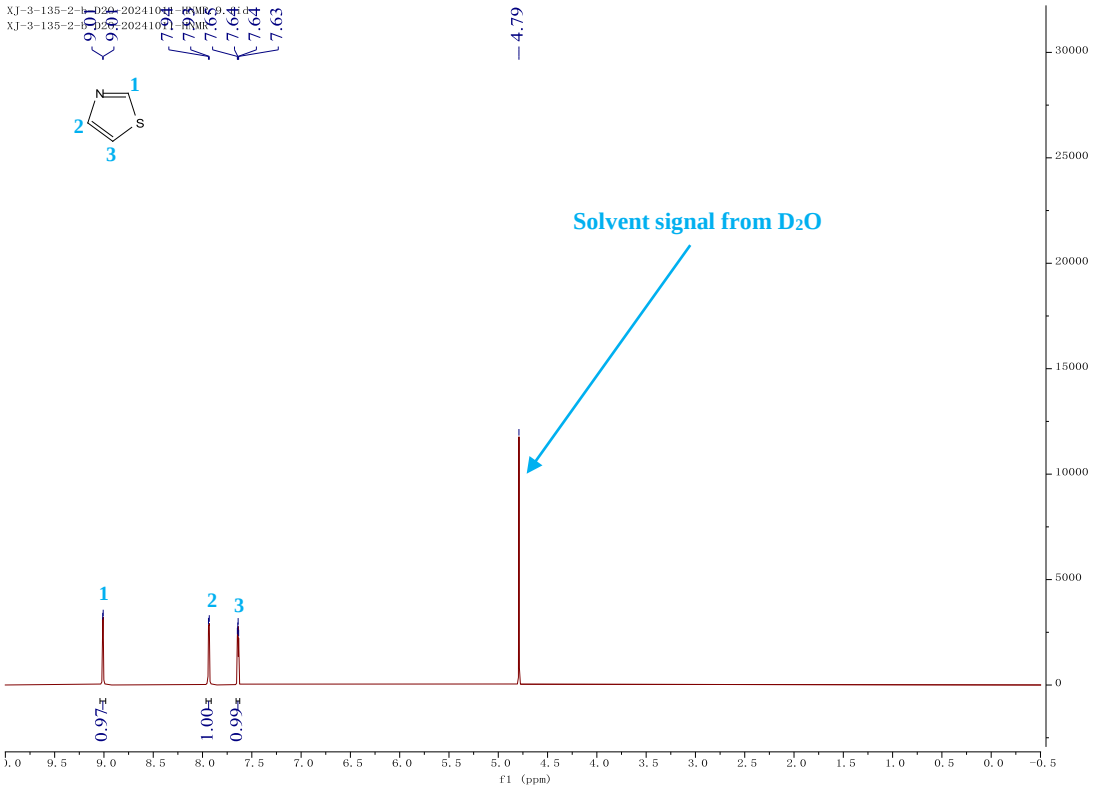

^{1}H NMR (400 MHz, D_2O) of product **12b**

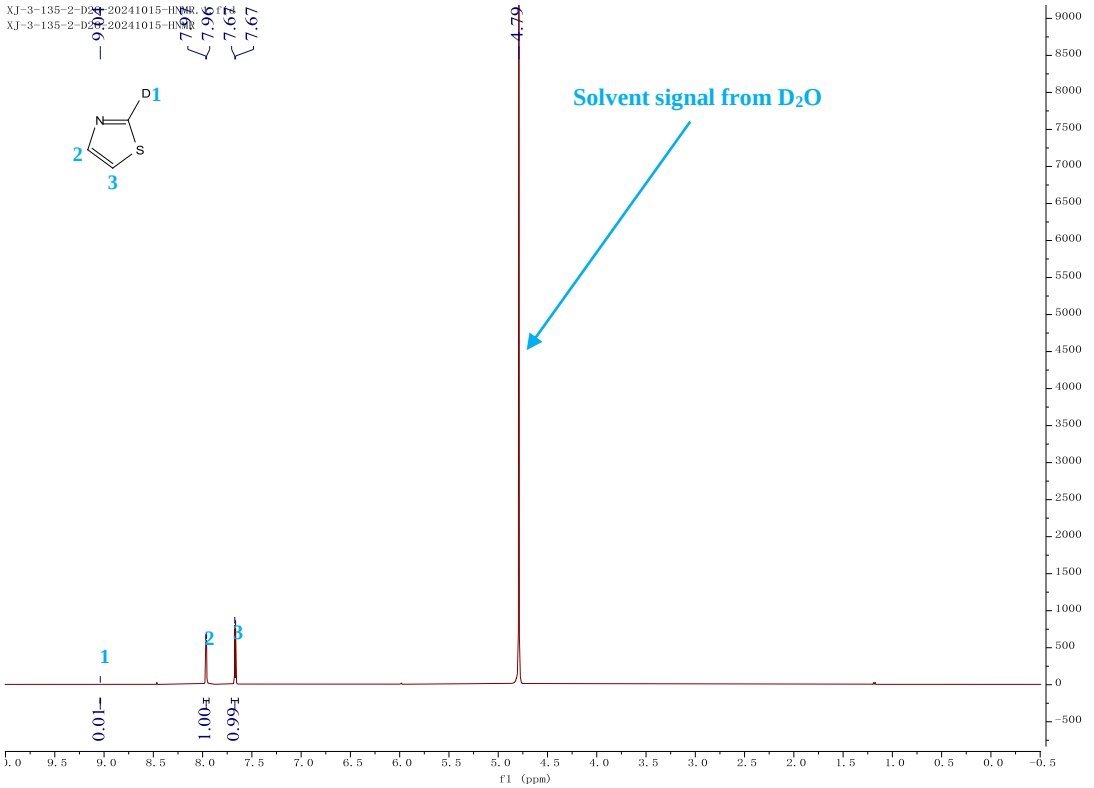

^{1}H NMR (400 MHz, D_2O) of feed material **13a**

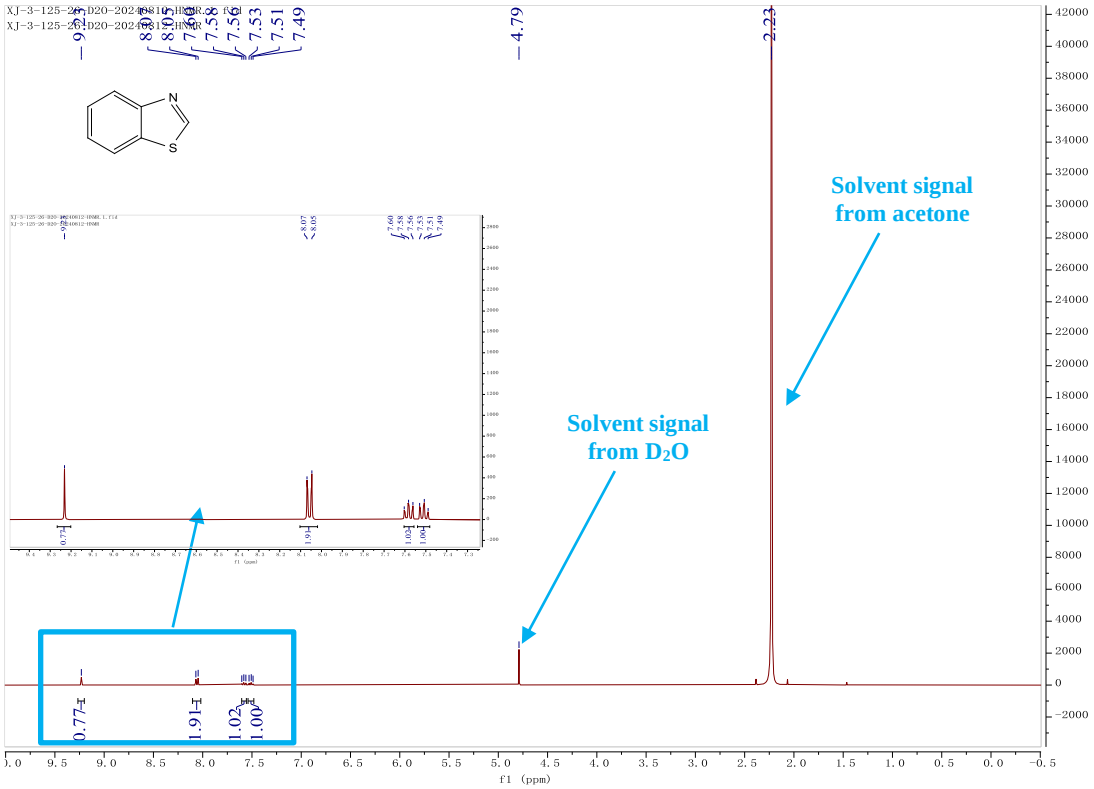

^{1}H NMR (400 MHz, D_2O) of product **13b**

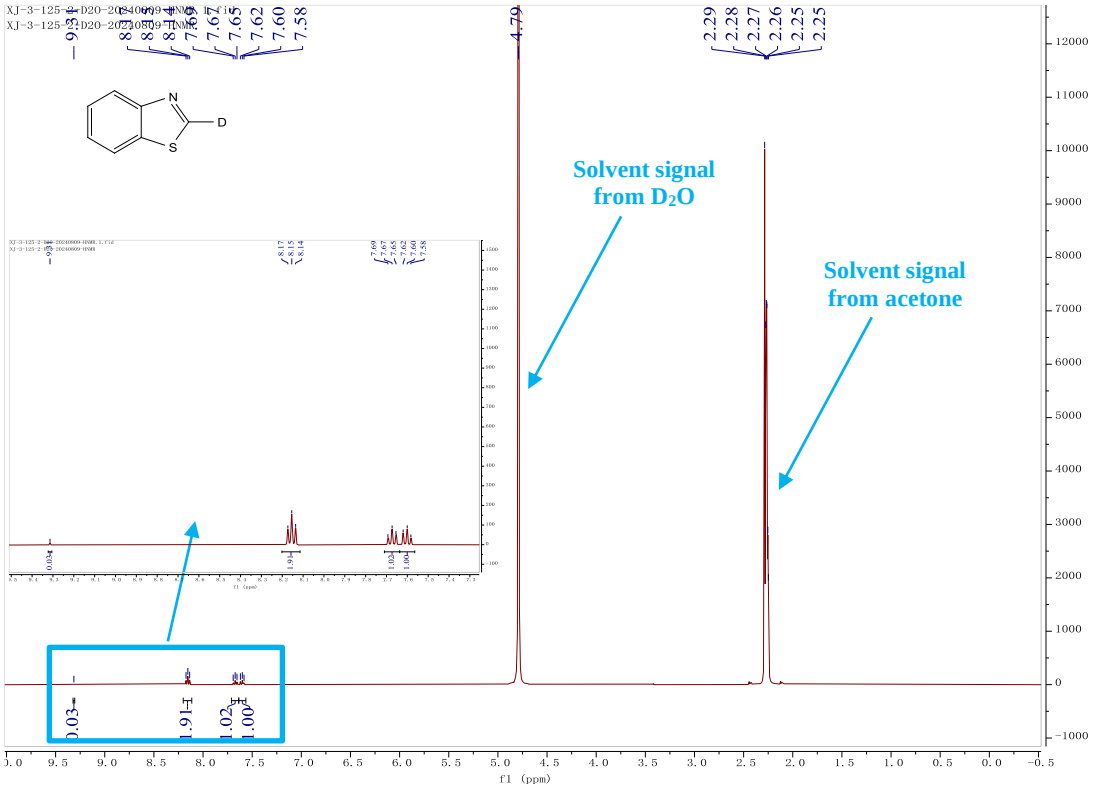

^{1}H NMR (400 MHz, D_2O) of feed material **14a**

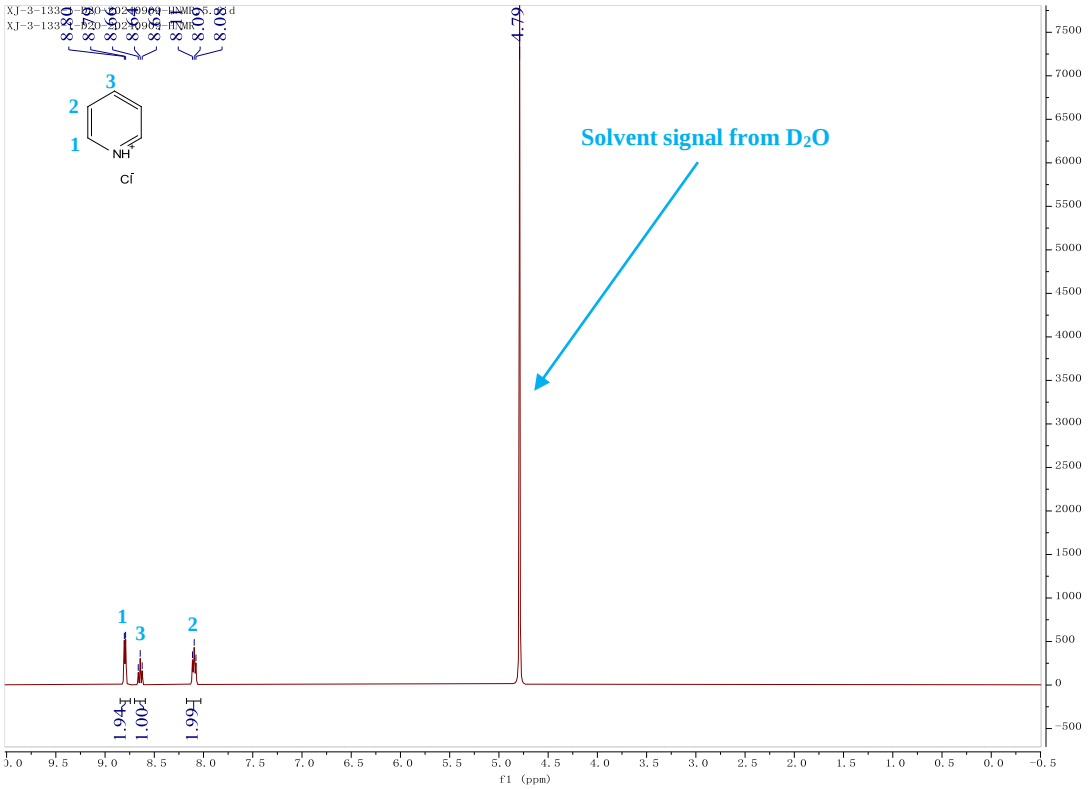

^{1}H NMR (400 MHz, D_2O) of product **14b**

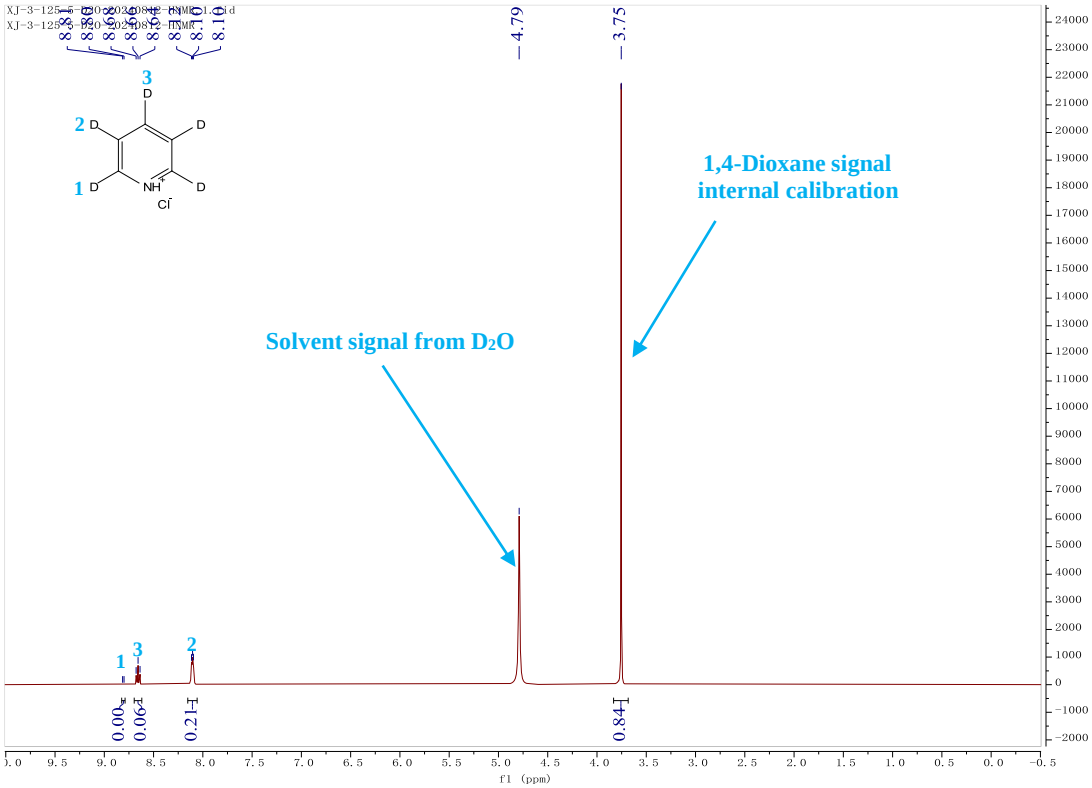

^{1}H NMR (400 MHz, $CDCl_3$) of feed material **16a**

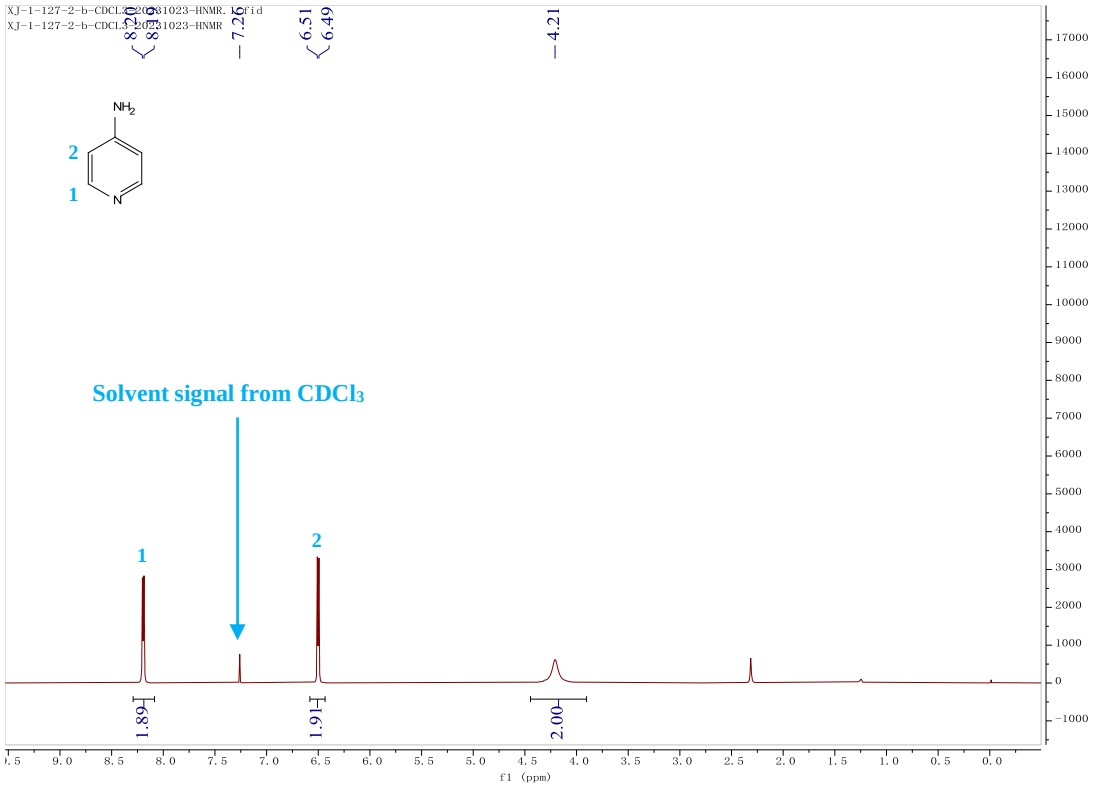

^{1}H NMR (400 MHz, $CDCl_3$) of product **16b**

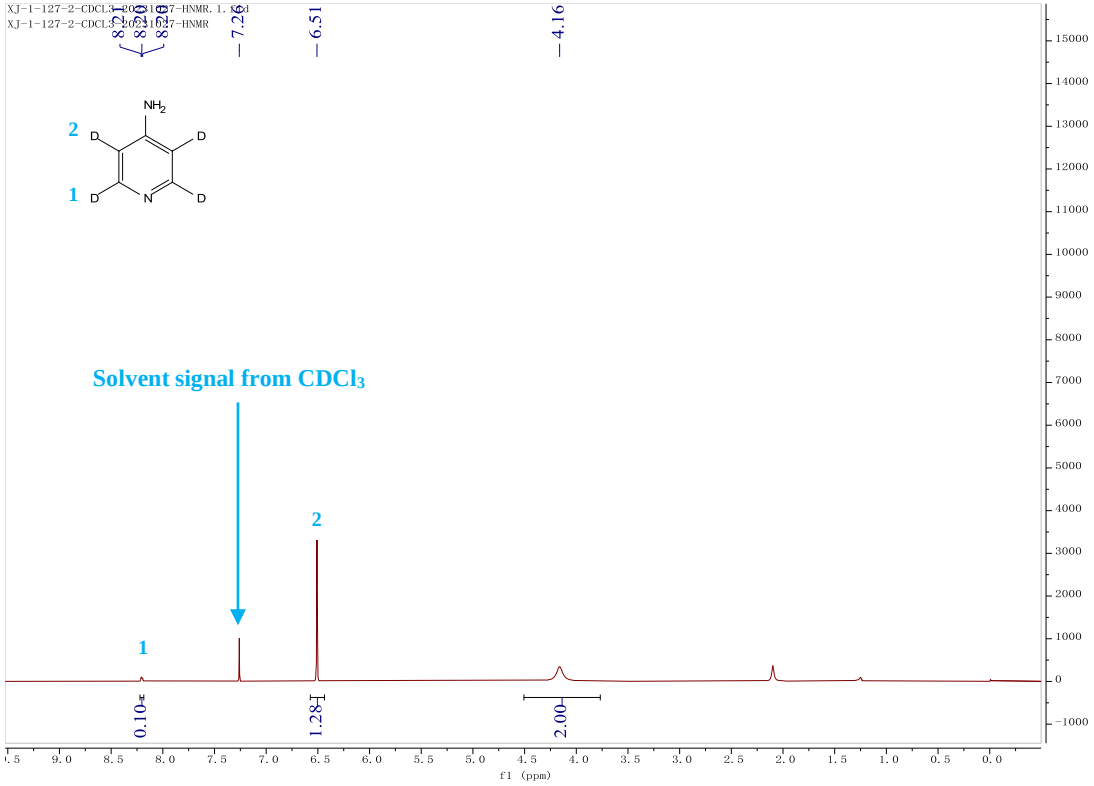

^{1}H NMR (400 MHz, $CDCl_3$) of feed material **17a**

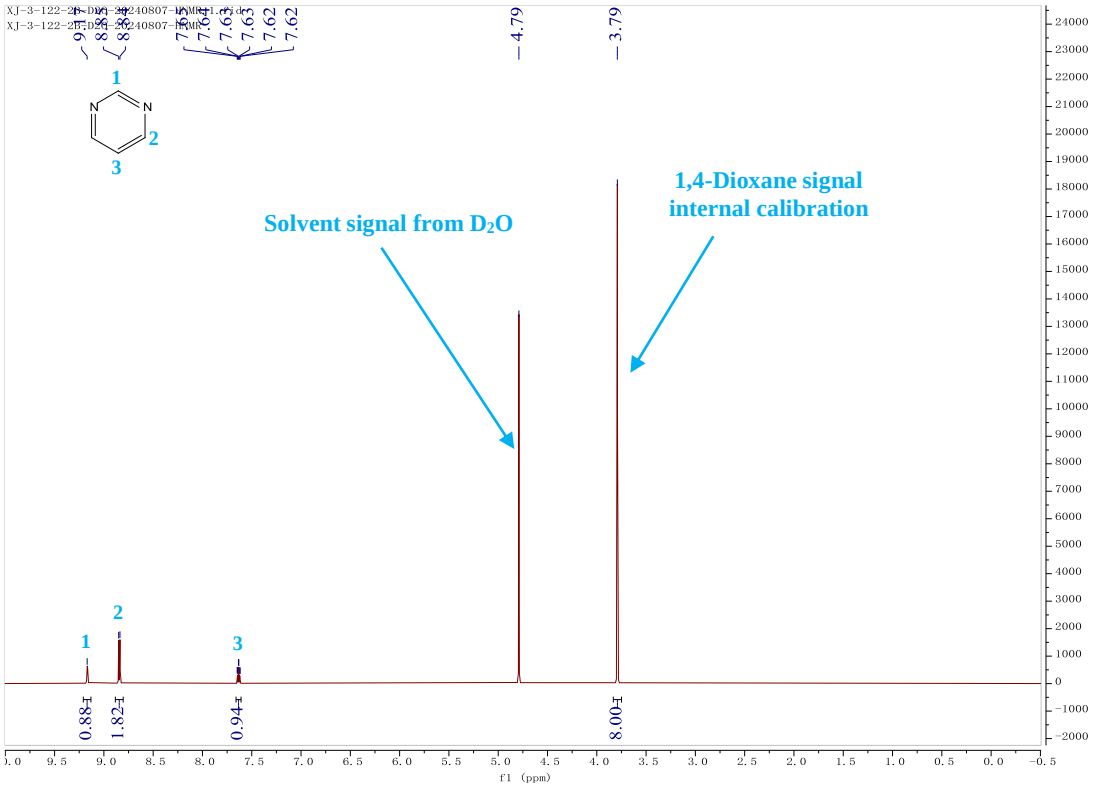

^{1}H NMR (400 MHz, $CDCl_3$) of product **17b**

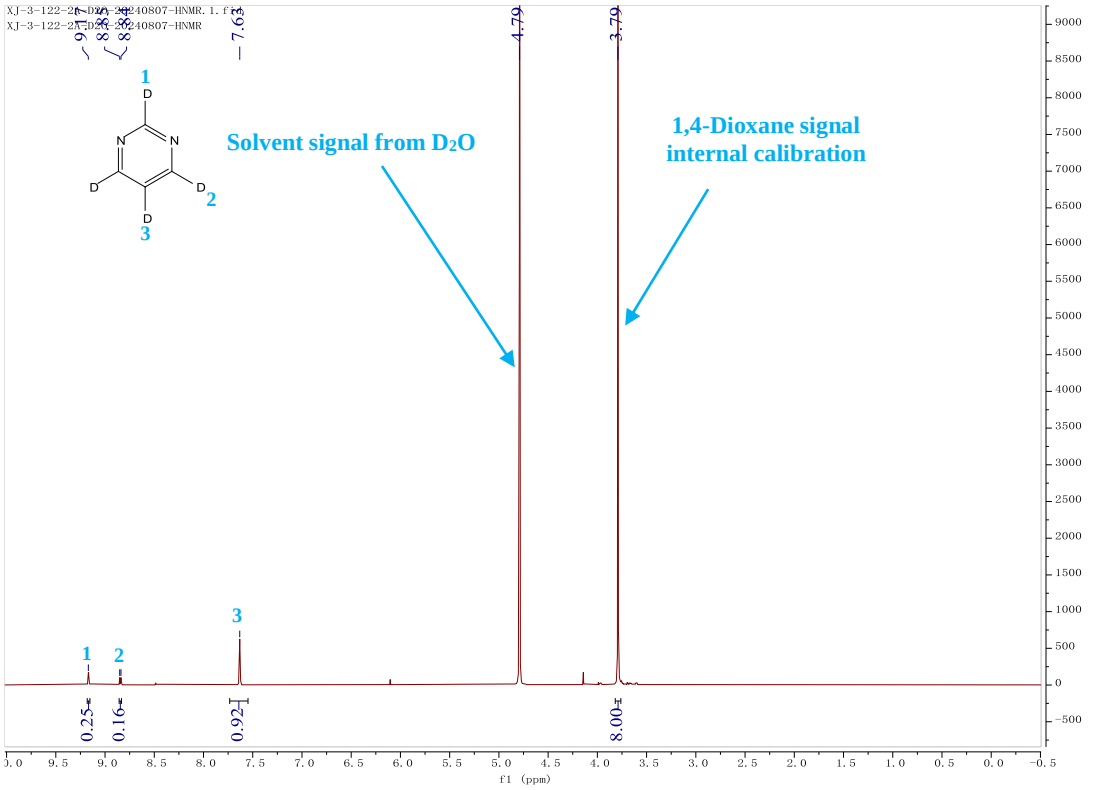

^{1}H NMR (400 MHz, D_2O) of feed material **18a**

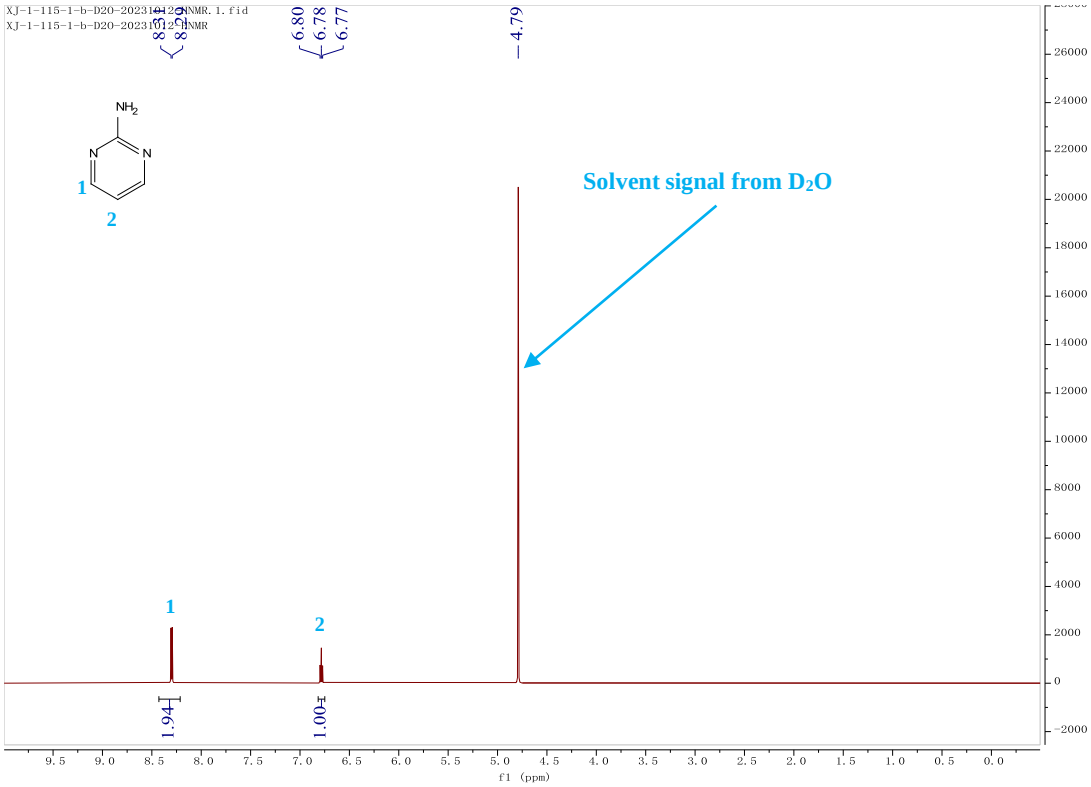

^{1}H NMR (400 MHz, D_2O) of product **18b**

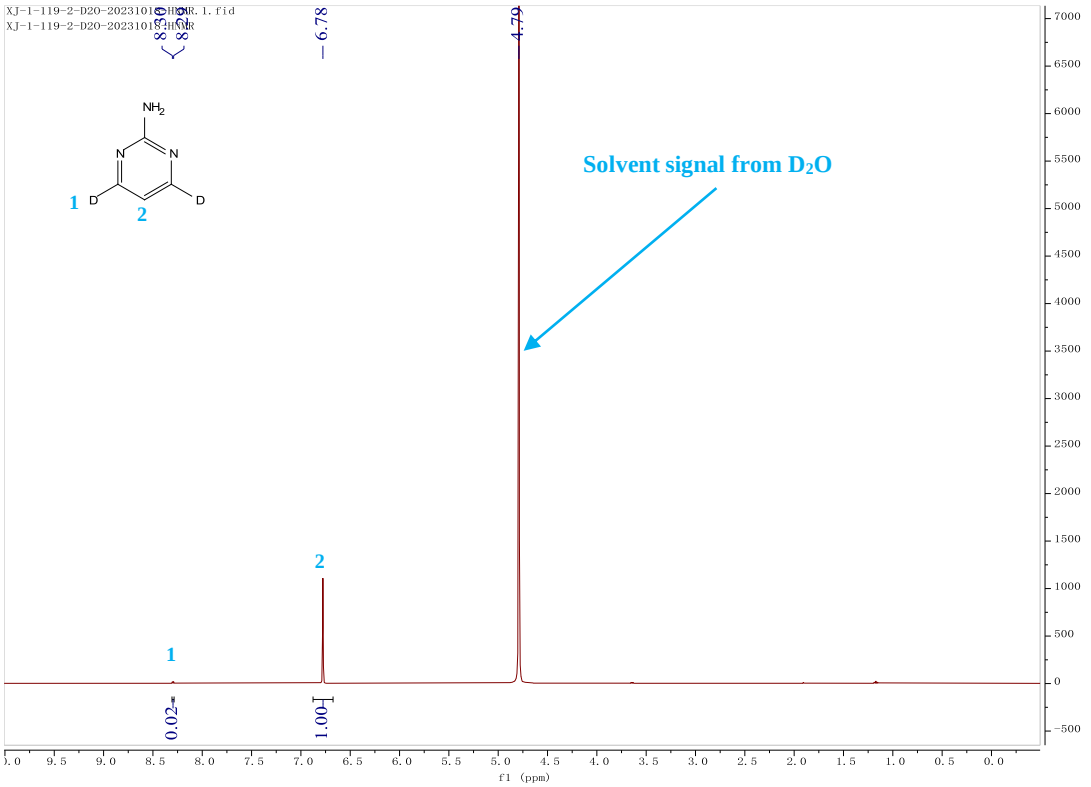

^{1}H NMR (400 MHz, D_2O) of feed material **19a**

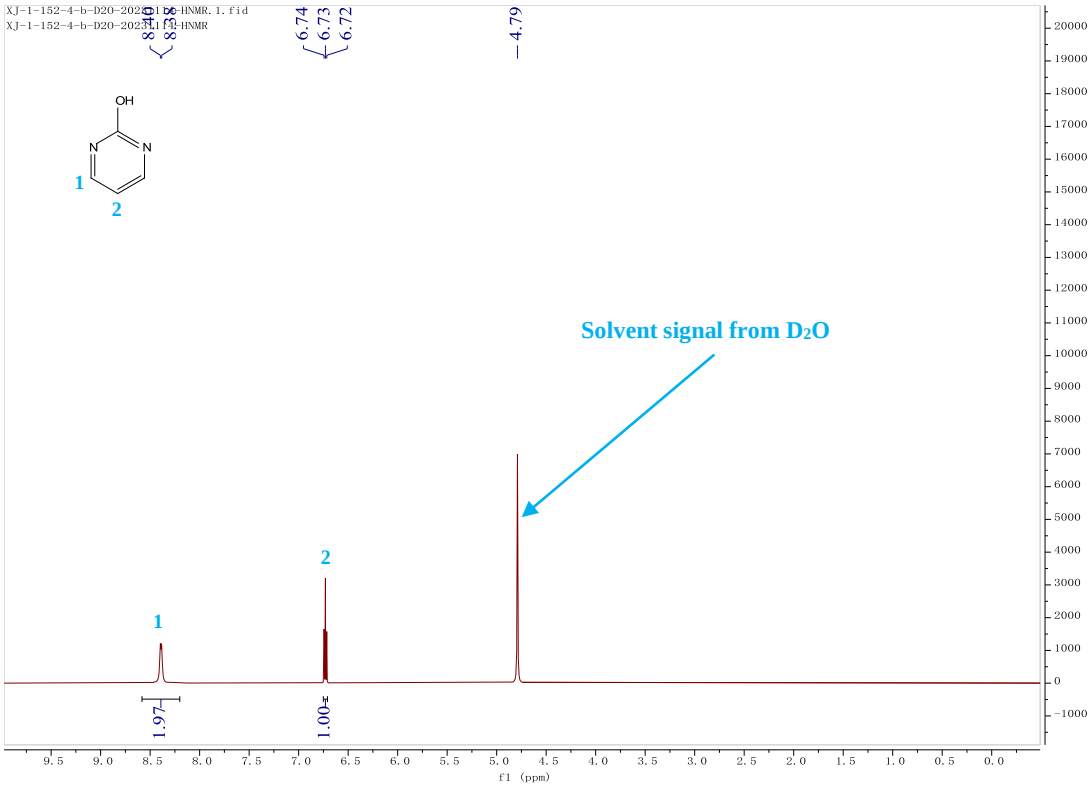

^{1}H NMR (400 MHz, D_2O) of product **19b**

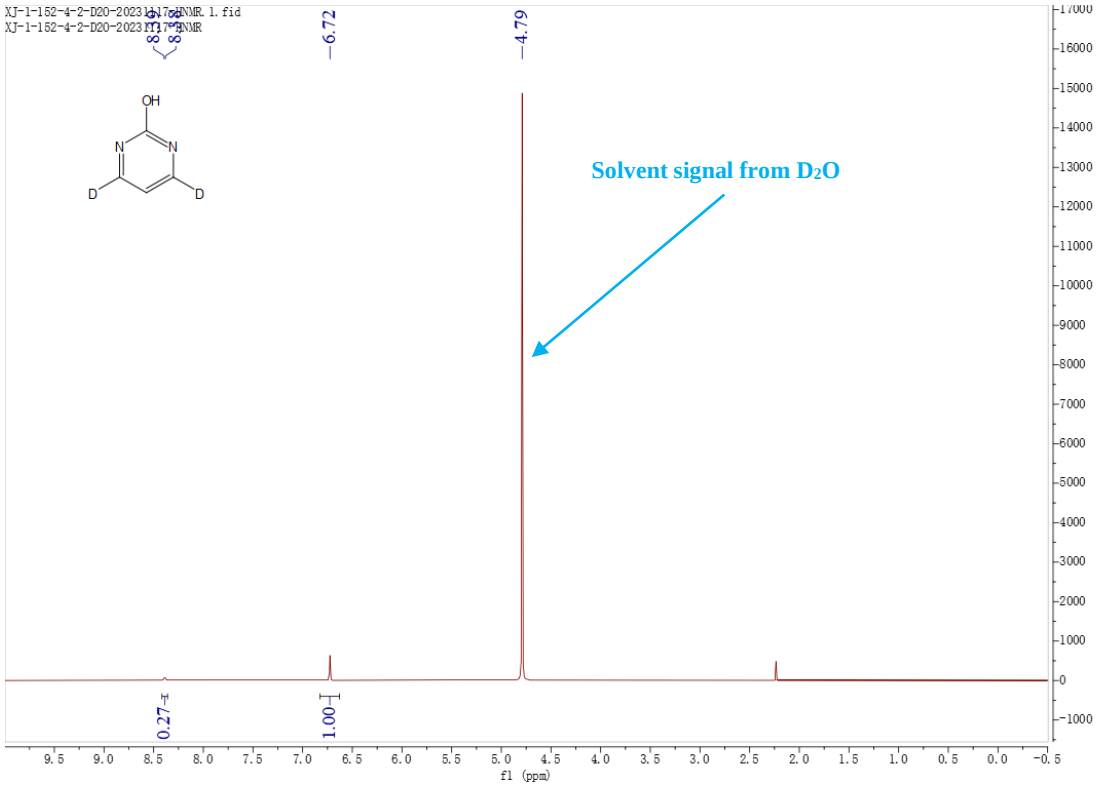

1 2

^{1}H NMR (400 MHz, D_2O) of feed material **20a**

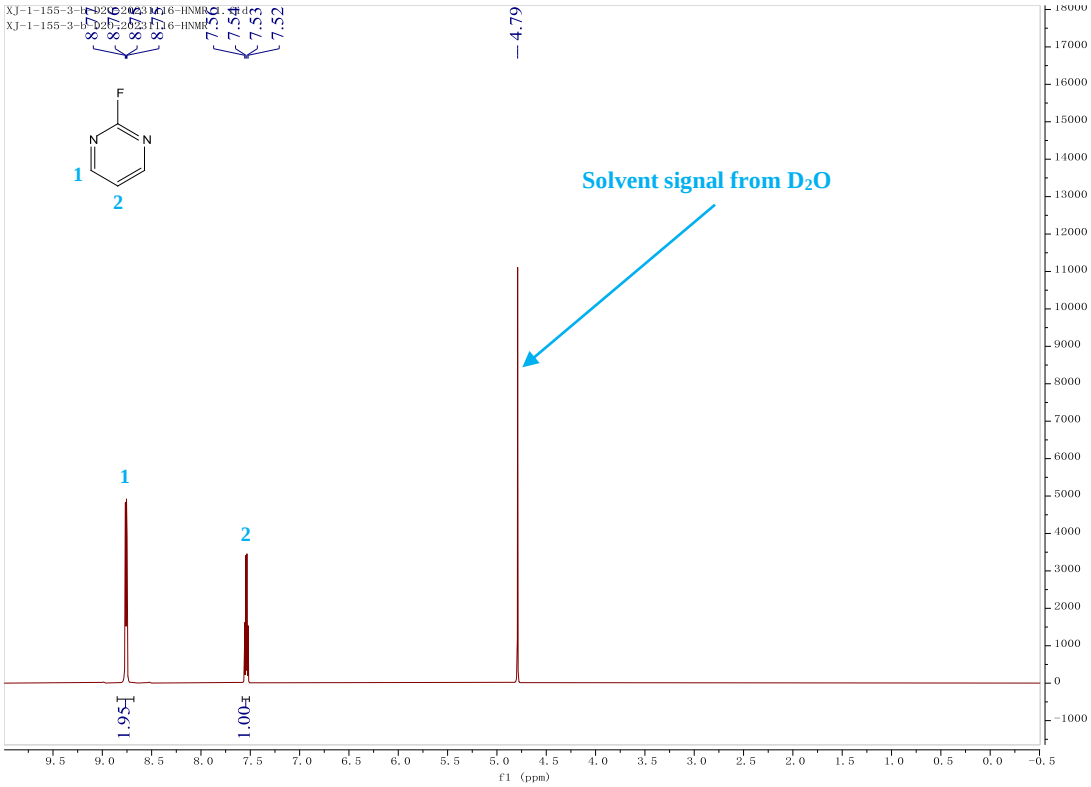

^{19}F NMR (376 MHz, D_2O) of feed material **20a**

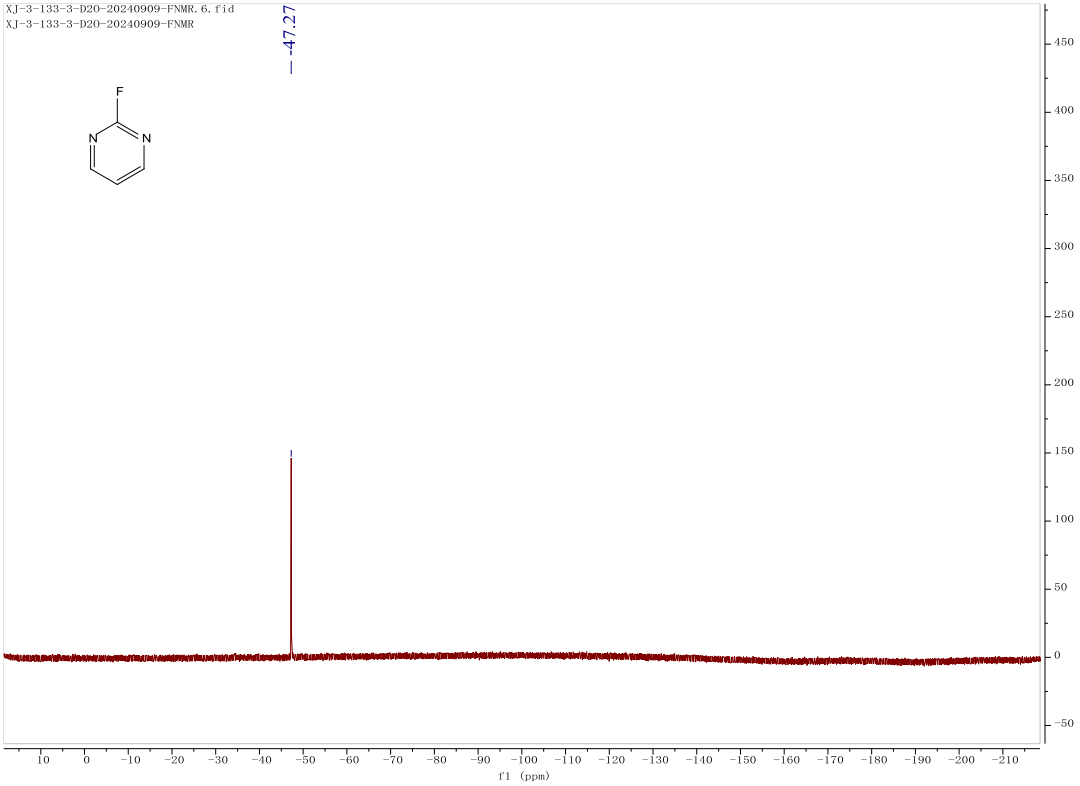

^{1}H NMR (400 MHz, D_2O) of product **20b**

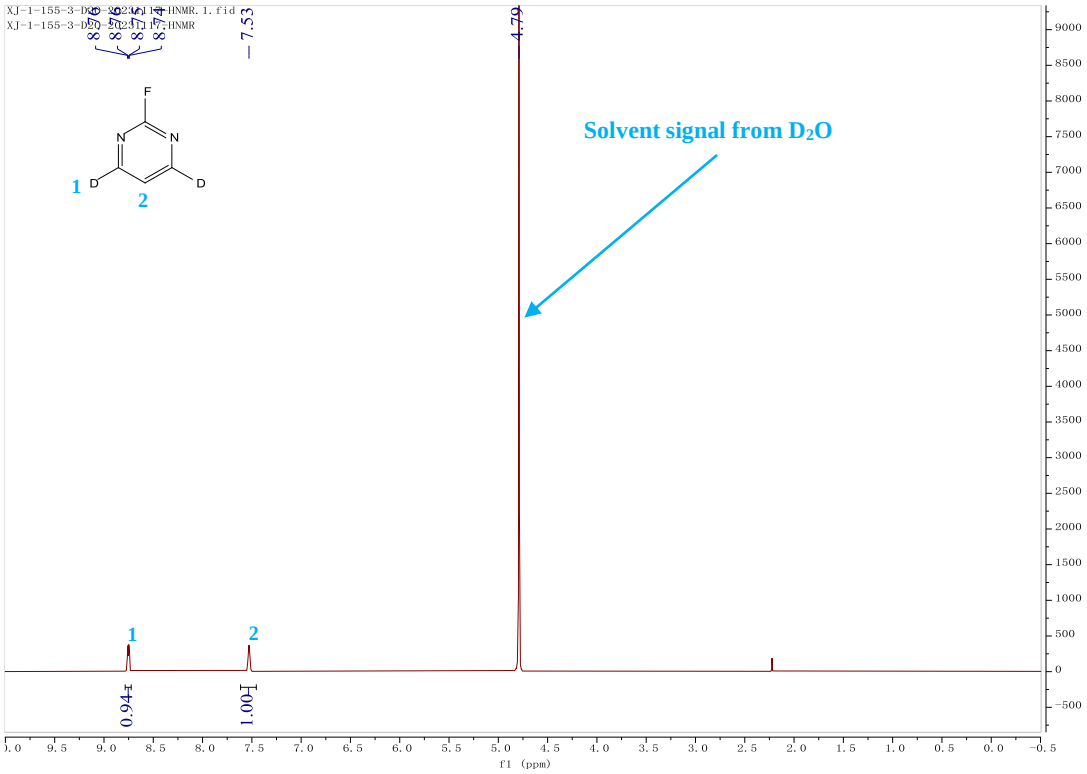

^{19}F NMR (376 MHz, D_2O) of product **20b**

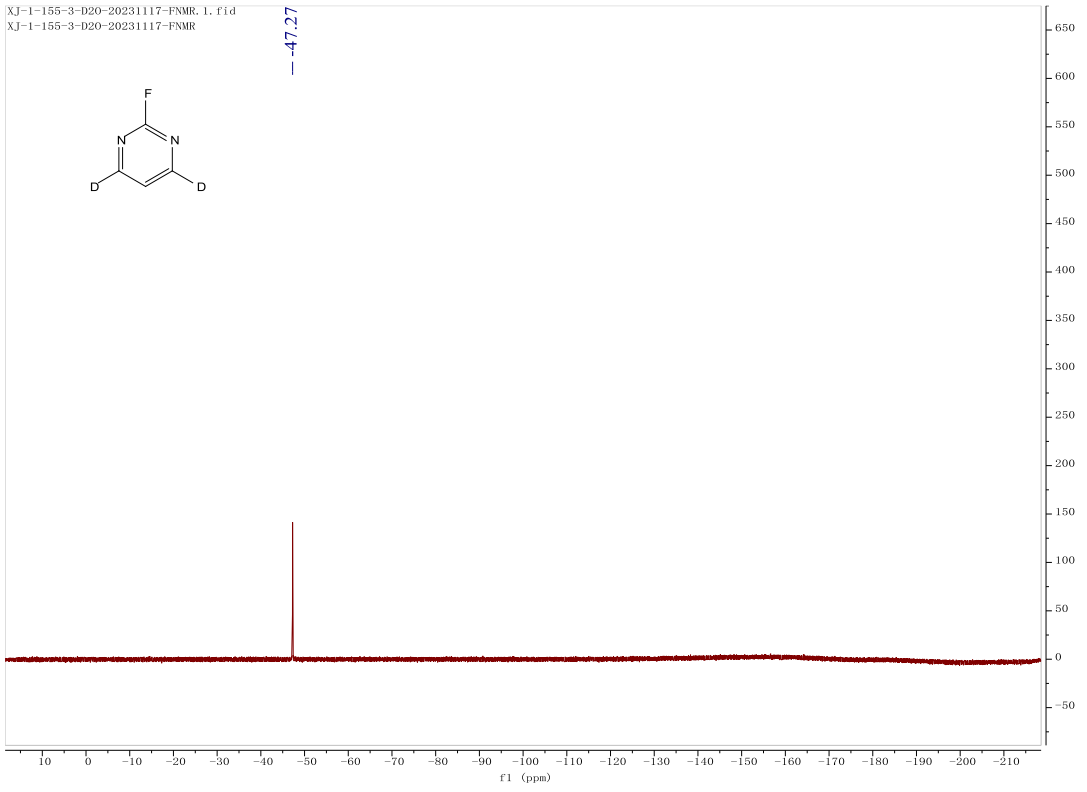

^{1}H NMR (400 MHz, D_2O) of feed material **21a**

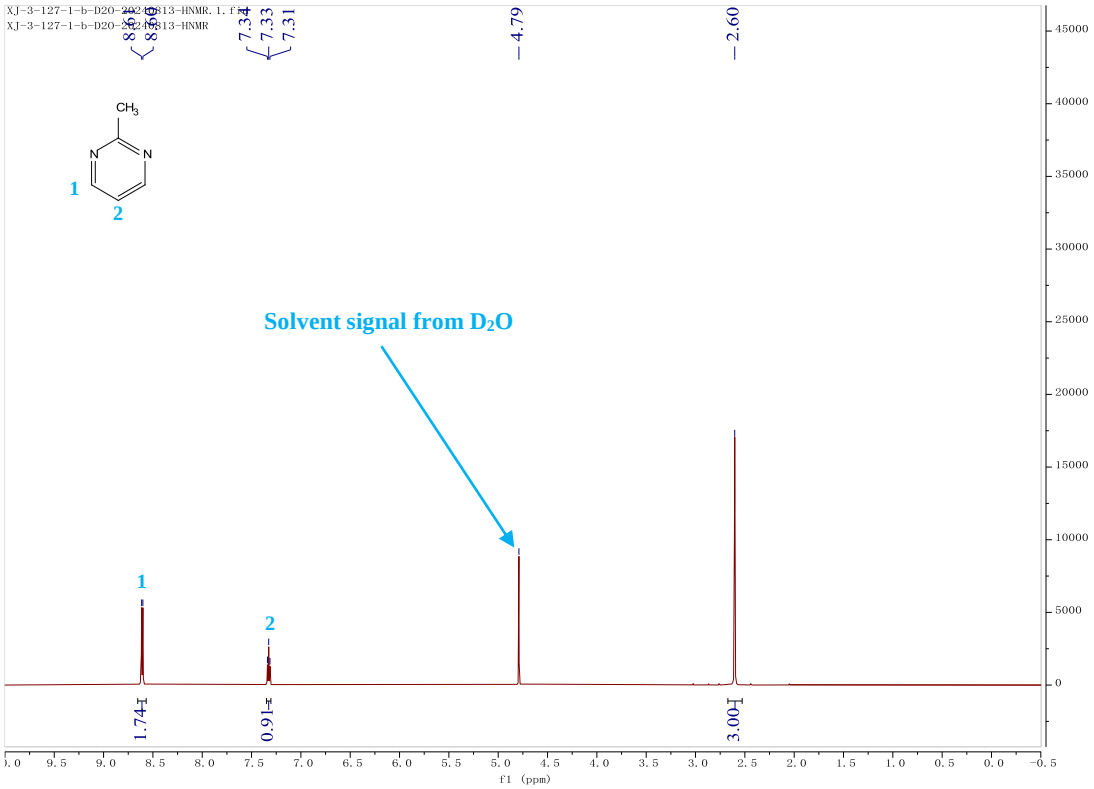

^{1}H NMR (400 MHz, D_2O) of product **21b**

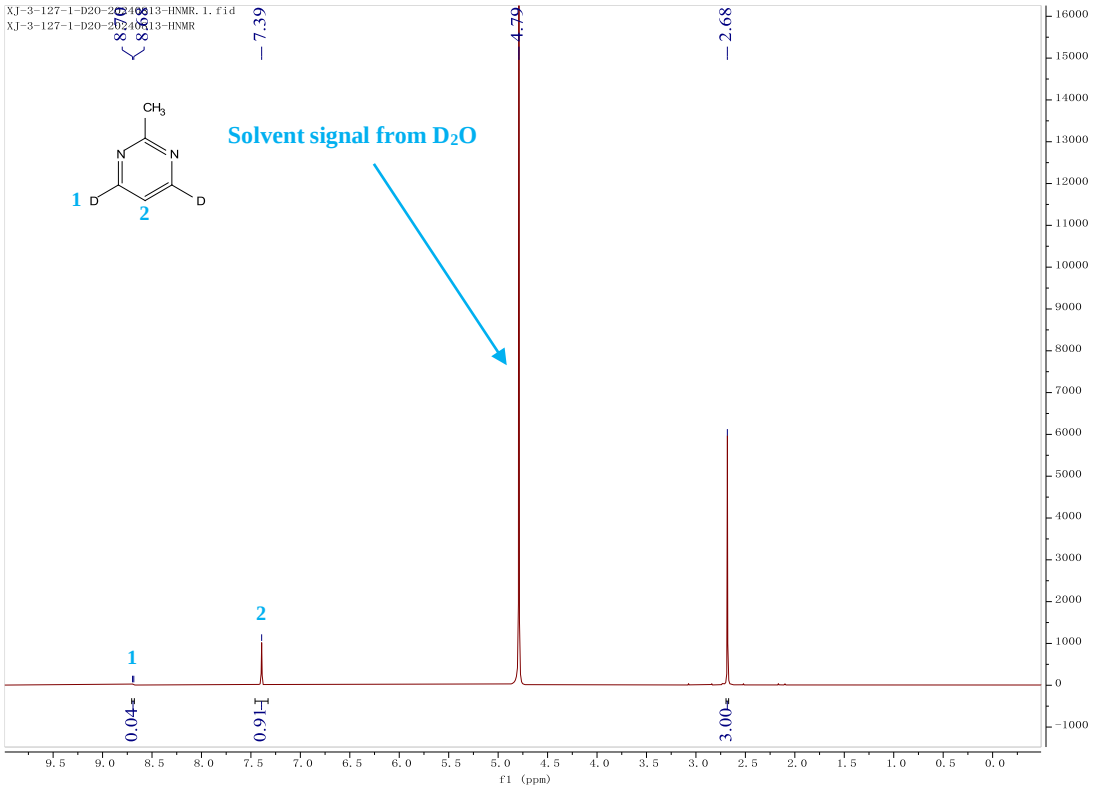

^{1}H NMR (400 MHz, D_2O) of feed material **22a**

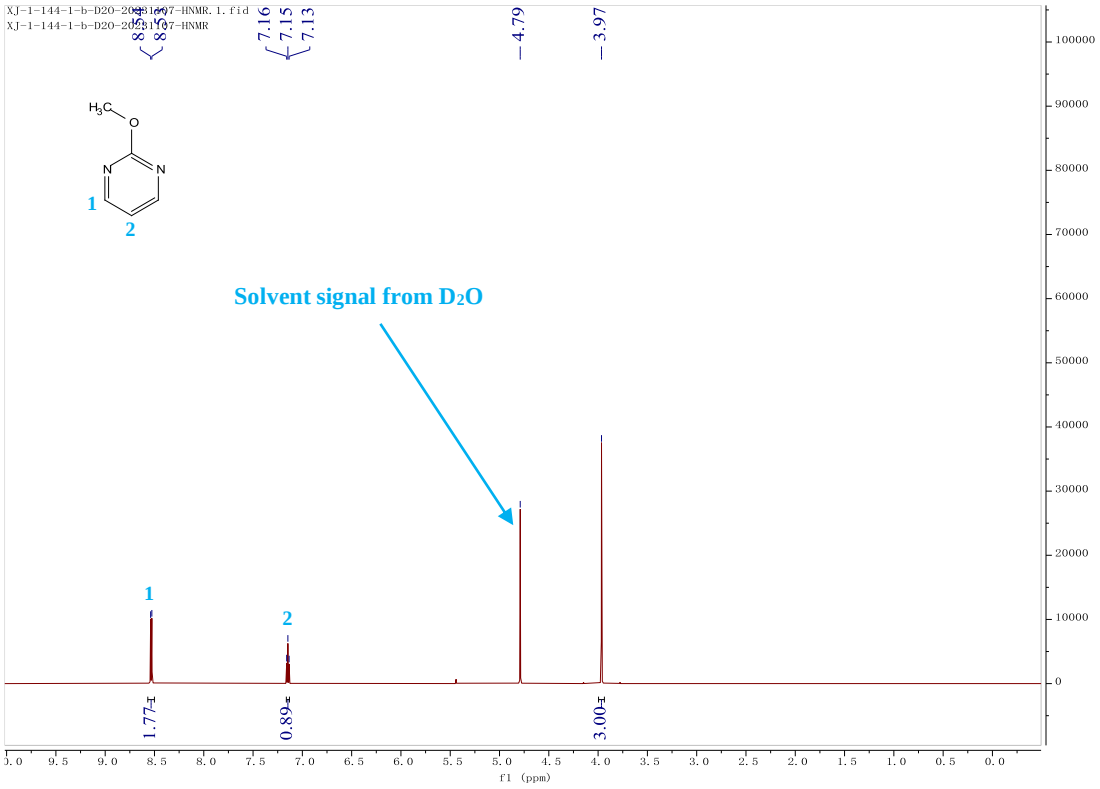

^{1}H NMR (400 MHz, D_2O) of product **22b**

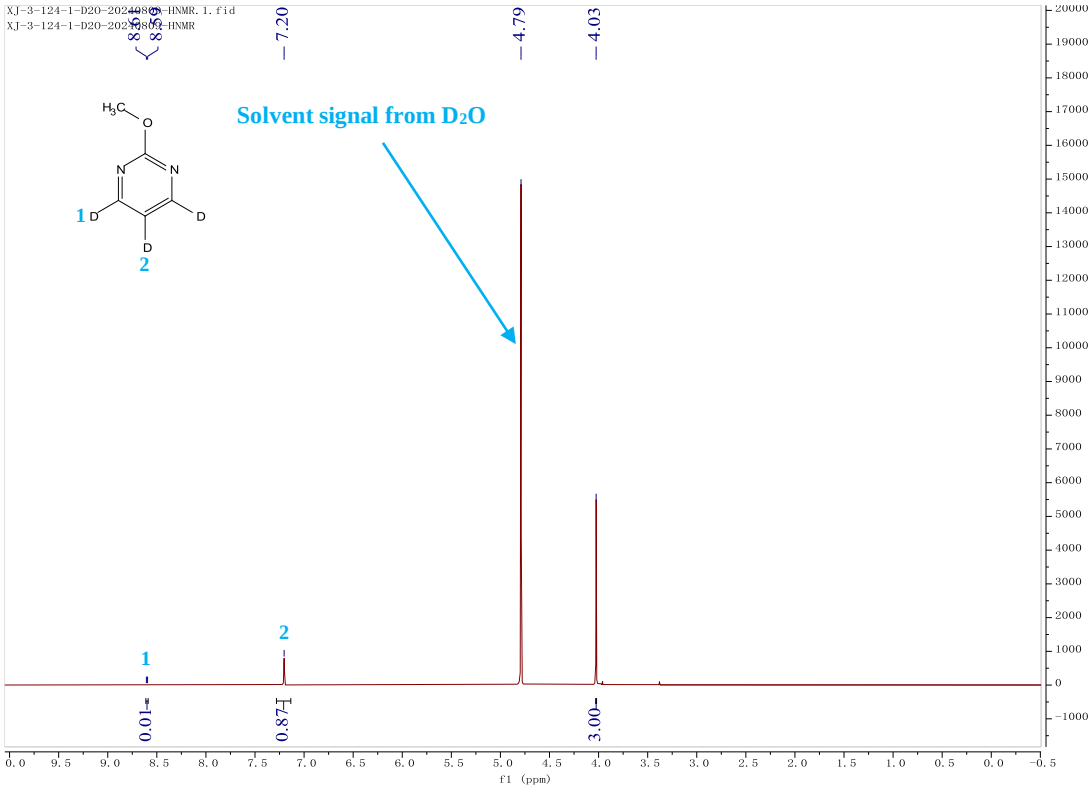

^{1}H NMR (400 MHz, D_2O) of feed material **23a**

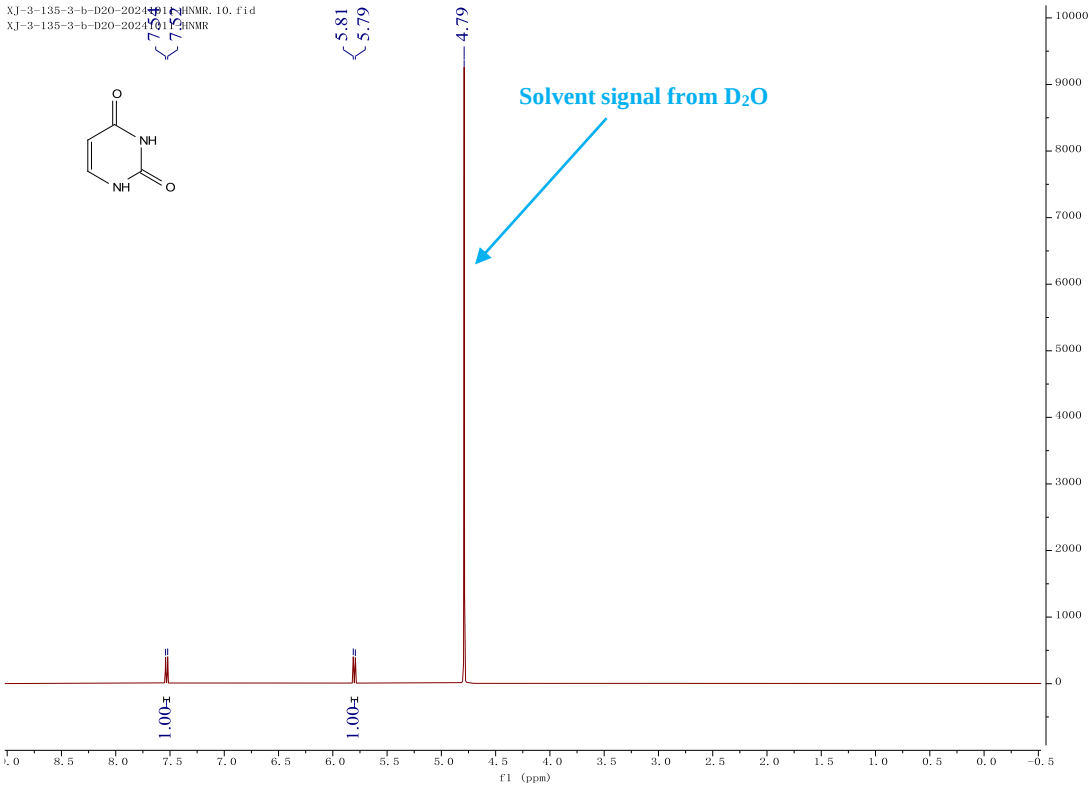

^{1}H NMR (400 MHz, D_2O) of product **23b**

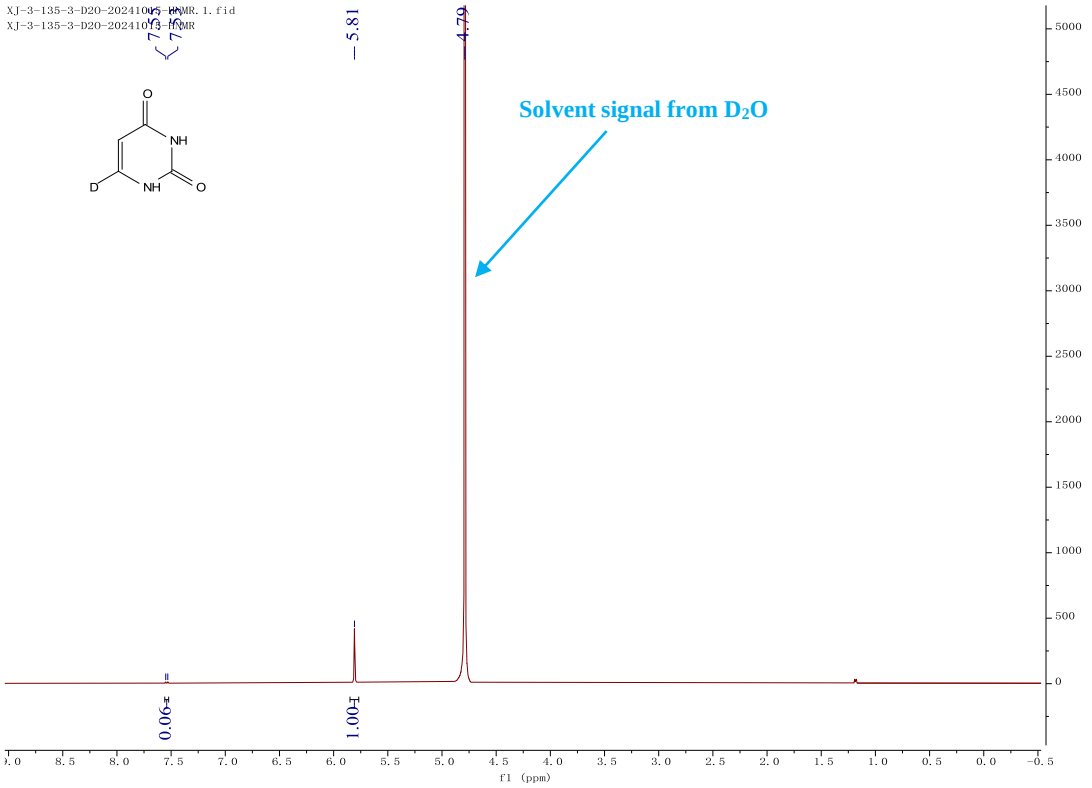

^{1}H NMR (400 MHz, D_2O) of feed material **24a**

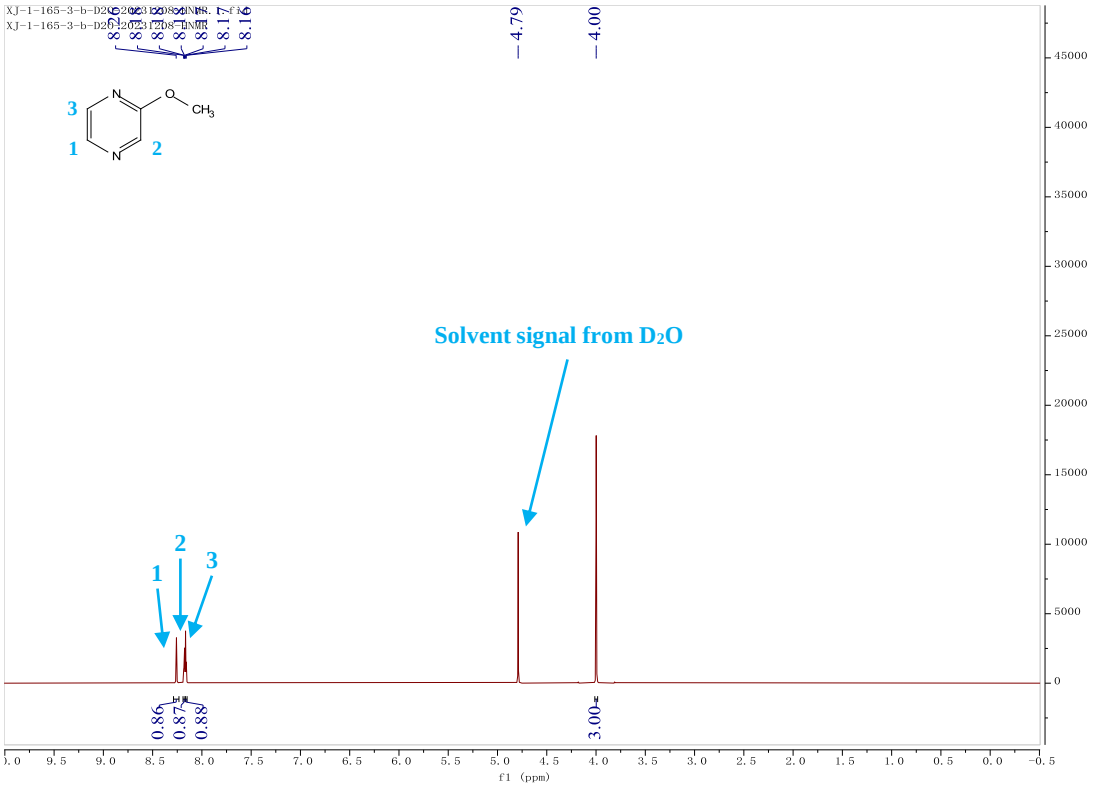

^{1}H NMR (400 MHz, D_2O) of product **24b**

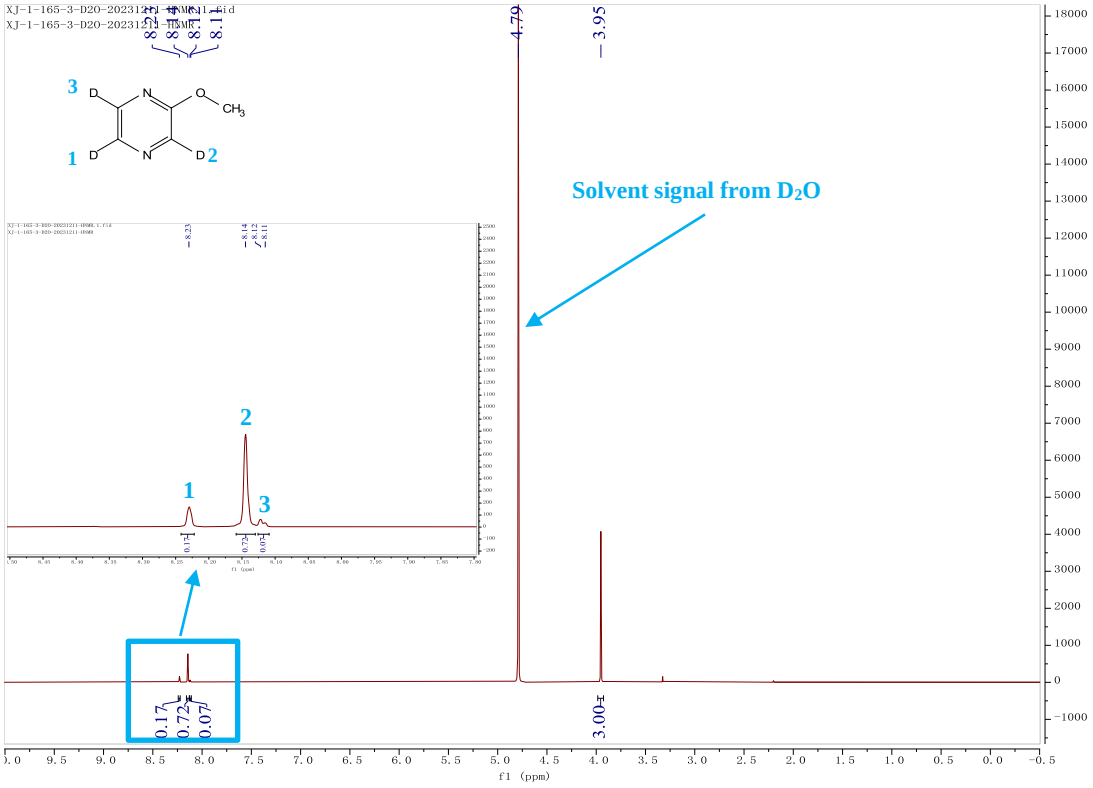

^{1}H NMR (400 MHz, D_2O) of feed material **25a**

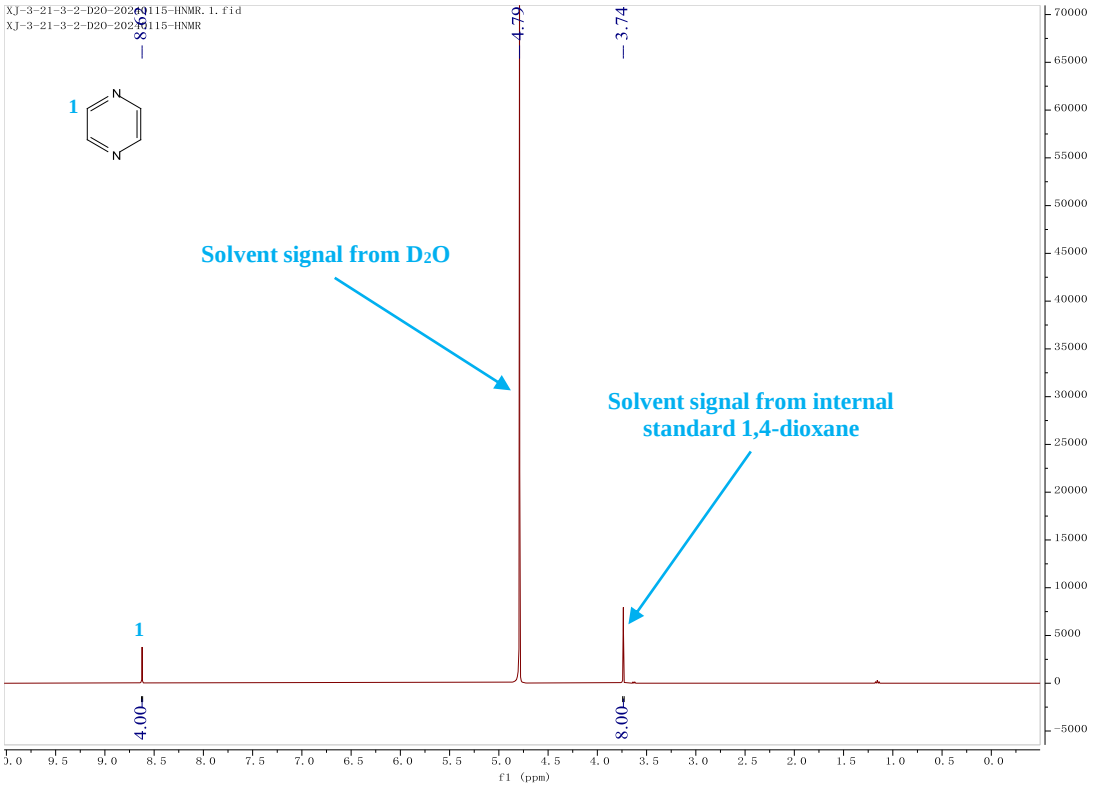

^{1}H NMR (400 MHz, D_2O) of product **25b**

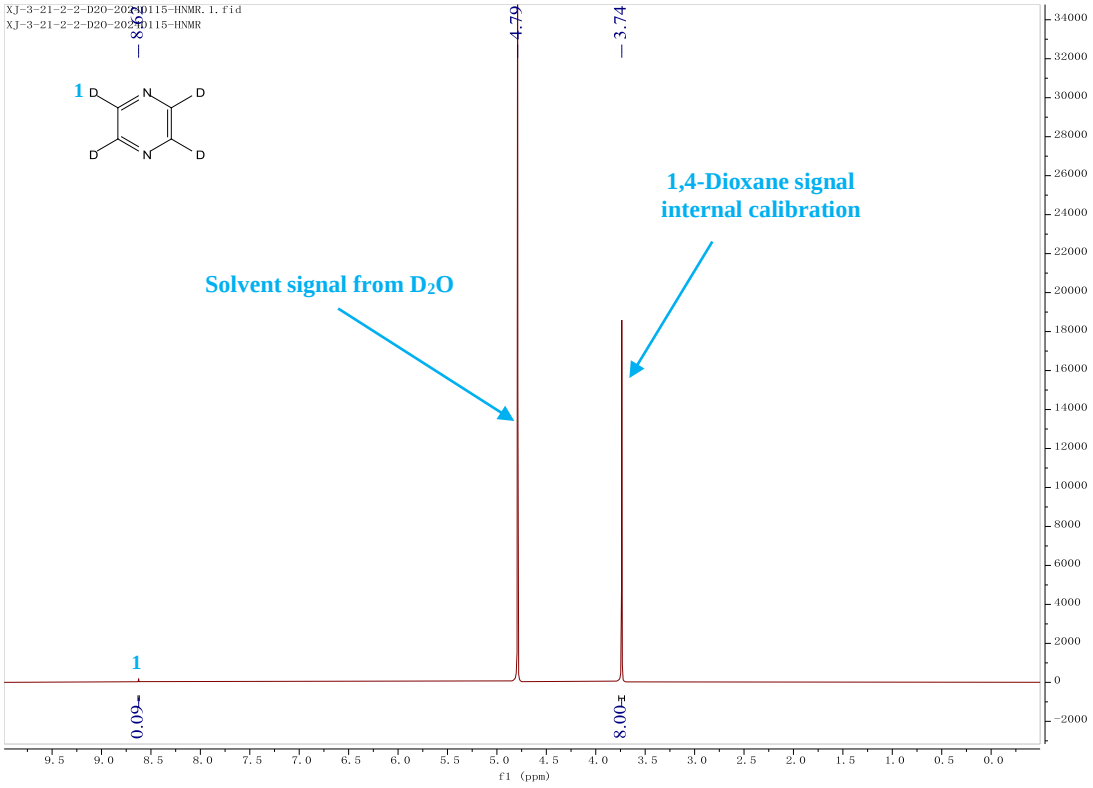

^{1}H NMR (400 MHz, DMSO-d_6) of feed material **26a**

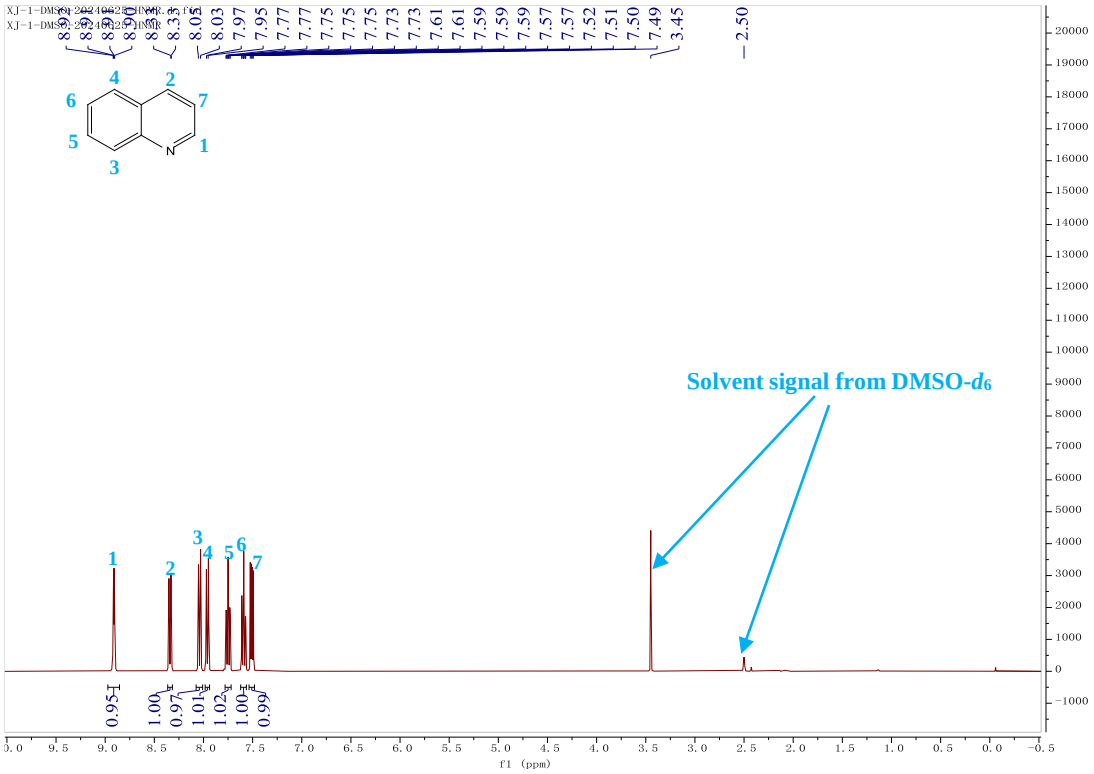

^{1}H NMR (400 MHz, D_2O) of product **26b**

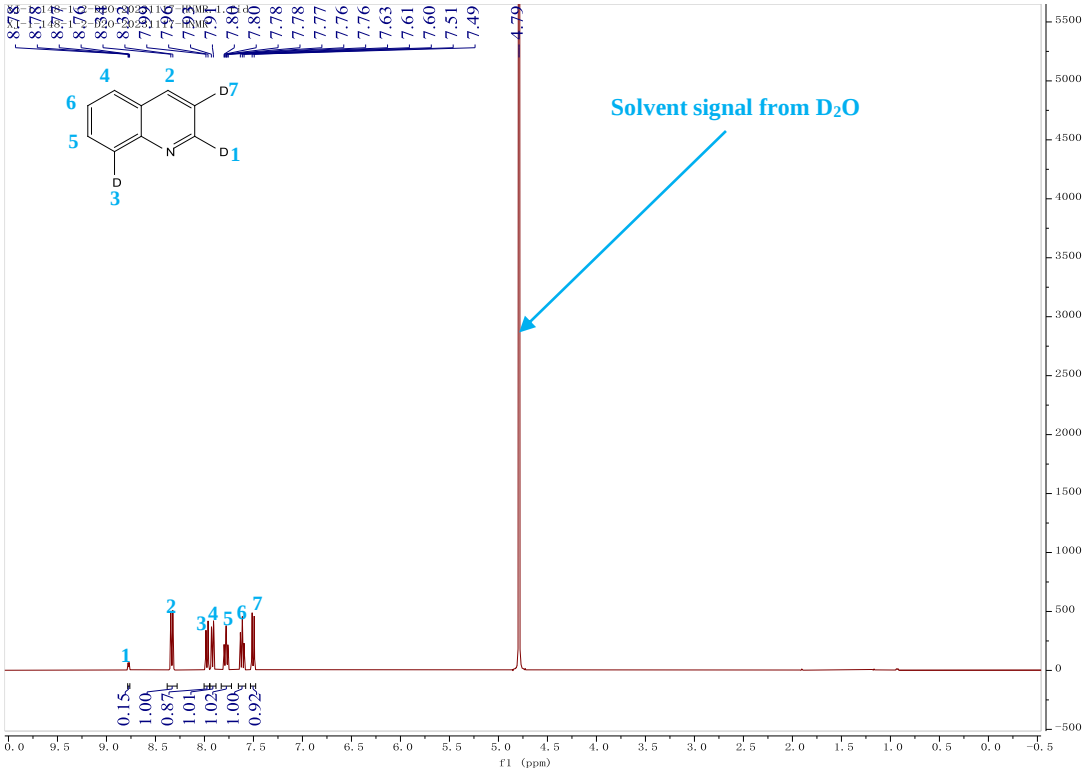

^{1}H NMR (400 MHz, $CDCl_3$) of feed material **27a**

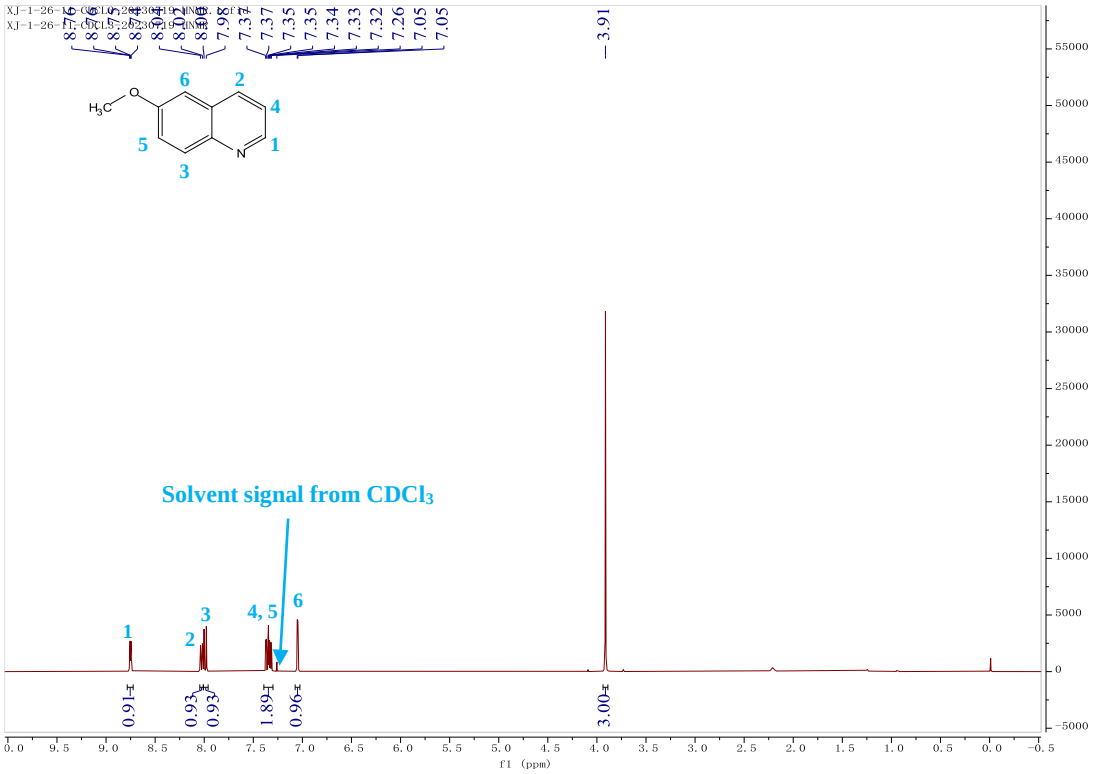

^{1}H NMR (400 MHz, $CDCl_3$) of product **27b**

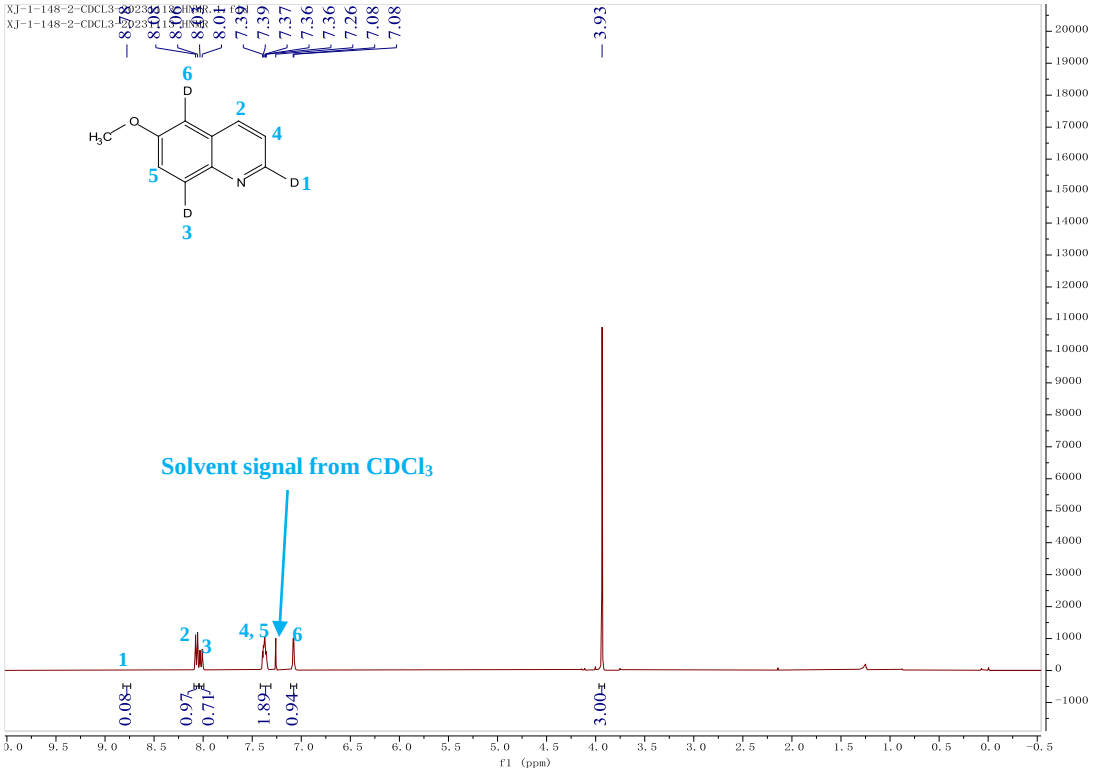

^{1}H NMR (400 MHz, D_2O) of feed material **28a**

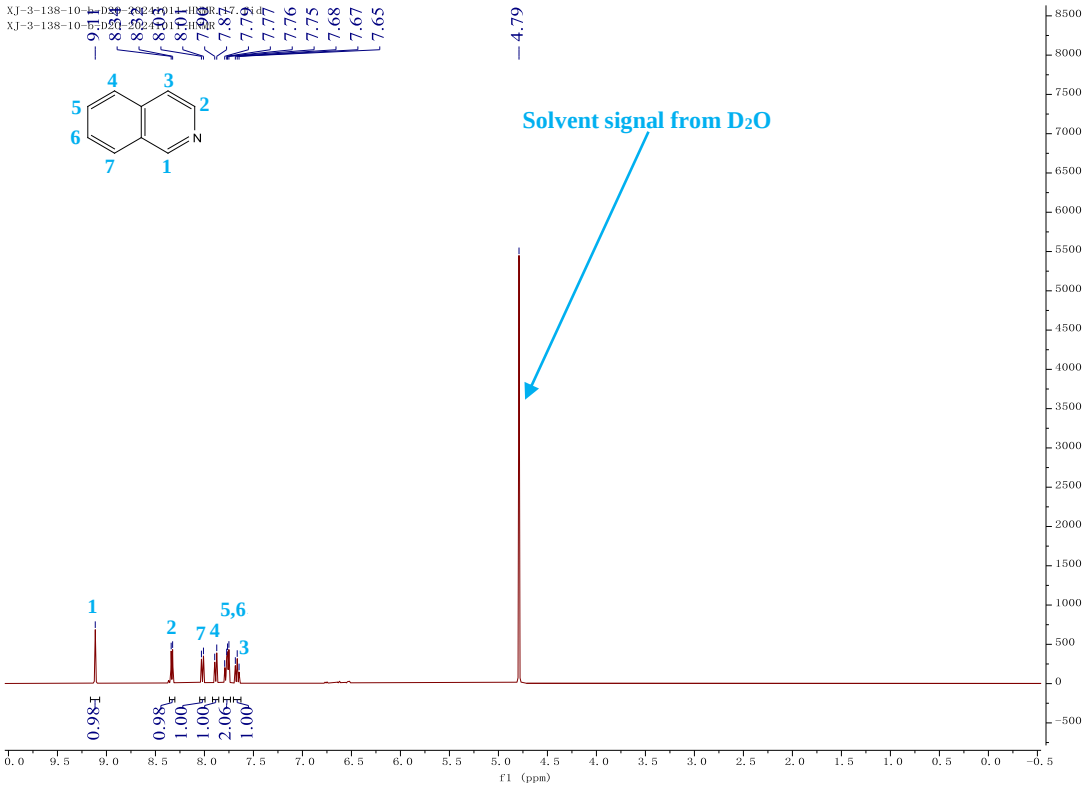

^{1}H NMR (400 MHz, D_2O) of product **28b**

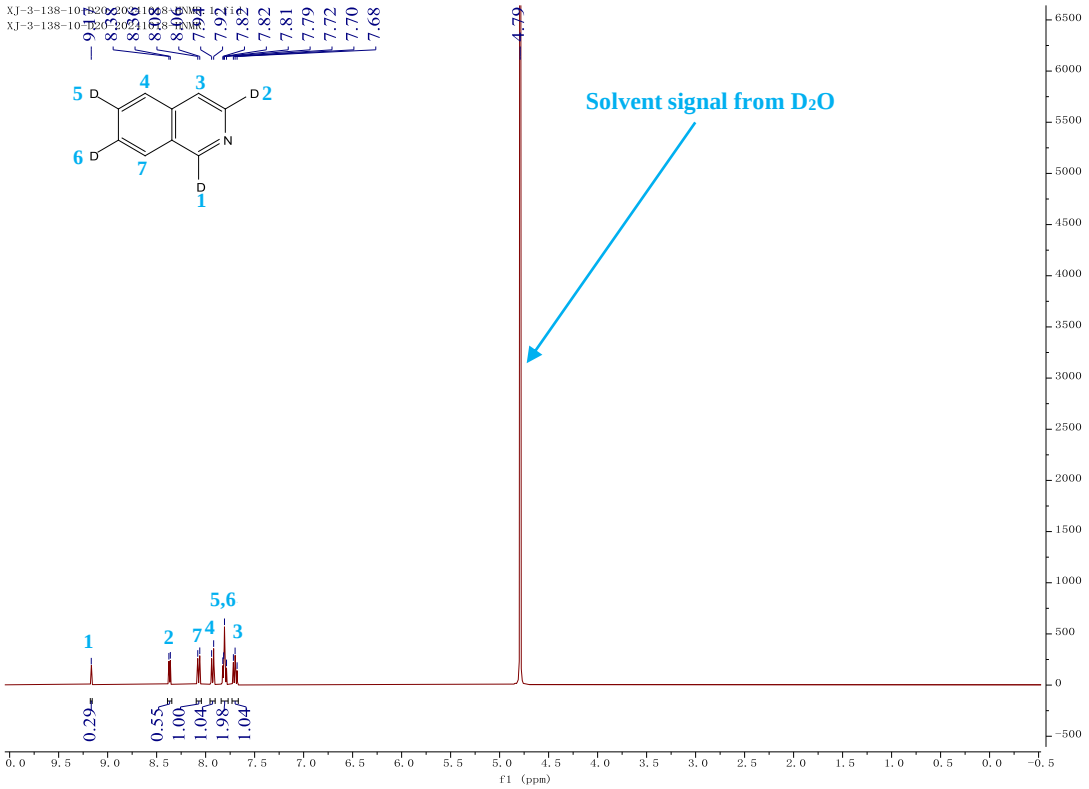

^{1}H NMR (400 MHz, D_2O) of feed material **29a**

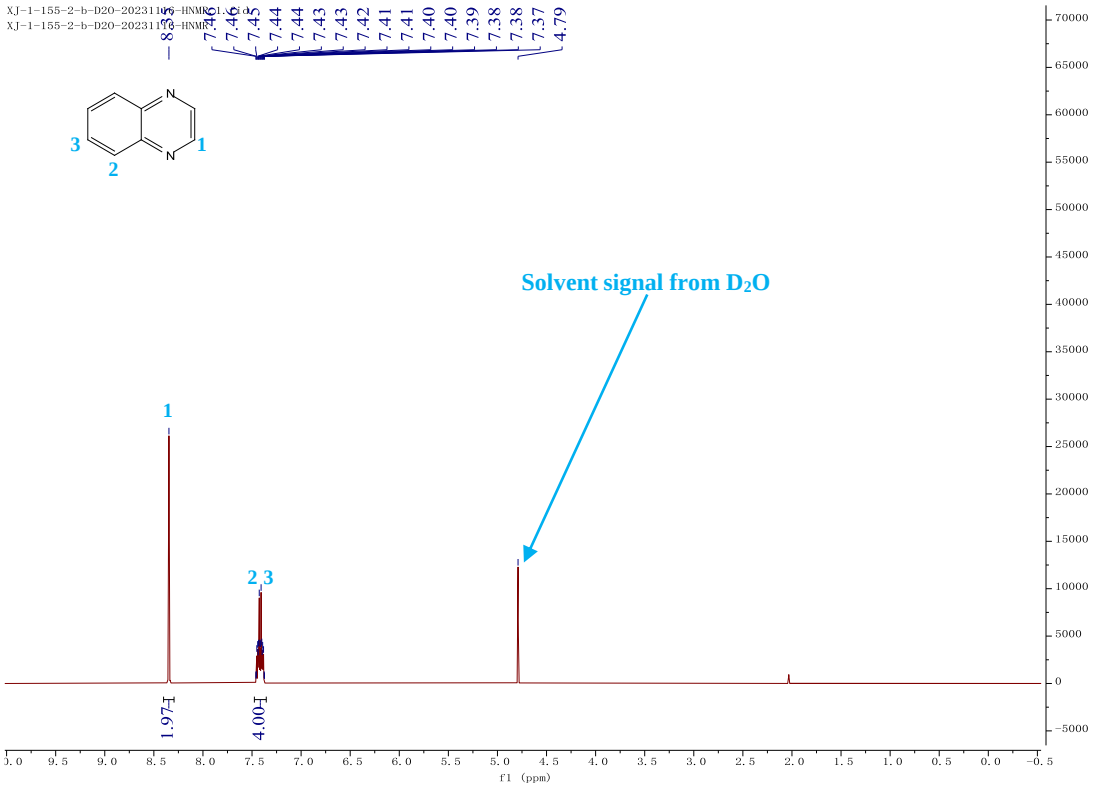

^{1}H NMR (400 MHz, D_2O) of product **29b**

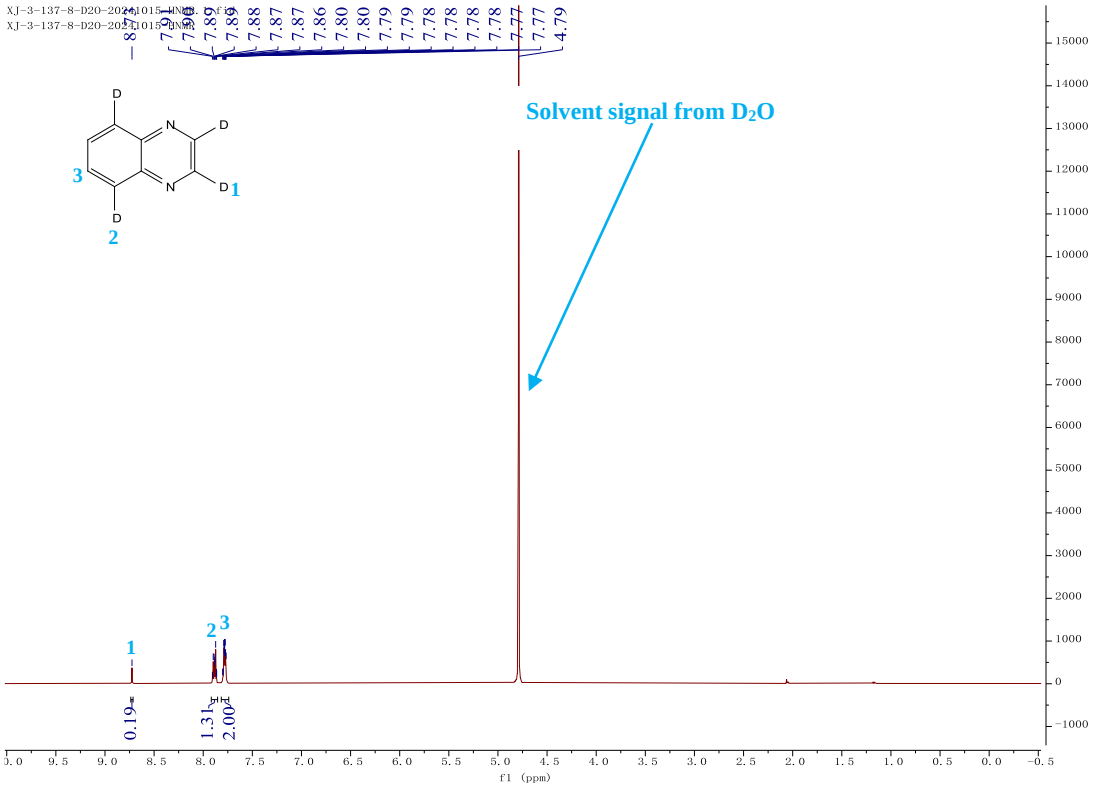

^{1}H NMR (400 MHz, D_2O) of feed material **30a**

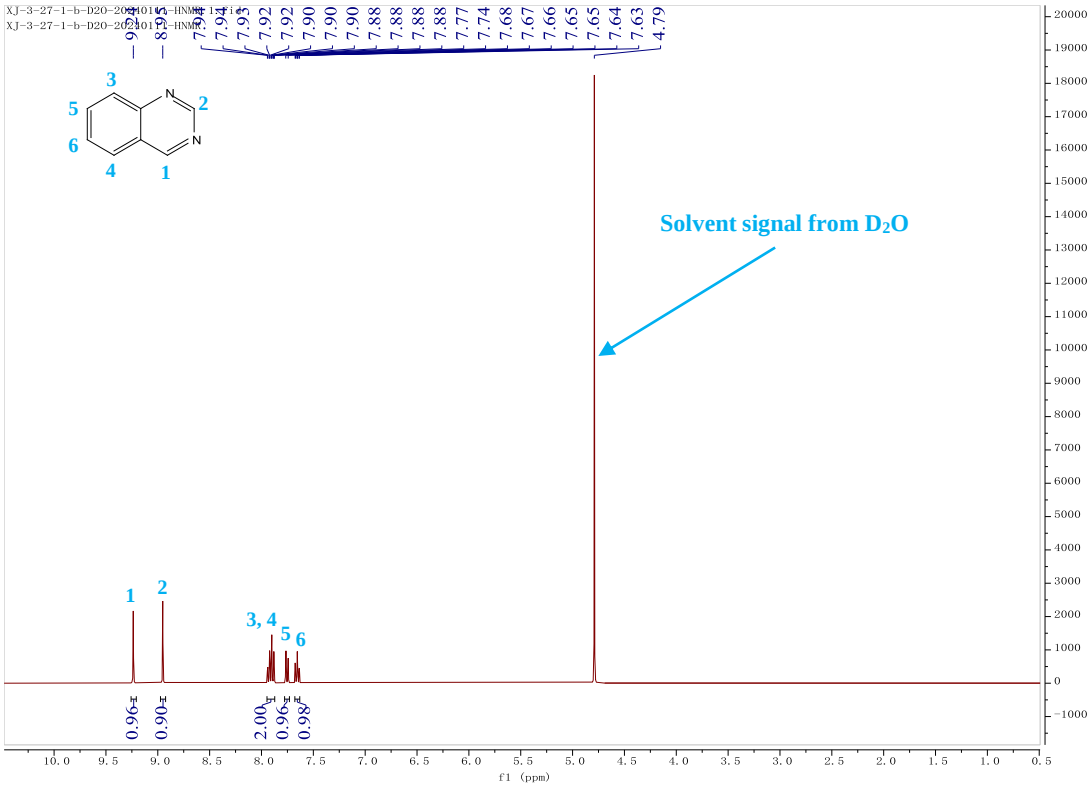

^{1}H NMR (400 MHz, D_2O) of product **30b**

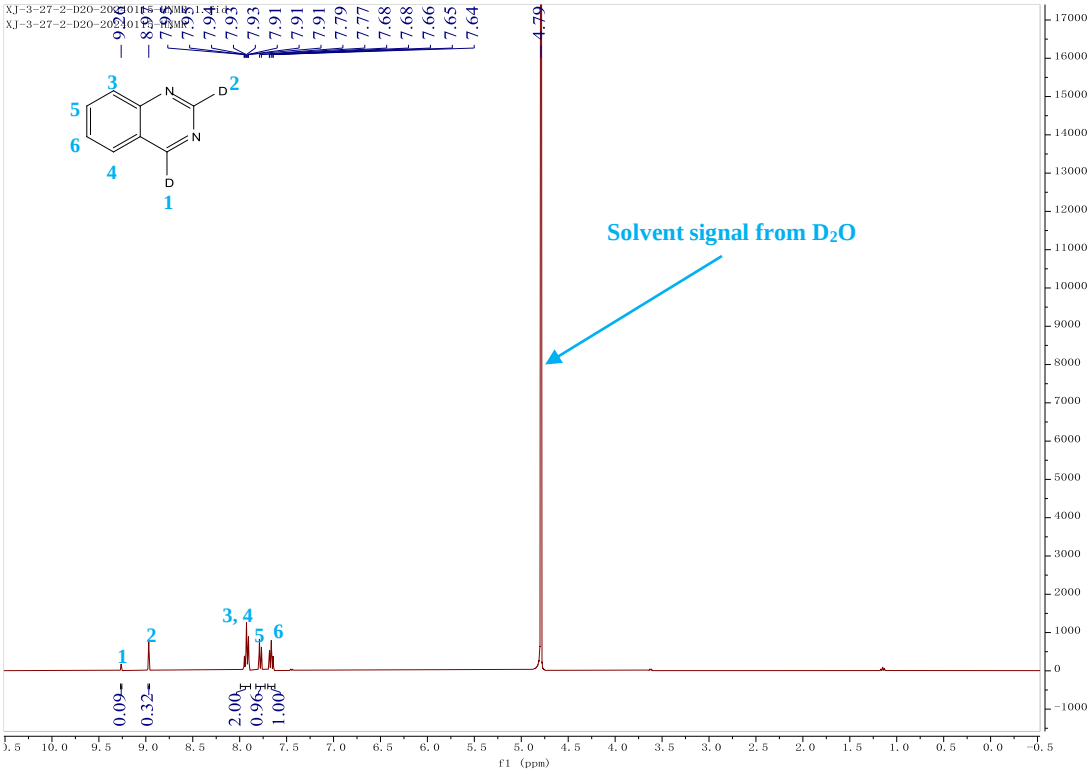

^{1}H NMR (400 MHz, DMSO-d_6) of feed material **31a**

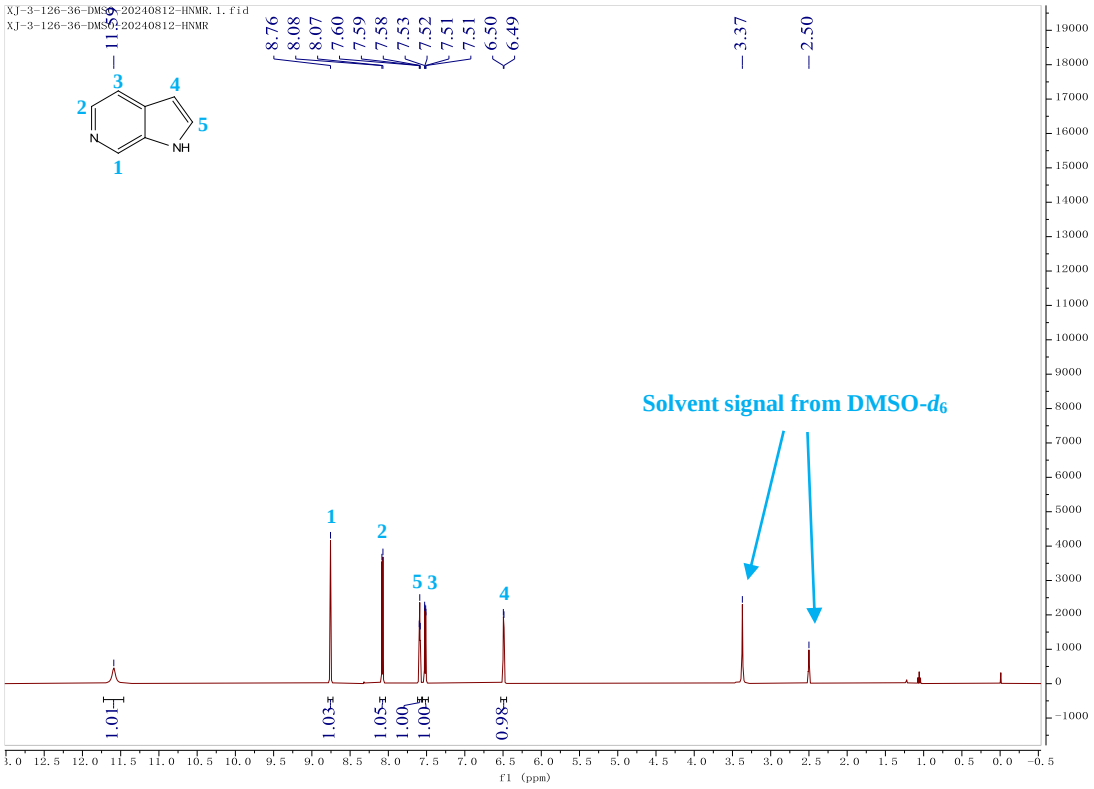

^{1}H NMR (400 MHz, DMSO-d_6) of product **31b**

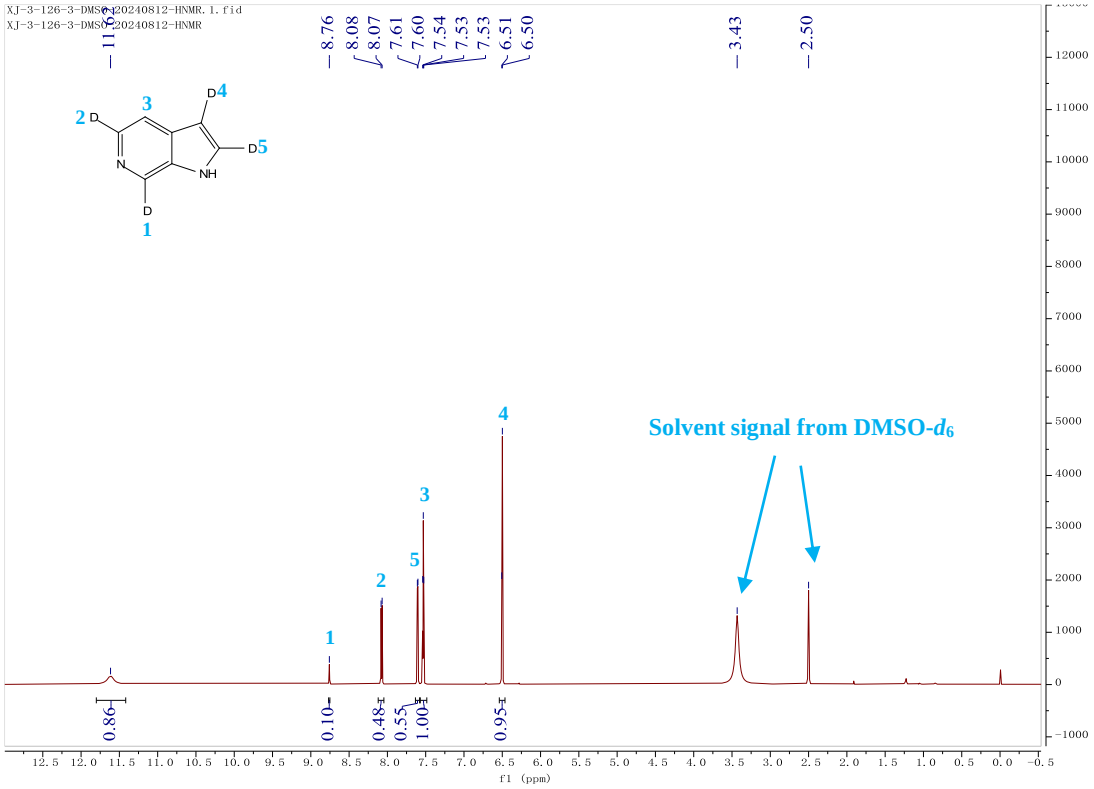

^{1}H NMR (400 MHz, DMSO-d_6) of feed material **32a**

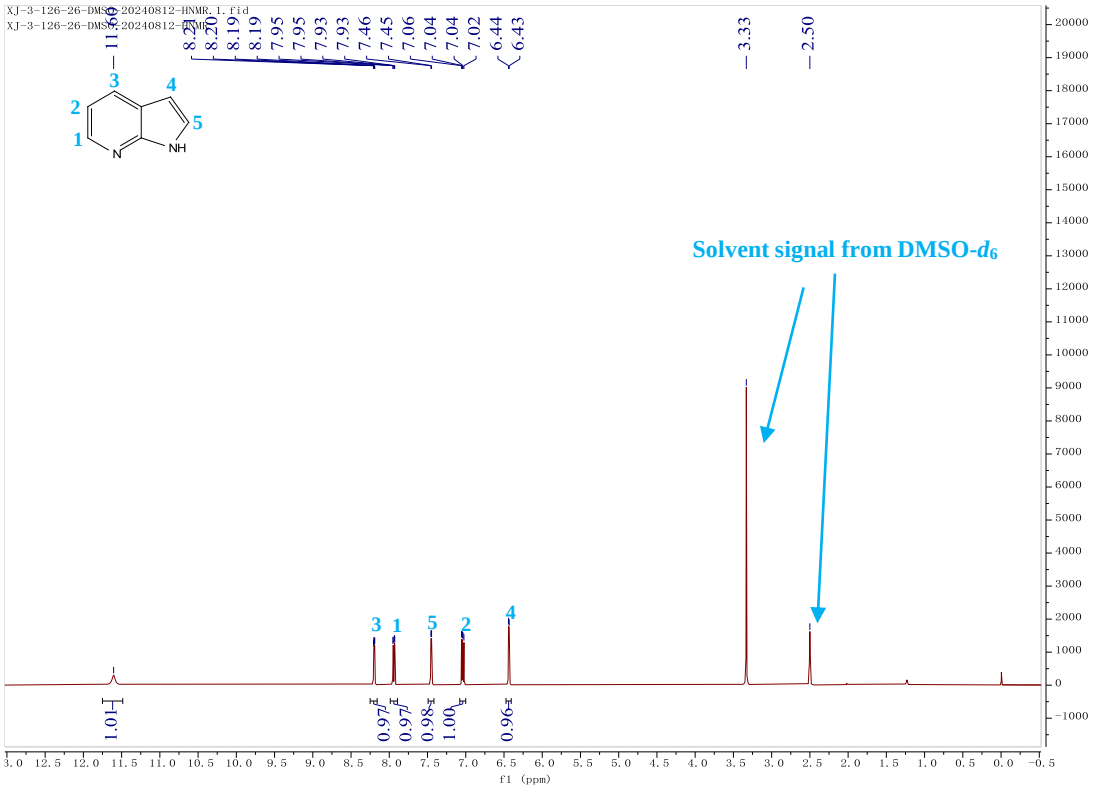

^{1}H NMR (400 MHz, DMSO-d_6) of product **32b**

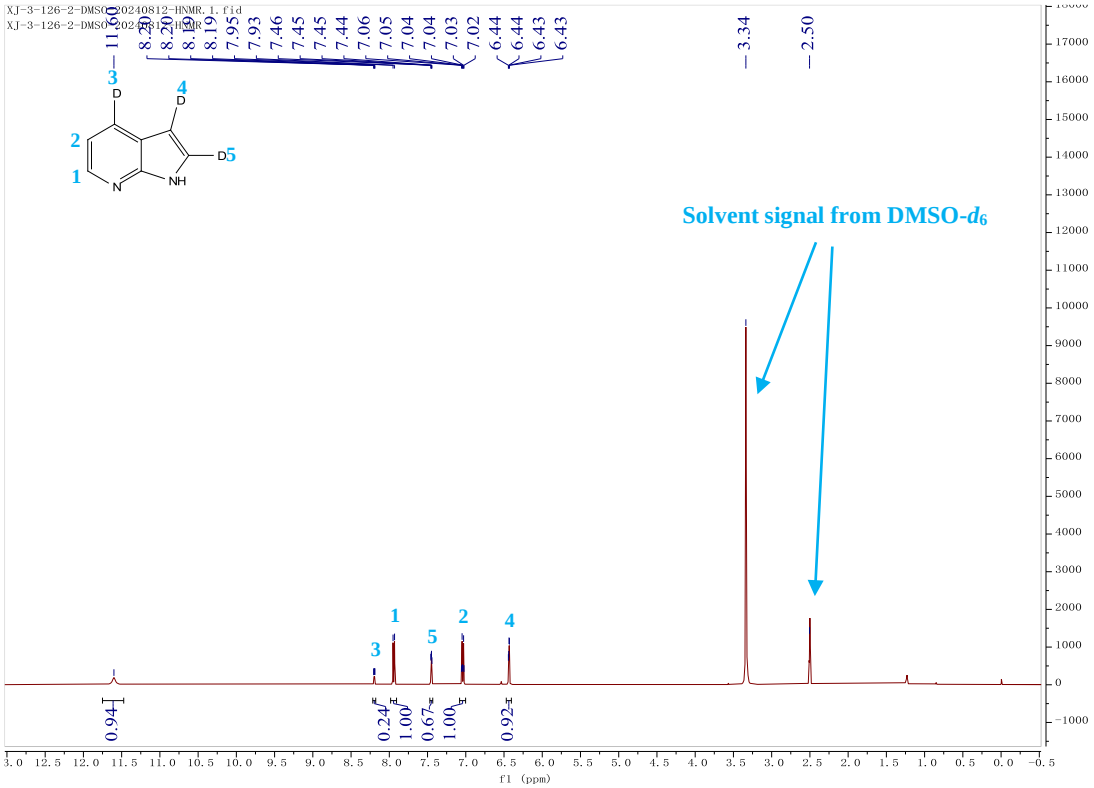

^{1}H NMR (400 MHz, $CDCl_3$) of feed material **33a**

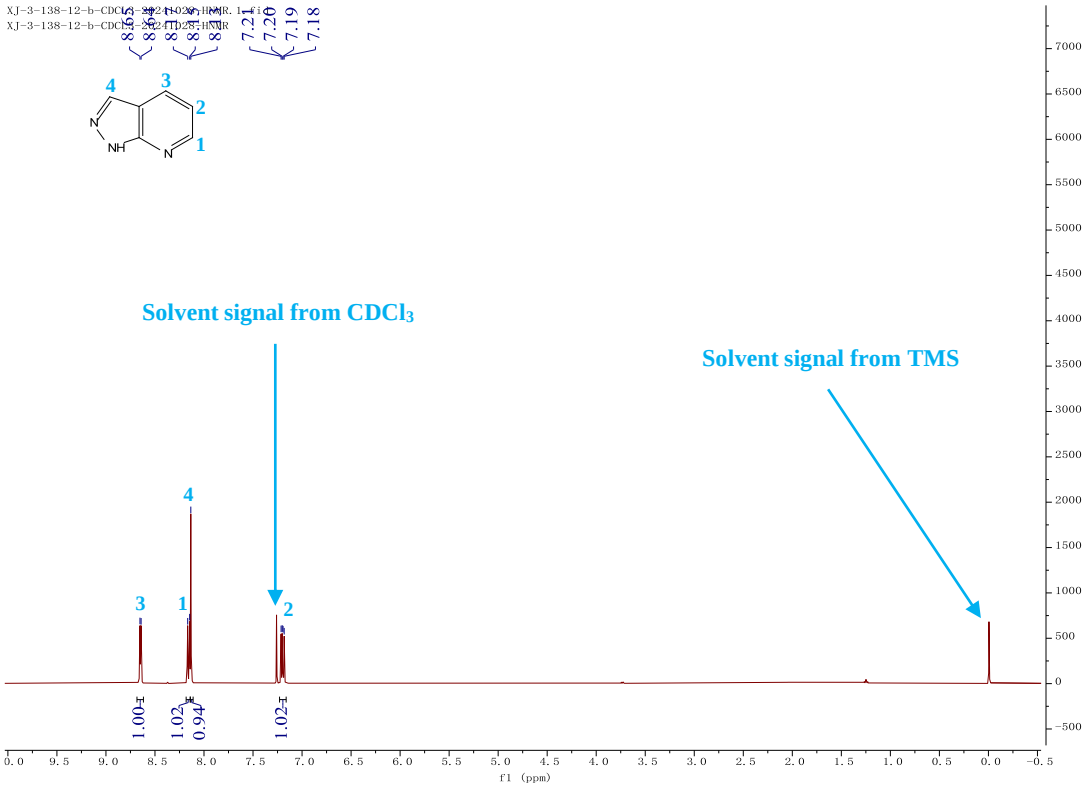

^{1}H NMR (400 MHz, $CDCl_3$) of product **33b**

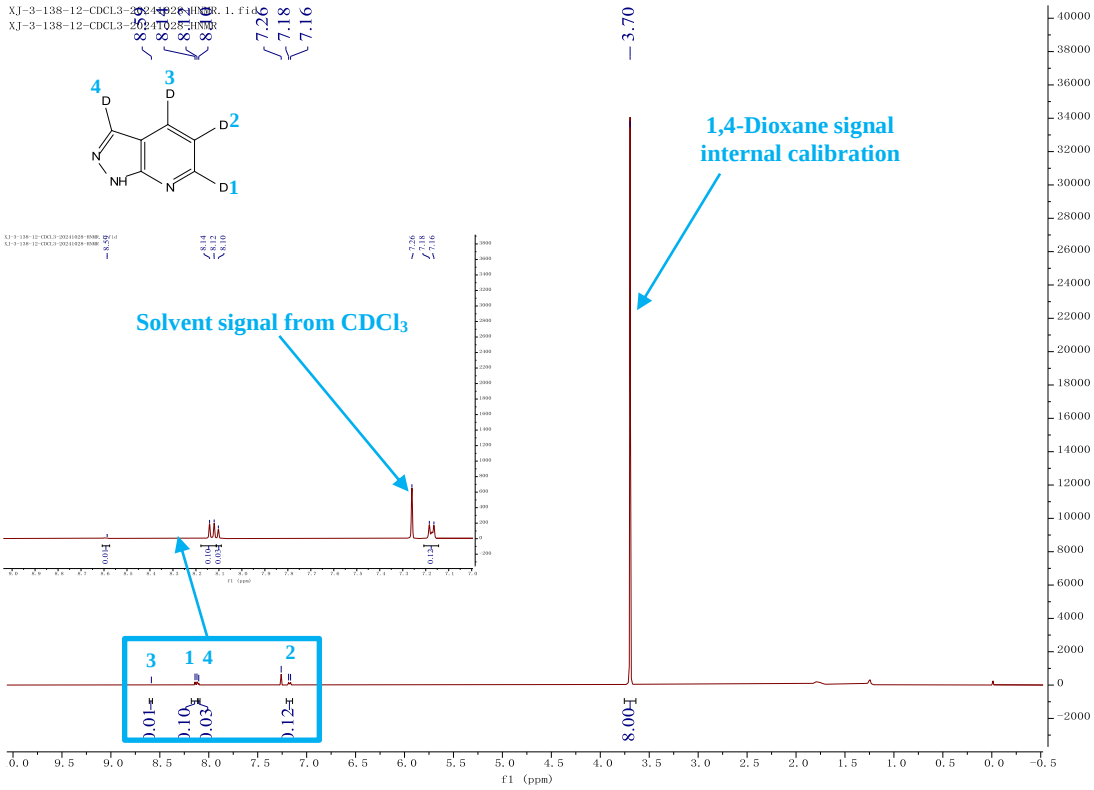

^{1}H NMR (400 MHz, $CDCl_3$) of feed material **34a**

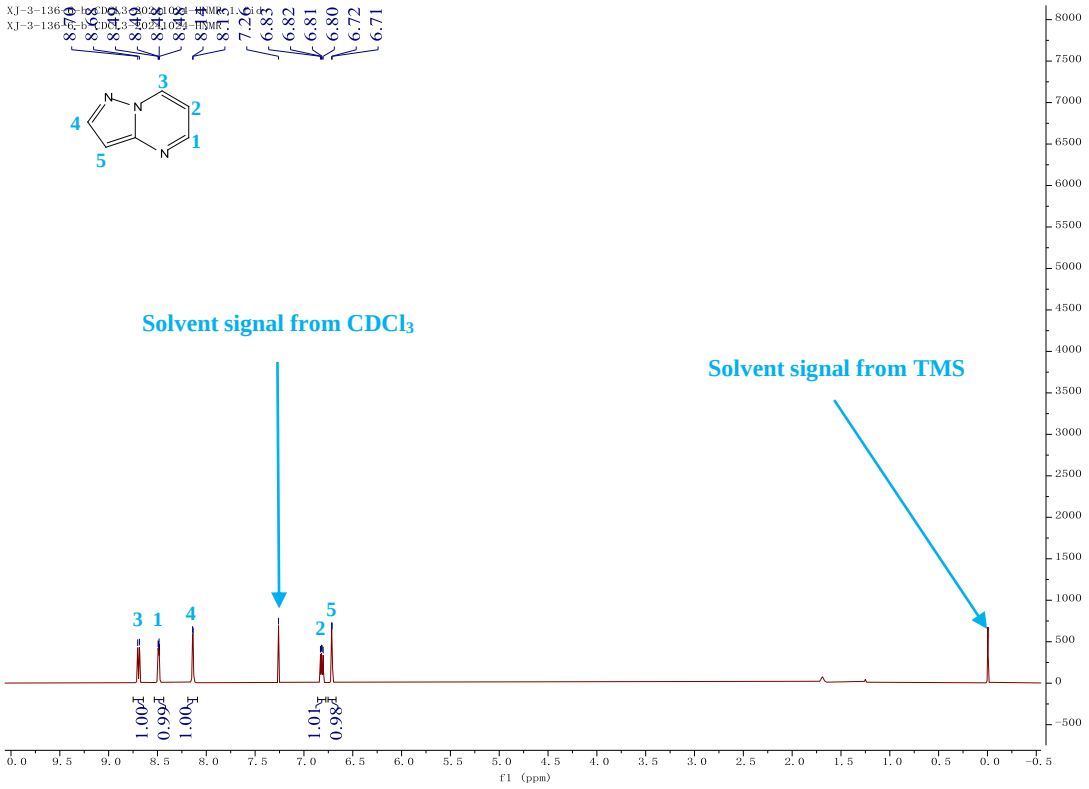

^{1}H NMR (400 MHz, $CDCl_3$) of product **34b**

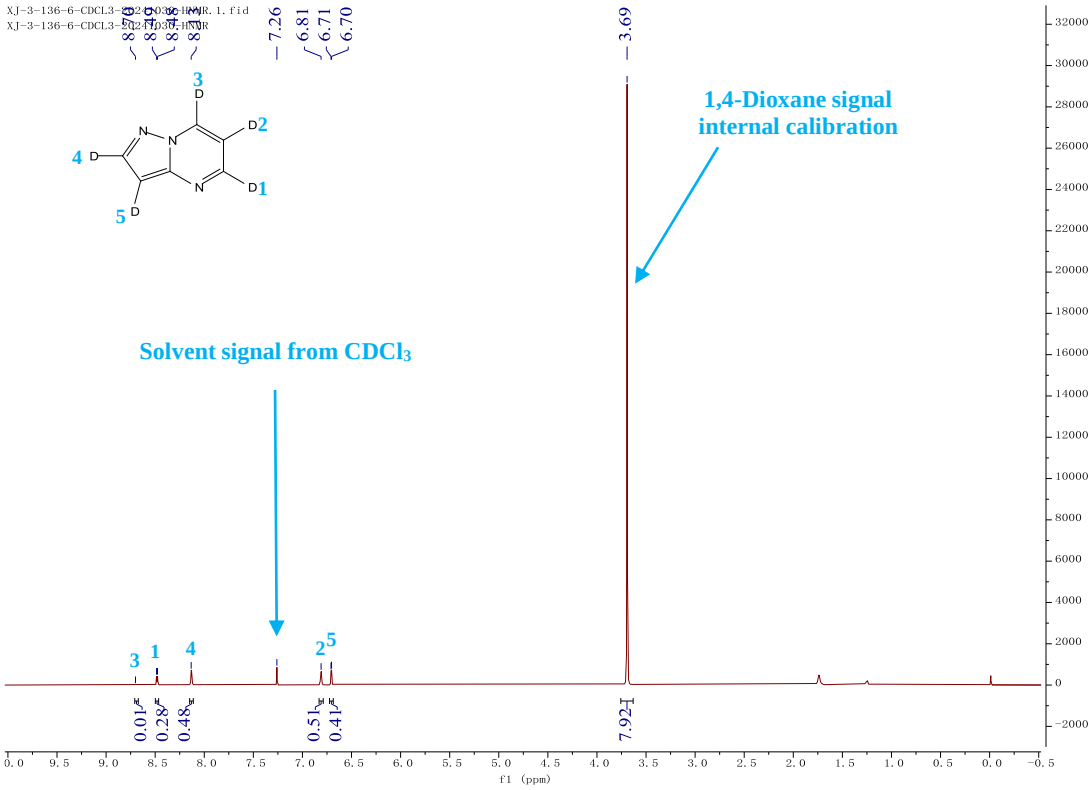

^{1}H NMR (400 MHz, $CDCl_3$) of feed material **35a**

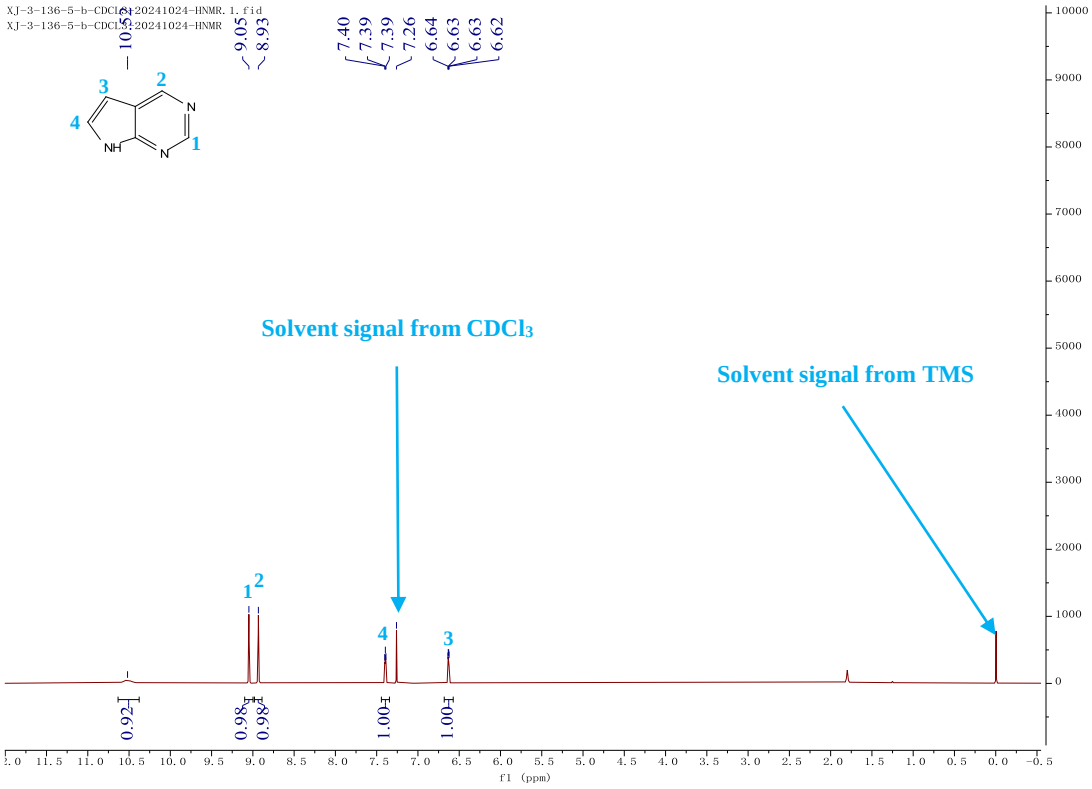

^{1}H NMR (400 MHz, $CDCl_3$) of product **35b**

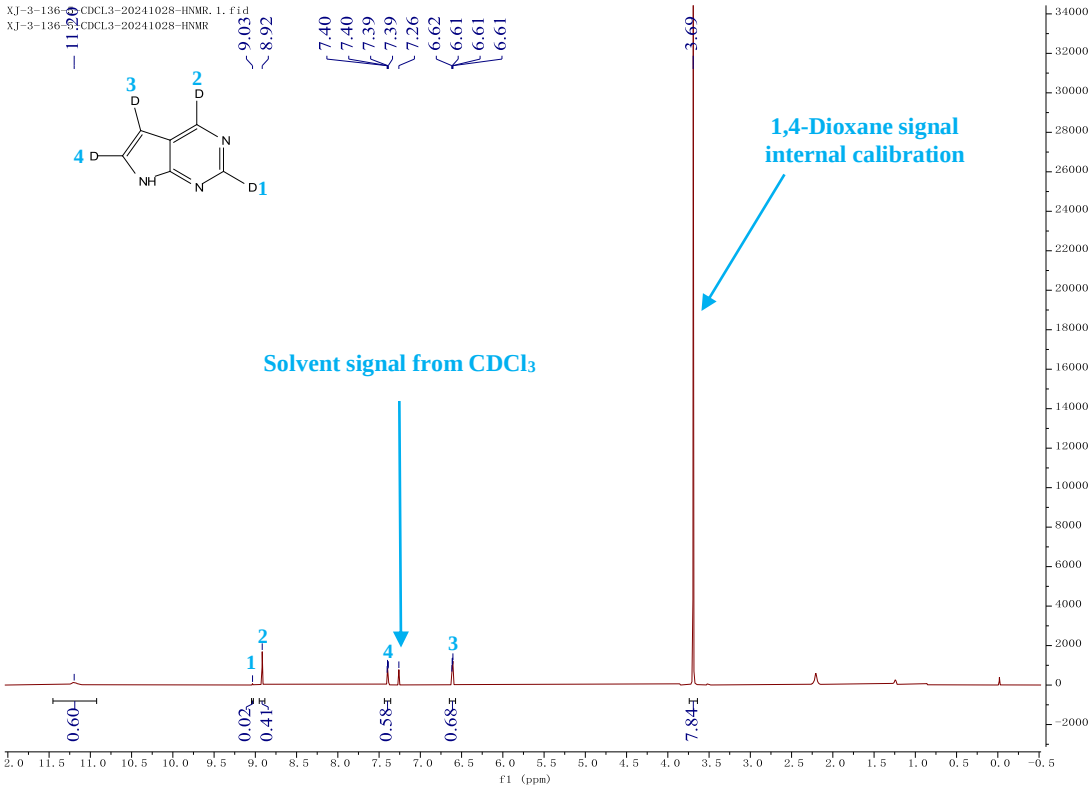

^{1}H NMR (400 MHz, D_2O) of feed material **36a**

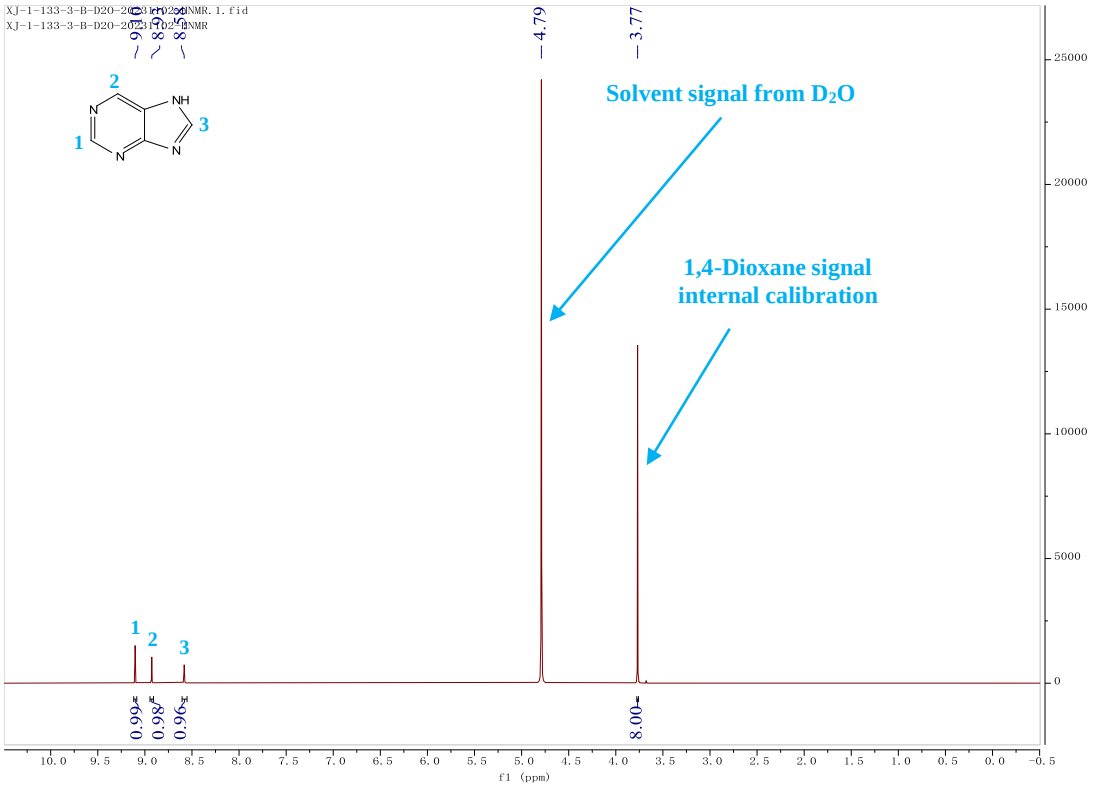

^{1}H NMR (400 MHz, D_2O) of product **36b**

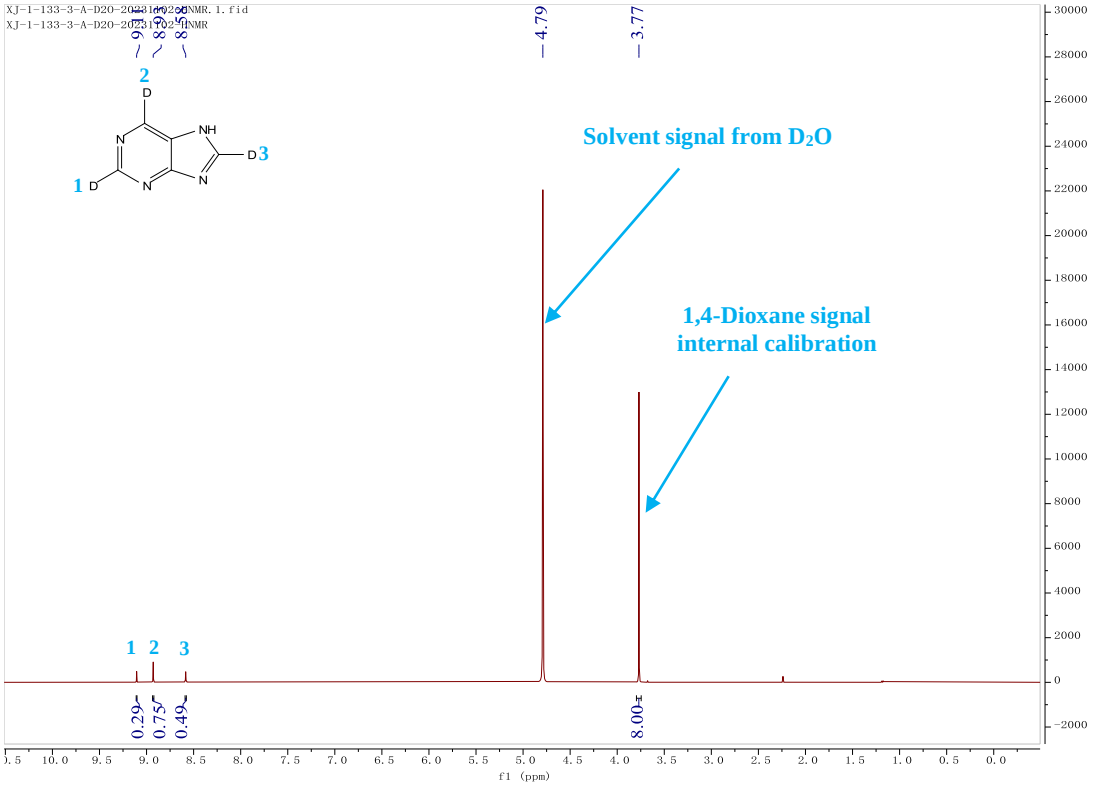

^{1}H NMR (400 MHz, D_2O) of feed material **37a**

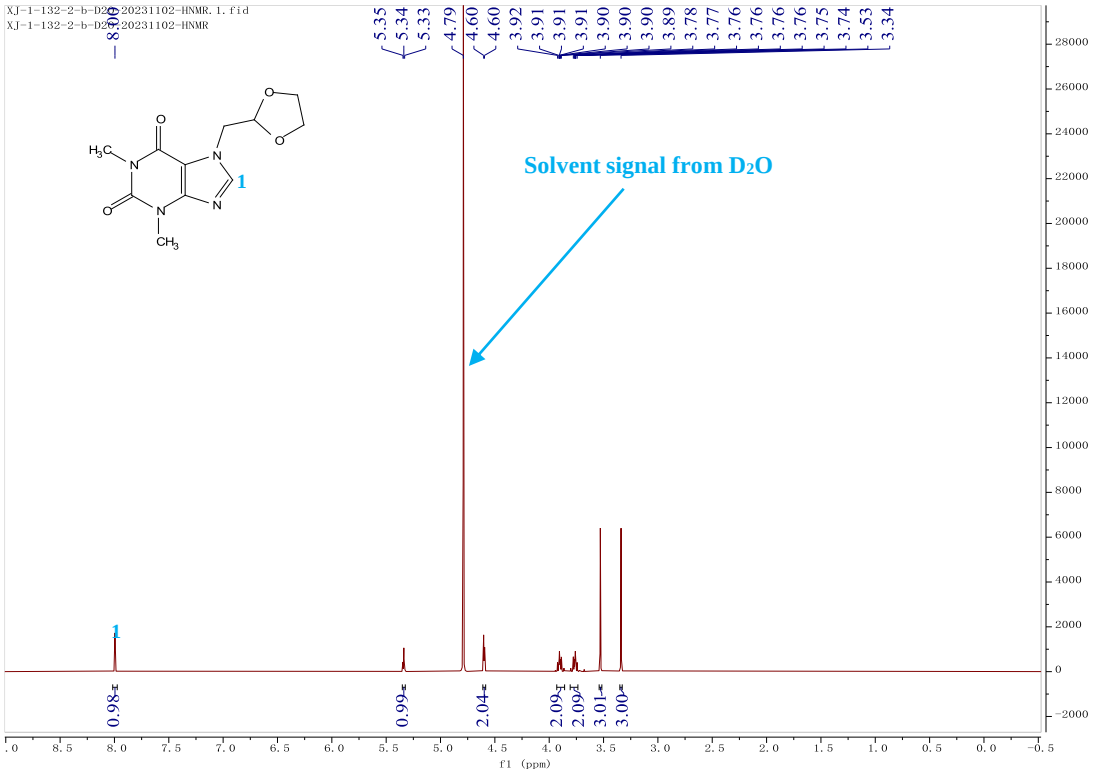

^{1}H NMR (400 MHz, D_2O) of product **37b**

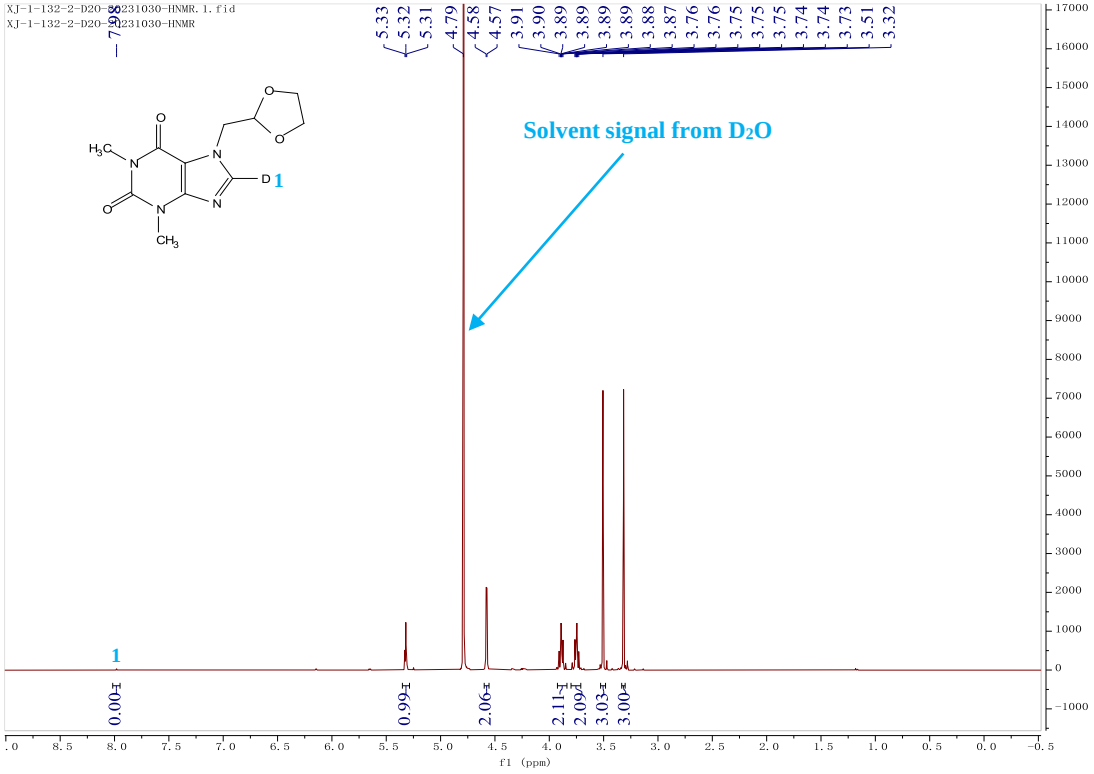

^{1}H NMR (400 MHz, D_2O) of feed material **38a**

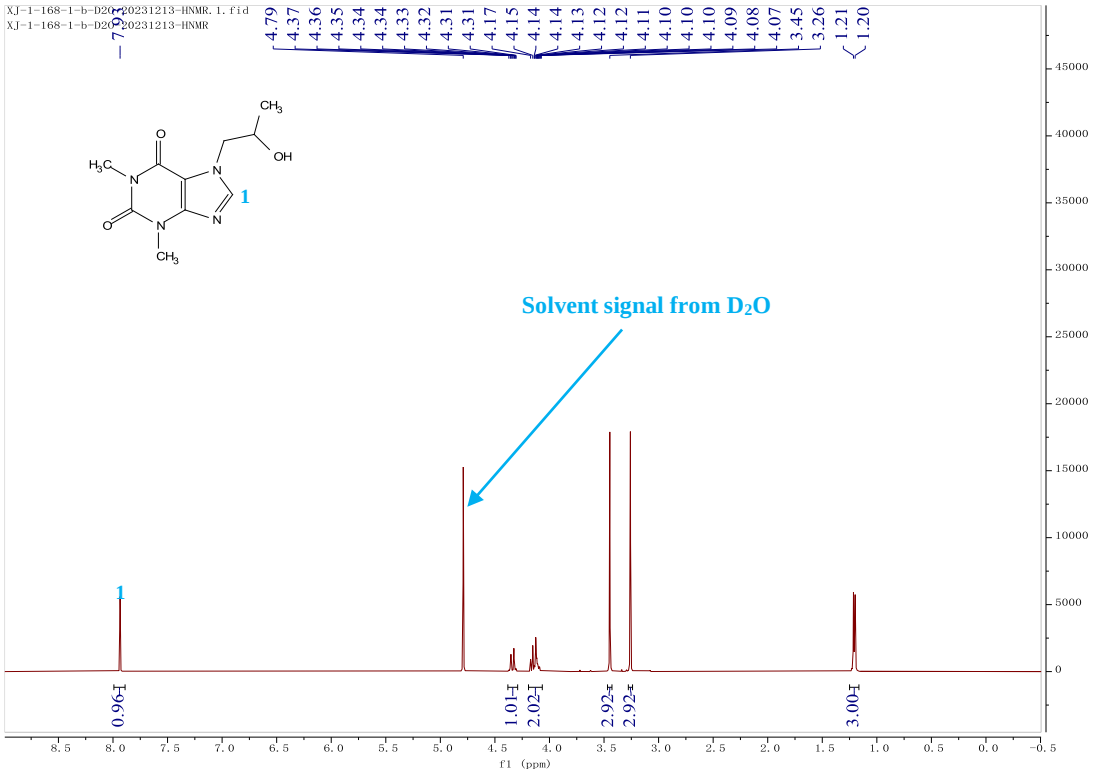

^{1}H NMR (400 MHz, D_2O) of product **38b**

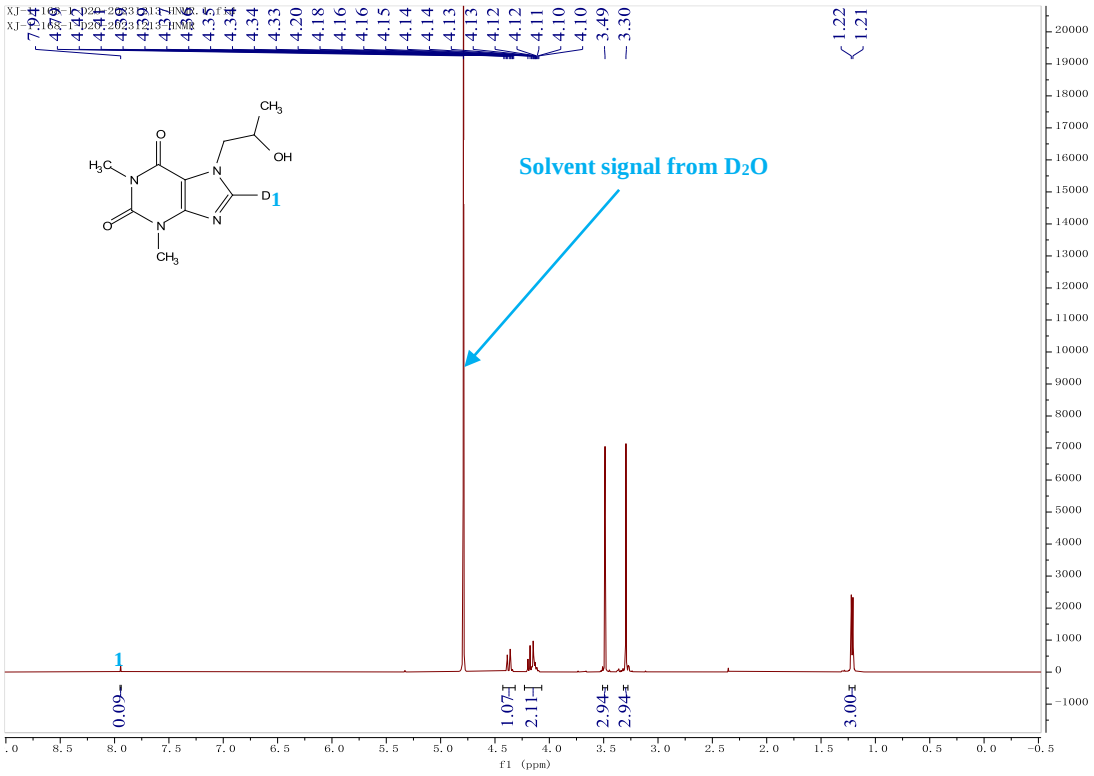

^{1}H NMR (400 MHz, D_2O) of feed material **39a**

^{1}H NMR (400 MHz, D_2O) of product **39b**

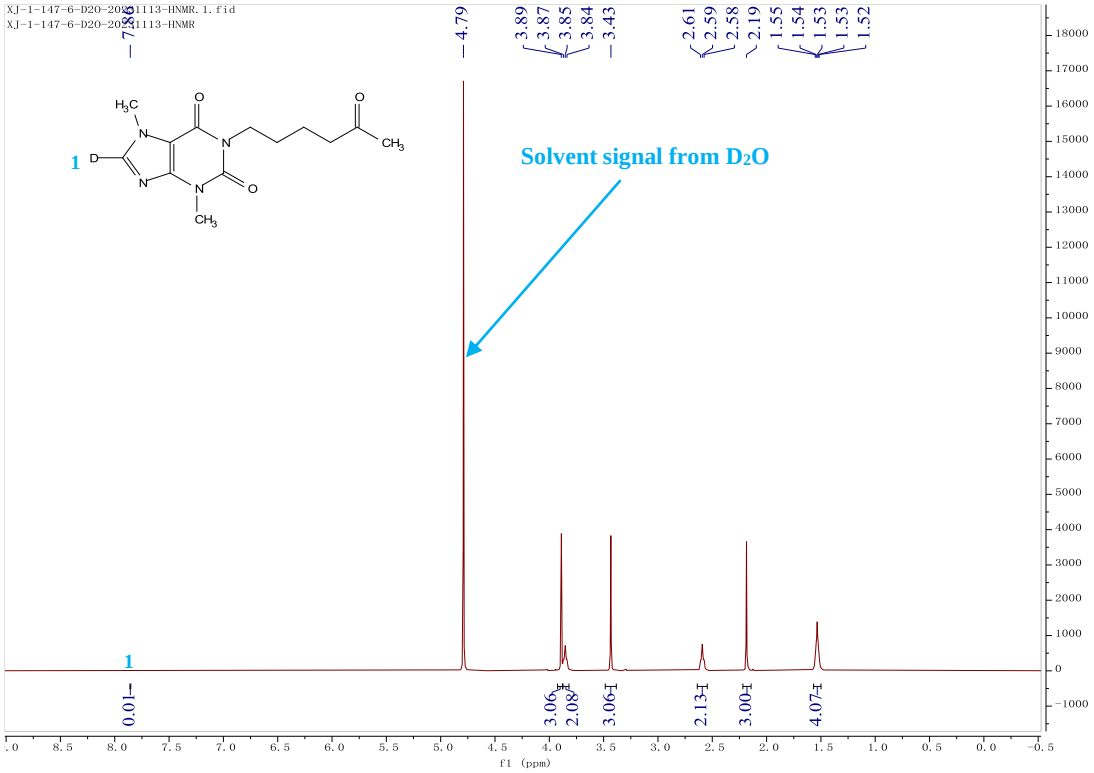

^{1}H NMR (400 MHz, D_2O) of feed material **40a**

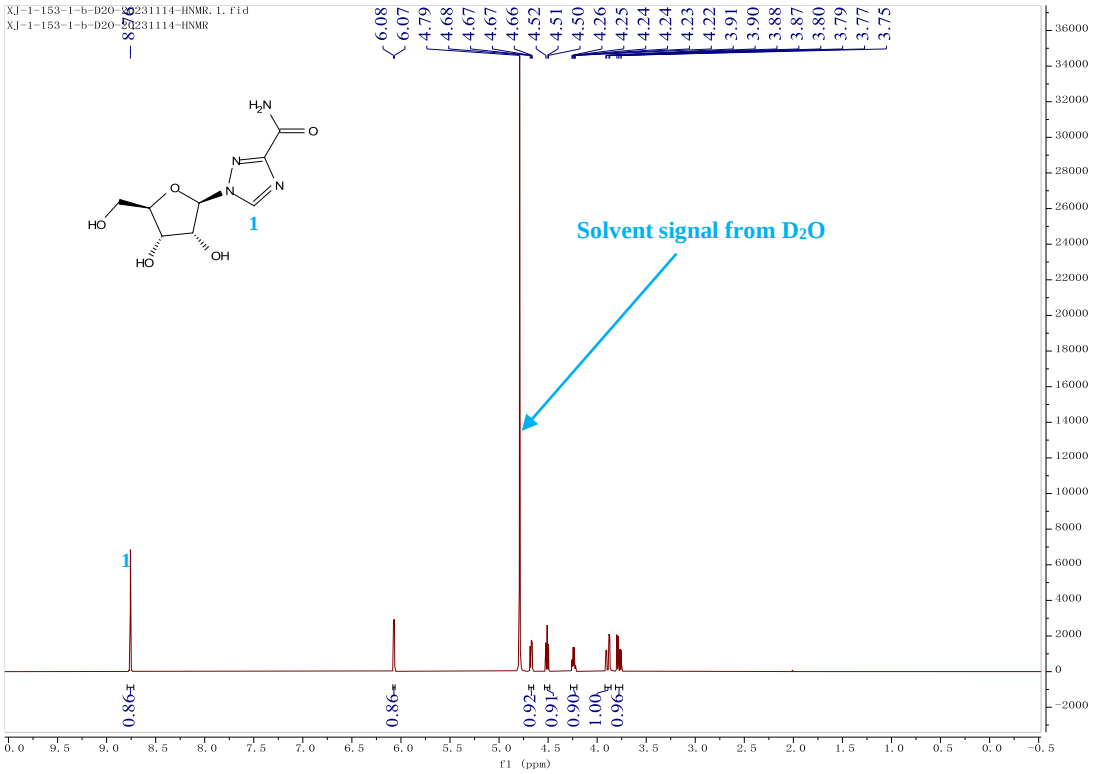

^{1}H NMR (400 MHz, D_2O) of product **40b**

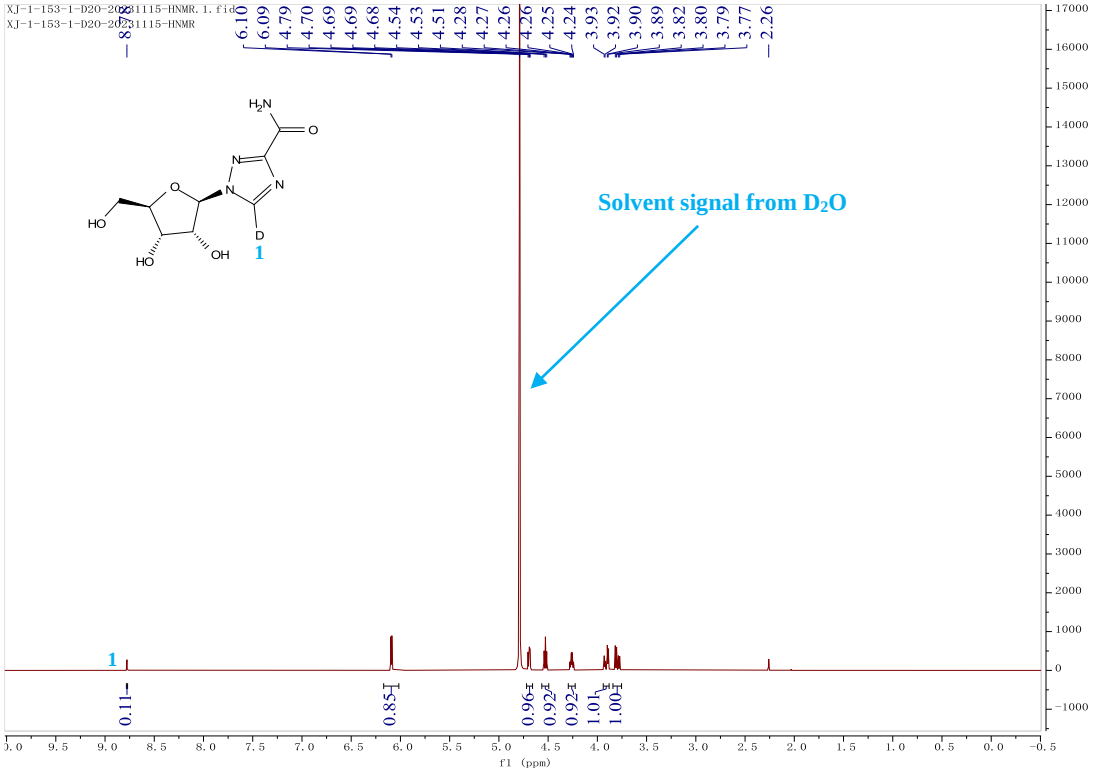

^{1}H NMR (400 MHz, DMSO-d_6) of feed material **41a**

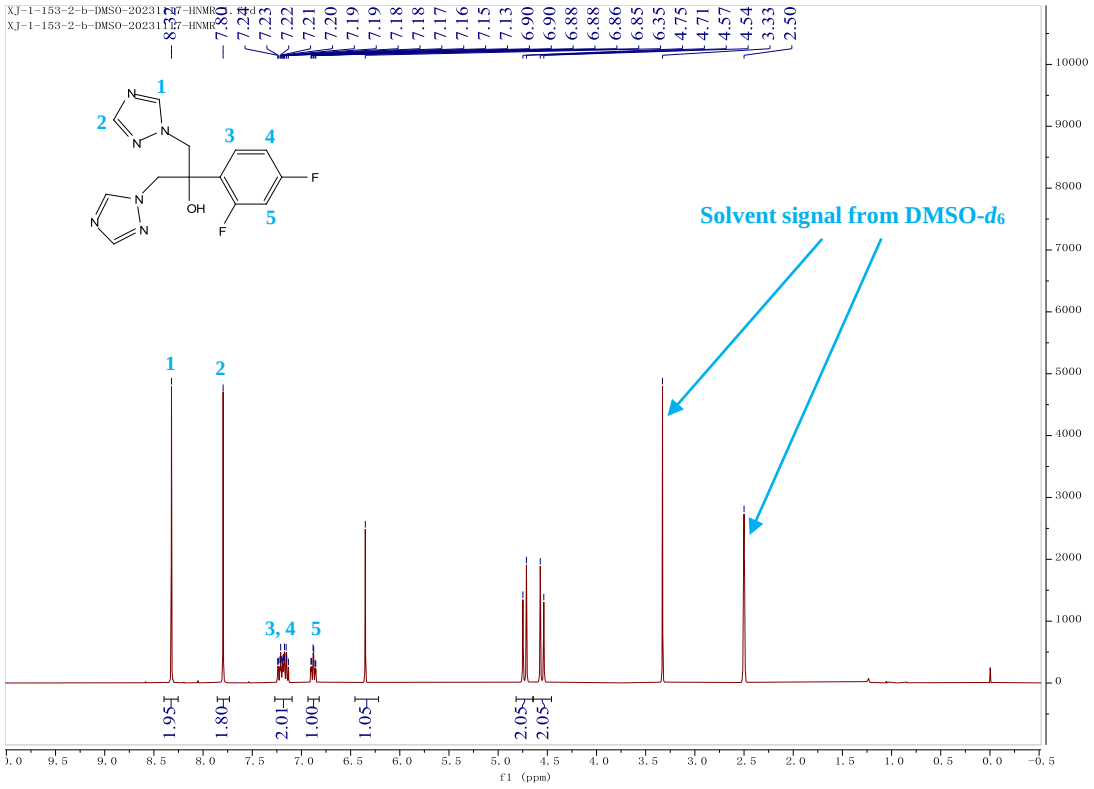

^{1}H NMR (400 MHz, DMSO-d_6) of product **41b**

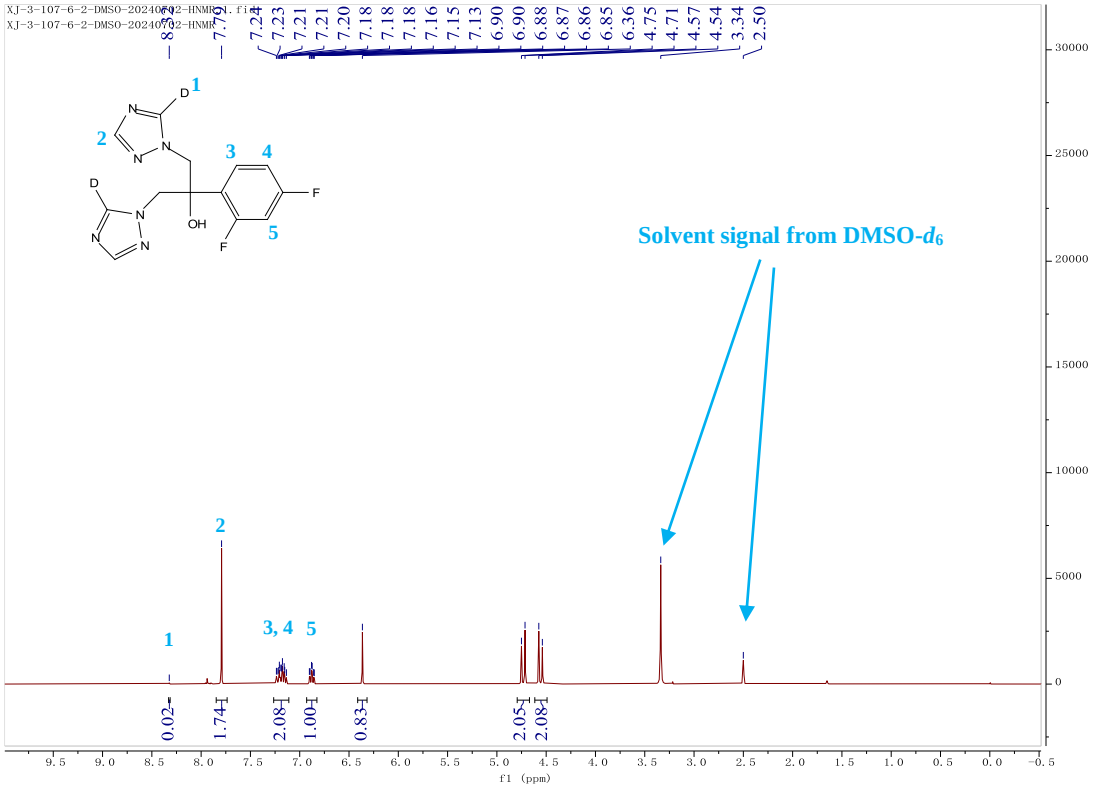

^{1}H NMR (400 MHz, D_2O) of feed material **42a**

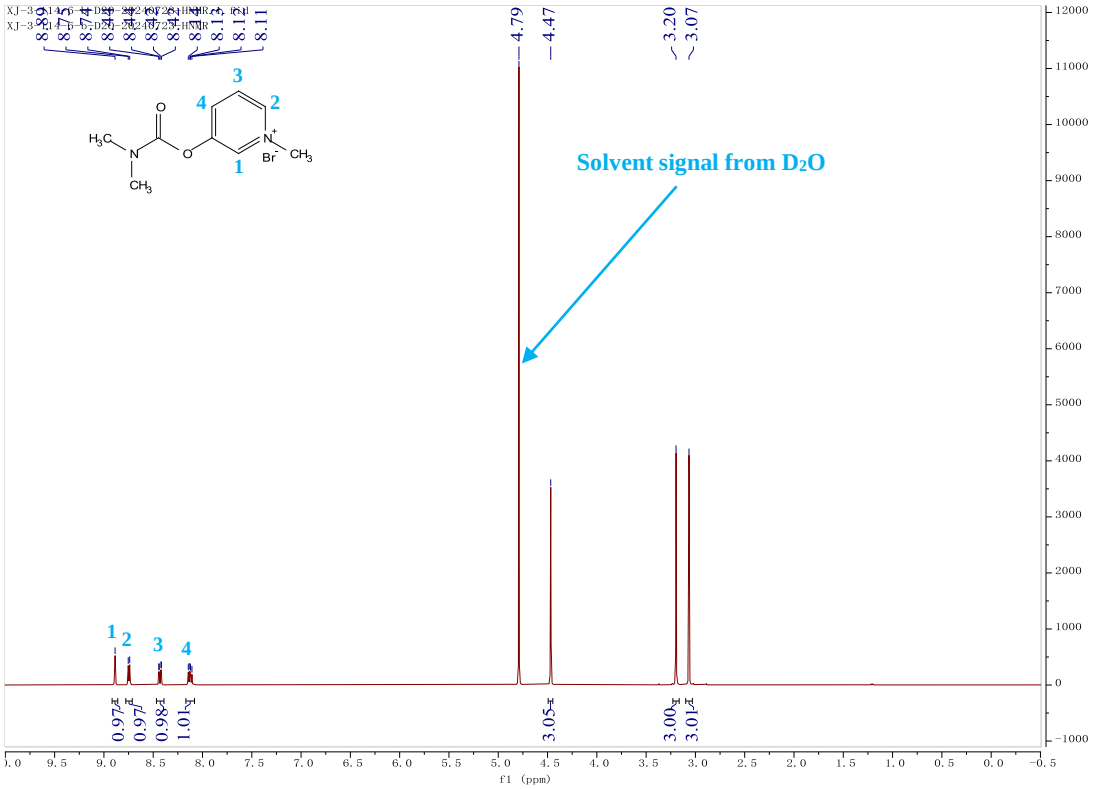

^{1}H NMR (400 MHz, D_2O) of product **42b**

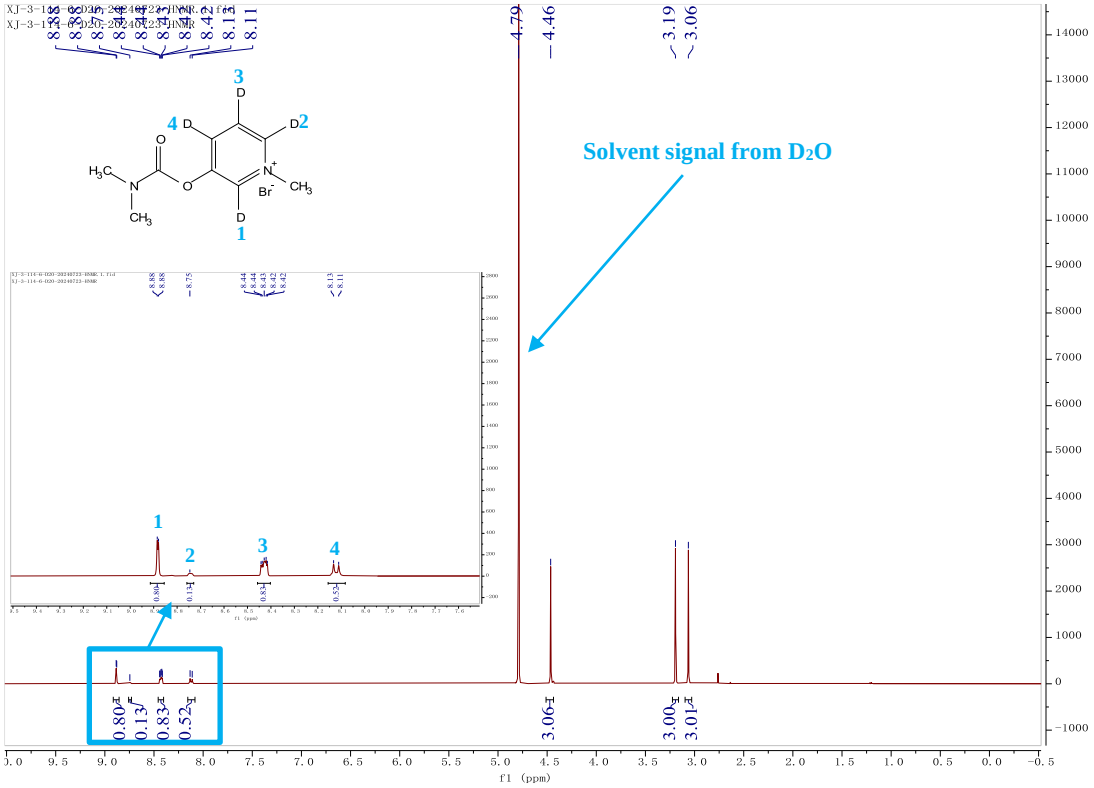

^{1}H NMR (400 MHz, D_2O) of feed material **43a**

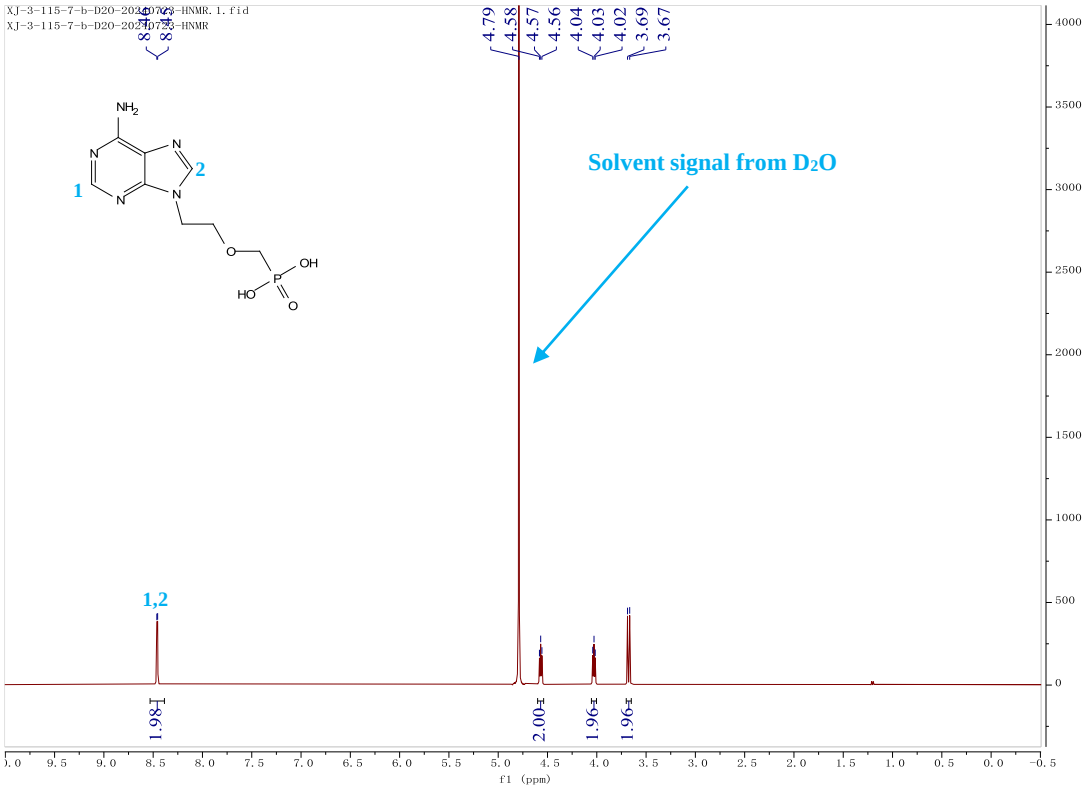

^{1}H NMR (400 MHz, D_2O) of product **43b**

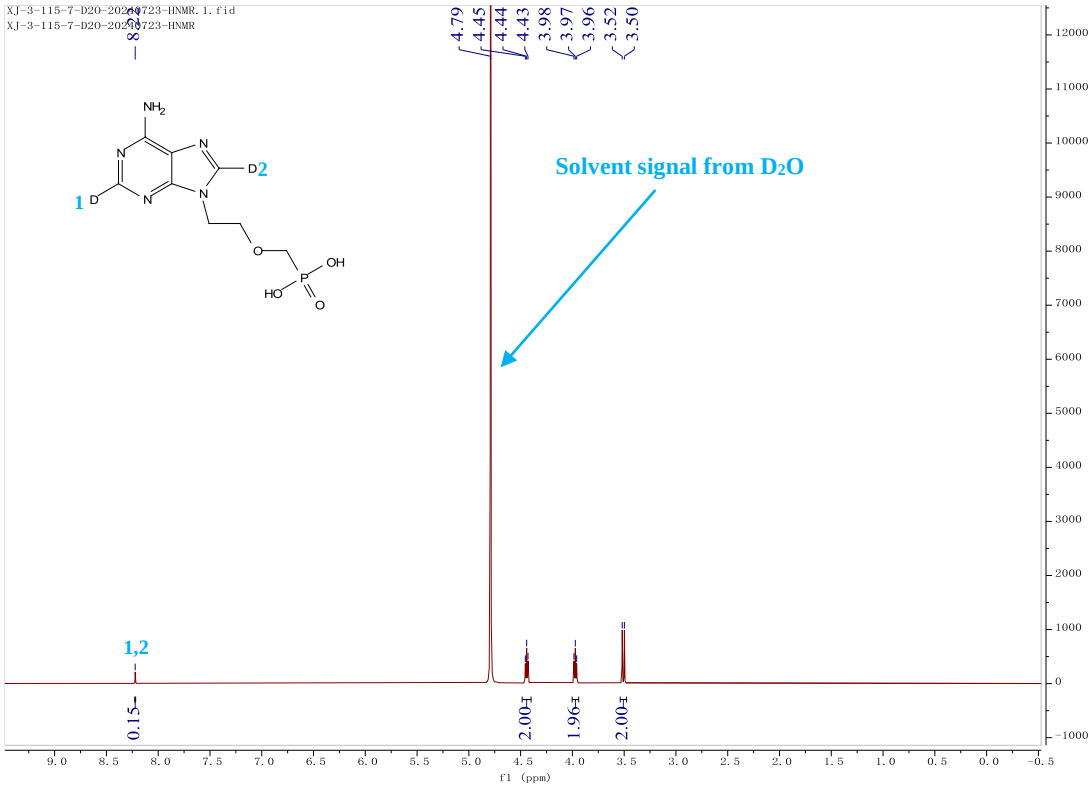

^{1}H NMR (400 MHz, D_2O) of feed material **44a**

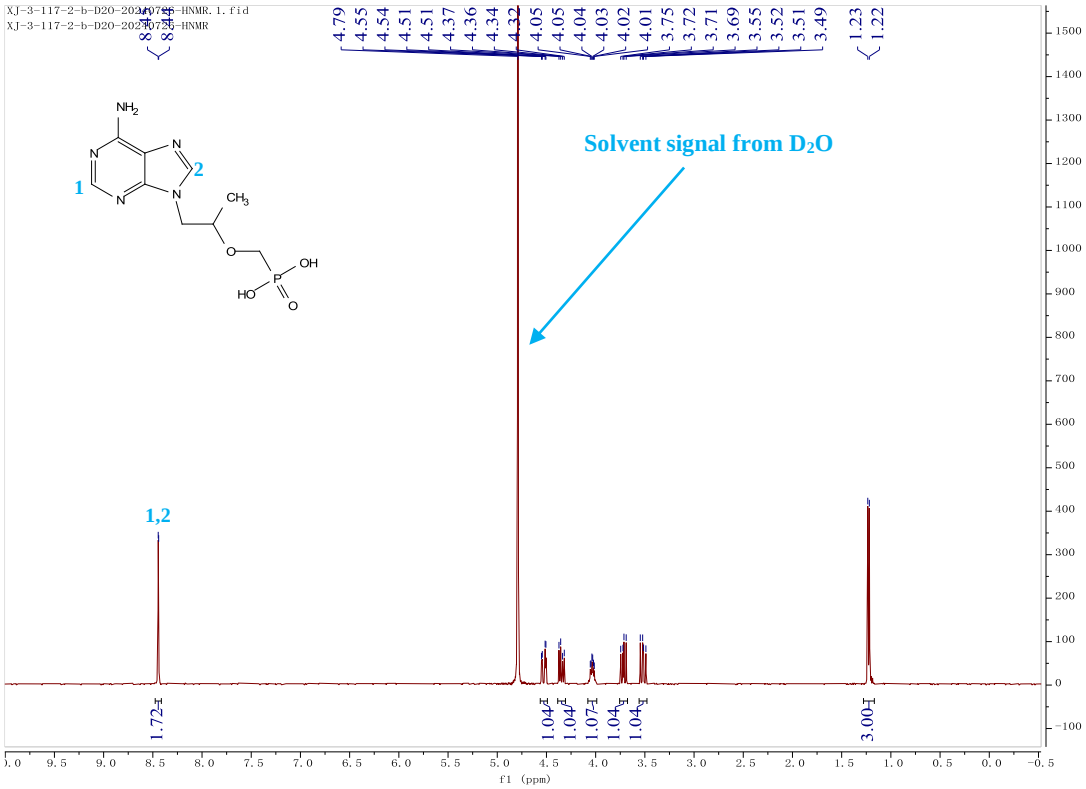

^{1}H NMR (400 MHz, D_2O) of product **44b**

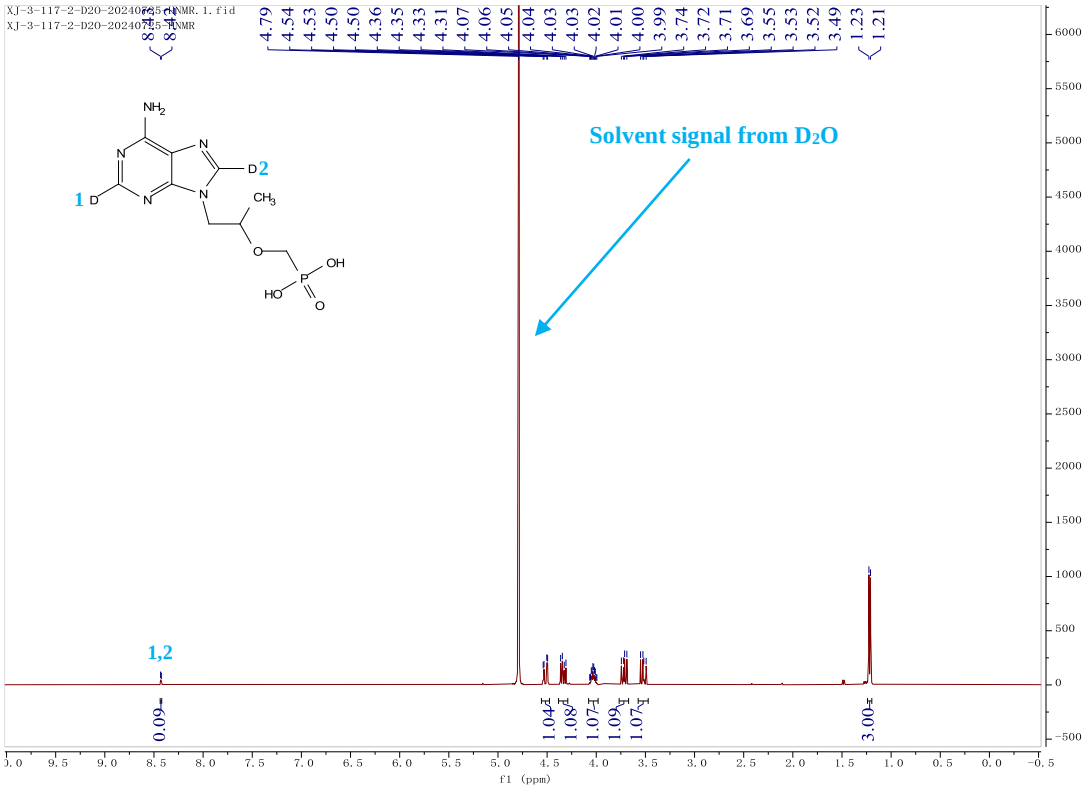

^{1}H NMR (400 MHz, D_2O) of feed material **45a**

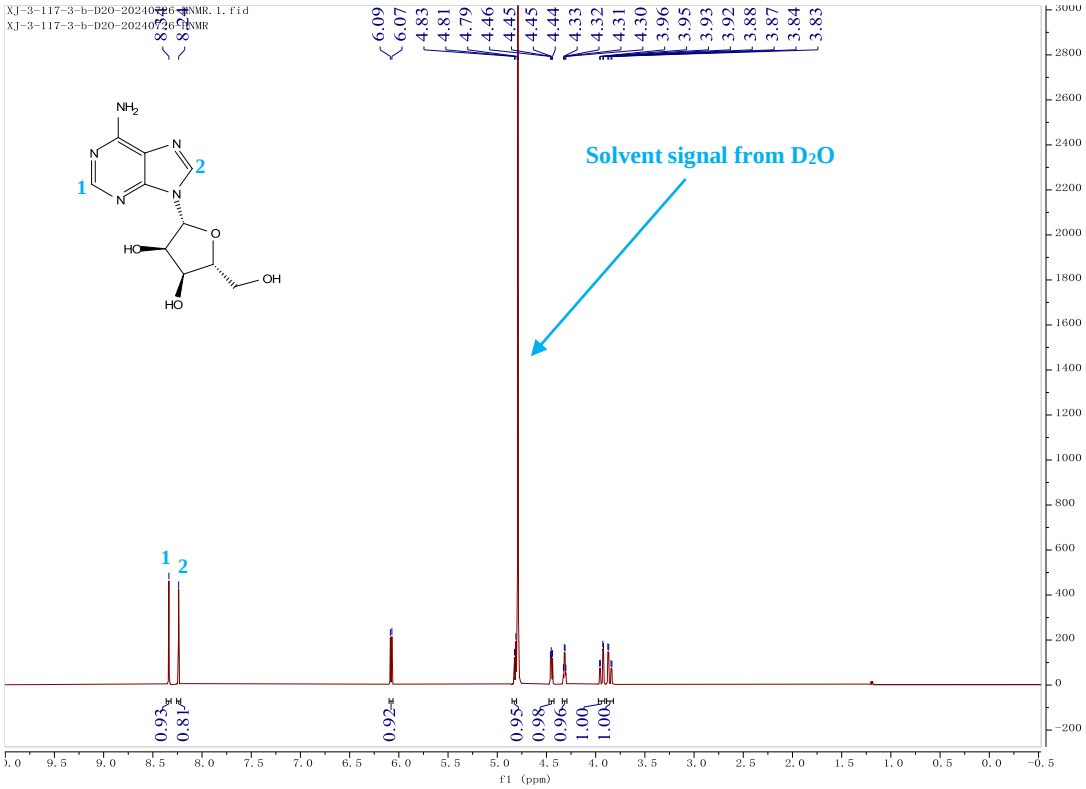

^{1}H NMR (400 MHz, D_2O) of product **45b**

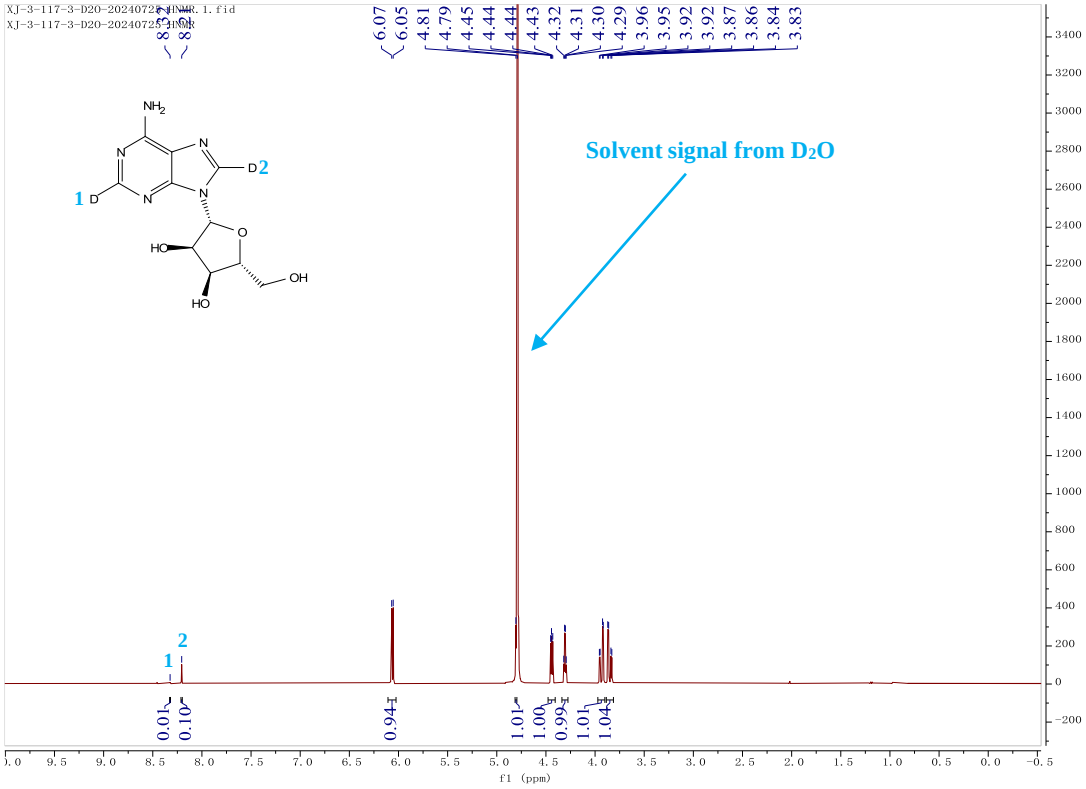

^{1}H NMR (400 MHz, D_2O) of feed material **46a**

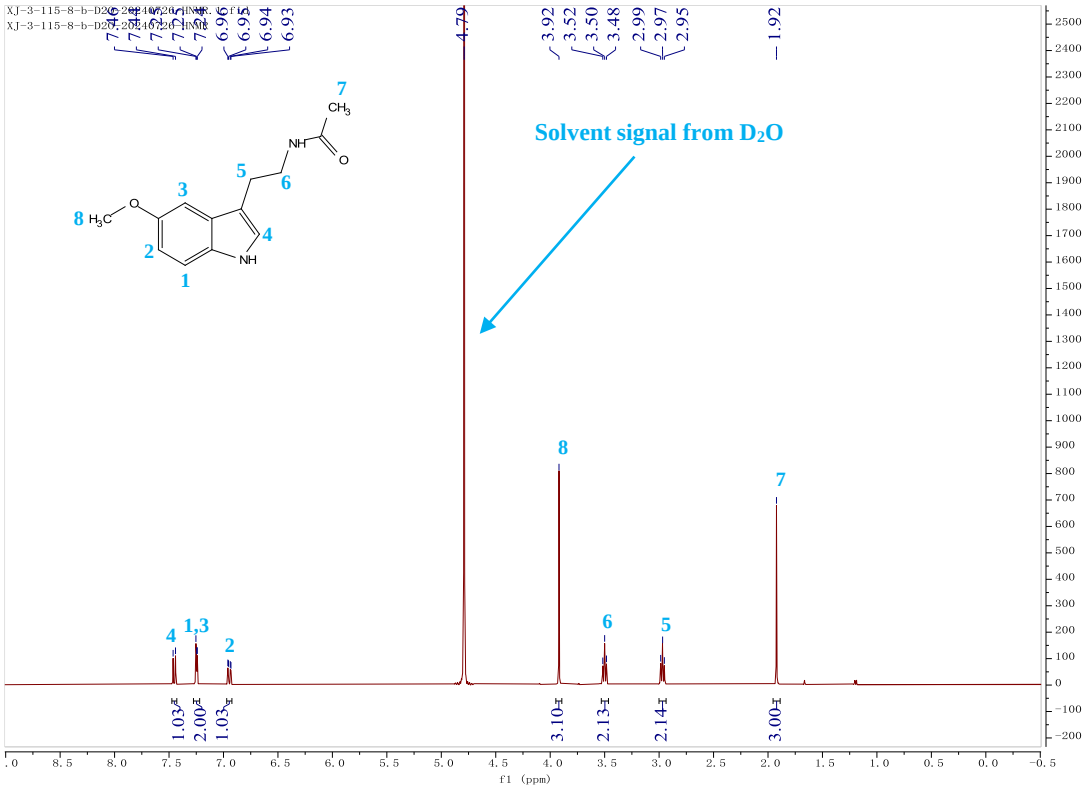

^{1}H NMR (400 MHz, D_2O) of product **46b**

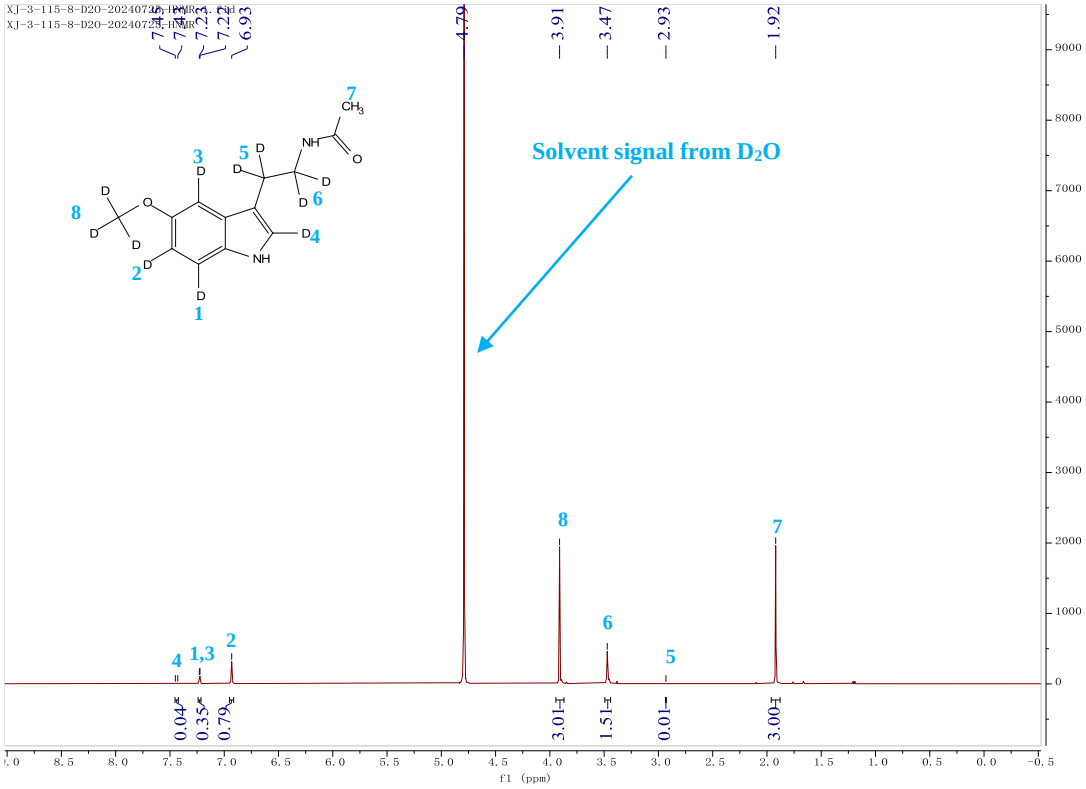

10. Supplementary References

1 Liu, P. *et al*. Photochemical route for synthesizing atomically dispersed palladium catalysts. *Science* **352**, 797-800 (2016).

2 Jiang, X., Li, M., Li, H. & Jin, Z. ZIF-9 derived cobalt phosphide and In_2O_3 as co-catalysts for efficient hydrogen production. *Mol. Catal.* **507**, 111551 (2021).

3 Edström, P. Examination of the revised Kubelka-Munk theory: considerations of modeling strategies. *J. Opt. Soc. Am. A* **24**, 548-556 (2007).

4 Tauc, J., Grigorovici, R. & Vancu, A. Optical Properties and Electronic Structure of Amorphous Germanium. *Phys. Status Solidi B* **15**, 627-637 (1966).

5 Lang, X., Chen, X. & Zhao, J. Heterogeneous visible light photocatalysis for selective organic transformations. *Chem. Soc. Rev.* **43**, 473-486 (2014).

6 Mansfeldova, V. *et al.* Work Function of TiO_2 (Anatase, Rutile, and Brookite) Single Crystals: Effects of the Environment. *J. Phys. Chem. C* **125**, 1902-1912 (2021).

7 Kuo, C.-T. *et al.* 18.1% single palladium atom catalysts on mesoporous covalent organic framework for gas phase hydrogenation of ethylene. *Cell Rep. Phys. Sci.* **2**, 100495 (2021).

8 Ball, M. R. *et al.* AgPd and CuPd Catalysts for Selective Hydrogenation of Acetylene. *ACS Catal.* **10**, 8567-8581 (2020).

9 Rebelli, J., Rodriguez, A. A., Ma, S., Williams, C. T. & Monnier, J. R. Preparation and characterization of silica-supported, group IB–Pd bimetallic catalysts prepared by electroless deposition methods. *Catal. Today* **160**, 170-178 (2011).

10 Dines, T. J., MacGregor, L. D. & Rochester, C. H. IR Spectroscopy of N-Methylpyrrole Adsorbed on Oxides—A Probe of Surface Acidity. *J. Colloid Interface Sci.* **245**, 221-229 (2002).

11 Gaussian 16 Rev. B.01 (Wallingford, CT, 2016).

12 Ditchfield, R., Hehre, W. J. & Pople, J. A. Self-consistent molecular-orbital methods. IX. An extended Gaussian-type basis for molecular-orbital studies of organic molecules. *J. Chem. Phys.* **54**, 724-728 (1971).

13 Zhao, Y. & Truhlar, D. G. The M06 suite of density functionals for main group thermochemistry, thermochemical kinetics, noncovalent interactions, excited states, and transition elements: two new functionals and systematic testing of four M06-class functionals and 12 other functionals. *Theor. Chem. Acc.* **120**, 215-241 (2008).

14 Hehre, W. J., Ditchfield, R. & Pople, J. A. Self-consistent molecular orbital methods. XII. Further extensions of Gaussian-type basis sets for use in molecular orbital studies of organic molecules. *J. Chem. Phys.* **56**, 2257-2261 (1972).

15 Kashinski, D. *et al.* Harmonic vibrational frequencies: approximate global scaling factors for TPSS, M06, and M11 functional families using several common basis sets. *J. Phys. Chem. A* **121**, 2265-2273 (2017).

16 Teng, Z. *et al.* Atomically dispersed low-valent Au boosts photocatalytic hydroxyl radical production. *Nat. Chem.* **16**, 1250-1260 (2024).

17 Akyüz, S. & Akyüz, T. FT-IR spectroscopic investigations of surface and intercalated 2-aminopyrimidine adsorbed on sepiolite and montmorillonite from Anatolia. *J. Mol. Struct.* **651-653**, 205-210 (2003).